SUPPORTING INFORMATION

Self-Assembly Can Direct Covalent Bond Formation Towards Diversity or Specificity

Dávid Komáromy, Marc C. A. Stuart, Guillermo Monréal Santiago, Meniz Tezcan, Victor V. Krasnikov and Sijbren Otto

Contents

1. General remarks

All chemicals, unless otherwise stated, were purchased from Sigma-Aldrich and used as received. Acetonitrile (ULC-MS grade), water (ULC-MS grade) and trifluoroacetic acid (HPLC grade) were purchased from Biosolve BV. Reagent grade solvents were purchased from Macron and used as received. Anhydrous solvents used in synthesis were freshly collected from a dry solvent purification system prior to use. Flash column chromatography was performed on a Reveleris ® X2 Flash Chromatography System (Grace Davison Discovery Sciences, Deerfield IL) on normal phase silica cartridges. NMR spectra were taken using a Varian VXR400 spectrometer. HRMS spectra were recorded on a LTQ Orbitrap XL instrument in ESI ionization mode. Fluorescence measurements were performed on a JASCO FP 6200 fluorimeter using quartz cuvettes with 1 cm path length at an excitation wavelength of 553 nm.

Sample preparation

Generally, samples were diluted to 100 μM with a 7: 3 V:V mixture of water (UPLC grade) and DMF (HPLC grade), containing 0.1 V/V% TFA (HPLC grade) and 5 μL of this diluted sample was injected for UPLC measurements. In experiments studying the co-solvent dependence of the composition of the DCLs (Figure 2a), 1 μL of undiluted samples was injected. In experiments studying the concentration dependence of LMC content (**Figure 2b**), 10 μL of undiluted samples were injected. In experiments studying the disassembly of $\mathbf{1_6}$ in methanol, 2.5 μL of undiluted samples were injected.

UPLC analysis

UPLC measurements were performed on a Waters Acquity H-class system equipped with a PDA detector, at a detection wavelength of 254 nm. UPLC analyses, unless otherwise stated, were performed on an Aeris WIDEPORE 3.6 μm XB-C18 (150 × 2.1 mm) column, purchased from Phenomenex, using ULC-MS grade water (eluent A) and ULC-MS grade acetonitrile (eluent B), containing 0.1 V/V % TFA as a modifier. A flow rate of 0.3 mL/min and a column temperature of 35 °C were applied.

Methods for the analysis of DCLs prepared from **1** and **2**:

t / min	% A
0	60
7	38
10	34
17	5
18	5
19	60
20	60

Method for the analysis of DCLs prepared from **3**:

t / min	% A
0	60
17	25
18	25
19	60
20	60

UPLC-MS analysis

UPLC-MS measurements were performed using a Waters Acquity UPLC H-class system coupled to a Waters Xevo-G2 TOF. The mass spectrometer was operated in the positive electrospray ionization mode with the following ionization parameters: capillary voltage: 3 kV, sampling cone voltage: 20 V, extraction cone voltage : 4 V, source gas temperature: 120°C, desolvation gas temperature: 450°C, cone gas flow (nitrogen): 1 L/h, desolvation gas flow (nitrogen): 800 L/h.

Negative-staining Transmission Electron Microscopy

Samples were diluted to 60-fold using UPLC grade water. A small drop (5 µL) of sample was then deposited on a 400 mesh copper grid covered with a thin carbon film (supplied by Agar Scientific). After 30 seconds, the droplet was blotted on filter paper. The sample was then stained with a solution of 2% uranyl acetate (4 µL) deposited on the grid, subsequently washed and blotted on filter paper after 30 seconds. The staining procedure was repeated a second time, this time without the washing and blotting step. The grids were observed in a Philips CM12 electron microscope operating at 120 kV. Images were recorded on a slow scan CCD camera.

Cryo Transmission Electron Microscopy

A 10 µL drop of the sample was placed on a Quantifoil 3.5/1 holey carbon coated grid. Blotting and vitrification in ethane was done in a Vitrobot (FEI, Eindhoven, the Netherlands). The grids were observed in a Tecnai T20 cryo-electron microscope operating at 200 keV with a Gatan model 626 cryo-stage. Images were recorded under low-dose conditions with a slow-scan CCD camera.

Atomic Force Microscopy

AFM samples were prepared by depositing 100 µL of the sample (diluted to 10 µM building block concentration with UPLC grade water) onto a clean mica surface (Grade V1, Van Loenen Instruments). Subsequently, the solvent was evaporated in a gentle stream of air in ca. 20 minutes. The surface was then washed with 100 µL of UPLC grade water and blotted into a piece of paper twice and finally air-dried. The AFM measurements have been performed using a Bruker Multimode 8 instrument in Scan Asyst-Air imaging mode. Measurements were performed in air at room temperature. As a probe, a ScanAsyst Air (Bruker) silicon tip on a nitride cantilever was used with the following parameters: length: 115 µm, width: 25 µm, resonance frequency: 70 kHz, force constant: 0.4 N/m. The images were recorded with frequencies between 0.5 and 1.5 Hz and analyzed with NanoScope Analysis 1.50 software (Bruker Corporation, 2015).

Optical Microscopy

Optical microscopy was performed on a Nikon Eclipse TS 100 instrument. Length calibration was performed by recording the image of a 40 µm scale bar with the same settings as for the corresponding image. The images were processed using ImageJ software.

Confocal Fluorescence Microscopy

Confocal fluorescence microscopy measurements were performed on a MicroTime 200 instrument (PicoQuant, Berlin, Germany), using an excitation wavelength of 532 nm (the excitation power was set at 4 µW), with a 542 nm long-pass edge emission filter (BLPO1-532R, Semrock, New York). For the measurement, 50 µL sample was deposited on the microscope slide and 5.0 µL of Nile Red (1.0 µM solution in methanol) was added. The measurements were performed after an incubation time of 2 minutes The images were processed using ImageJ software. .

Dynamic Light Scattering

Dynamic light scattering measurements were performed on a NanoBrook 90Plus PALS Particle Size Analyzer (Brookhaven, NY), using a 659 nm laser at 90º detection angle. Samples were prepared using 50 mM aqueous borate buffer (pH = 8.2), previously filtered with a 0.2 µm pore size filter. For each measurement, 10 parallels were recorded.

2. Synthetic Procedures

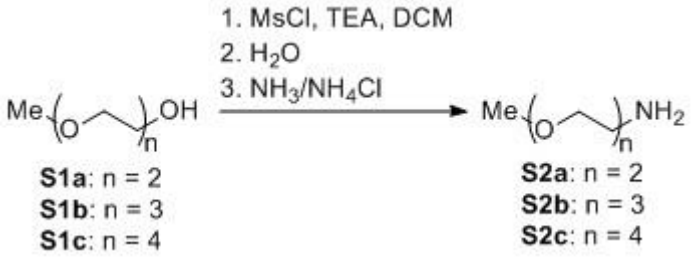

To a vigorously stirred, ice-cooled solution of the monomethylated oligoethylene glycol (50 mmol) and triethylamine (8.5 mL, 61 mmol, 1.2 eq) in anhydrous DCM (60 mL) a solution of methylsulfonyl chloride (5.4 mL, 70 mmol, 1.4 eq) in anhydrous DCM (20 mL) was added dropwise. The reaction mixture was stirred overnight at 0-5°C in a cold room. The mixture was warmed to room temperature. DCM (20 mL) and deionized water (50 mL) was added and the solution stirred for 30 minutes to obtain a clear biphasic mixture. The layers were separated and the organic layer was washed with 1M HCl (540 mL) and water (500 mL). The combined aqueous layers were back-extracted with DCM (5 ×100 mL). The combined organic layers were dried over Na_2SO_4 and concentrated. The obtained crude mesylate was dissolved in a mixture of 25 w/w% NH_3 in water (600 mL) and NH_4Cl (90 g) and stirred for 48 h. NaCl (90 g) was dissolved in the reaction mixture, which was extracted with DCM (3 ×500 mL). The combined organic layers were dried over $Na_2SO_4$and concentrated to obtain the corresponding amine as a yellow oil, which was used without further purification in the following reactions.

S2a. Yield: 4.05 g (67%). ^{1}H NMR (400 MHz, $CDCl_3$) δ 3.35 (dtt, *J* = 4.6, 2.2, 1.1 Hz, 2H), 3.28 (dddd, *J* = 5.1, 4.0, 2.2, 1.1 Hz, 2H), 3.24 (td, *J* = 5.3, 1.2 Hz, 2H), 3.15 – 3.08 (m, 3H), 2.64 – 2.57 (m, 2H). ^{13}C NMR (101 MHz, $CDCl_3$) δ 73.29, 71.65, 69.95, 58.70, 58.67, 41.53. ESI-HRMS: $[M+H]^+$ found: 120.1017 Da (expected: 120.1019 Da). Analytical data matched that reported previously in ref 2.

S2b. Yield: 7.24 g (88%). 1H NMR (400 MHz, $CDCl_3$) δ 5.26 (s, 2H), 3.58 (th, J = 5.6, 2.6 Hz, 6H), 3.50 – 3.46 (m, 2H), 3.44 (t, J = 5.2 Hz, 2H), 3.31 (s, 3H), 2.79 (t, J = 5.2 Hz, 2H), 1.44 (s, 2H). 13C NMR (101 MHz, $CDCl_3$) δ 73.29, 71.79, 70.45, 70.13, 58.84, 53.41, 41.66. ESI-HRMS: $[M+H]^+$ found: 164.1280 Da (expected: 164.1281 Da). Analytical data matched that reported previously in ref 2.

S2c. Yield: 8.65 g (84%). ^{1}H NMR (400 MHz, $CDCl_3$) δ 3.66 – 3.50 (m, 10H), 3.48 (dd, *J* = 5.7, 3.6 Hz, 2H), 3.44 (t, *J* = 5.2 Hz, 2H), 3.31 (s, 3H), 2.79 (t, *J* = 5.2 Hz, 2H), 1.46 (s, 2H). ^{13}C NMR (101 MHz $CDCl_3$) δ 73.30, 71.82, 70.50, 70.47, 70.46, 70.40, 70.17, 58.89, 41.70. ESI-HRMS: $[M+H]^+$ found: 208.1542 Da (expected: 208.1543 Da). Analytical data matched that reported previously in ref 3.

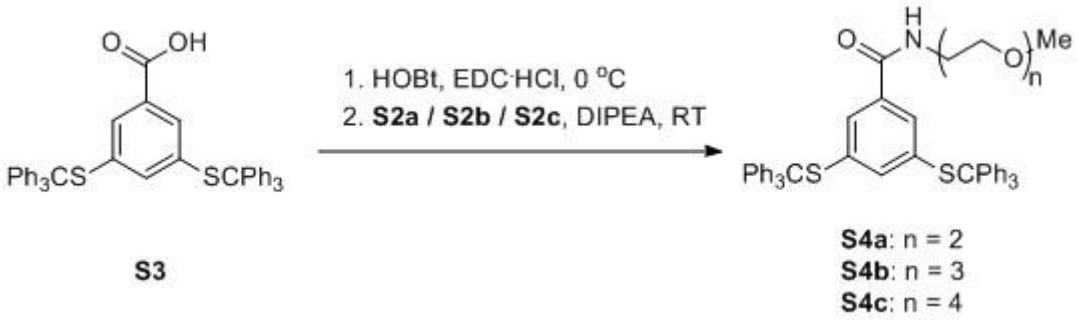

S3

S4a: n = 2
S4b: n = 3
S4c: n = 4

To an ice-cooled suspension of 3.5-bis(trithyltio)benzoic acid **S3**[1] (1.2 g, 1.8 mmol) and HOBt (0.364 g, 2.4 mmol, 1.3 eq) in anhydrous DCM (60 mL) was added EDC·HCl (0.934 g, 4.9 mmol, 2.7 eq). A clear yellow solution was obtained. Subsequently, an ice-cooled solution of the corresponding amine **S2a**-**S2c** (2.7 mmol, 1.5 eq) and diisopropylethylamine (3.1 mL, 18 mmol, 10 eq) in anhydrous DCM (30 mL) was added dropwise. The mixture was allowed to warm to room temperature and stirred overnight. DCM (50 mL) was added and the solution was washed with 1M HCl (30 mL), saturated $NaHCO_3$ solution (30 mL) and water (30 mL). The organic phase was dried over $MgSO_4$ and concentrated *in vacuo*. The residue was dissolved in DCM (4 mL) and purified by flash column chromatography to obtain the product as a white foamy solid.

S4a: Yield: 83% (1.14 g). Gradient for flash column chromatography (24 g silica): 0 min: 100% DCM, 0-2 min: 100% DCM to 100% hexanes, 2-3 min: 100% hexanes, 3-13 min: 100% hexanes to 50% hexanes in EtOAc, 13-15 min: 50% hexanes in EtOAc, 15-17 min : 50% hexanes in EtOAc to 60% hexanes in EtOAc, 17-18 min: 60% hexanes in EtOAc, 18-20 min : 60% hexanes in EtOAc to 100% EtOAc, 20-27 min: 100% EtOAc.

^{1}H NMR (400 MHz, $CDCl_3$) δ 7.39 – 7.30 (m, 12H), 7.21 (m, 18H), 7.12 (t, *J* = 1.7 Hz, 1H), 6.88 (d, *J* = 1.6 Hz, 2H), 3.63 (dd, *J* = 5.8, 2.9 Hz, 2H), 3.59 – 3.52 (m, 4H), 3.47 (q, *J* = 5.4 Hz, 2H), 3.39 (s, 3H). ^{13}C NMR (101 MHz, $CDCl_3$) δ 165.96, 144.14, 142.29, 134.80, 134.05, 132.40, 130.19, 129.92, 127.81, 127.58, 126.81, 77.45, 77.13, 76.81, 71.90, 71.34, 70.32, 69.90, 60.40, 59.09, 39.63, 14.25. ESI-HRMS: $[M+H]^+$ found: 772.2914 Da (expected: 772.2914 Da), $[M+Na]^+$ found: 794.2740 Da (expected: 794.2733 Da).

S4b: Yield: 47% (0.715 g, 1.2 g scale), 67 % (2.303 g, 3 g scale). Gradient for flash column chromatography (24 g silica): 0 min: 100% DCM, 0-1 min: 100% DCM to 100% hexanes, 2-4 min: 100% hexanes, 4-18 min: 100% hexanes to 50% hexanes in EtOAc, 18-19 min: 50% hexanes in EtOAc, 19-21 min : 50% hexanes in EtOAc to 100% EtOAc, 21-29 min: 100% EtOAc.

^{1}H NMR (400 MHz, $CDCl_3$) δ 7.23 (dt, *J* = 5.4, 3.3 Hz, 12H), 7.14 – 7.05 (m, 18H), 7.01 (t, *J* = 1.6 Hz, 1H), 6.77 (d, *J* = 1.6 Hz, 2H), 5.66 (t, *J* = 5.4 Hz, 1H), 3.60 – 3.52 (m, 6H), 3.47 – 3.41 (m, 4H), 3.35 (dd, *J* = 10.1, 5.0 Hz, 2H), 3.22 (s, 3H), 1.95 (s, 1H). ^{13}C NMR (101 MHz, $CDCl_3$) δ 165.92, 144.12, 142.27, 134.76, 134.04, 132.41, 129.89, 127.79, 126.79, 71.95, 71.31, 70.60, 70.57, 70.37, 69.89, 59.02, 39.65. ESI-HRMS: $[M+H]^+$ found: 816.3168 Da (expected: 816.3176 Da). $[M+Na]^+$ found: 838.2992 Da (expected: 838.2995 Da).

S4c: Yield: 55% (0.852 g). Gradient for flash column chromatography (24 g silica): 0 min: 100% DCM, 0-2 min: 100% DCM to 100% hexanes, 2-3 min: 100% hexanes, 3-19 min: 100% hexanes to 100% EtOAc, 19-21 min: 100% EtOAc.

^{1}H NMR (400 MHz, $CDCl_3$) δ 7.38 – 7.29 (m, 12H), 7.20 (dd, m, 18H), 7.11 (t, *J* = 1.7 Hz, 1H), 6.88 (d, *J* = 1.7 Hz, 2H), 5.82 (t, *J* = 5.4 Hz, 1H), 3.71 – 3.57 (m, 10H), 3.57 – 3.49 (m, 4H), 3.46 (q, *J* = 5.0 Hz, 2H), 3.35 (s, 3H). ^{13}C NMR (101 MHz, $CDCl_3$) δ 165.92, 144.12, 142.27, 134.74, 134.03, 132.44, 129.89, 127.79, 126.79, 71.90, 71.32, 70.63, 70.60, 70.51, 70.37, 69.91, 59.02, 39.67. ESI-HRMS: [M+H]+ found: 860.3438 Da (expected: 860.3438 Da).

S4a: n = 2
S4b: n = 3
S4c: n = 4

2: n = 2
1: n = 3
3: n = 4

9 mL TFA was degassed through 3 freeze-pump-thaw cycles in a 25-mL Schlenk tube and added to a 50-mL round-bottomed flask containing protected amide **S4a**-**S4c** (1.4 mmol) under nitrogen. The orange solution was sonicated for 1 minute and stirred at room temperature for 15 minutes. Subsequently, Et_3SiH (1.0 mL, 6.3 mmol, 4.5 eq) was added dropwise and the solution stirred for further 15 minutes. TFA was removed in vacuo via the Schlenk line and condensed into a cold trap immersed in liquid nitrogen. The remaining suspension was dissolved in 70 mL of a degassed mixture of MeOH-H_2O (9:1, 70 mL) and washed with 3*100 mL heptane. Methanol was removed *in vacuo* at 40°C and the remaining suspension was freeze-dried for 36 hours to furnish the corresponding building block **1**-**3.**

1: Sticky, yellow solid. Yield: 90% (0.416 g). ^{1}H NMR (400 MHz, $(CD_3)_2SO$) δ 8.47 (t, *J* = 5.6 Hz, 1H), 7.46 (d, *J* = 1.7 Hz, 2H), 7.36 (t, *J* = 1.7 Hz, 1H), 5.67 (s, 2H), 3.48 (ddd, *J* = 7.1, 3.1, 1.5 Hz, 8H), 3.40 – 3.32 (m, 4H), 3.20 (s, 3H). ^{13}C NMR (101 MHz, CD_3OD) δ 167.55, 135.77, 133.83, 130.38, 123.68, 71.48, 70.10, 69.94, 69.85, 68.98, 57.66, 39.60. ESI-HRMS: $[M+H]^+$ found: 332.0985 Da (expected: 332.0985 Da), $[M+Na]^+$ found: 354.0802 Da (expected: 354.0810 Da).

2: White-yellow solid**.** Yield: 98% (0.393 g). ^{1}H NMR (400 MHz, DMSO-d_6) δ 8.49 (t, *J* = 5.6 Hz, 1H), 7.46 (d, *J* = 1.7 Hz, 2H), 7.36 (t, *J* = 1.7 Hz, 1H), 5.70 (s, 2H), 3.52 – 3.45 (m, 4H), 3.44 – 3.39 (m, 2H), 3.36 (t, *J* = 5.8 Hz, 2H), 3.21 (s, 3H). ^{13}C NMR (101 MHz, cd_3od) δ 167.60, 135.75, 133.84, 130.35, 123.64, 71.52, 69.60, 69.03, 57.77, 39.55. ESI-HRMS: $[M+Na]^+$ found: 310.0543 Da (expected: 310.0542 Da).

3: Yellow oil**.** Yield: 93% (0.488 g). ^{1}H NMR (400 MHz, $(CD_3)_2SO$) δ 8.47 (s, 1H), 7.46 (d, *J* = 1.5 Hz, 2H), 7.36 (s, 1H), 5.67 (s, 2H), 3.48 (dd, *J* = 13.3, 4.8 Hz, 12H), 3.42 – 3.31 (m, 4H), 3.20 (s, 3H). ^{13}C NMR (101 MHz, CD_3OD) δ 167.47, 135.75, 133.83, 130.40, 123.75, 71.51, 70.12, 70.07, 69.91, 69.88, 69.02, 57.70, 39.67. ESI-HRMS: [M+H]+ found: 376.1246 Da (expected: 376.1247 Da), [M+Na]+ found: 398.1062 Da (expected: 398.1066 Da).

3. NMR Spectra

 **S2a**

^{1}H NMR (400 MHz, $CDCl_3$)

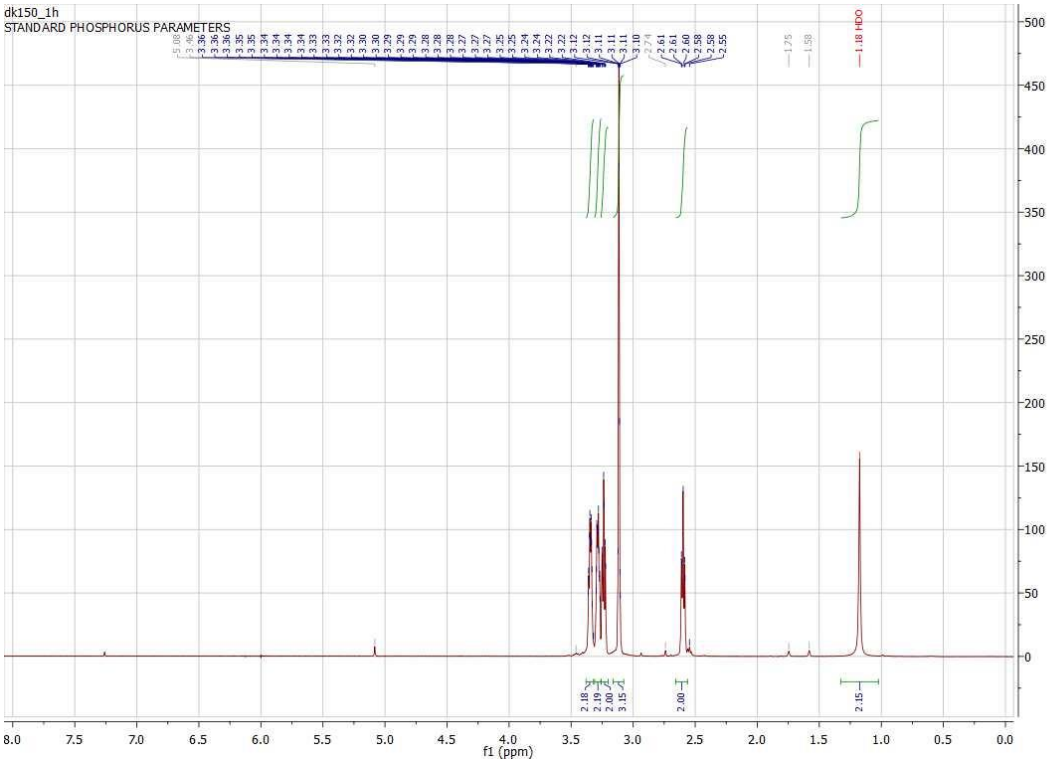

^{13}C NMR (101 MHz, $CDCl_3$)

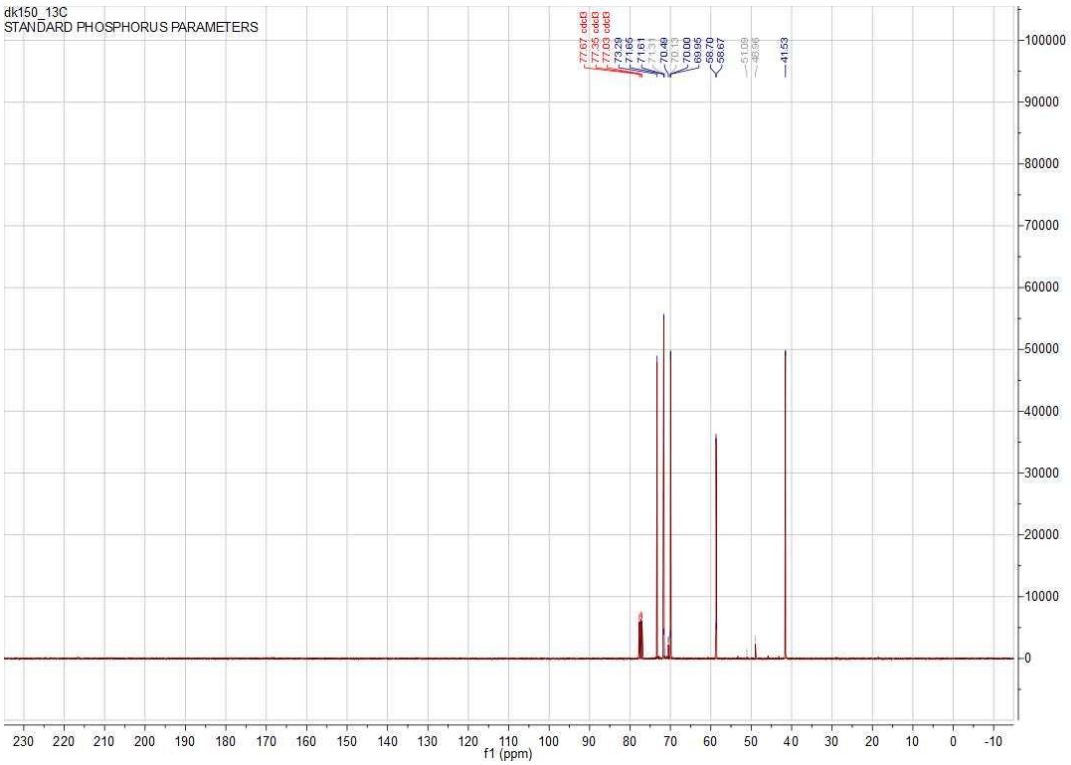

S2b

^{1}H NMR (400 MHz, $CDCl_3$)

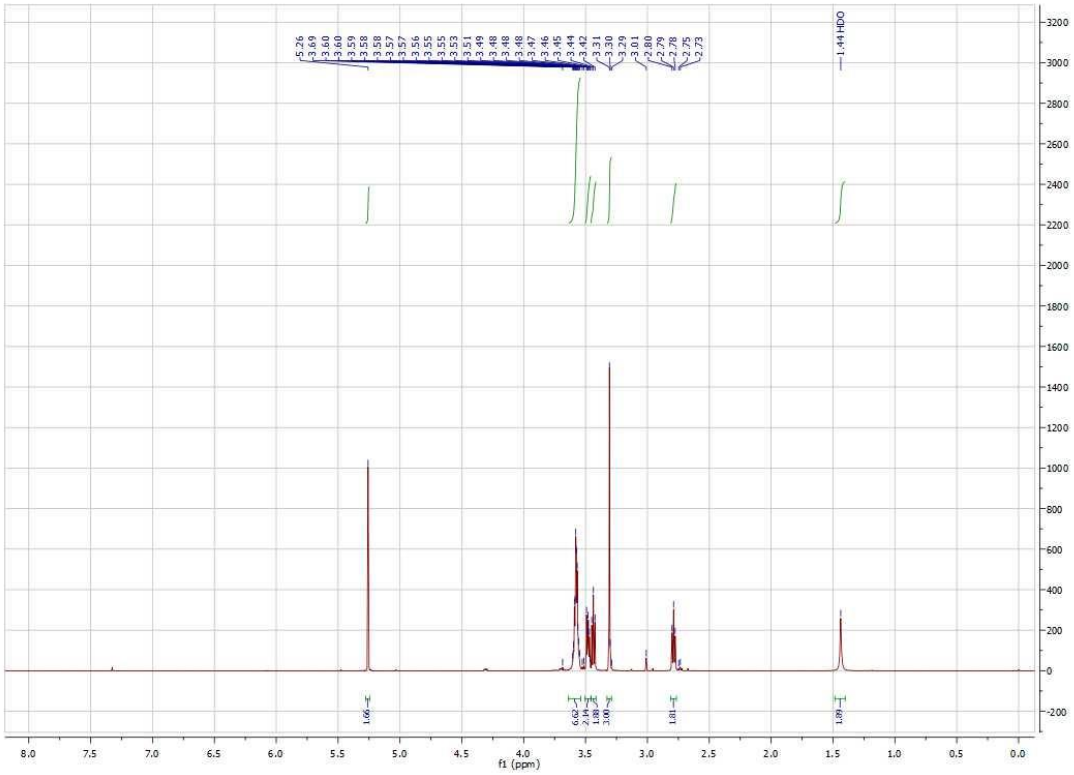

^{13}C NMR (101 MHz, $CDCl_3$)

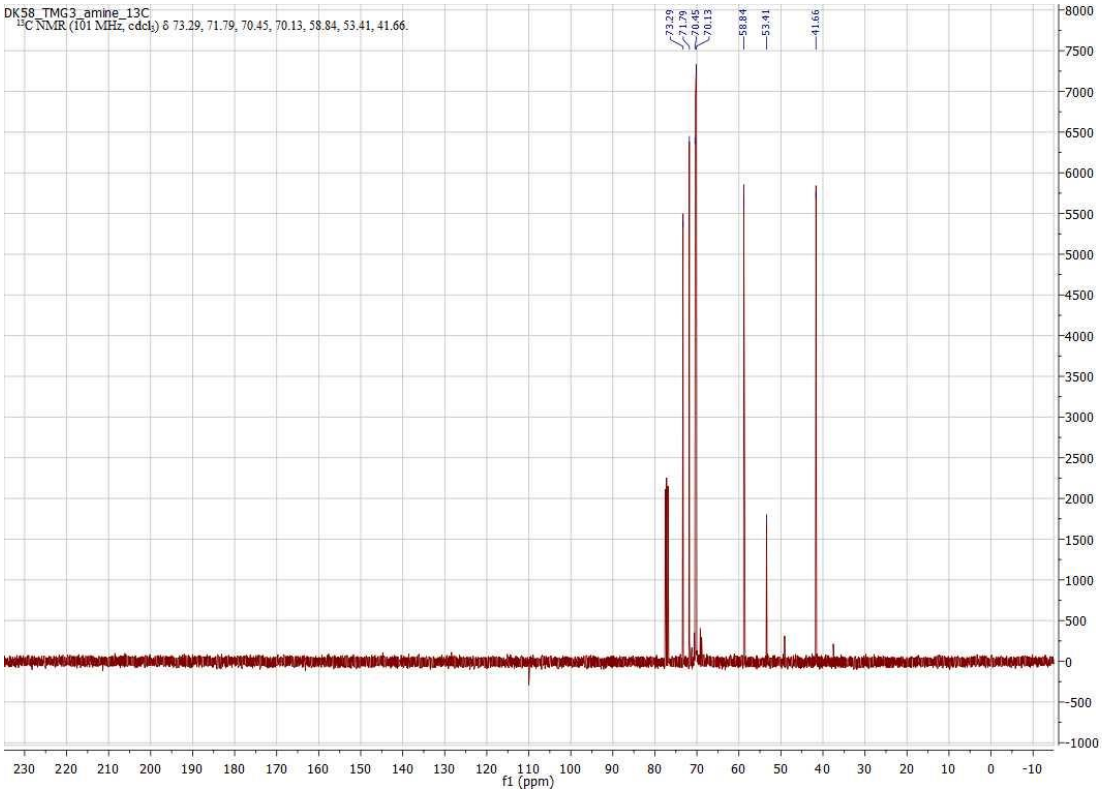

S2c

^{1}H NMR (400 MHz, $CDCl_3$)

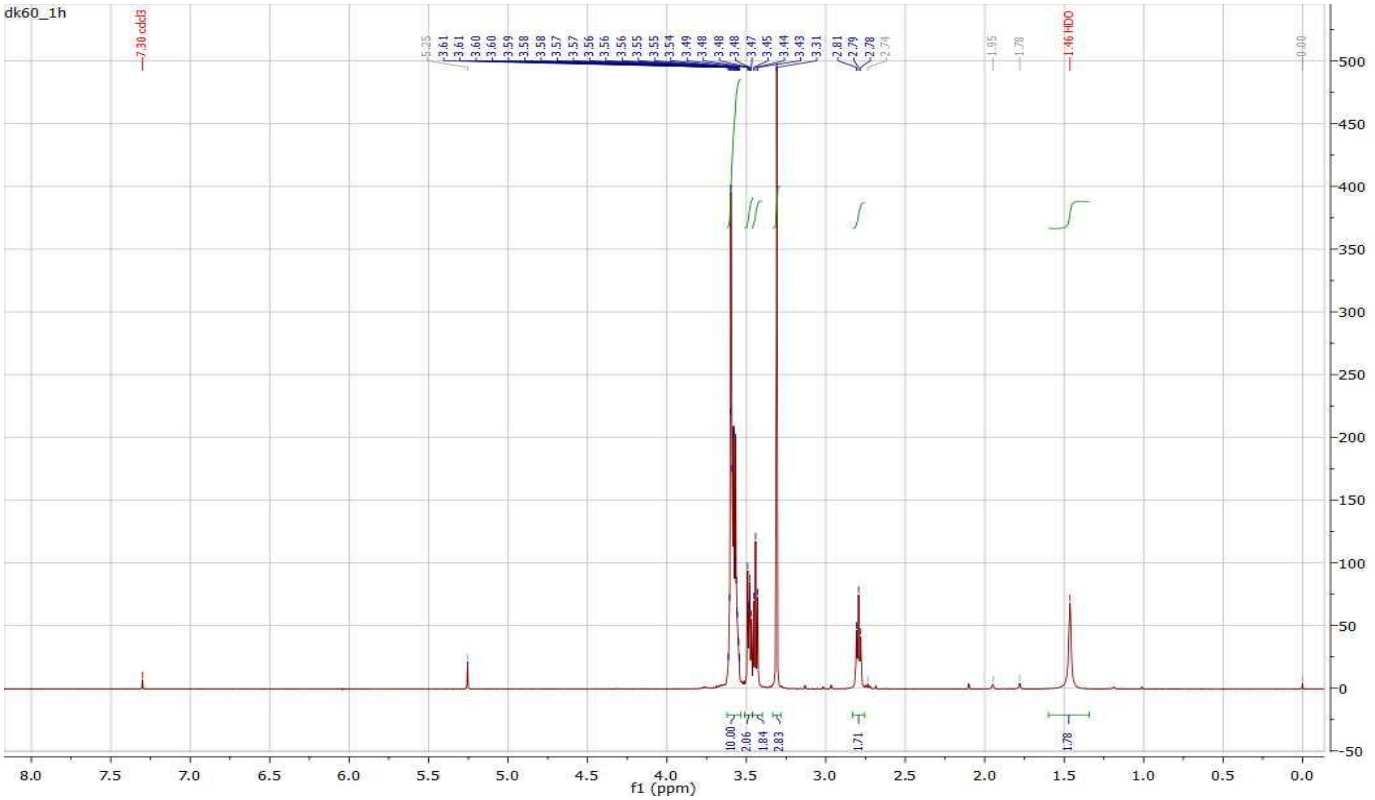

^{13}C NMR (101 MHz, $CDCl_3$)

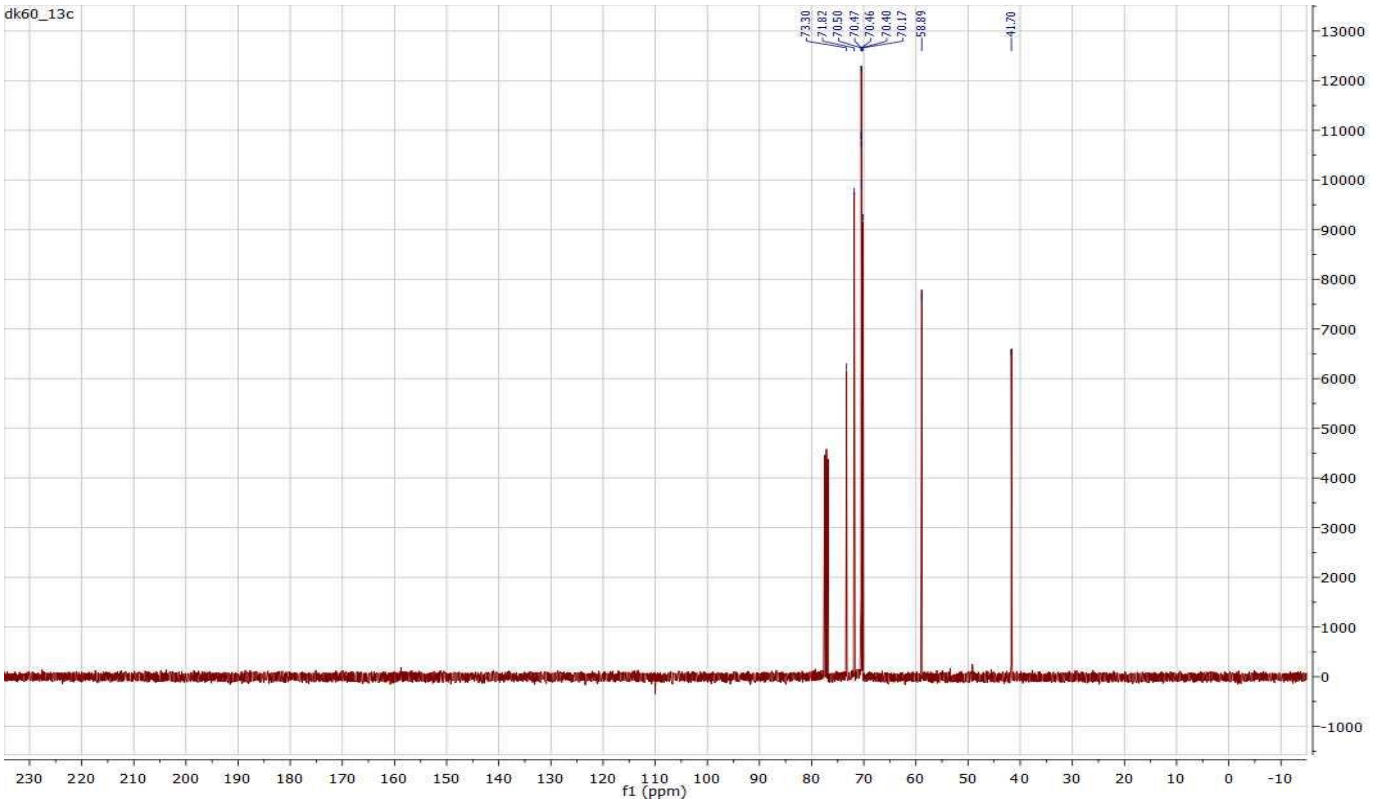

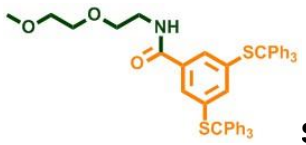

S4a

^{1}H NMR (400 MHz, $CDCl_3$)

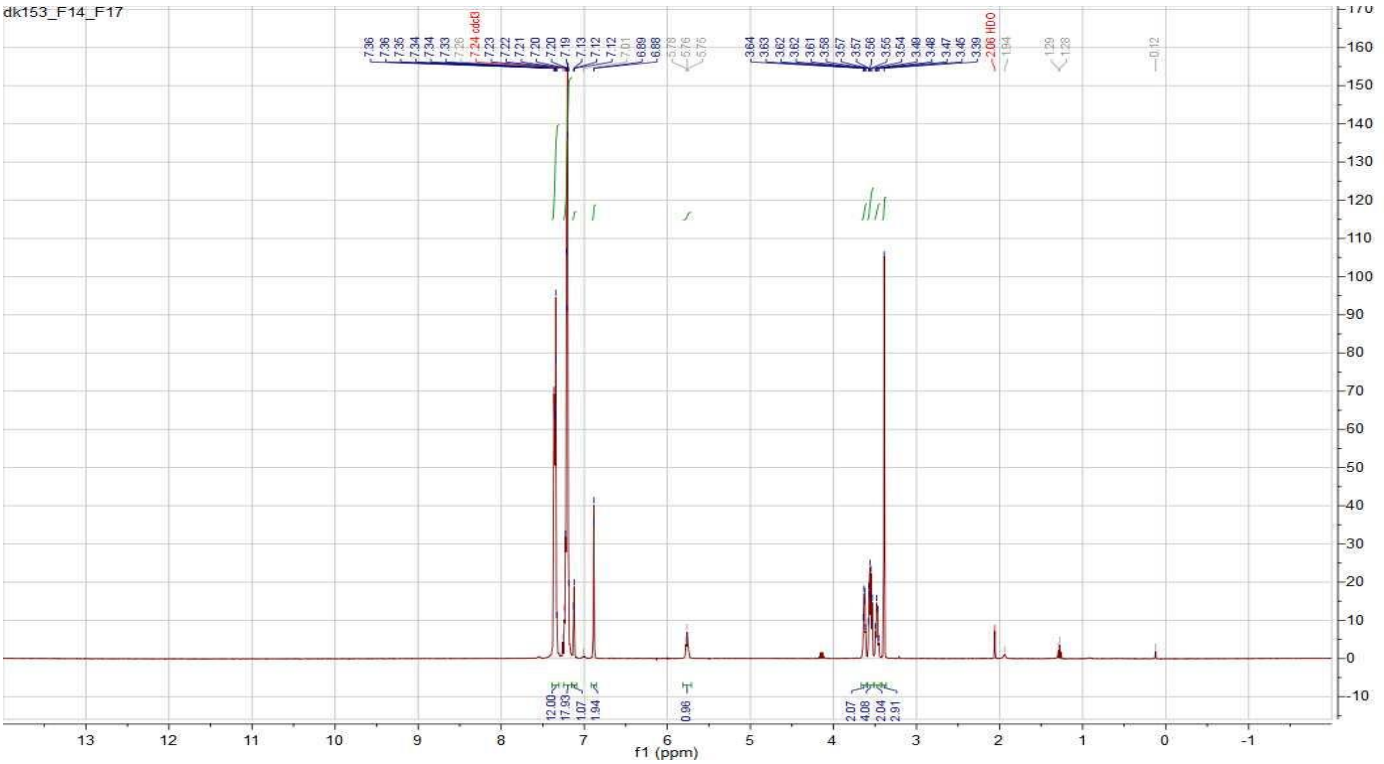

^{13}C NMR (101 MHz, $CDCl_3$)

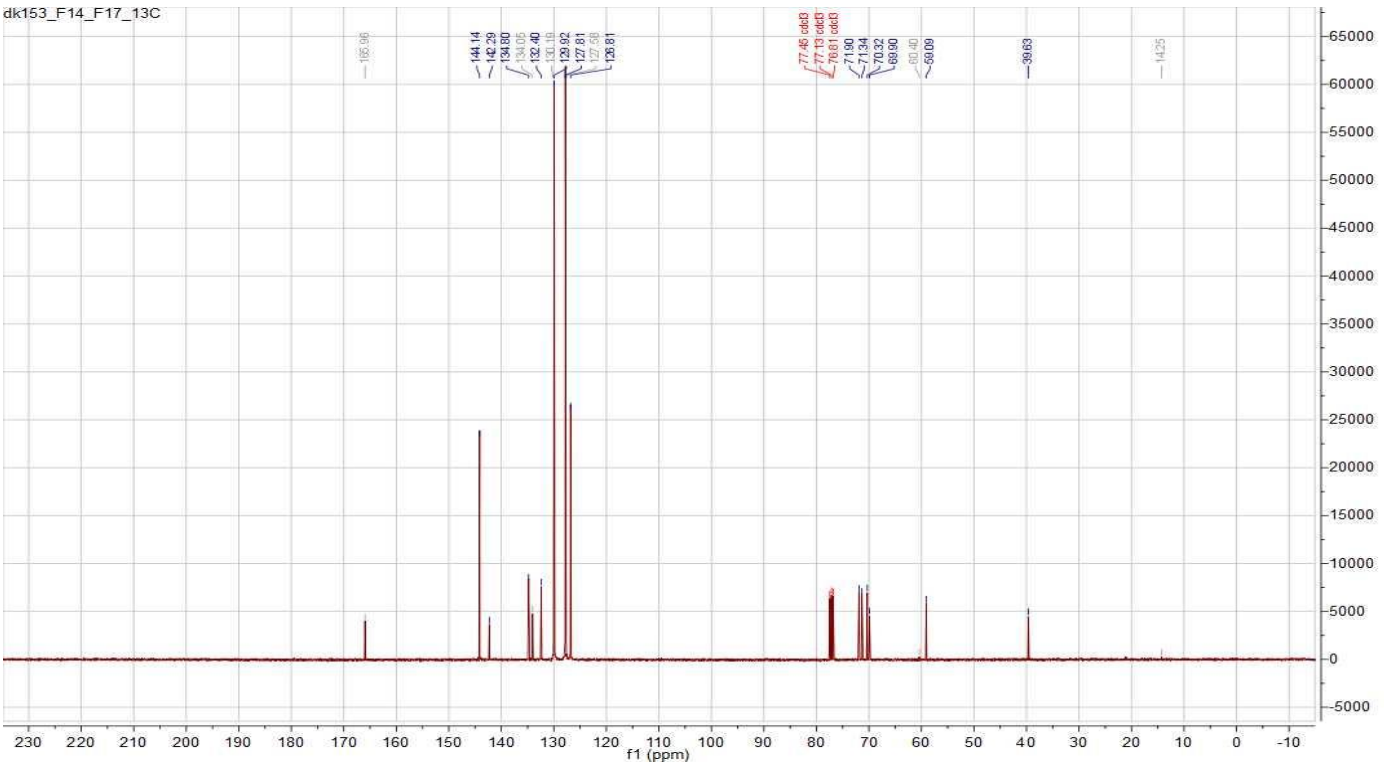

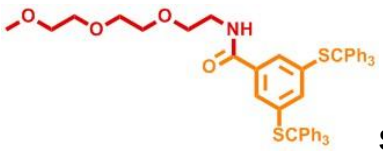

S4b

^{1}H NMR (400 MHz, $CDCl_3$)

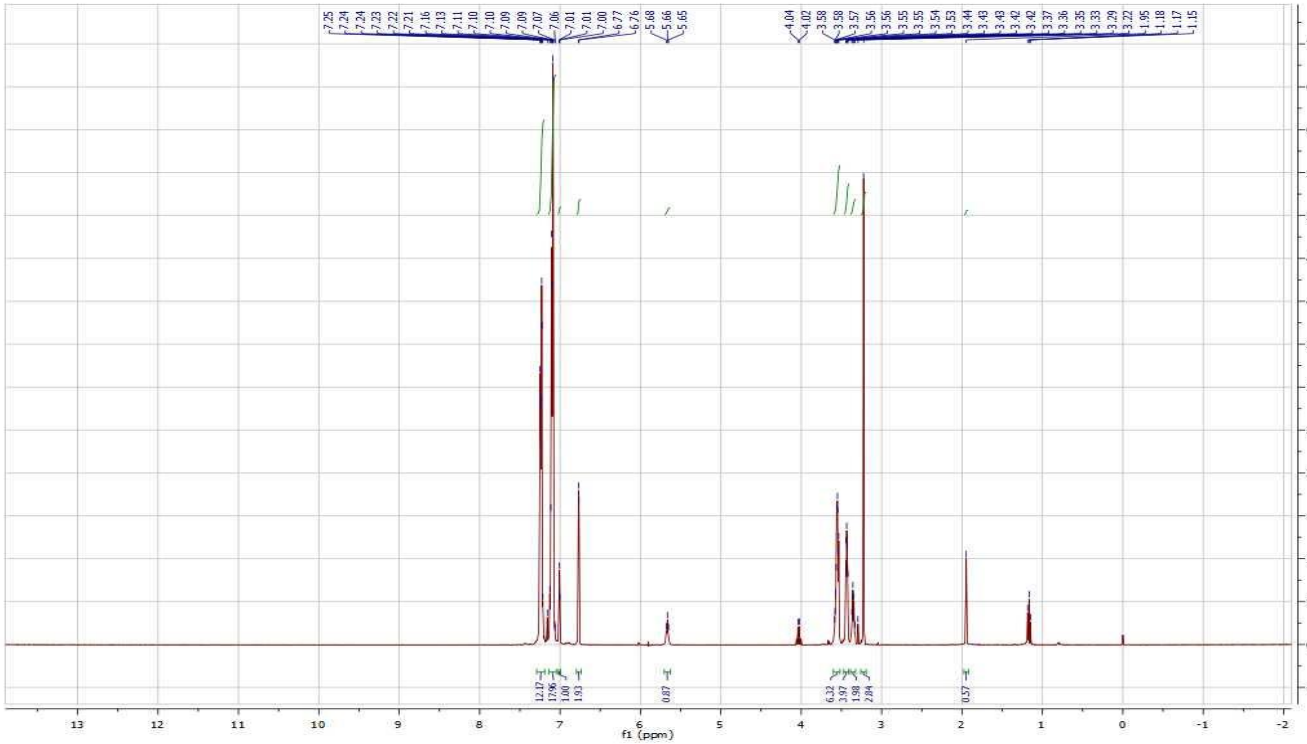

^{13}C NMR (101 MHz, $CDCl_3$)

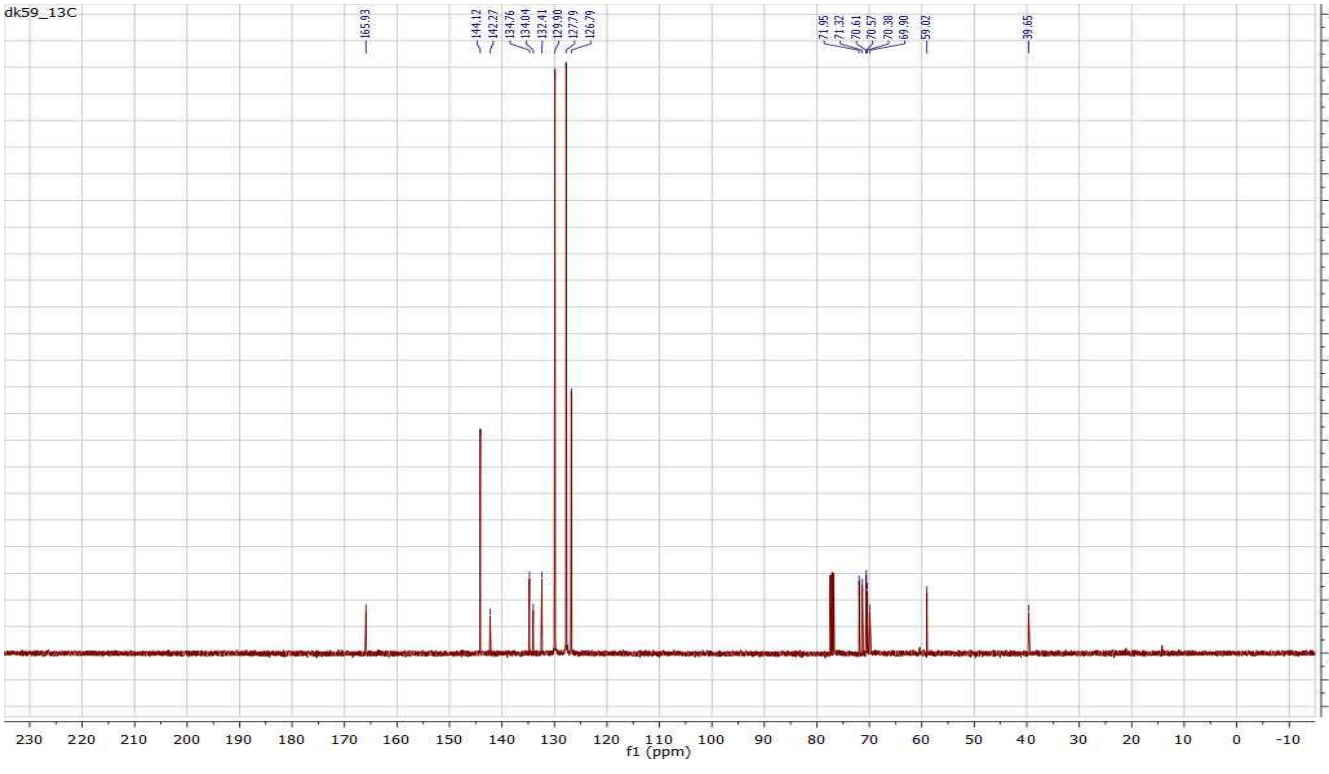

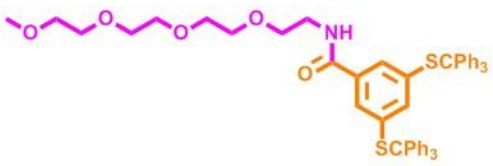

S4c

^{1}H NMR (400 MHz, $CDCl_3$)

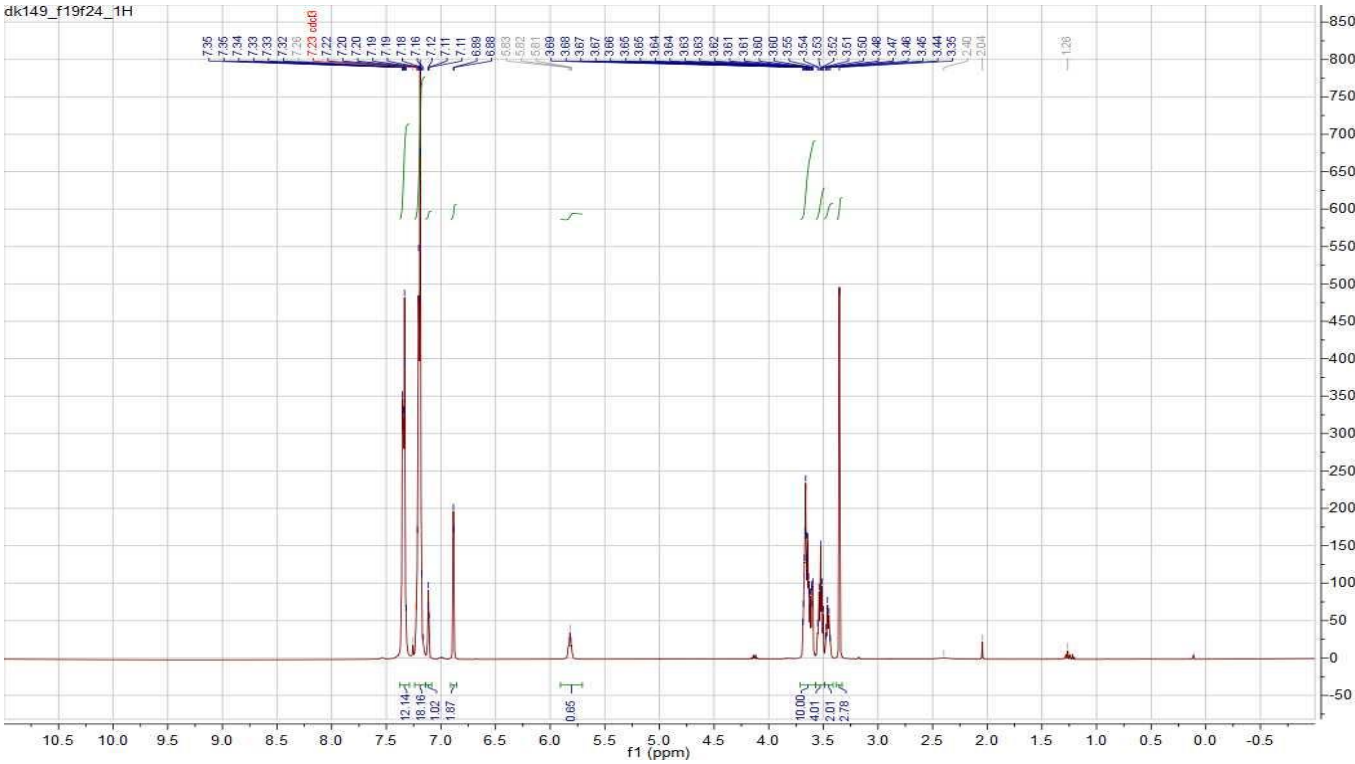

^{13}C NMR (101 MHz, $CDCl_3$)

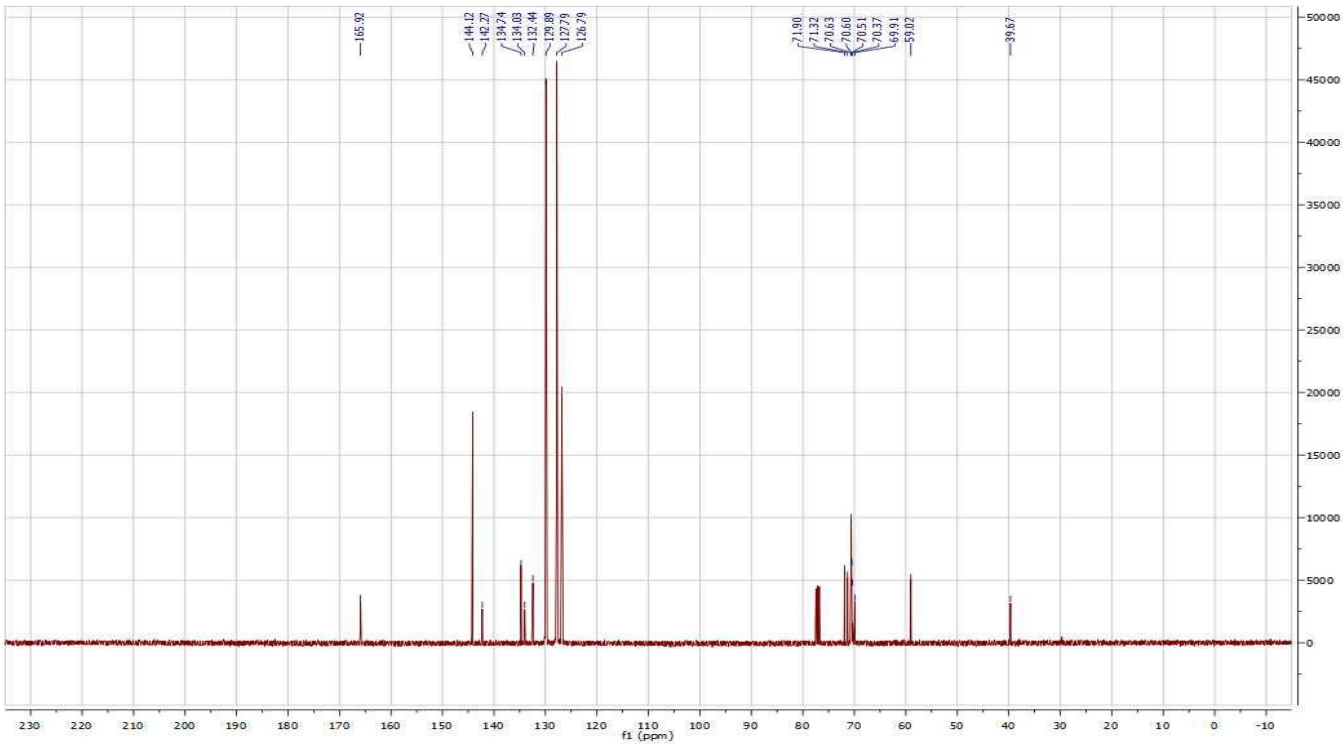

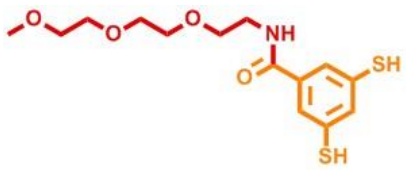
O
O
O
NH
O
SH
SH

1

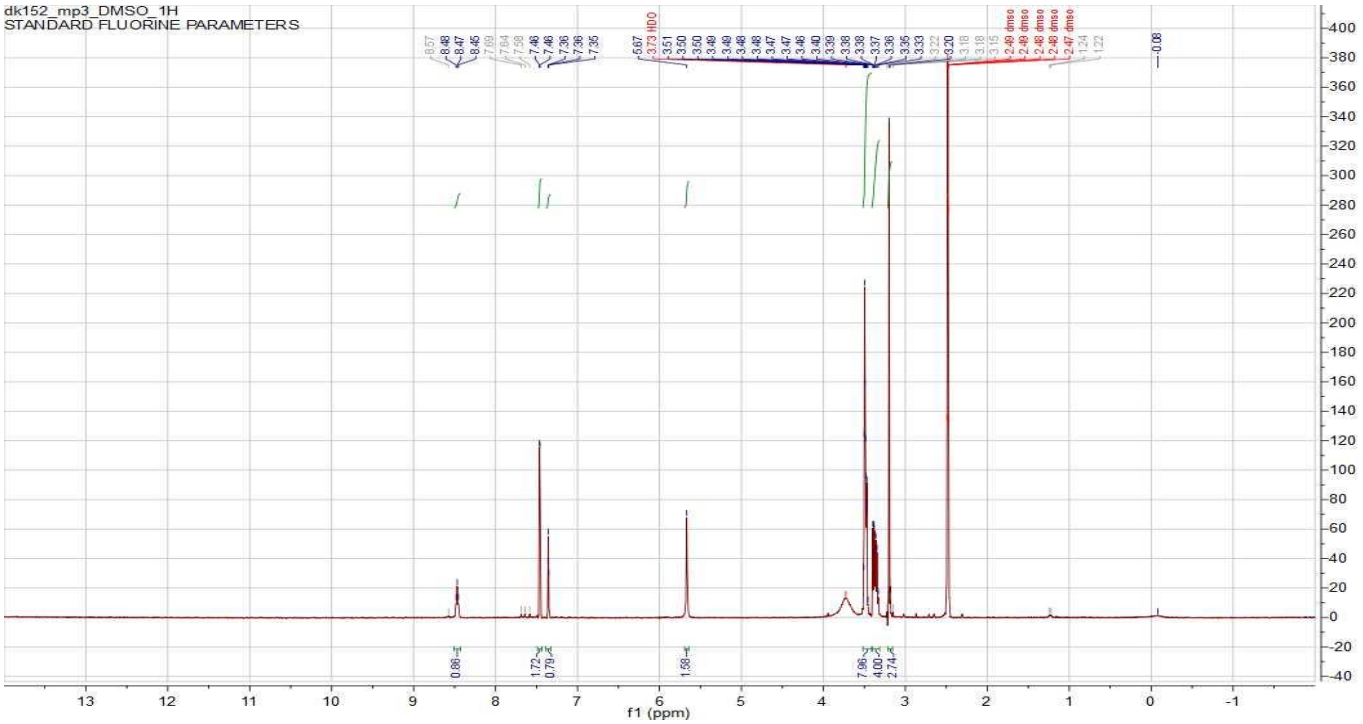
dk152_mp3_DMSO_1H
STANDARD FLUORINE PARAMETERS
f1 (ppm)

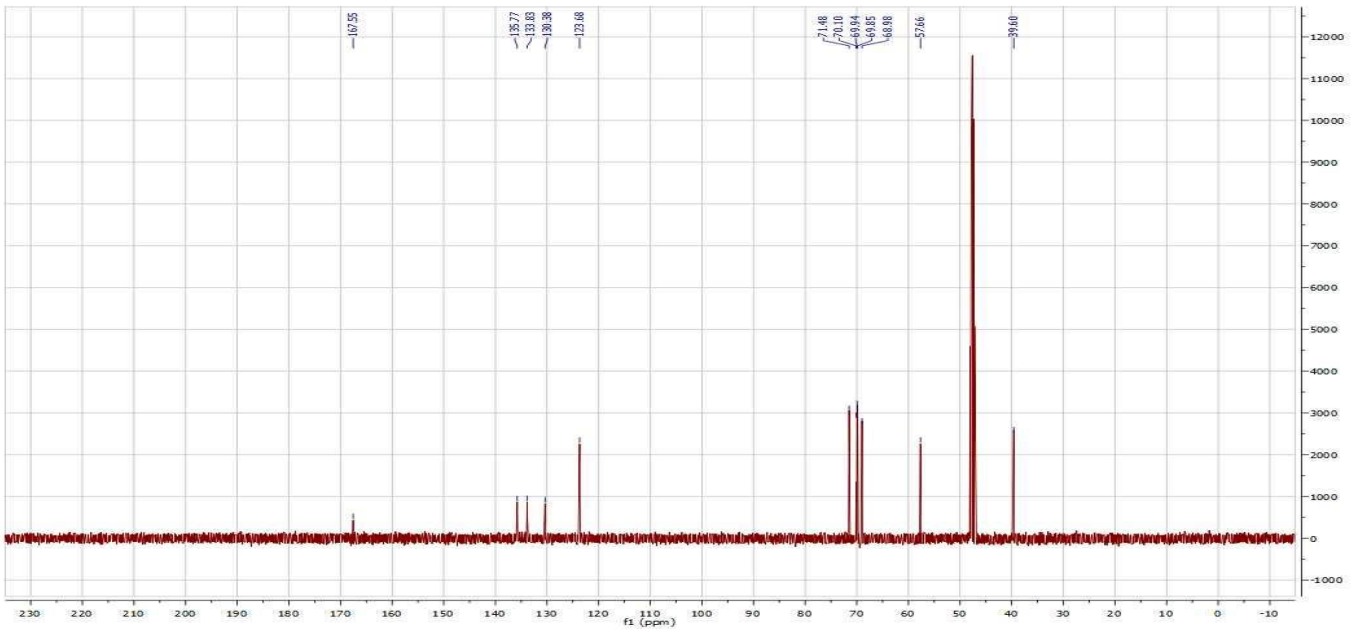
f1 (ppm)

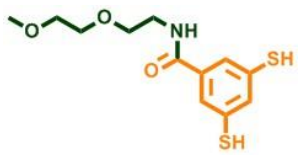

2

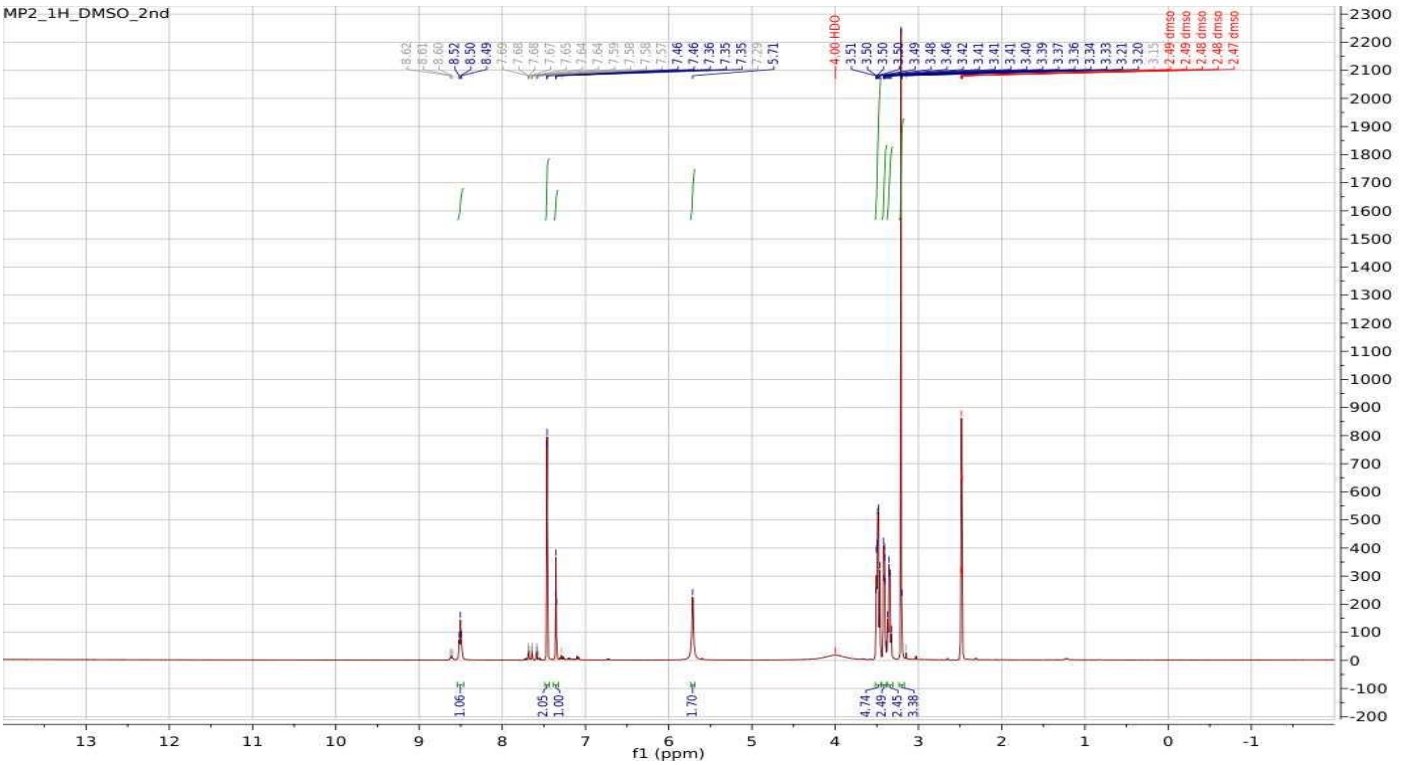

^{13}C NMR (101 MHz, CD_3OD)

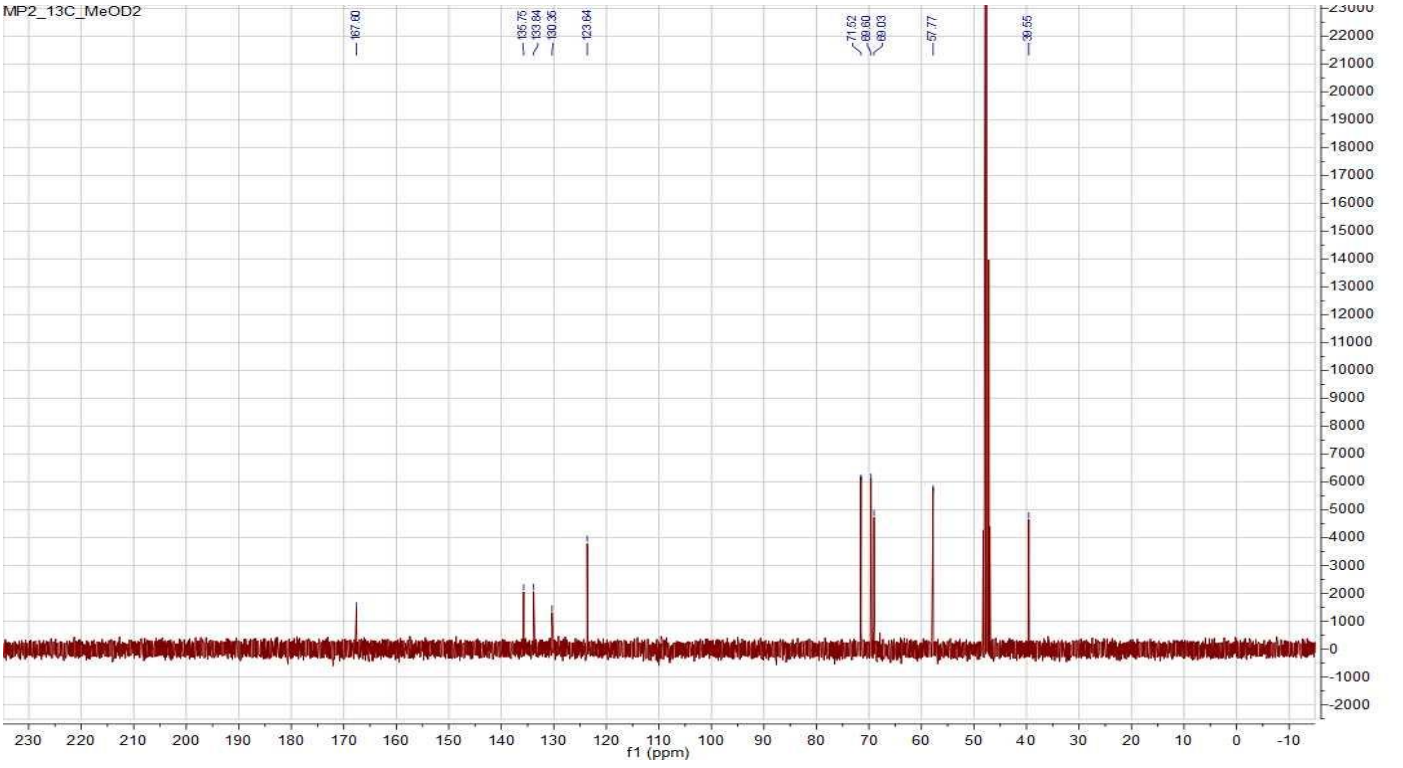

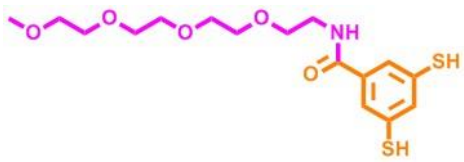

3

^{1}H NMR (400 MHz, $(CD_3)_2SO$)

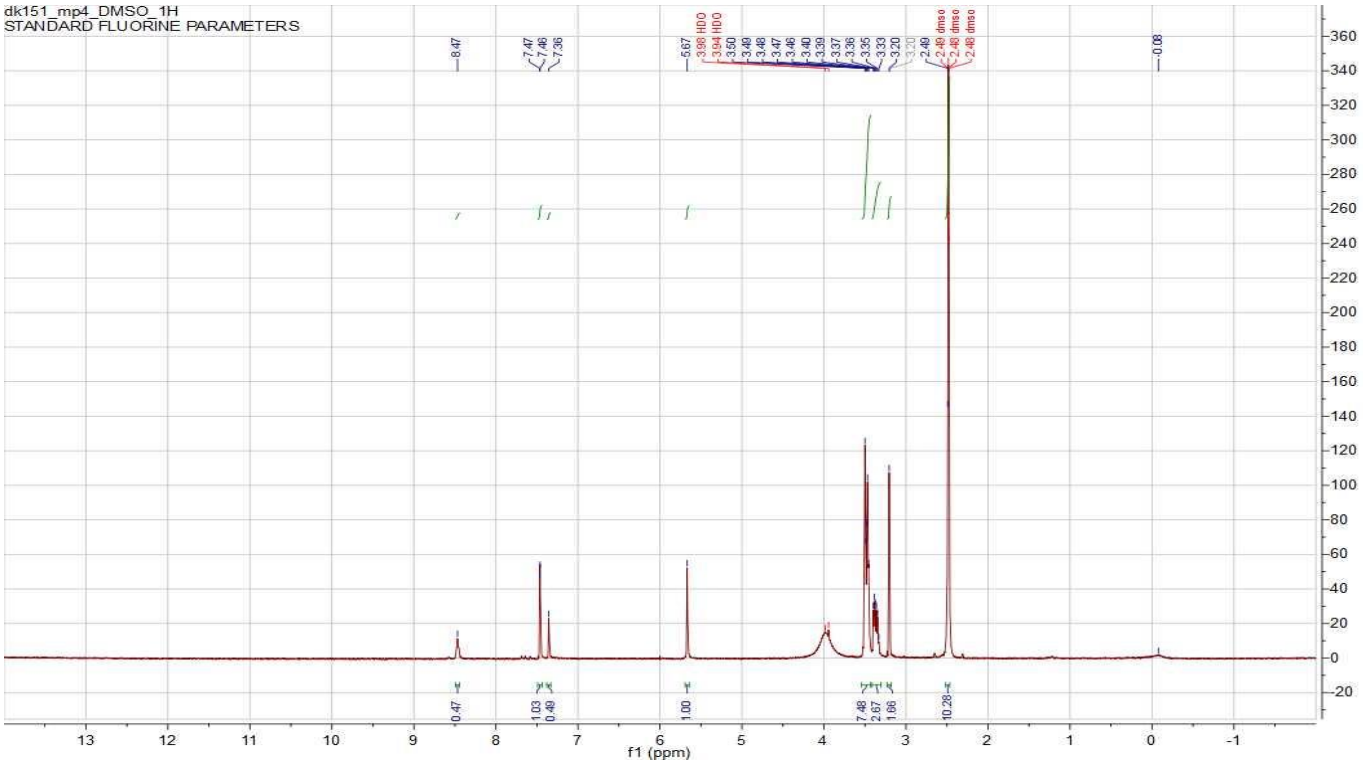

^{13}C NMR (101 MHz, CD_3OD)

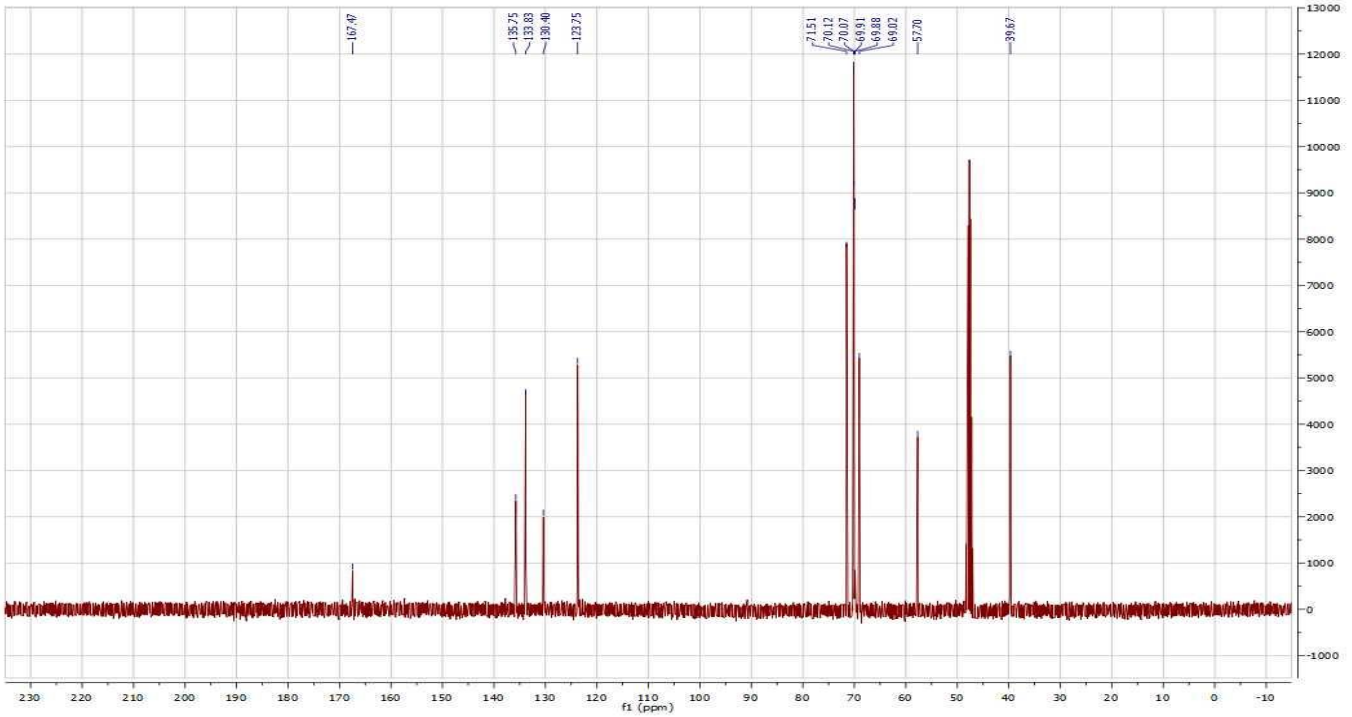

4. UPLC chromatograms of monomers 1, 2, and 3.

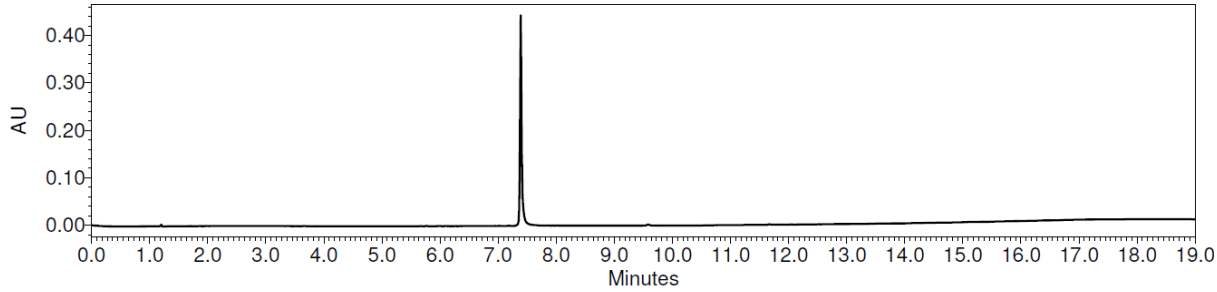

Figure S 1. UPLC chromatogram of **1** (BEH C18 column, 5 to 95 % MeCN in H_2O, detection wavelength 254 nm.)

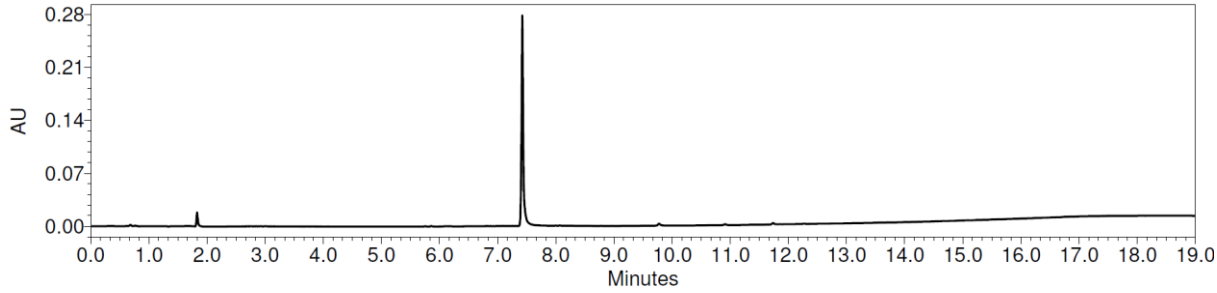

Figure S 2. UPLC chromatogram of **2** (BEH C18 column, 5 to 95 % MeCN in H_2O, detection wavelength 254 nm.)

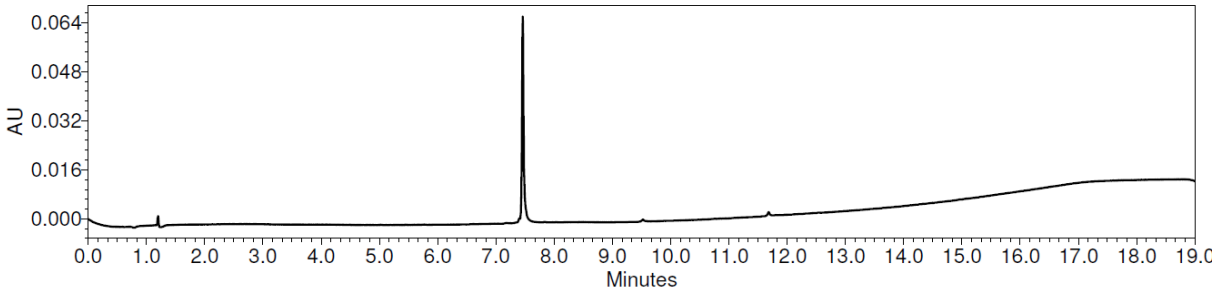

Figure S 3. UPLC chromatogram of **3** (BEH C18 column, 5 to 95 % MeCN in H_2O, detection wavelength 254 nm.)

5. *Procedure for preparation of DCLs with perborate-mediated oxidation*

The following shows a typical example. A DCL made from **1** (6.0 mM), pre-oxidized with $NaBO_3$ to 80% in borate buffer in the presence of 20 V/V % DMF, was prepared in the following manner:

1. 4.03 mg $NaBO_3 \cdot 4H_2O$ (26.2 µmol) was weighed in a vial.
2. As the overall building block concentration is 6 mM, a 60 mM solution was prepared in borate buffer. This required $\frac{26.2\ \mu mol}{60\ \mu mol/mL}$ = 437 µL borate buffer.
3. 437 µL borate buffer was added to the vial containing $NaBO_3 \cdot 4H_2O$ and the solution was sonicated for 2 minutes until the entire amount of salt was dissolved.
4. 2.62 mg **1** (7.92 µmol) is weighed in a 2 mL vial containing a small stirring bar.
5. This required a total solvent volume of $\frac{7.92\ \mu mol}{6\ \mu mol/mL}$ = 1320 µL solvent.
6. This required 1320 ×20% = 264 µL DMF.
7. This required a total amount of $\frac{1320\ \mu L \times 6\ mM \times 80\%}{60\ mM}$ = 106 µL $NaBO_3$ solution.
8. To fill up the remaining volume, 1320 – 264 -106 = 950 µL buffer was required.
9. Thus, 264 µL DMF was added to the vial containing the building block (with a Hamilton syringe).
10. Subsequently, 950 µL buffer was added (with an Eppendorf pipette).
11. The oxidant was added **in portions** (to avoid over-oxidation of the thiol groups). 2.5 - 3% oxidant was added at once safely in 1-minute intervals without the risk of over-oxidation. I.e. 80 % of oxidant was added in $\frac{80\ \%}{2.5\%\ /\ min}$= 32 portions of $\frac{106\ \mu L}{32}$ = 3.31 µL, adding one portion in every minute, under vigorous stirring (1200 rpm).
12. After adding the last portion of oxidant, stirring was discontinued. According to our experience, no replication happened during this period and the composition of the libraries prepared in this manner was similar to those prepared by oxidation with air in the absence of stirring.
13. The composition of the resulting DCL was monitored with UPLC over the course of 7-40 days.

6. LC-MS analyses of DCLs

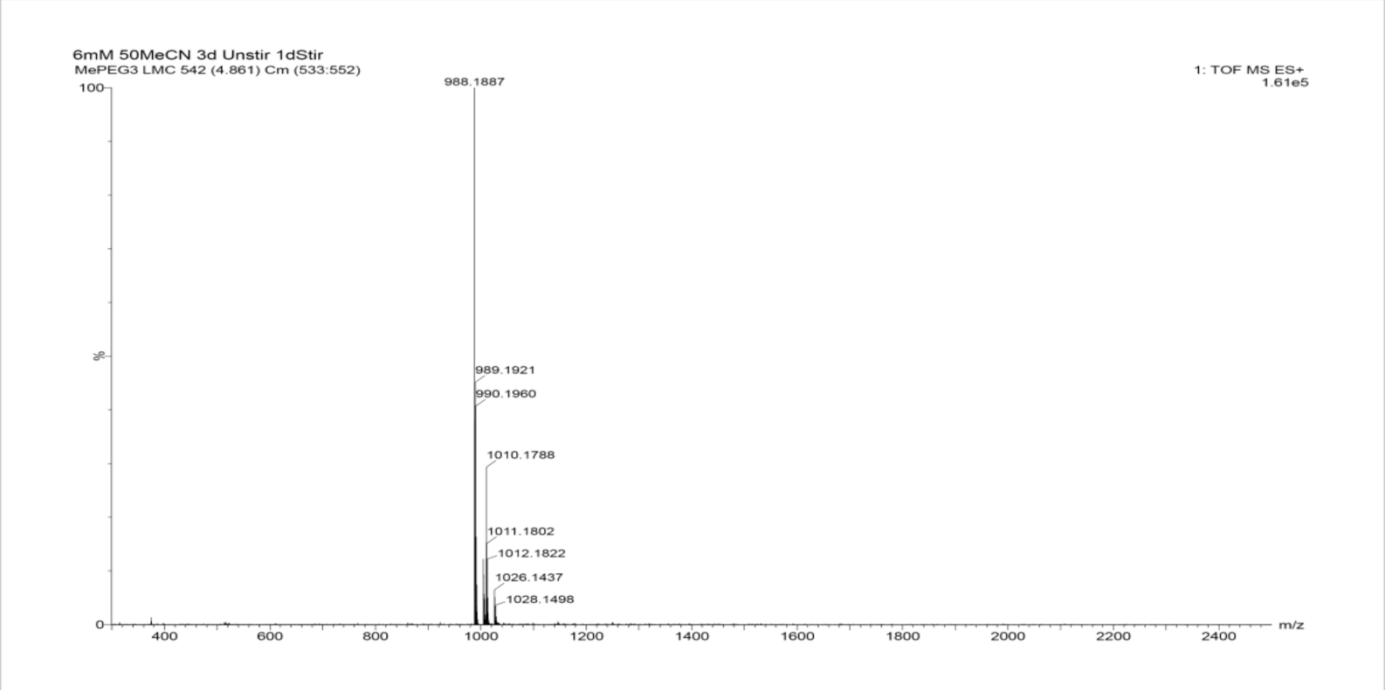

Figure S4. Mass spectrum of (**1**)$_3$ (t_R =4.9 min) from the LC-MS analysis of a DCL made from **1**.
m/z calculated: 988.23 $[M+H]^+$, 1010.22 $[M+Na]^+$; m/z observed: 988.19 $[M+H]^+$, 1010.18 $[M+Na]^+$.

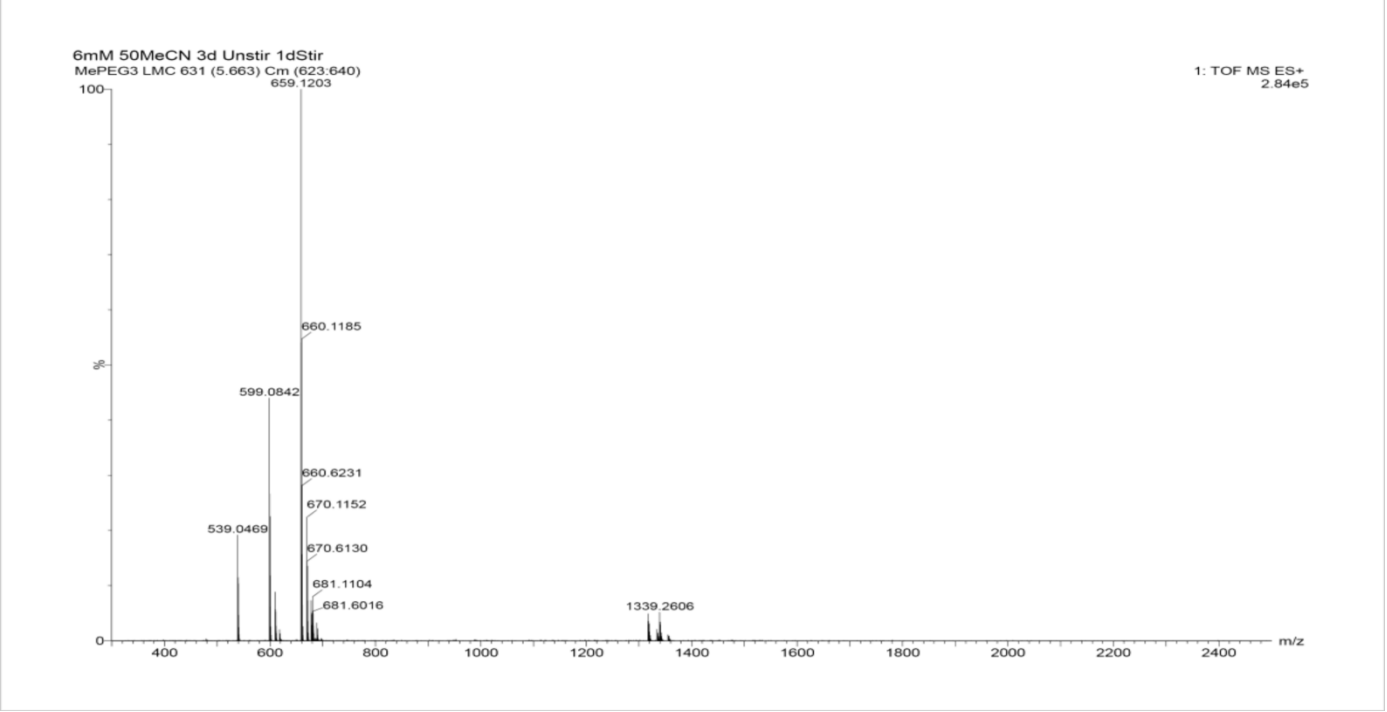

Figure S5. Mass spectrum of (**1**)$_4$ (t_R =5.7 min) from the LC-MS analysis of a DCL made from **1**.
m/z calculated: 659.16 $[M+2H]^{2+}$, 1339.29 $[M+Na]^+$; m/z observed: 659.12 $[M+H]^+$, 1339.27 $[M+Na]^+$.

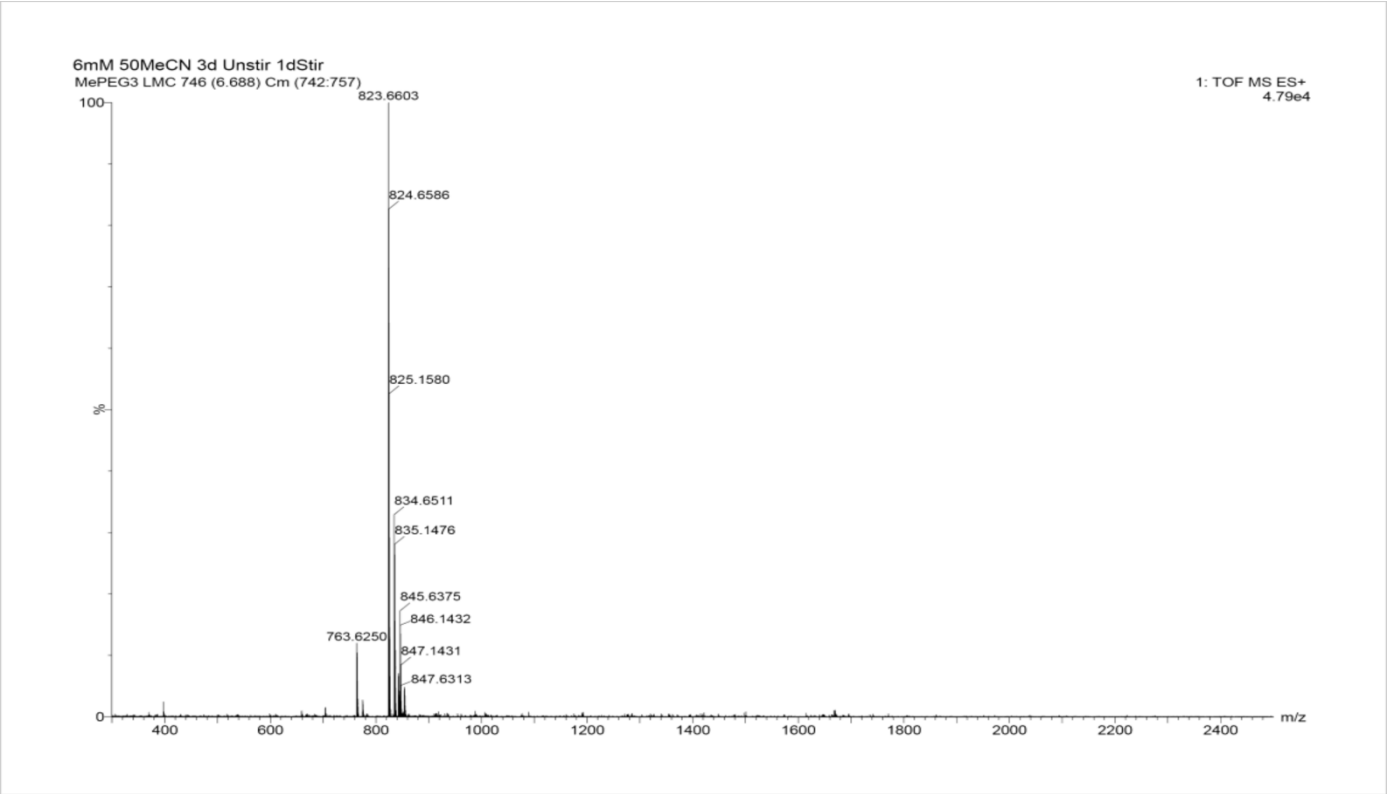

Figure S6. Mass spectrum of $(\mathbf{1})_5$ (t_R =6.7 min) from the LC-MS analysis of a DCL made from **1**.
m/z calculated: 823.70 $[M+2H]^{2+}$; m/z observed: 823.66 $[M+2H]^{2+}$.

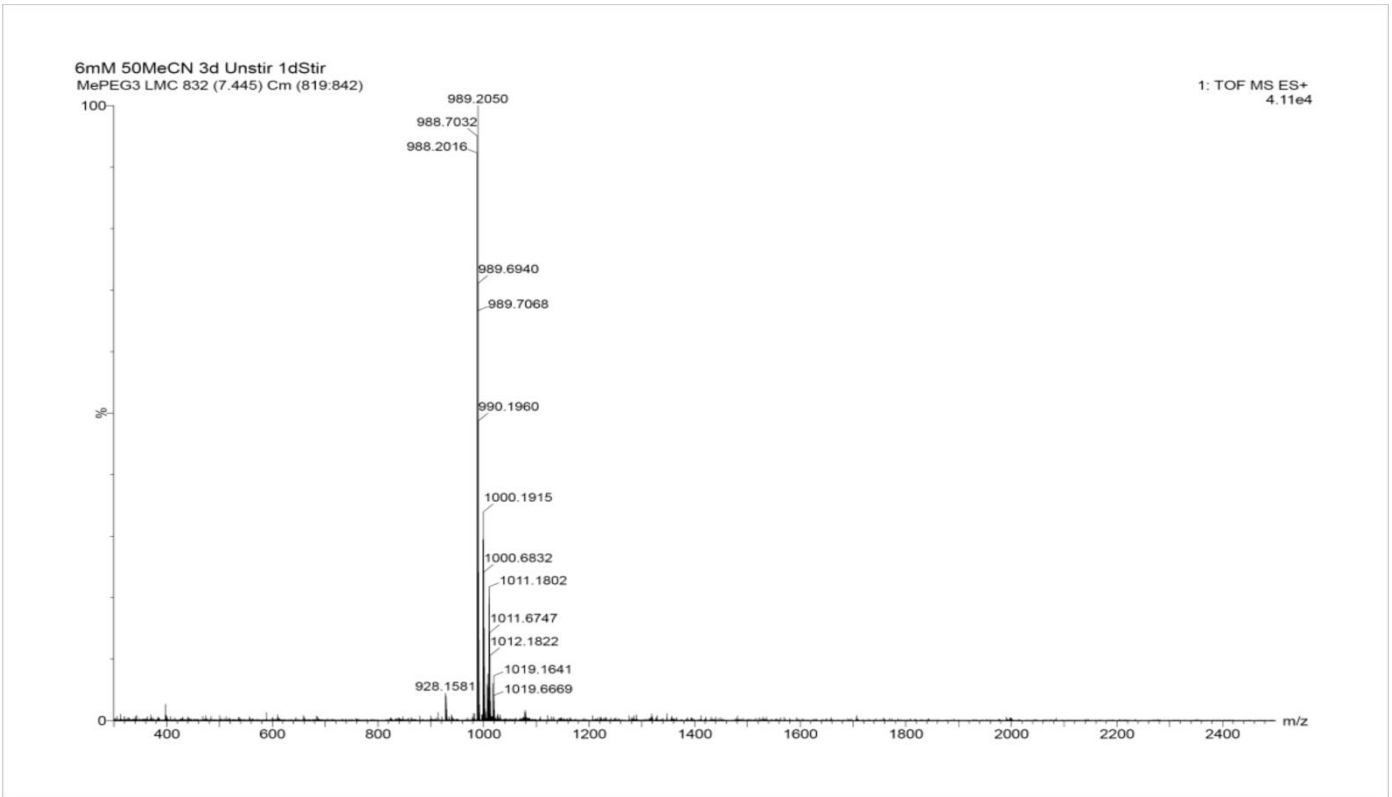

Figure S7. Mass spectrum of $(\mathbf{1})_6$ (t_R =7.45 min) from the LC-MS analysis of a DCL made from **1**.
m/z calculated: 988.23 $[M+2H]^{2+}$; m/z observed: 988.20 $[M+2H]^{2+}$.

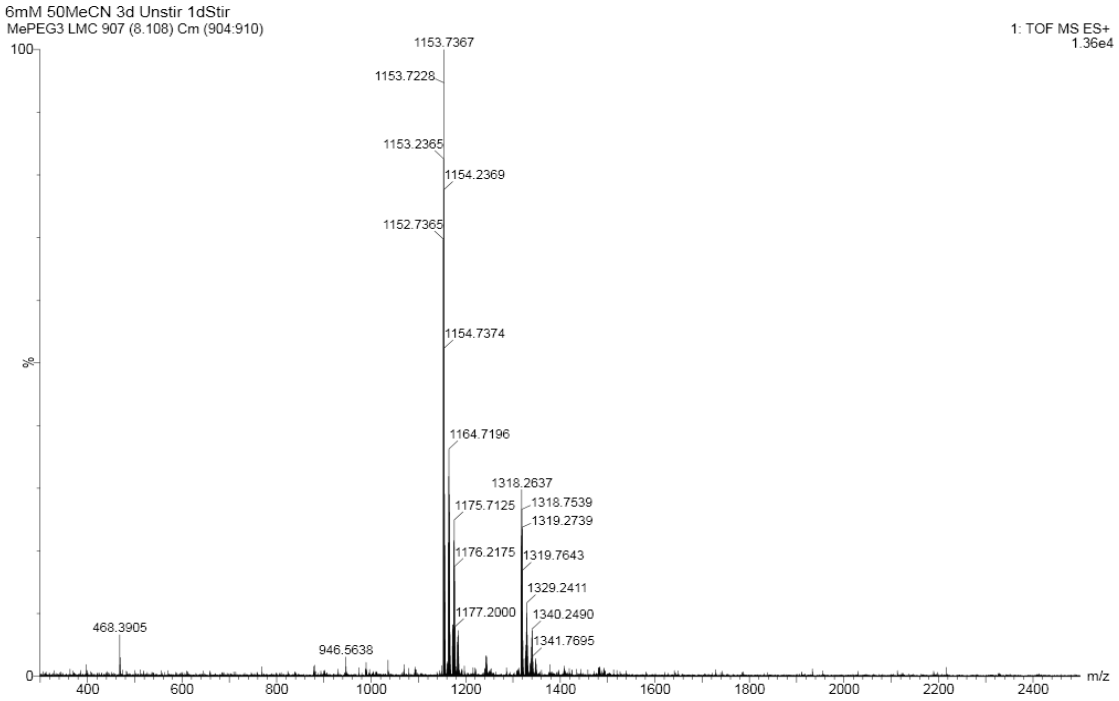

Figure S8. Mass spectrum of $(\mathbf{1})_7$ and $(\mathbf{1})_8$ (t_R =8.11 min) from the LC-MS analysis of a DCL made from **1**.
$(\mathbf{1})_7$: m/z calculated: 1152.77 $[M+2H]^{2+}$; m/z observed: 1152.74 $[M+2H]^{2+}$.
$(\mathbf{1})_8$ **:** m/z calculated: 1317.31 $[M+2H]^{2+}$; m/z observed: 1317.27 $[M+2H]^{2+}$.

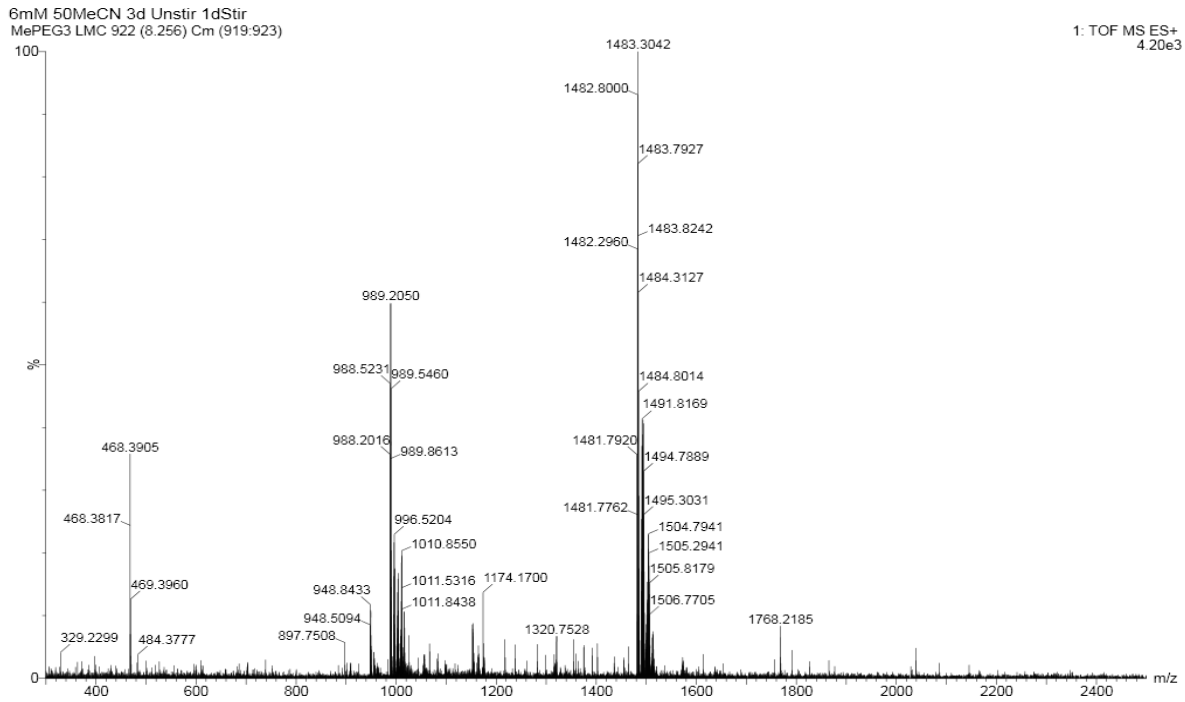

Figure S9. Mass spectrum of $(\mathbf{1})_9$ (t_R =8.26 min) from the LC-MS analysis of a DCL made from **1**.
m/z calculated: 1481.85 $[M+2H]^{2+}$, 988.23 $[M+3H]^{3+}$; m/z observed: 1481.81 $[M+2H]^{2+}$, 988.20 $[M+3H]^{3+}$.

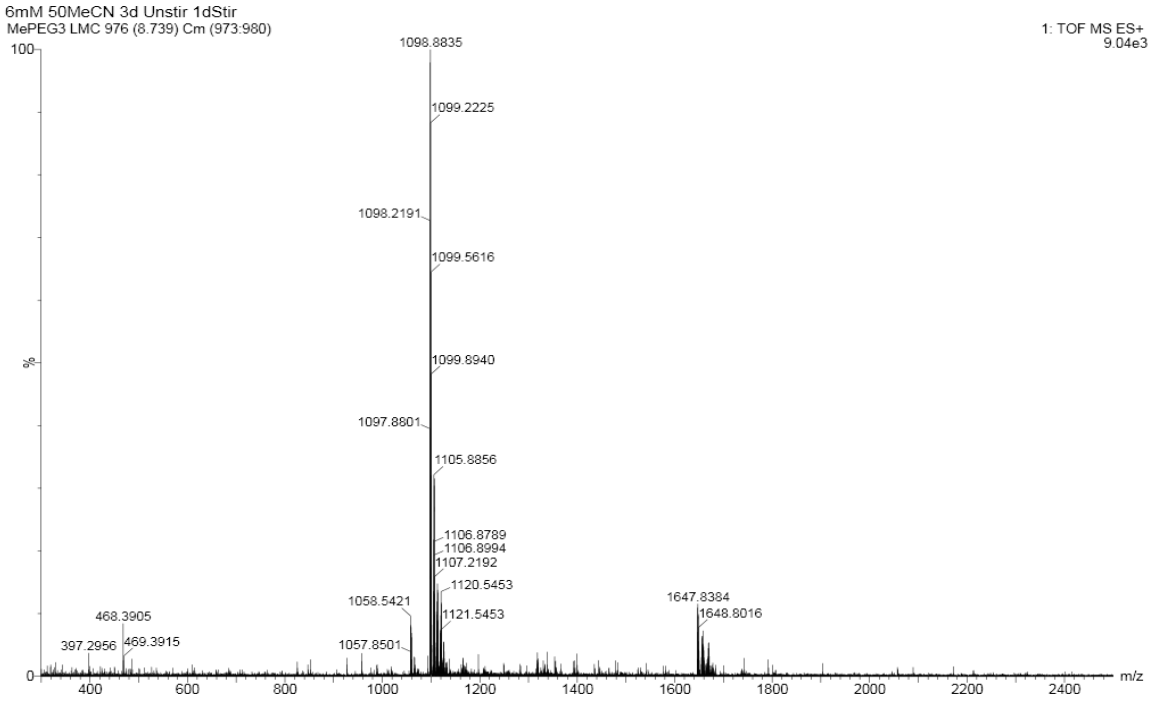

Figure S 10. Mass spectrum of $(\mathbf{1})_{10}$ (t_R =8.74 min) from the LC-MS analysis of a DCL made from **1**.
m/z calculated: 1646.39 $[M+2H]^{2+}$, 1097.93 $[M+3H]^{3+}$; m/z observed: 1646.33 $[M+2H]^{2+}$, 1097.88 $[M+3H]^{3+}$.

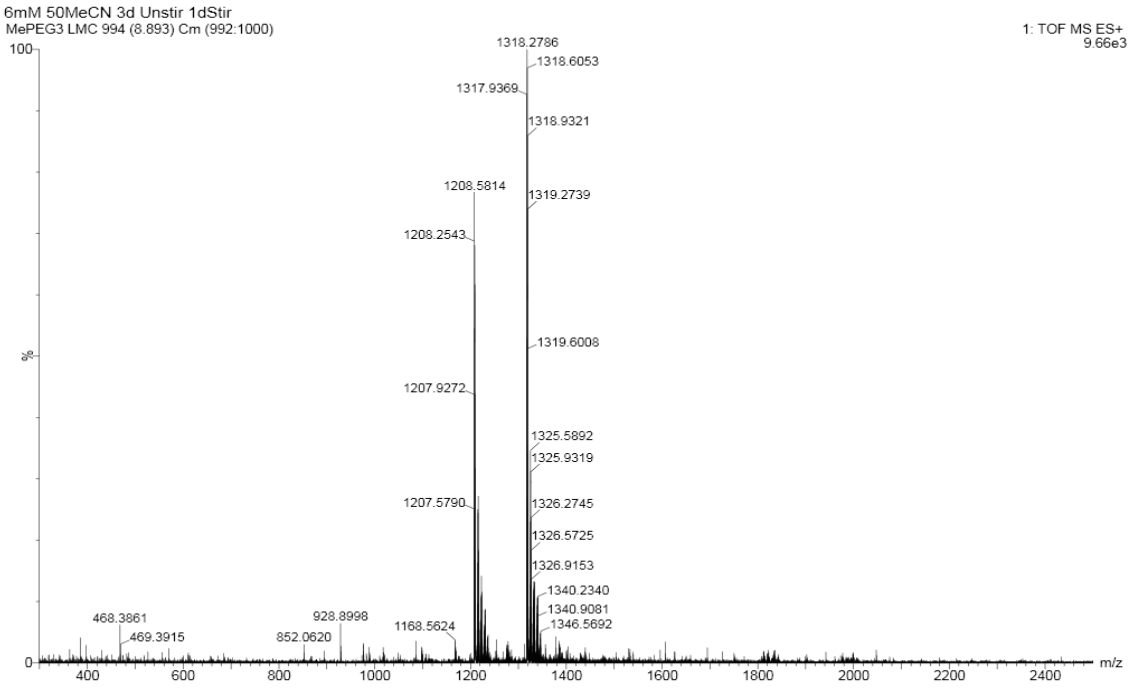

Figure S11. Mass spectrum of $(\mathbf{1})_{11}$ and $(\mathbf{1})_{12}$ (t_R =8.89 min) from the LC-MS analysis of a DCL made from **1**.
$(\mathbf{1})_{11}$:m/z calculated: 1207.62 $[M+3H]^{3+}$; m/z observed: 1207.58 $[M+3H]^{3+}$.
$(\mathbf{1})_{12}$:m/z calculated: 1317.31 $[M+3H]^{3+}$; m/z observed: 1317.27 $[M+3H]^{3+}$.

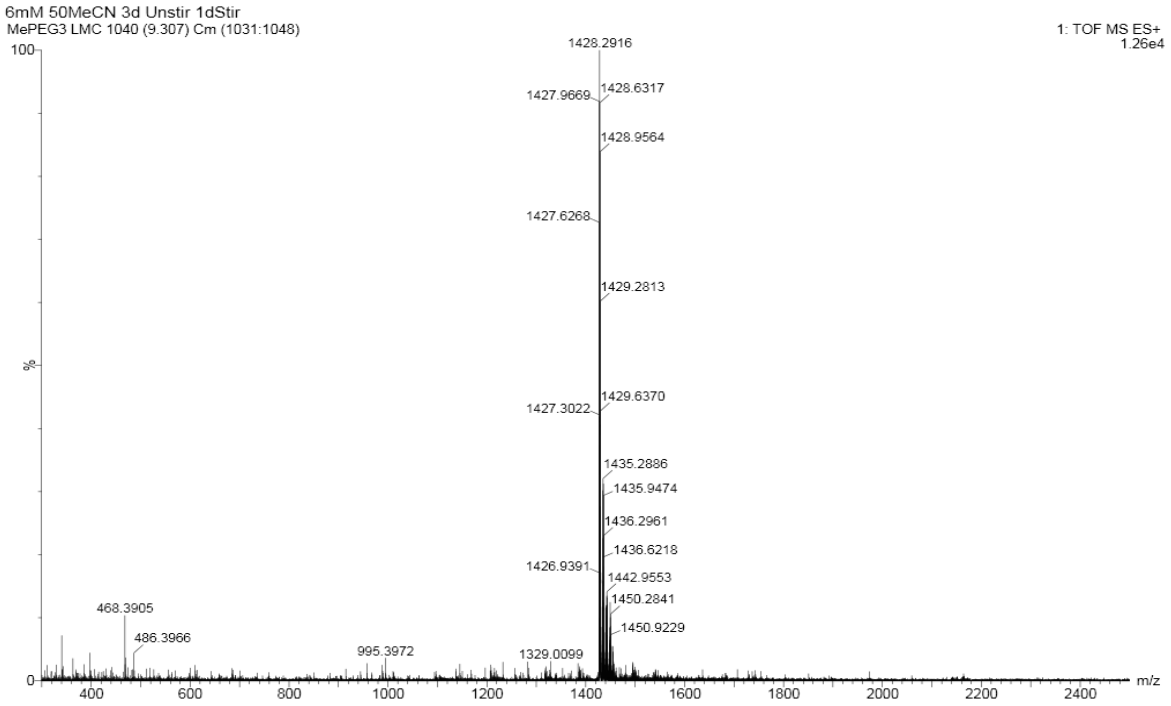

Figure S12. Mass spectrum of $(\mathbf{1})_{13}$ (t_R =9.31 min) from the LC-MS analysis of a DCL made from **1**. $(\mathbf{1})_{13}$:m/z calculated: 1427.00 $[M+3H]^{3+}$; m/z observed: 1426.94 $[M+3H]^{3+}$.

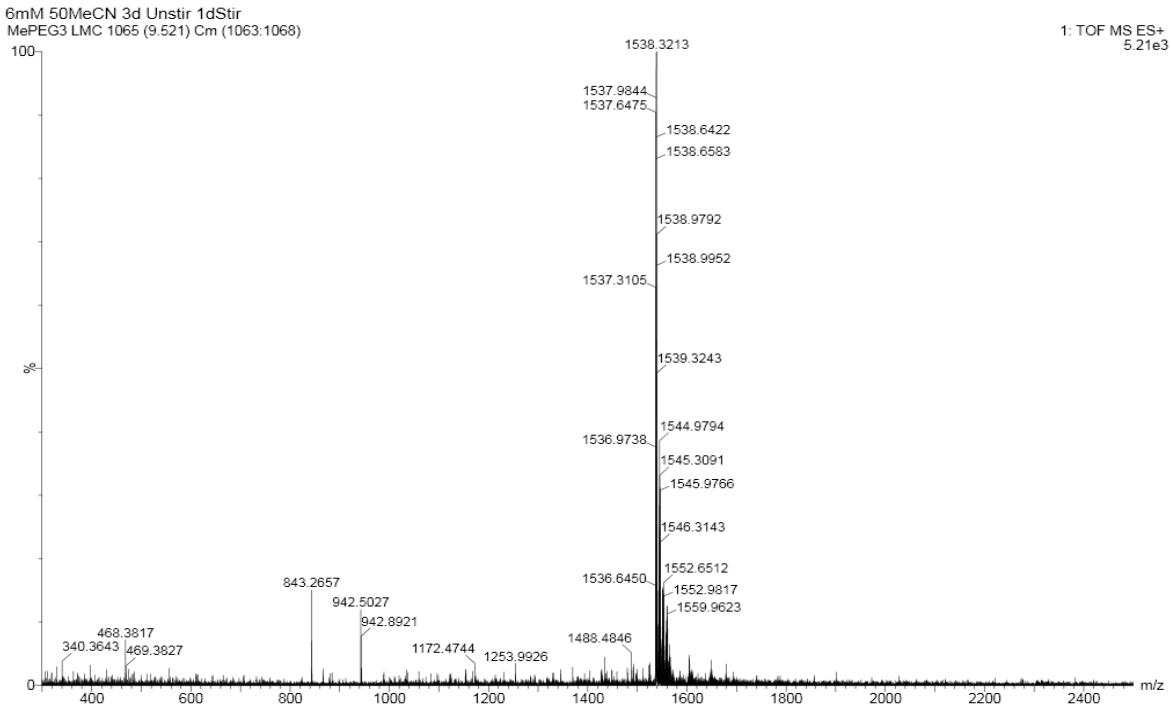

Figure S13. Mass spectrum of $(\mathbf{1})_{14}$ (t_R =9.52 min) from the LC-MS analysis of a DCL made from **1**. $(\mathbf{1})_{14}$:m/z calculated: 1536.69 $[M+3H]^{3+}$; m/z observed: 1536.65 $[M+3H]^{3+}$.

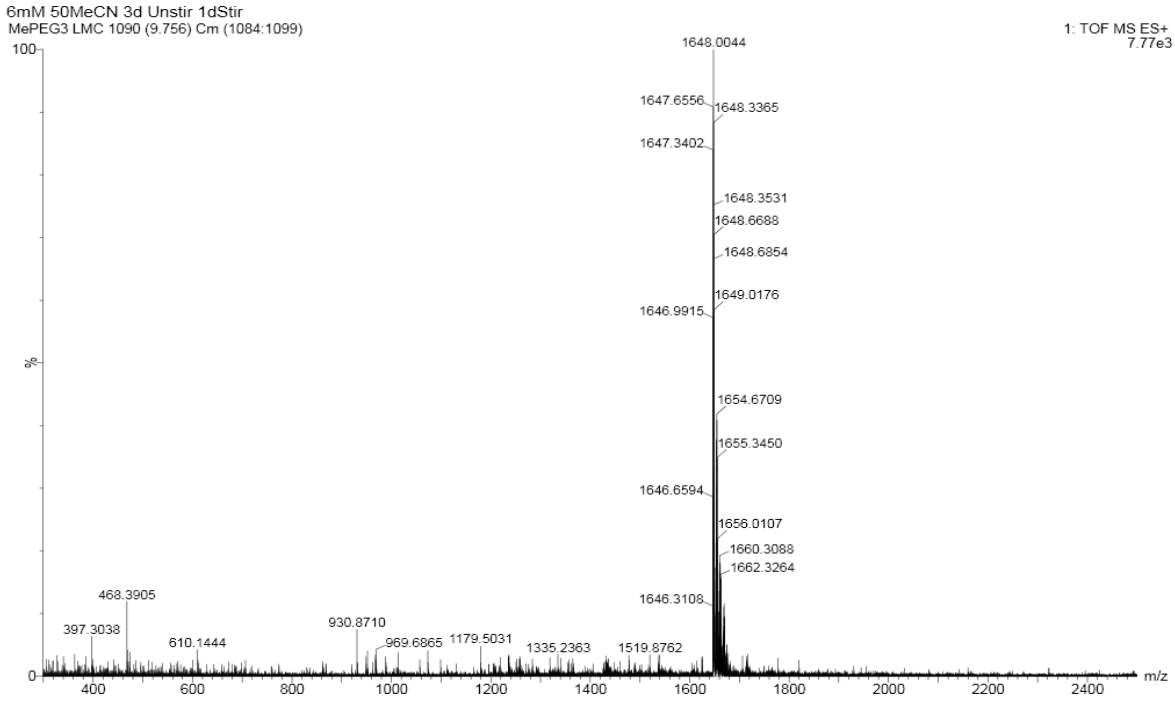

Figure S 14. Mass spectrum of $(\mathbf{1})_{15}$ (t_R =9.76 min) from the LC-MS analysis of a DCL made from **1**. $(\mathbf{1})_{15}$:m/z calculated: 1646.39 $[M+3H]^{3+}$; m/z observed: 1646.31 $[M+3H]^{3+}$.

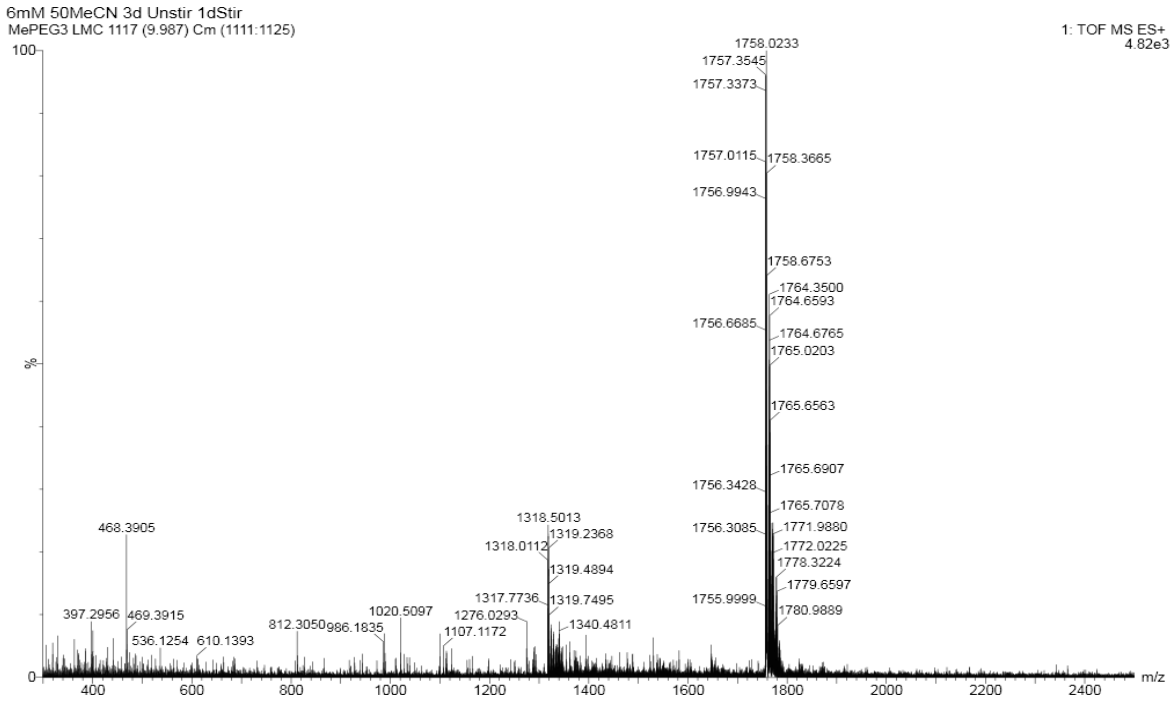

Figure S 15. Mass spectrum of $(\mathbf{1})_{16}$ (t_R =9.97 min) from the LC-MS analysis of a DCL made from **1**. $(\mathbf{1})_{16}$:m/z calculated: 1756.01 $[M+3H]^{3+}$, 1317.31 $[M+4H]^{4+}$; m/z observed: 1756.00 $[M+3H]^{3+}$, 1317.28 $[M+4H]^{4+}$.

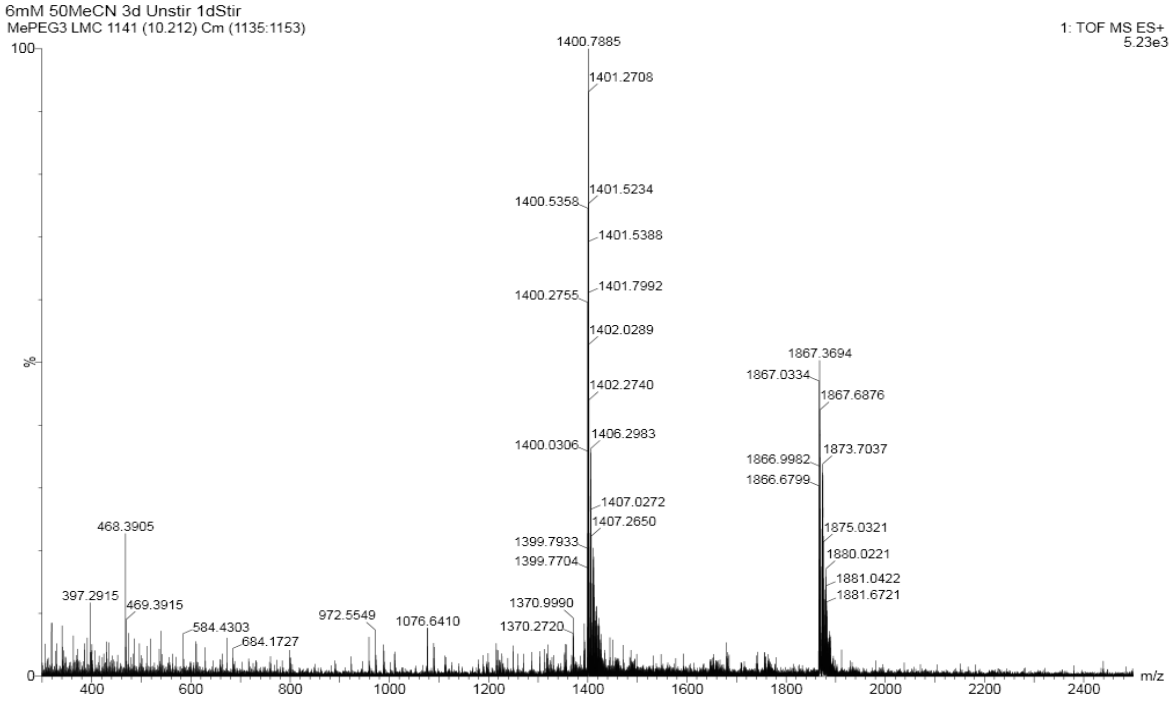

Figure S16. Mass spectrum of $(\mathbf{1})_{17}$ (t_R =10.21 min) from the LC-MS analysis of a DCL made from **1**. $(\mathbf{1})_{17}$:m/z calculated: 1865.77 $[M+3H]^{3+}$, 1399.58 $[M+4H]^{4+}$; m/z observed: 1865.72 $[M+3H]^{3+}$, 1399.55 $[M+4H]^{4+}$.

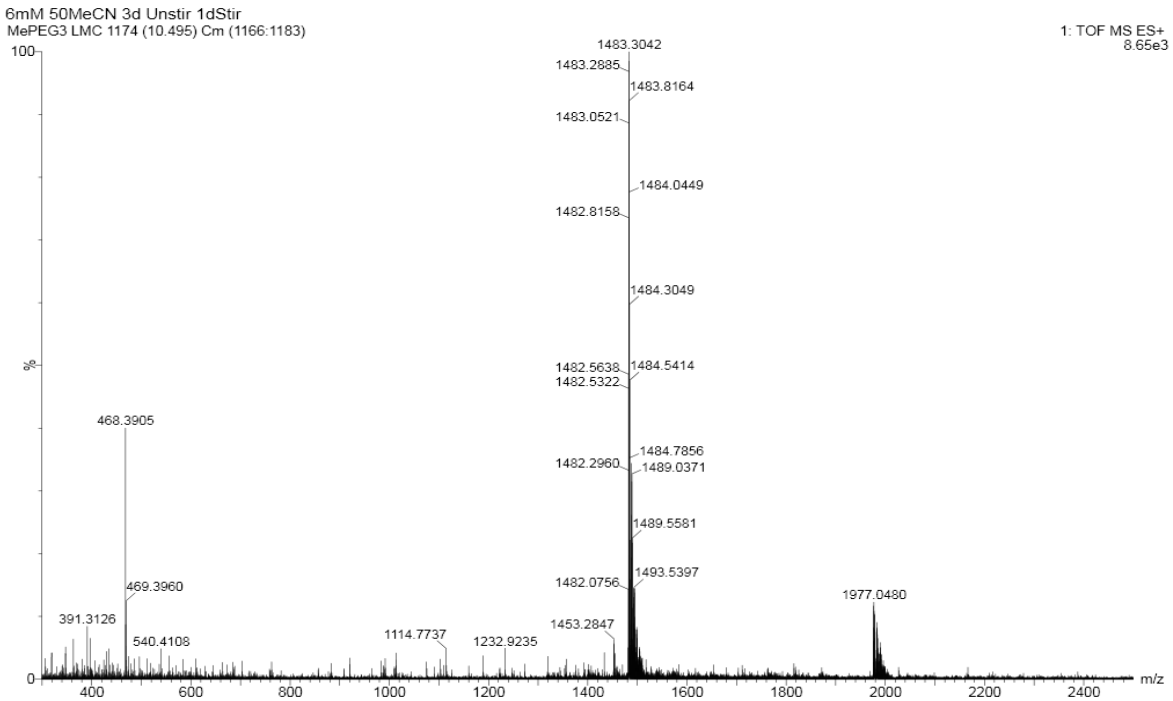

Figure S17. Mass spectrum of $(\mathbf{1})_{18}$ (t_R =10.50 min) from the LC-MS analysis of a DCL made from **1**. $(\mathbf{1})_{18}$:m/z calculated: 1975.46 $[M+3H]^{3+}$, 1481.85 $[M+4H]^{4+}$; m/z observed: 1975.37 $[M+3H]^{3+}$, 1481.81 $[M+4H]^{4+}$.

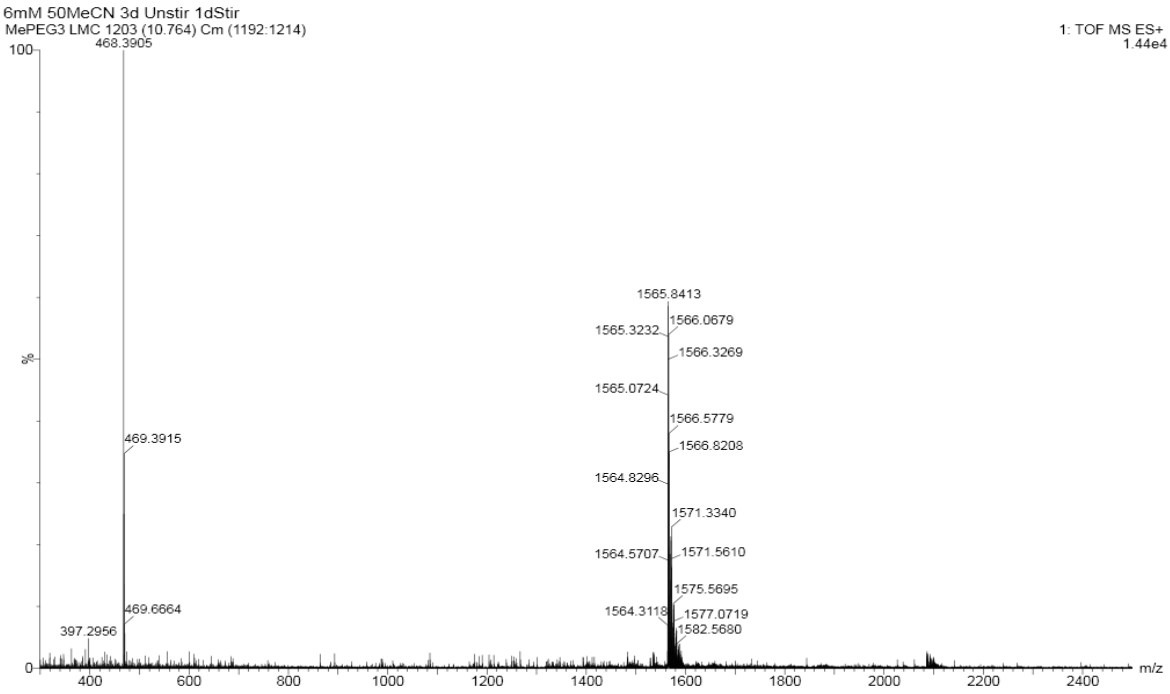

Figure S18. Mass spectrum of $(\mathbf{1})_{19}$ (t_R =10.76 min) from the LC-MS analysis of a DCL made from **1**. $(\mathbf{1})_{19}$:m/z calculated: 1564.12 $[M+4H]^{4+}$; m/z observed: 1564.06 $[M+4H]^{4+}$.

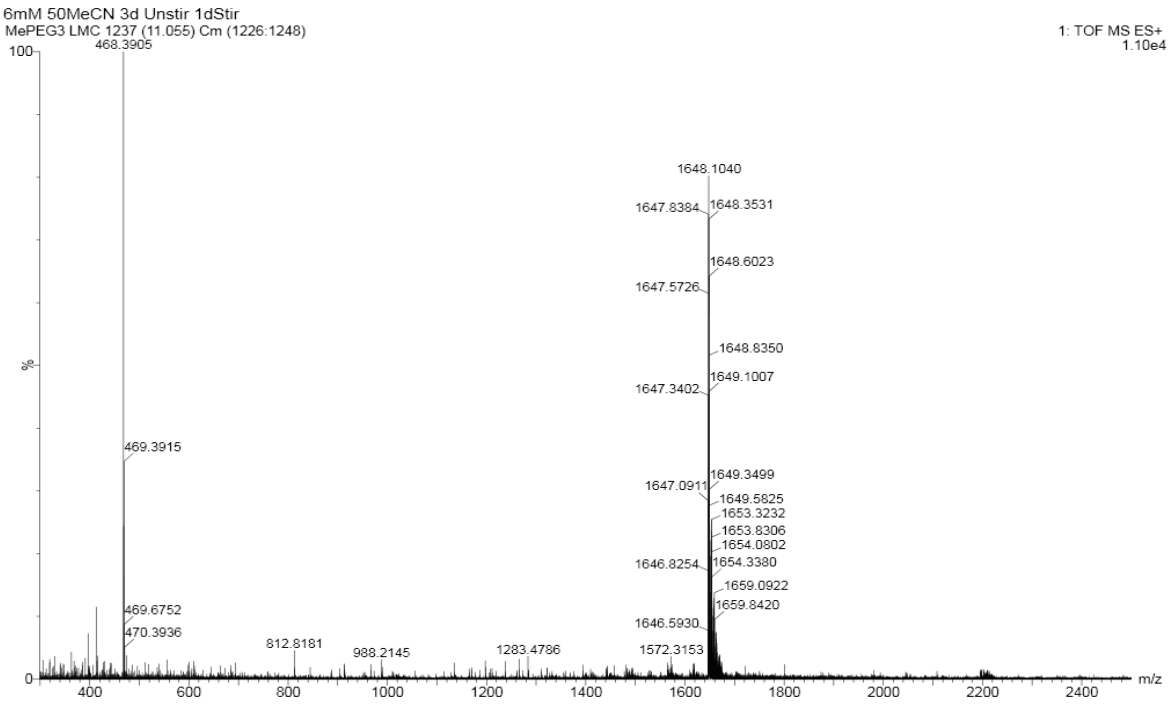

Figure S 19. Mass spectrum of $(\mathbf{1})_{20}$ (t_R =11.06 min) from the LC-MS analysis of a DCL made from **1**. $(\mathbf{1})_{20}$:m/z calculated: 1646.39 $[M+4H]^{4+}$; m/z observed: 1646.34 $[M+4H]^{4+}$.

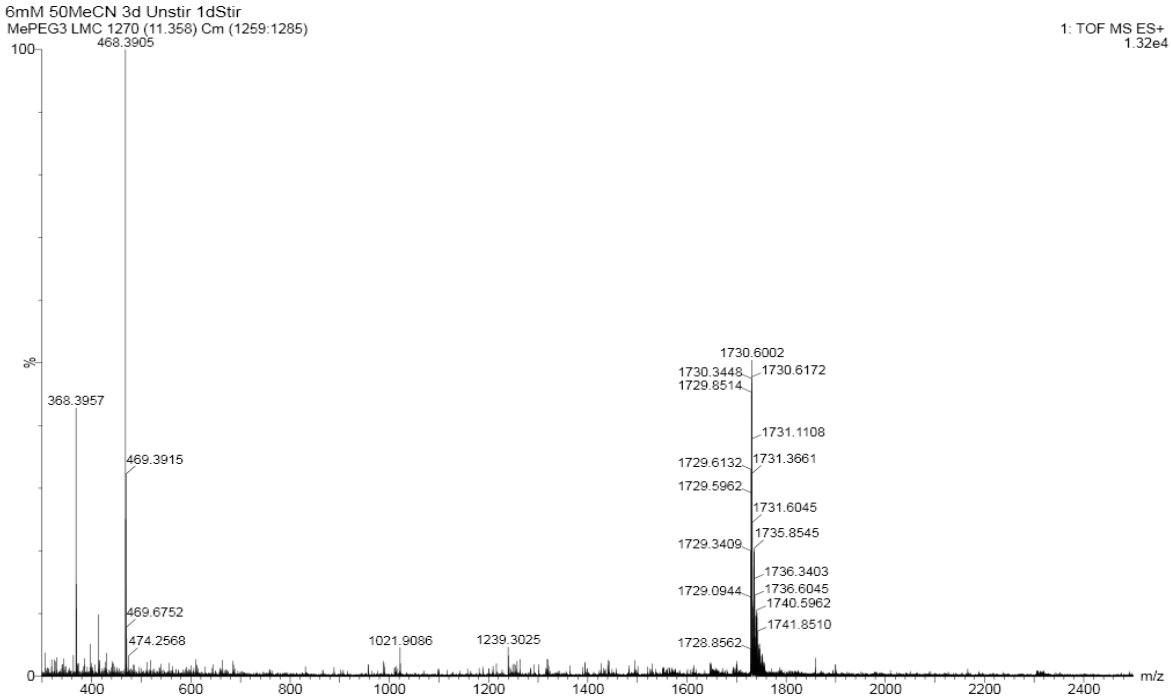

Figure S20. Mass spectrum of $(\mathbf{1})_{21}$ (t_R =11.36 min) from the LC-MS analysis of a DCL made from **1**. **$(1)_{21}$:**m/z calculated: 1728.65 $[M+4H]^{4+}$; m/z observed: 1728.59 $[M+4H]^{4+}$.

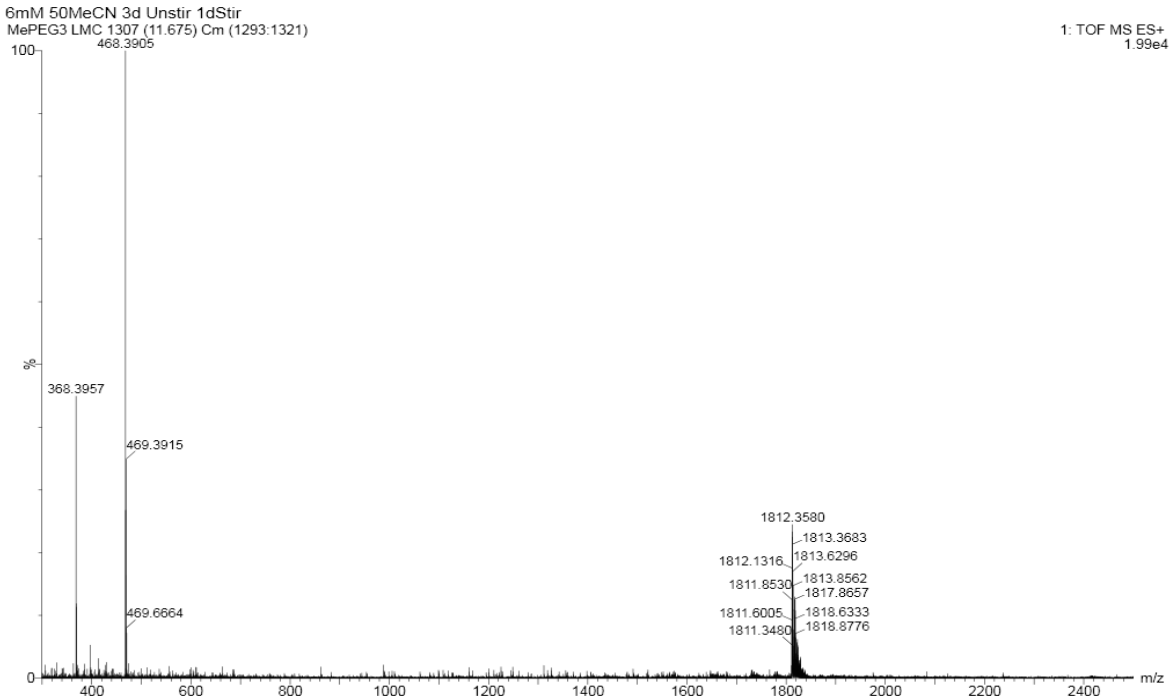

Figure S21. Mass spectrum of $(\mathbf{1})_{22}$ (t_R =11.68 min) from the LC-MS analysis of a DCL made from **1**. $(\mathbf{1})_{22}$:m/z calculated: 1810.92 $[M+4H]^{4+}$; m/z observed: 1811.09 $[M+4H]^{4+}$.

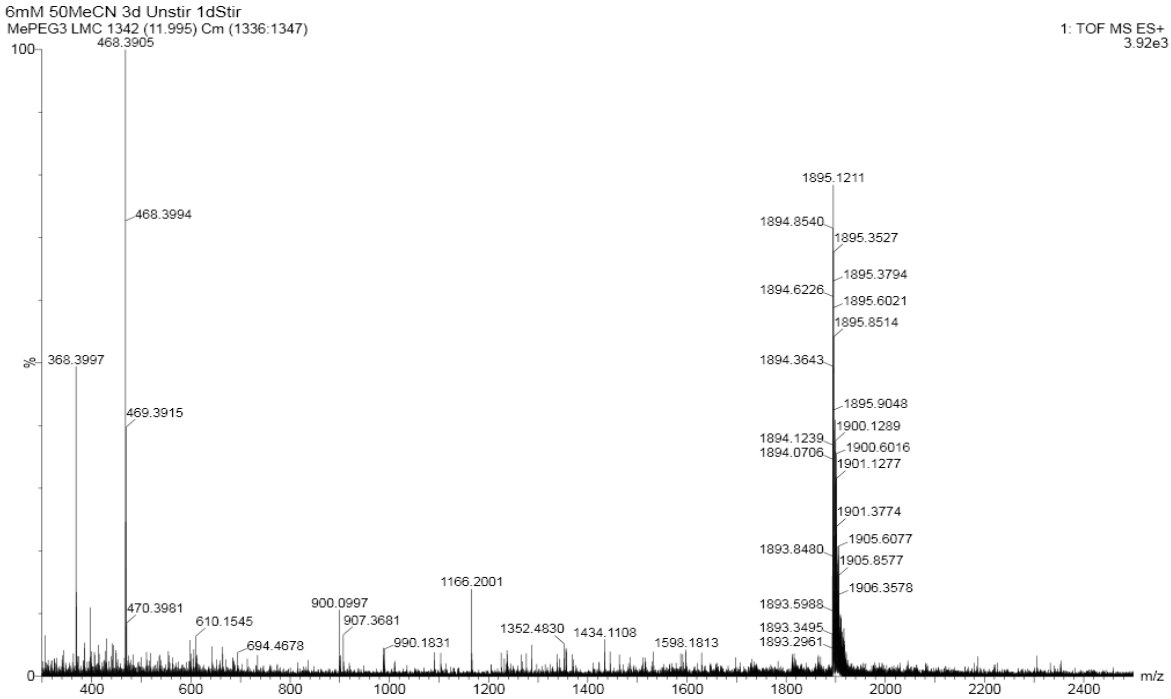

Figure S22. Mass spectrum of $(\mathbf{1})_{23}$ (t_R =11.99 min) from the LC-MS analysis of a DCL made from **1**. $(\mathbf{1})_{23}$:m/z calculated: 1893.12 $[M+4H]^{4+}$; m/z observed: 1893.14 $[M+4H]^{4+}$.

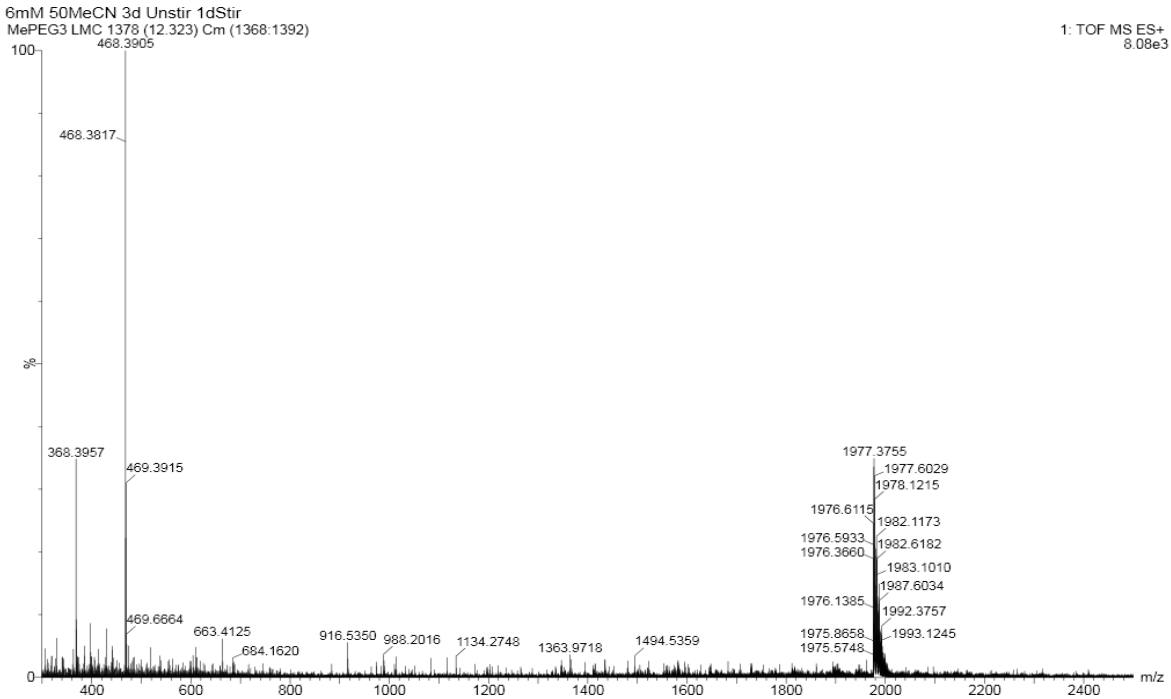

Figure S23. Mass spectrum of $(\mathbf{1})_{24}$ (t_R =12.32 min) from the LC-MS analysis of a DCL made from **1**. $(\mathbf{1})_{24}$:m/z calculated: 1975.46 $[M+4H]^{4+}$; m/z observed: 1975.57 $[M+4H]^{4+}$.

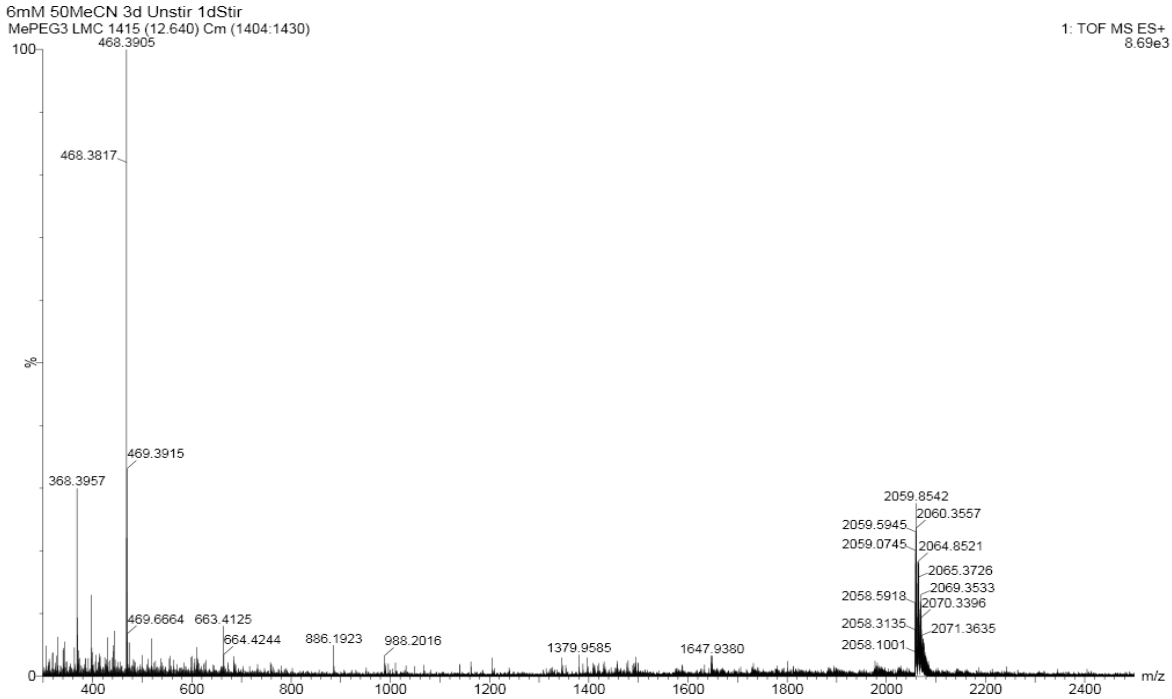

Figure S24. Mass spectrum of $(\mathbf{1})_{25}$ (t_R =12.64 min) from the LC-MS analysis of a DCL made from **1**. $(\mathbf{1})_{25}$:m/z calculated: 2057.58 $[M+4H]^{4+}$; m/z observed: 2057.58 $[M+4H]^{4+}$.

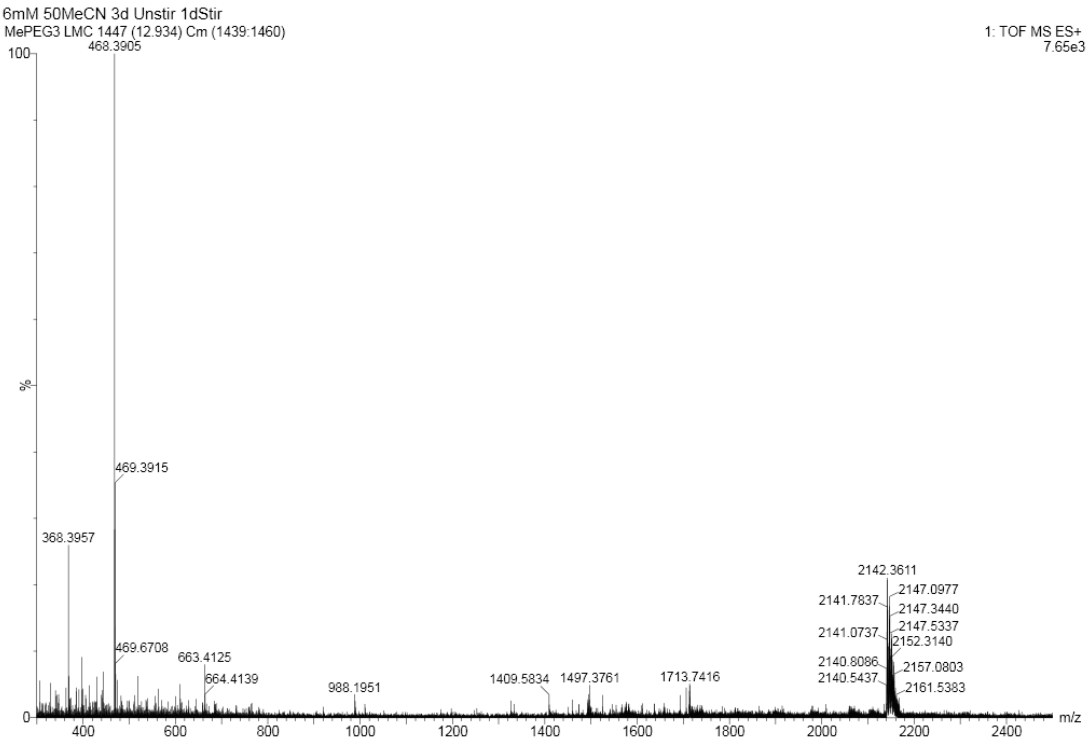

Figure S25. Mass spectrum of $(\mathbf{1})_{26}$ (t_R =12.93 min) from the LC-MS analysis of a DCL made from **1**. $\mathbf{(1)}_{26}$:m/z calculated: 2140.00 $[M+4H]^{4+}$; m/z observed: 2140.14 $[M+4H]^{4+}$.

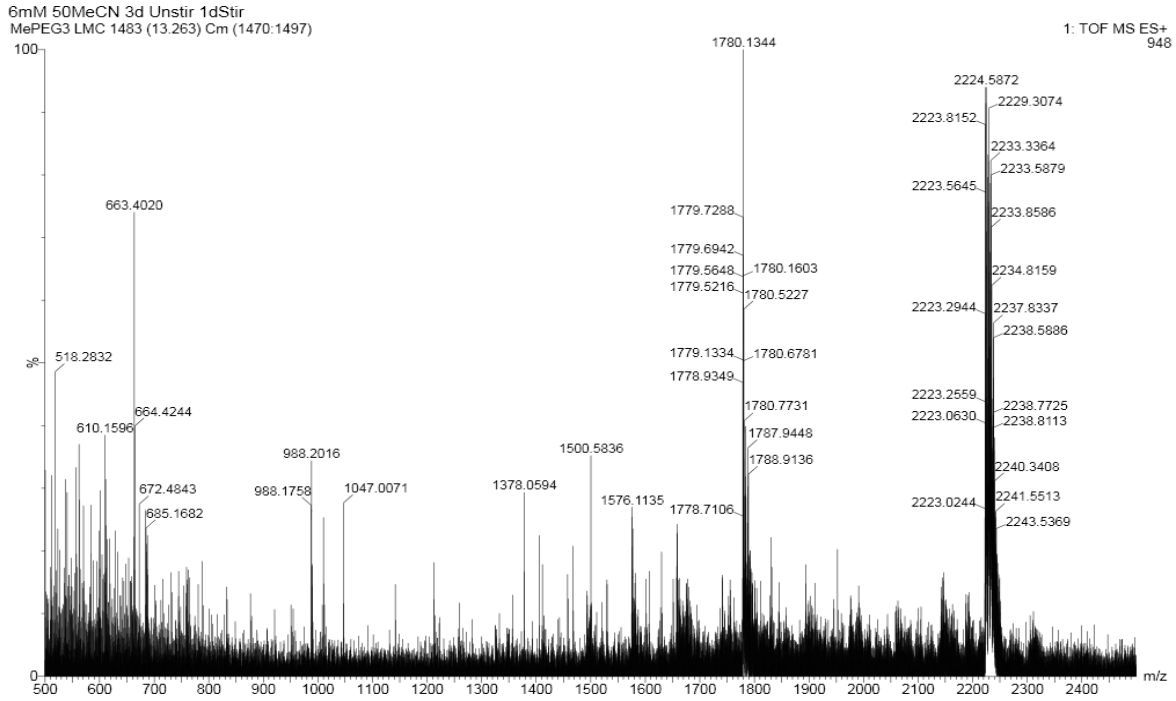

Figure S 26. Mass spectrum of $(\mathbf{1})_{27}$ (t_R =13.26 min) from the LC-MS analysis of a DCL made from **1**.
$(\mathbf{1})_{27}$:m/z calculated: 2222.27 $[M+4H]^{4+}$, 1778.02 $[M+5H]^{5+}$; m/z observed: 2222.24 $[M+4H]^{4+}$, 1777.96 $[M+5H]^{5+}$.

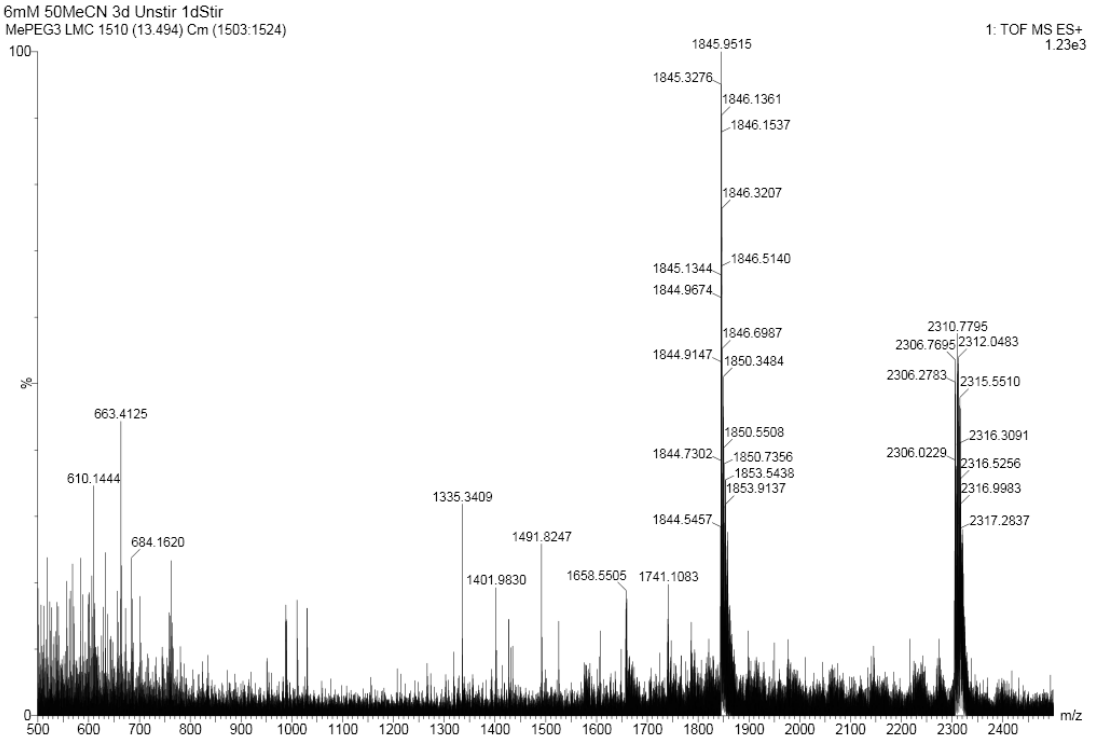

Figure S27. Mass spectrum of $(\mathbf{1})_{28}$ (t_R =13.49 min) from the LC-MS analysis of a DCL made from **1**.
$(\mathbf{1})_{28}$:m/z calculated: 2304.54 $[M+4H]^{4+}$, 1843.83 $[M+5H]^{5+}$; m/z observed: 2304.60 $[M+4H]^{4+}$, 1843.95 $[M+5H]^{5+}$.

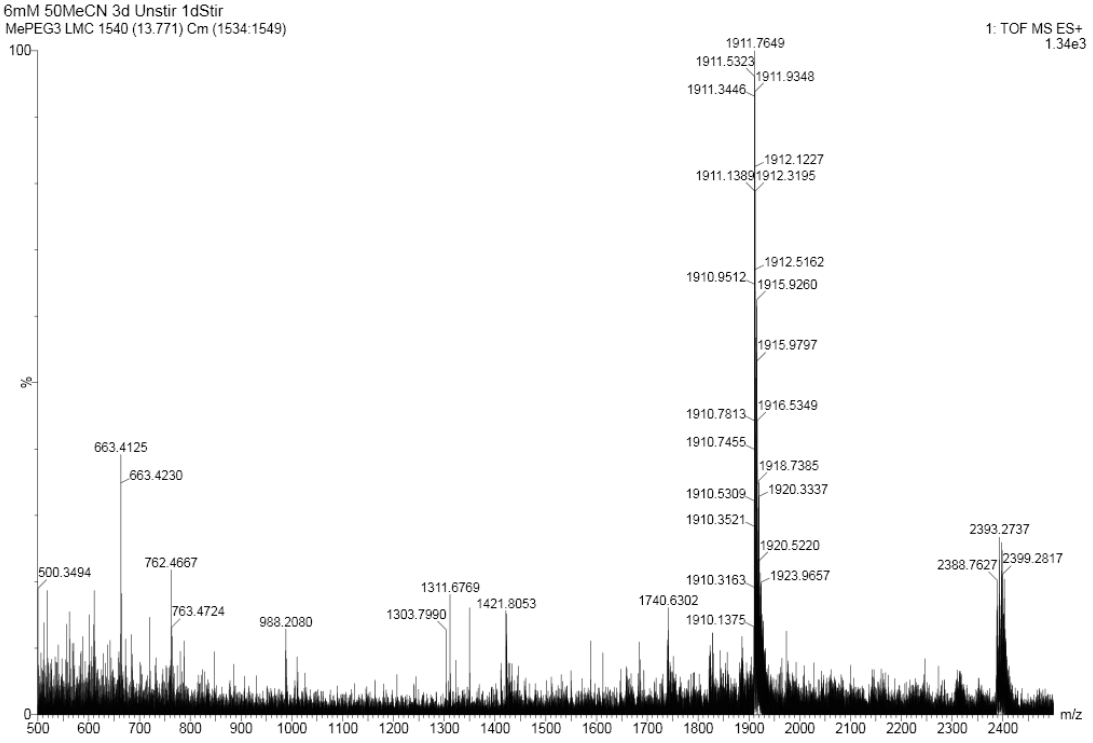

Figure S 28. Mass spectrum of $(\mathbf{1})_{29}$ (t_R =13.77 min) from the LC-MS analysis of a DCL made from **1**.
$(\mathbf{1})_{29}$:m/z calculated: 2386.81 $[M+4H]^{4+}$, 1909.65 $[M+5H]^{5+}$; m/z observed: 2386.74 $[M+4H]^{4+}$, 1909.69 $[M+5H]^{5+}$.

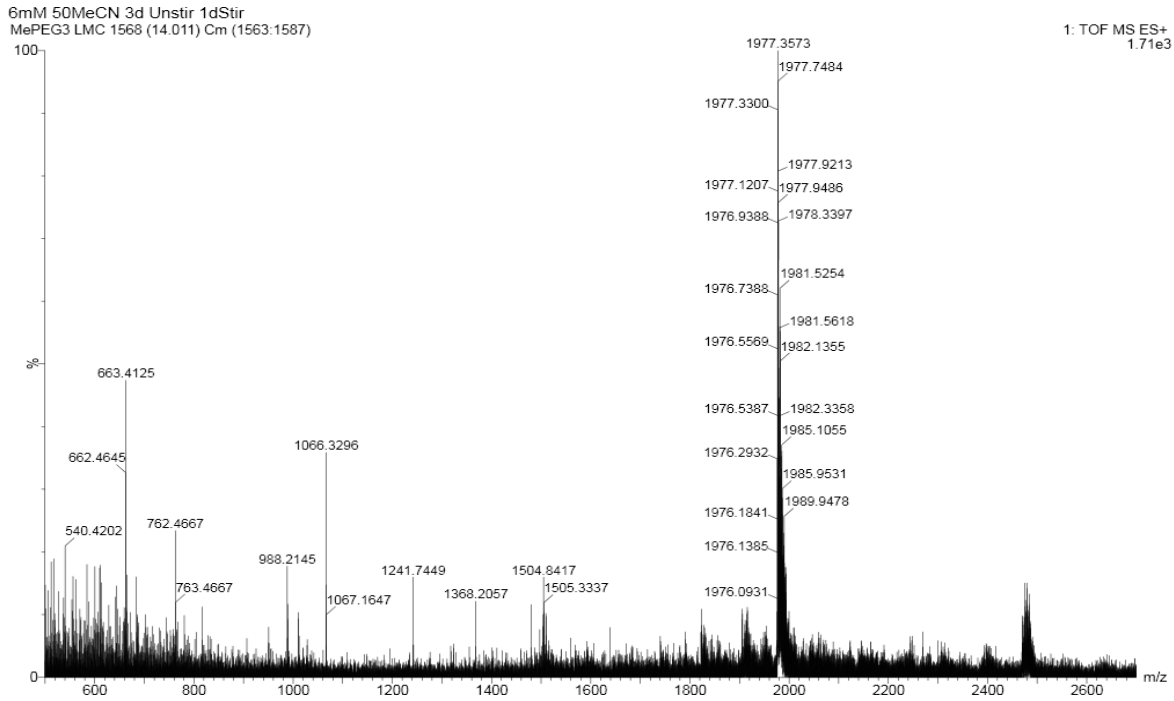

Figure S29. Mass spectrum of $(\mathbf{1})_{30}$ (t_R =14.01 min) from the LC-MS analysis of a DCL made from **1**.
$(\mathbf{1})_{30}$:m/z calculated: 2469.07 $[M+4H]^{4+}$, 1975.46 $[M+5H]^{5+}$; m/z observed: 2469.22 $[M+4H]^{4+}$, 1975.49 $[M+5H]^{5+}$.

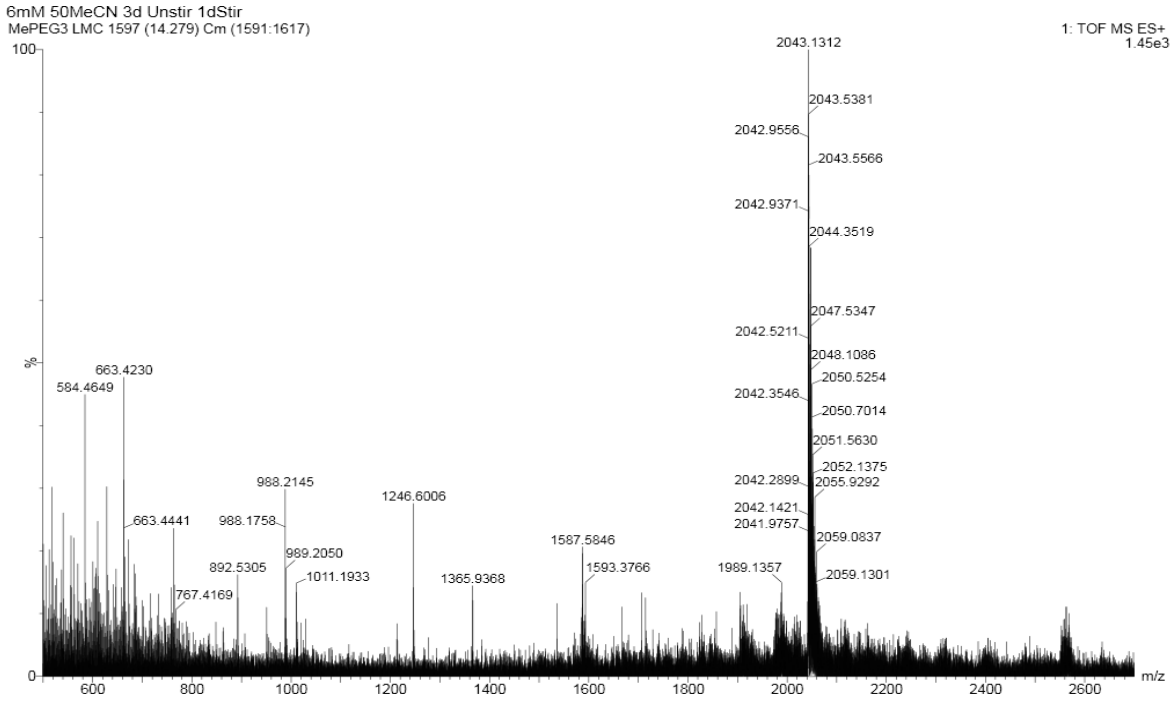

Figure S30. Figure 1: Mass spectrum of $(\mathbf{1})_{31}$ (t_R =14.28 min) from the LC-MS analysis of a DCL made from **1**. $(\mathbf{1})_{31}$:m/z calculated: 2041.27 $[M+5H]^{5+}$; m/z observed: 2041.30 $[M+5H]^{5+}$.

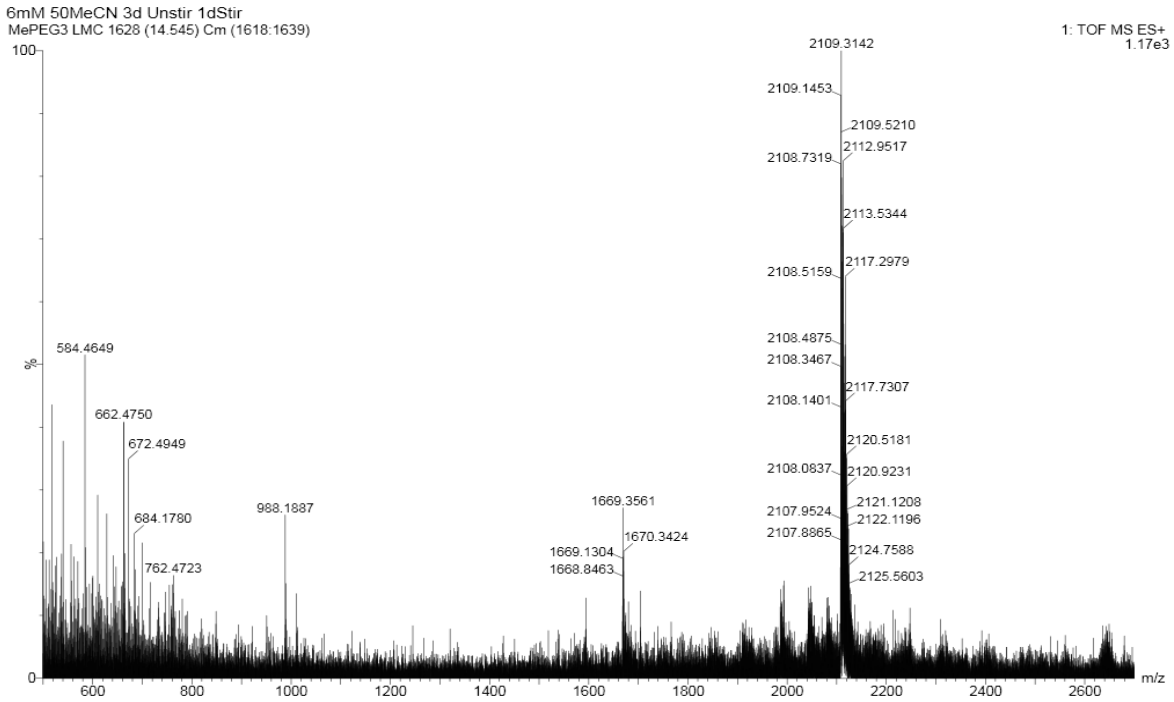

Figure S31. Mass spectrum of $(\mathbf{1})_{32}$ (t_R =14.55 min) from the LC-MS analysis of a DCL made from **1**. $(\mathbf{1})_{32}$:m/z calculated: 2107.09 $[M+5H]^{5+}$; m/z observed: 2107.10 $[M+5H]^{5+}$.

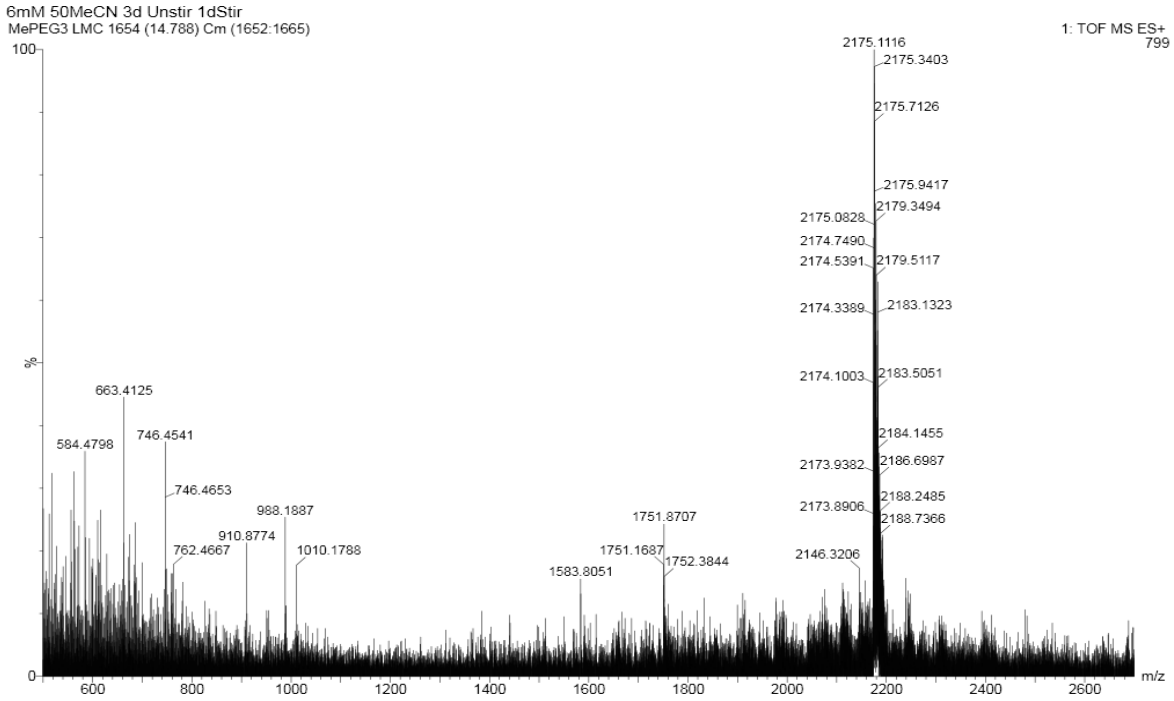

Figure S 32. Mass spectrum of $(\mathbf{1})_{33}$ (t_R =14.79 min) from the LC-MS analysis of a DCL made from **1**. $(\mathbf{1})_{33}$:m/z calculated: 2172.91 $[M+5H]^{5+}$; m/z observed: 2172.99 $[M+5H]^{5+}$.

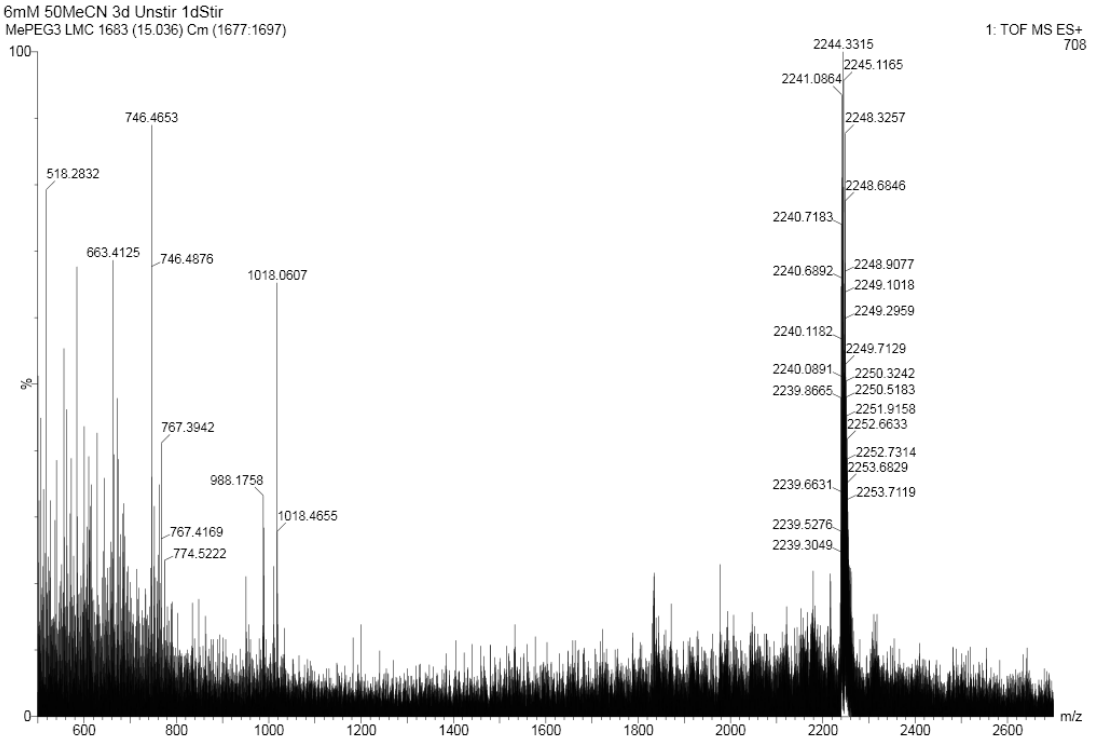

Figure S33. Mass spectrum of $(\mathbf{1})_{34}$ (t_R =15.04 min) from the LC-MS analysis of a DCL made from **1**. $(\mathbf{1})_{34}$:m/z calculated: 2238.72 $[M+5H]^{5+}$; m/z observed: 2238.84 $[M+5H]^{5+}$.

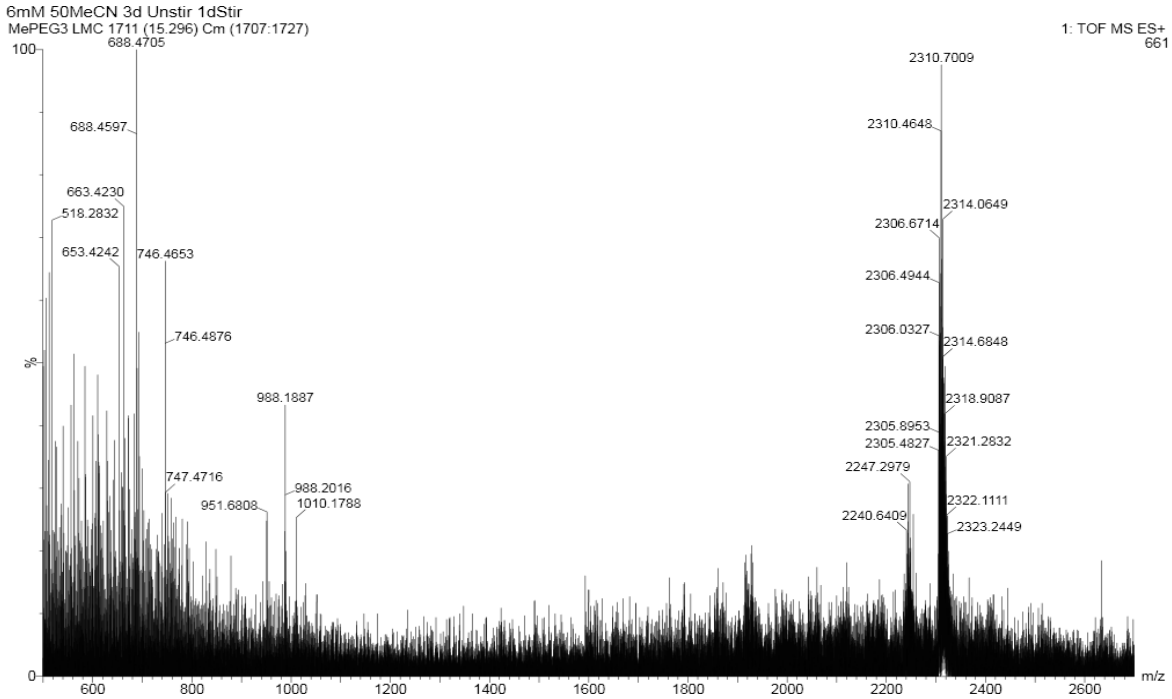

Figure S34. Mass spectrum of $(1)_{35}$ (t_R =15.29 min) from the LC-MS analysis of a DCL made from **1**. $(\mathbf{1})_{35}$:m/z calculated: 2304.54 $[M+5H]^{5+}$; m/z observed: 2304.64 $[M+5H]^{5+}$.

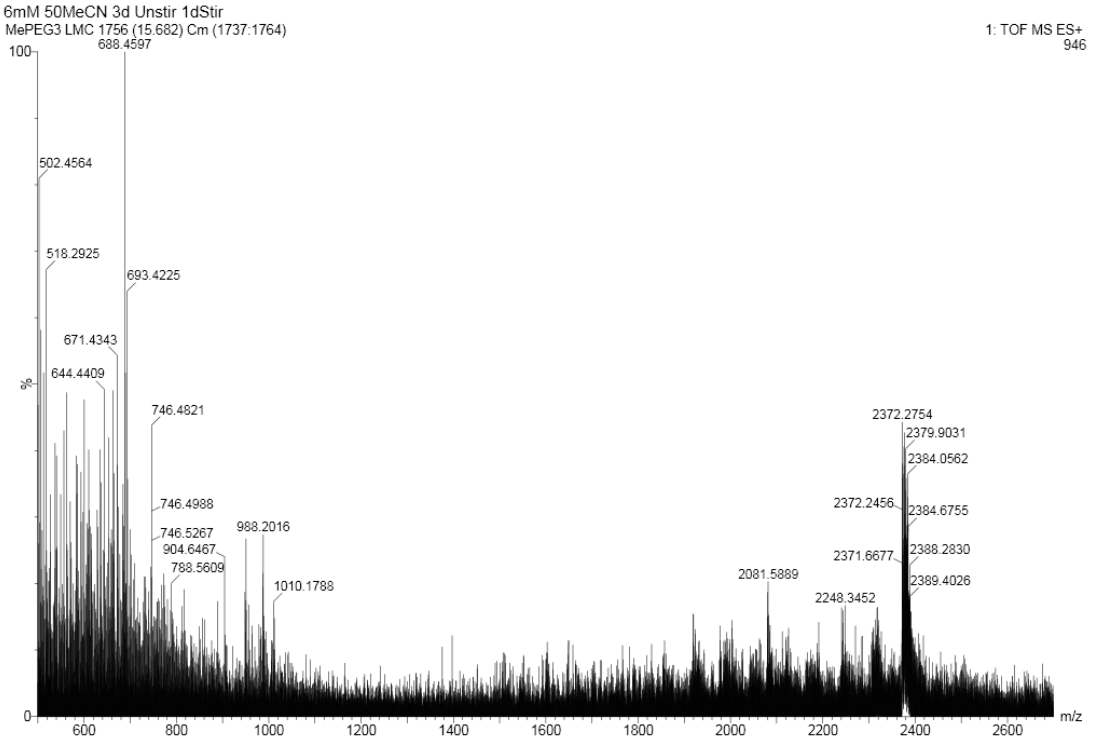

Figure S35. Mass spectrum of $(\mathbf{1})_{36}$ (t_R =15.68 min) from the LC-MS analysis of a DCL made from **1**. $(\mathbf{1})_{36}$:m/z calculated: 2370.35 $[M+5H]^{5+}$; m/z observed: 2370.35 $[M+5H]^{5+}$.

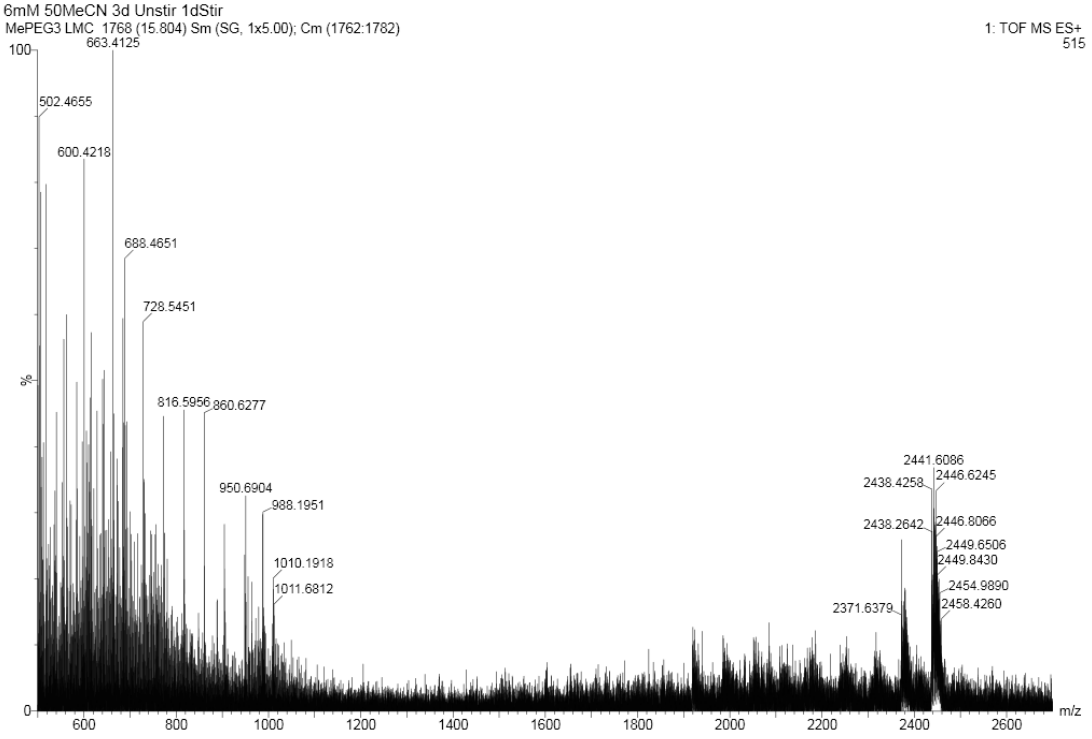

Figure S36. Mass spectrum of $(\mathbf{1})_{37}$ (t_R =15.81 min) from the LC-MS analysis of a DCL made from **1**. $(\mathbf{1})_{37}$:m/z calculated: 2436.17 $[M+5H]^{5+}$; m/z observed: 2436.00 $[M+5H]^{5+}$.

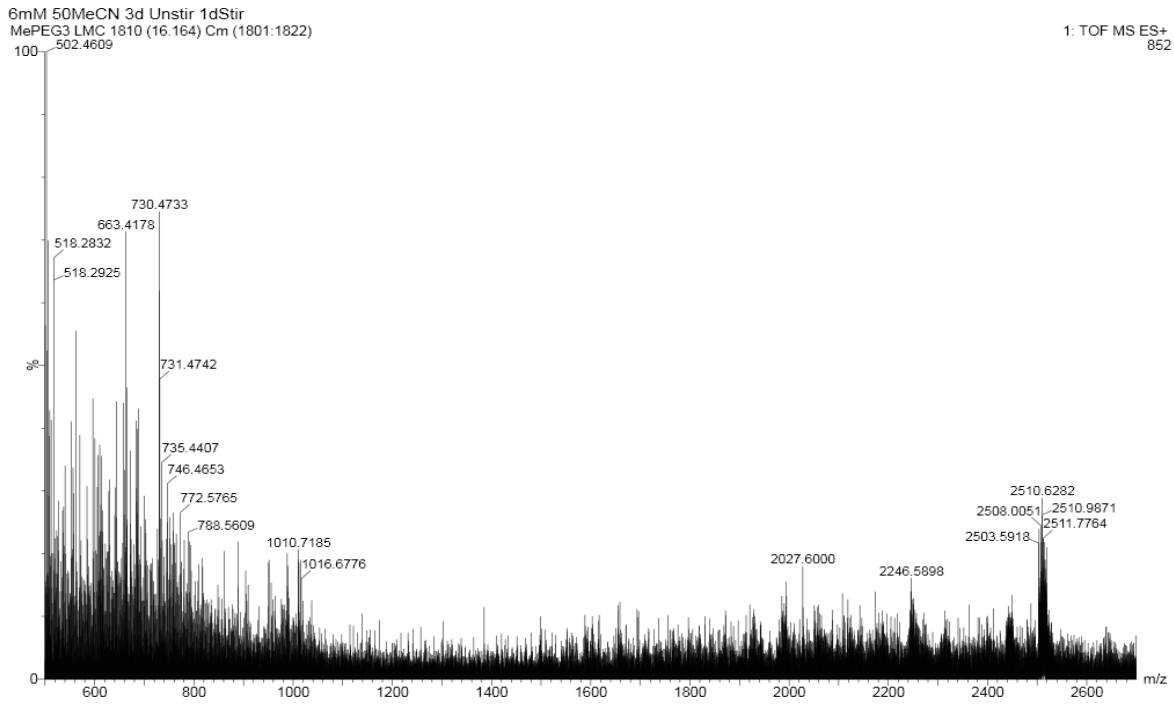

Figure S37. Mass spectrum of $(\mathbf{1})_{38}$ (t_R =16.16 min) from the LC-MS analysis of a DCL made from **1**. $(\mathbf{1})_{38}$:m/z calculated: 2501.91 $[M+5H]^{5+}$; m/z observed: 2501.94 $[M+5H]^{5+}$.

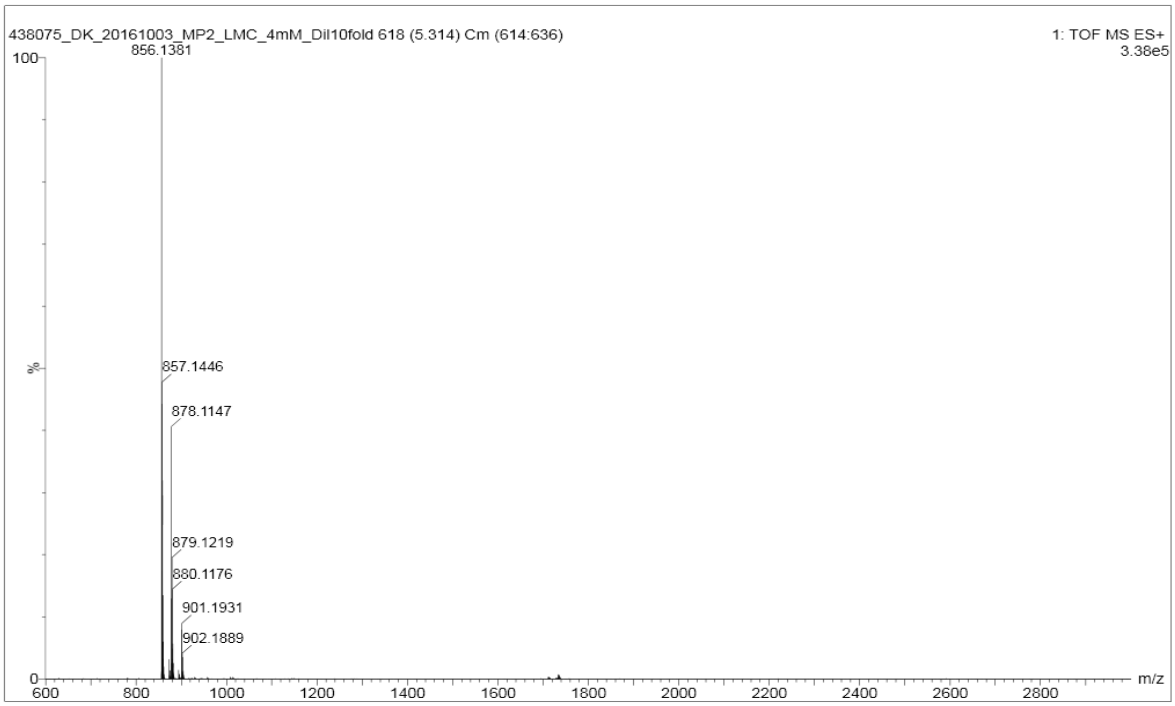

Figure S 38. Mass spectrum of $(\mathbf{2})_3$ (t_R =5.31 min) from the LC-MS analysis of a DCL made from **2**. $(\mathbf{2})_3$:m/z calculated: 856.16 $[M+H]^+$; m/z observed: 856.14 $[M+H]^+$.

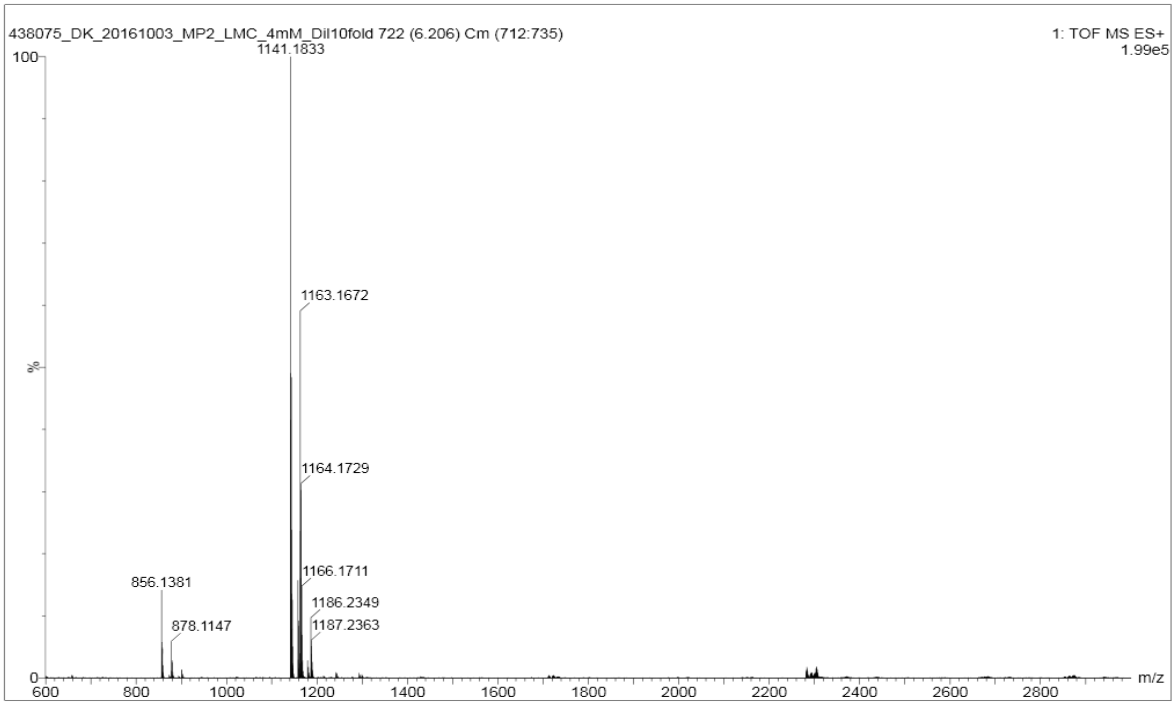

Figure S 39. Mass spectrum of $(\mathbf{2})_4$ (t_R =6.21 min) from the LC-MS analysis of a DCL made from **2**. $(\mathbf{2})_4$:m/z calculated: 1141.21 $[M+H]^+$; m/z observed: 1141.18 $[M+H]^+$.

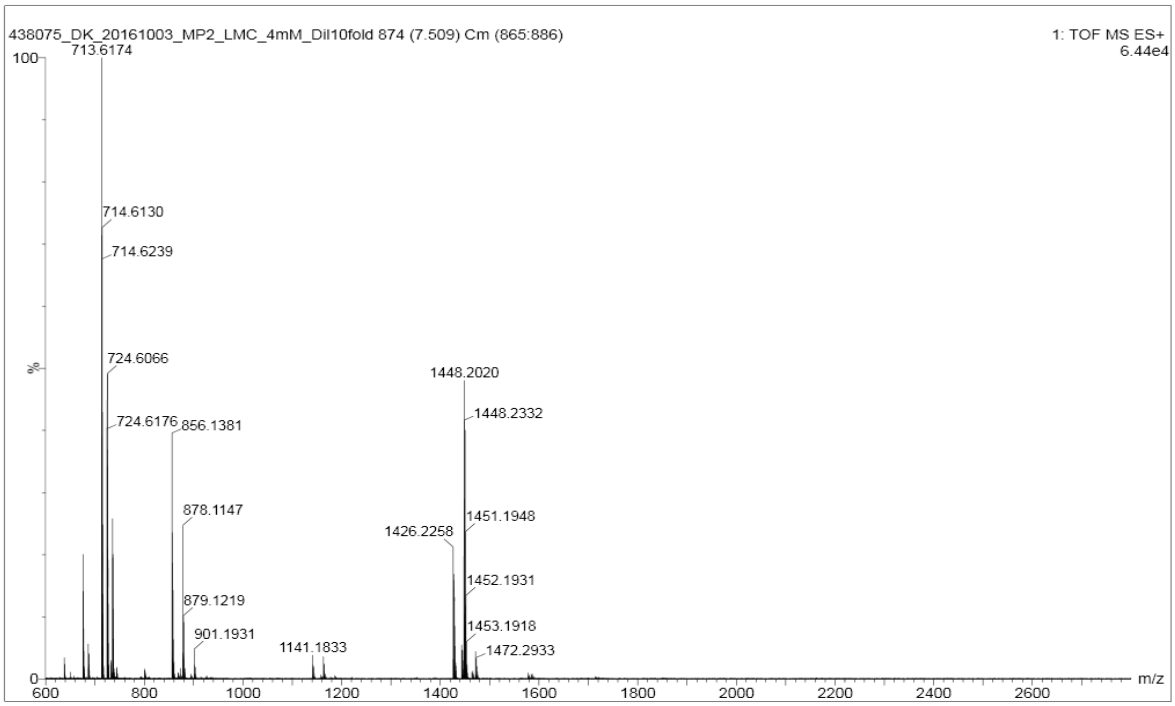

Figure S 40. Mass spectrum of $(\mathbf{2})_5$ (t_R =7.51 min) from the LC-MS analysis of a DCL made from **2**. $(\mathbf{2})_5$:m/z calculated: 1448.24 $[M+Na]^+$; m/z observed: 1448.20 $[M+Na]^+$.

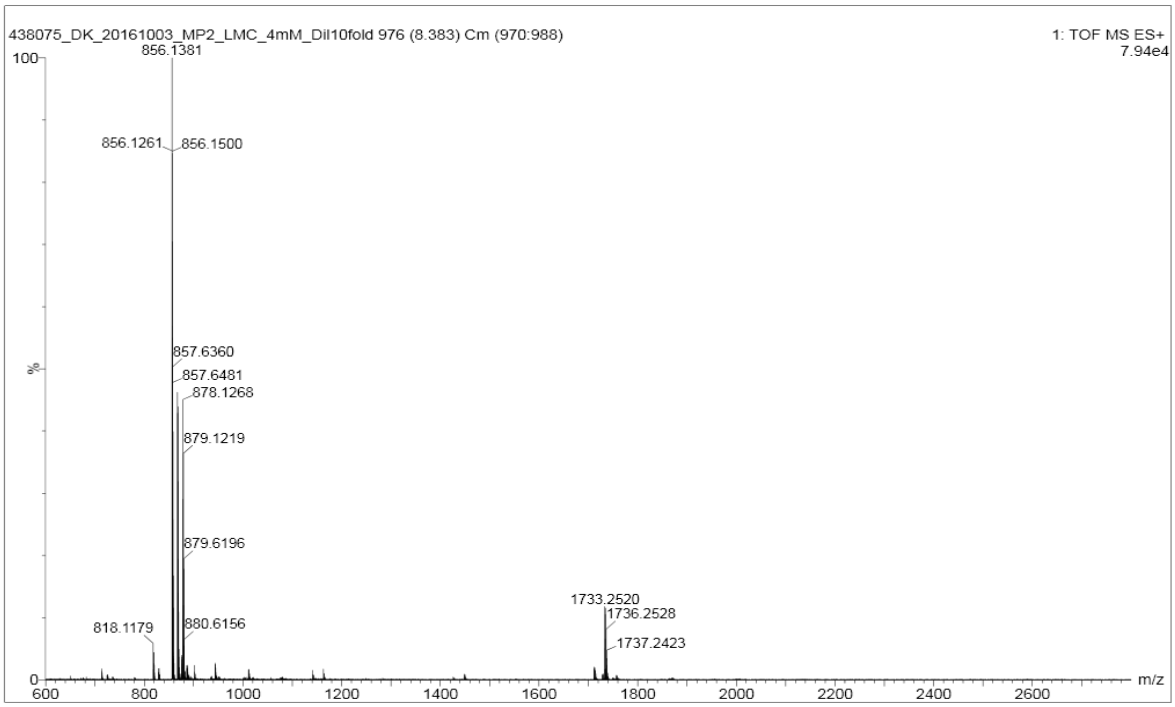

Figure S 41. Mass spectrum of $(\mathbf{2})_6$ (t_R =8.38 min) from the LC-MS analysis of a DCL made from **2**. $(\mathbf{2})_6$:m/z calculated: 856.16 $[M+2H]^{2+}$; m/z observed: 856.14 $[M+2H]^{2+}$.

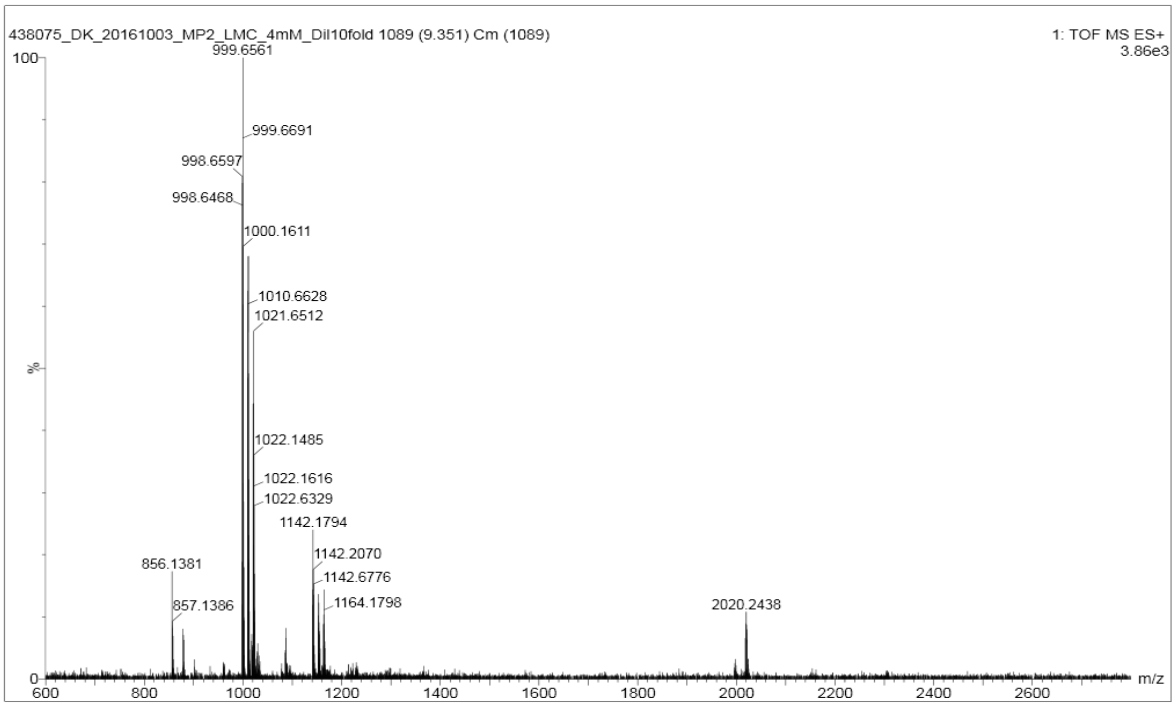

Figure S 42. Mass spectrum of $(\mathbf{2})_7$ and $(\mathbf{2})_8$ (t_R =9.35 min) from the LC-MS analysis of a DCL made from **2**.
$(\mathbf{2})_7$: m/z calculated: 998.65 $[M+2H]^{2+}$; m/z observed: 998.68 $[M+2H]^{2+}$.
$(\mathbf{2})_8$ **:** m/z calculated: 1141.21 $[M+2H]^{2+}$; m/z observed: 1141.08 $[M+2H]^{2+}$.

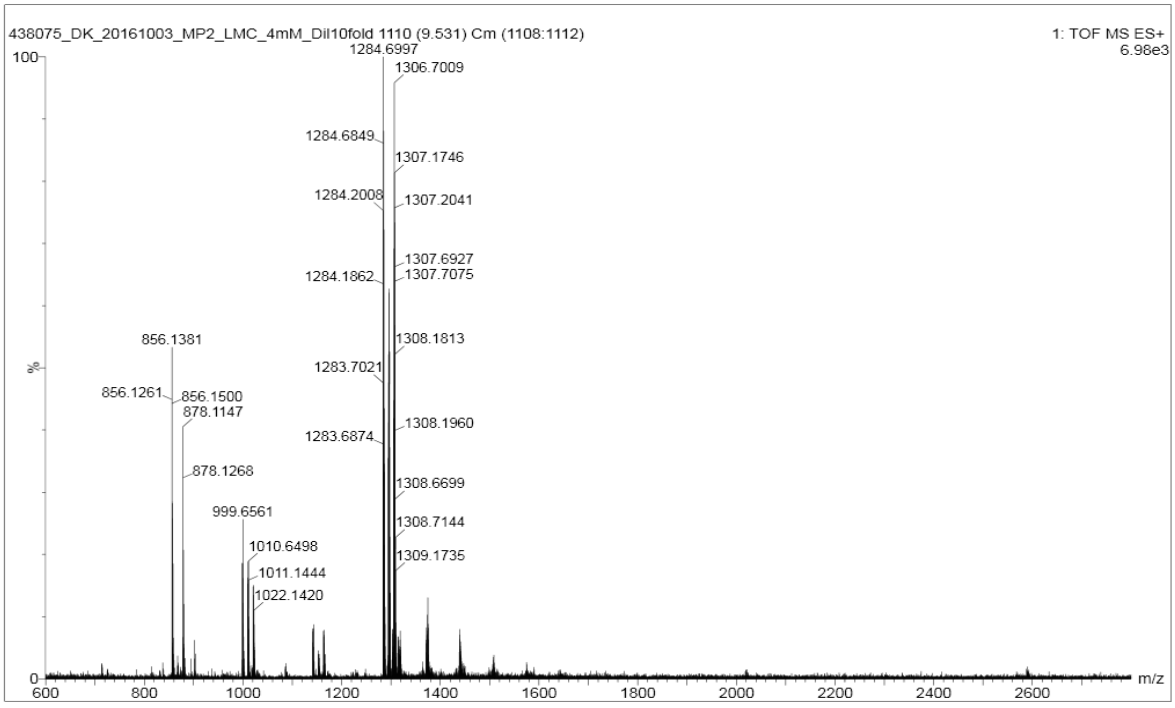

Figure S 43. Mass spectrum of $(\mathbf{2})_9$ (t_R =9.53 min) from the LC-MS analysis of a DCL made from **2**.
$(\mathbf{2})_9$:m/z calculated: 1283.73 $[M+2H]^{2+}$; m/z observed: 1283.70 $[M+2H]^{2+}$.

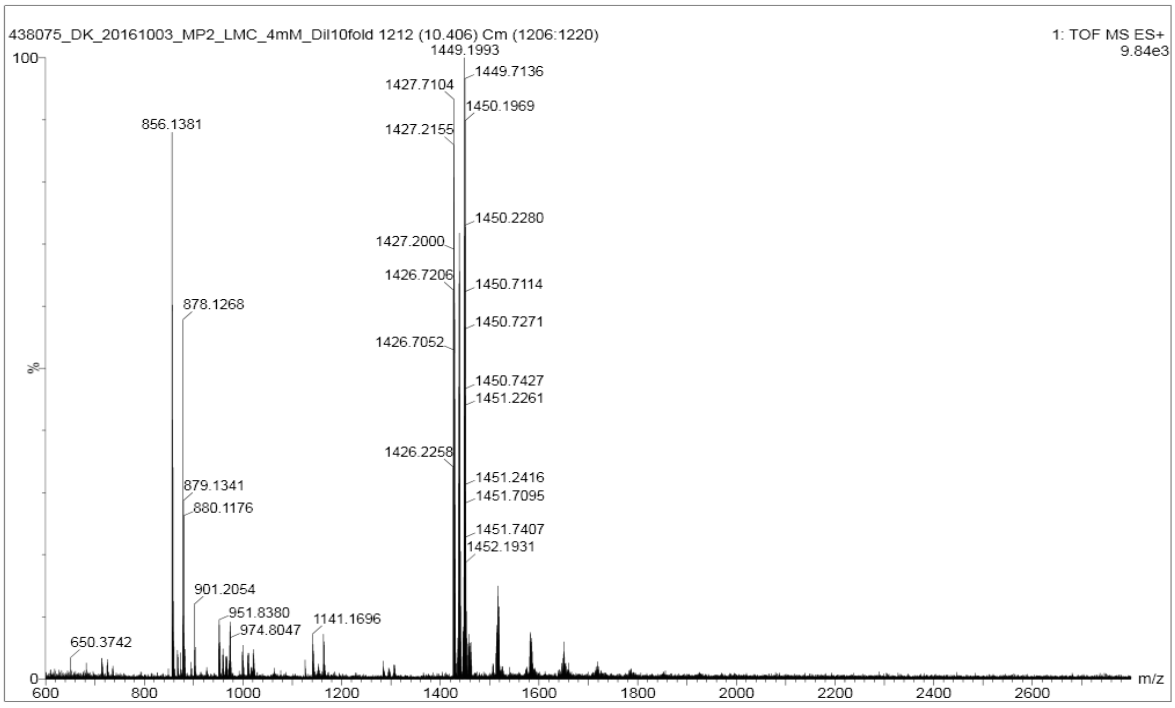

Figure S 44. Mass spectrum of $(\mathbf{2})_{10}$ (t_R =10.41 min) from the LC-MS analysis of a DCL made from **2**.
$(\mathbf{2})_{10}$:m/z calculated: 1426.23 $[M+2H]^{2+}$; m/z observed: 1426.25 $[M+2H]^{2+}$.

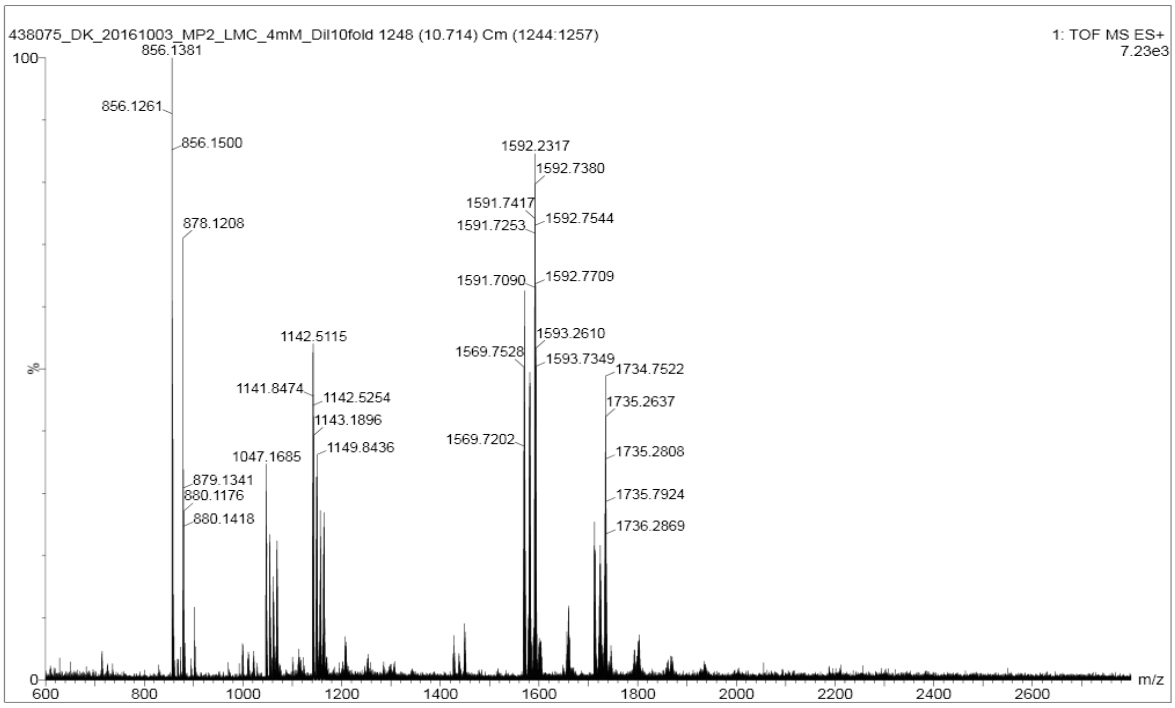

Figure S 45. Mass spectrum of $(\mathbf{2})_{11}$and $(\mathbf{2})_{12}$ (t_R =10.71 min) from the LC-MS analysis of a DCL made from **2**.
$(\mathbf{2})_{11}$: m/z calculated: 1568.78 $[M+2H]^{2+}$, 1046.19 $[M+3H]^{3+}$; m/z observed: 1568.75 $[M+2H]^{2+}$, 1046.15 $[M+3H]^{3+}$.
$(\mathbf{2})_{12}$ **:** m/z calculated: 1711.30 $[M+2H]^{2+}$, 1141.21 $[M+3H]^{3+}$; m/z observed: 1711.28 $[M+2H]^{2+}$, 1141.17 $[M+3H]^{3+}$.

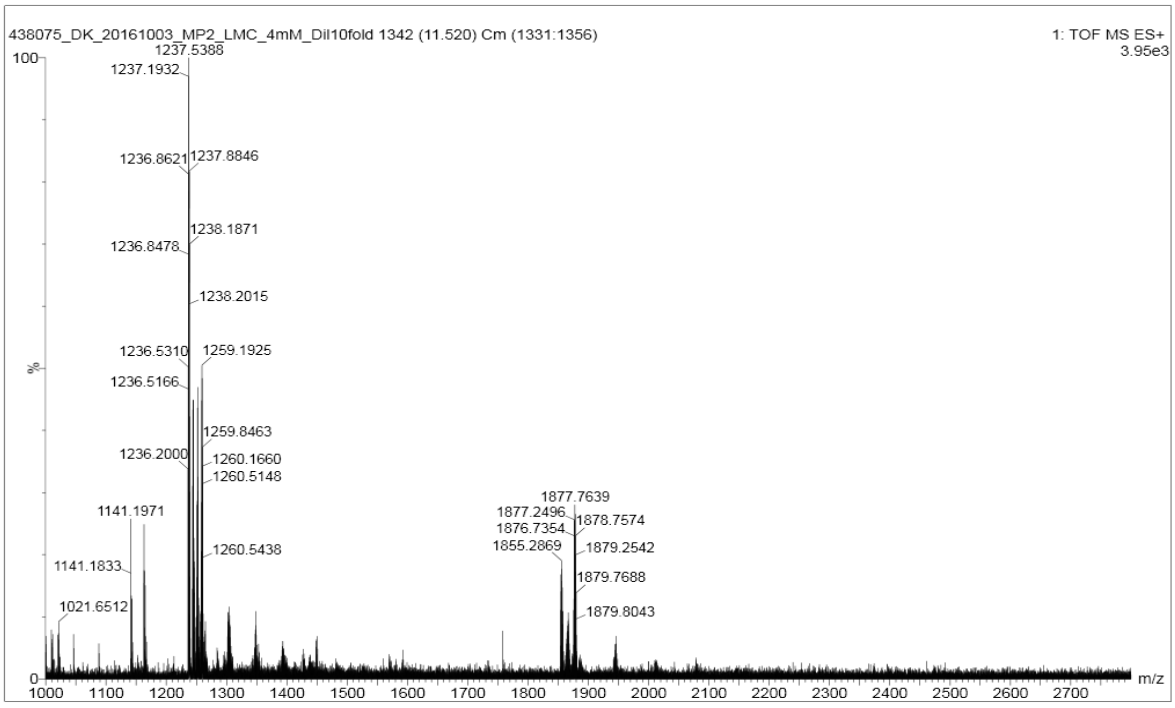

Figure S 46. Mass spectrum of $(\mathbf{2})_{13}$ (t_R =11.52 min) from the LC-MS analysis of a DCL made from **2**.
$(\mathbf{2})_{13}$:m/z calculated: 1853.83 $[M+2H]^{2+}$, 1236.22 $[M+3H]^{3+}$; m/z observed: 1853.79 $[M+2H]^{2+}$, 1236.20 $[M+3H]^{3+}$.

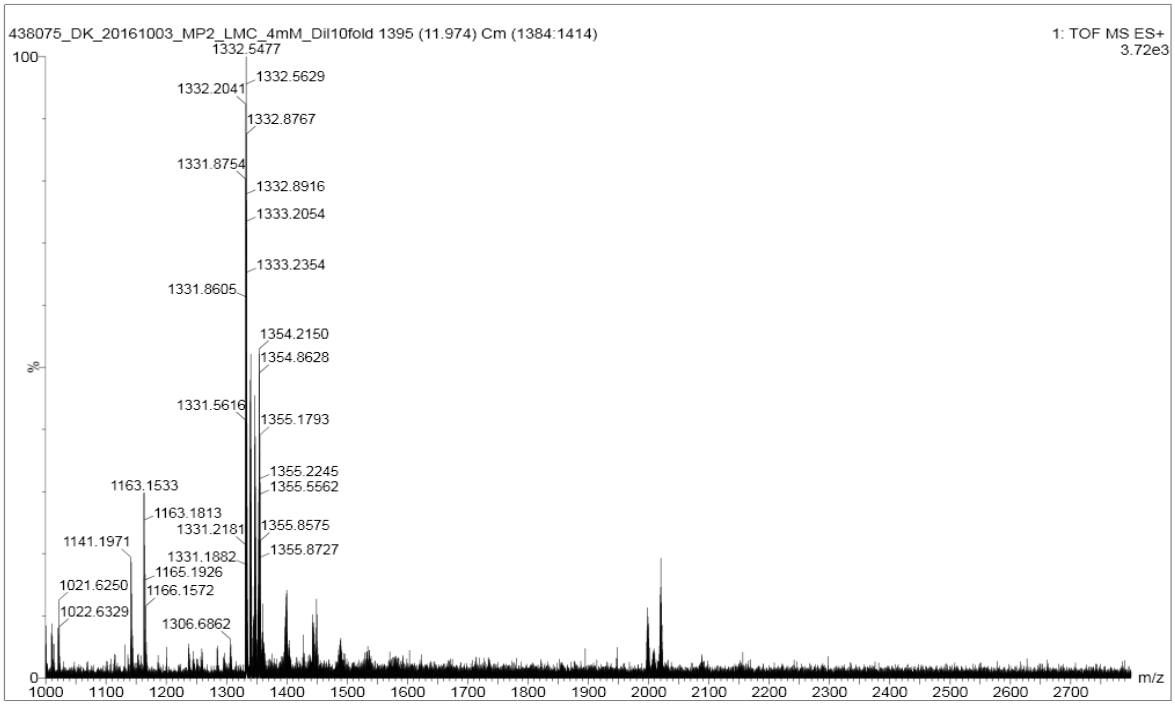

Figure S 47 Mass spectrum of $(\mathbf{2})_{14}$ (t_R =11.97 min) from the LC-MS analysis of a DCL made from **2**.
$(\mathbf{2})_{14}$:m/z calculated: 1331.24 $[M+3H]^{3+}$; m/z observed: 1331.22 $[M+3H]^{3+}$.

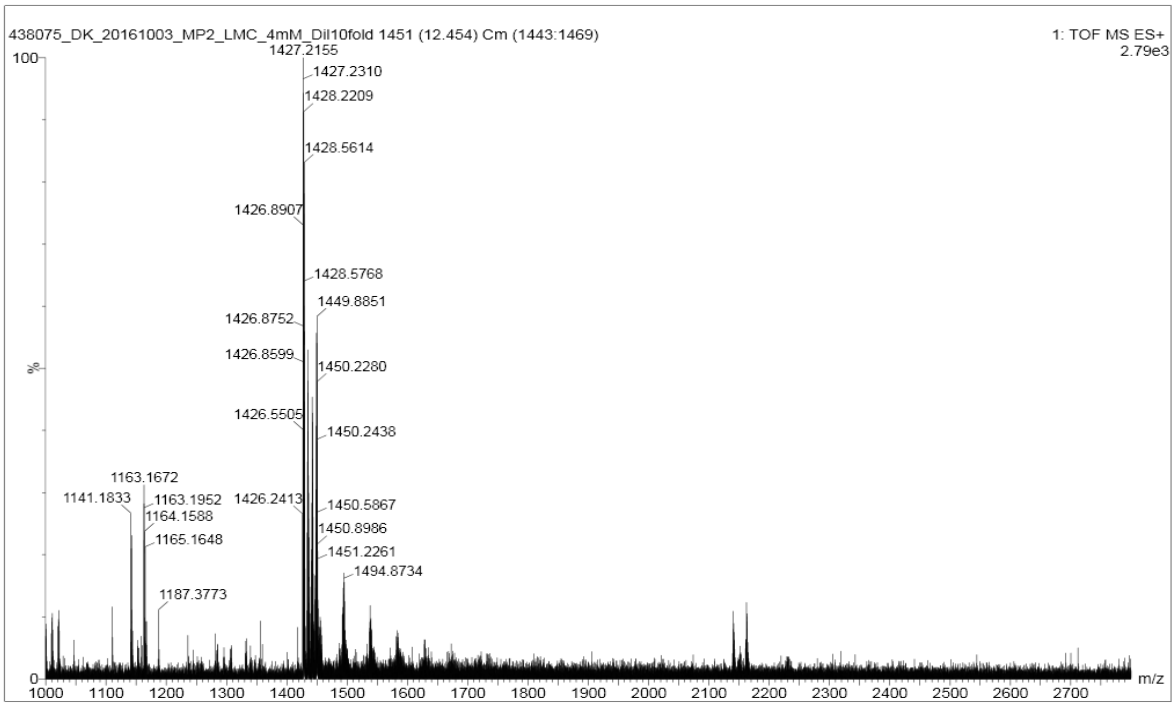

Figure S48: Mass spectrum of (**2**)$_{15}$ (t_R =12.45 min) from the LC-MS analysis of a DCL made from **2**.
(**2**)$_{15}$: m/z calculated: 1426.25 $[M+3H]^{3+}$; m/z observed: 1426.24 $[M+3H]^{3+}$.

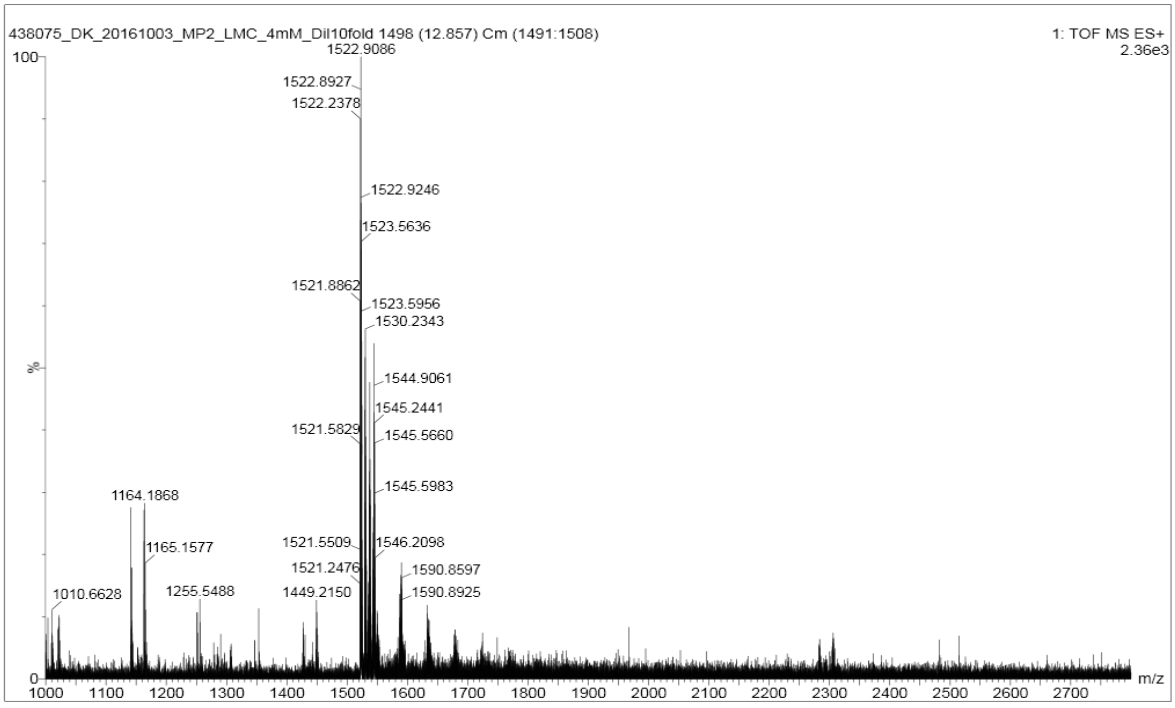

Figure S49. Mass spectrum of (**2**)$_{16}$ (t_R =12.86 min) from the LC-MS analysis of a DCL made from **2**.
(**2**)$_{16}$: m/z calculated: 1521.27 $[M+3H]^{3+}$; m/z observed: 1521.25 $[M+3H]^{3+}$.

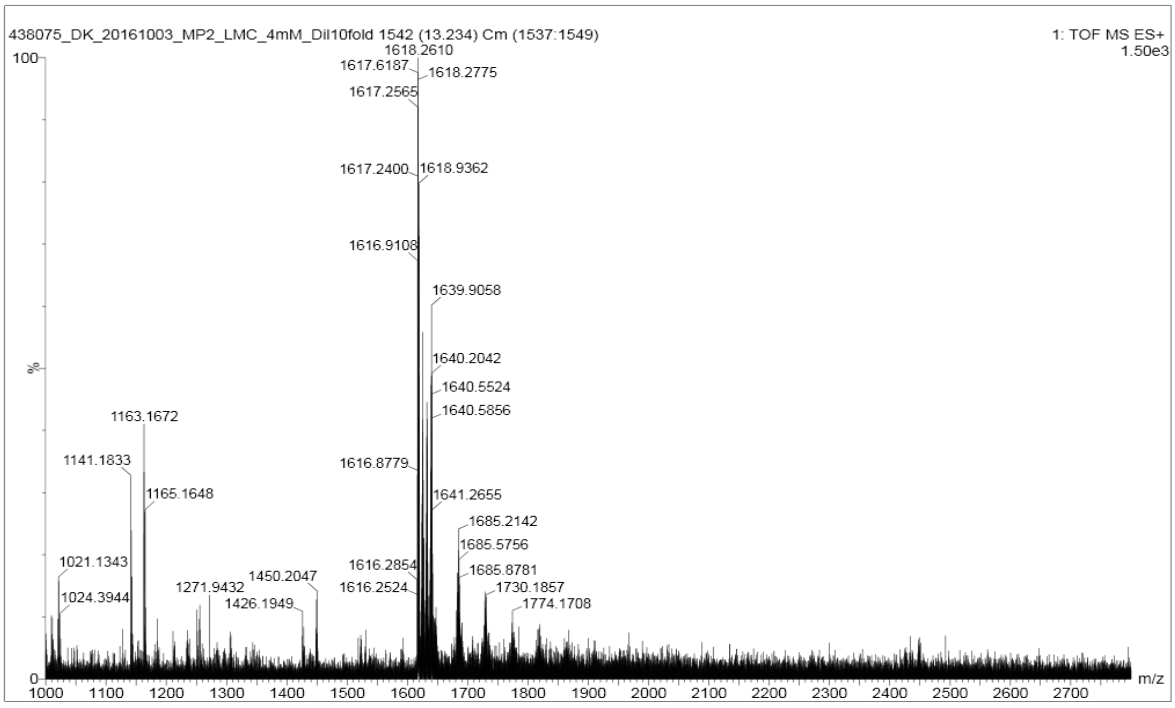

Figure S50. Mass spectrum of $(\mathbf{2})_{17}$ (t_R =13.23 min) from the LC-MS analysis of a DCL made from **2**. $(\mathbf{2})_{17}$: m/z calculated: 1616.29 $[M+3H]^{3+}$; m/z observed: 1616.25 $[M+3H]^{3+}$.

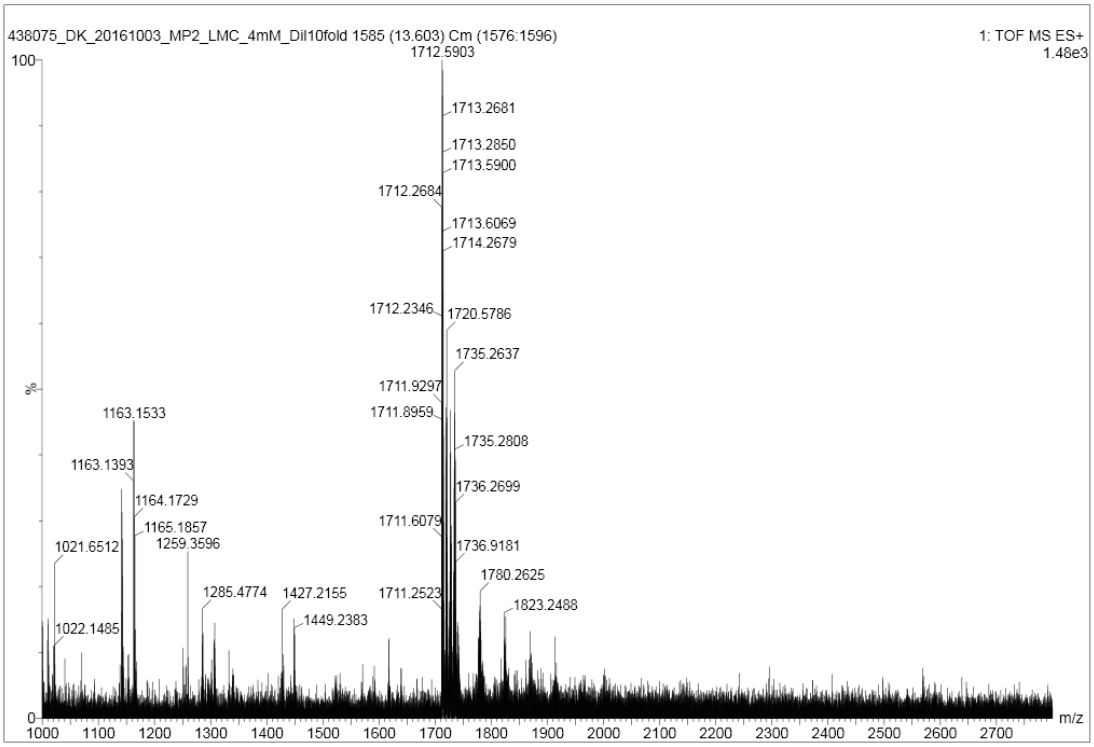

Figure S 51. Mass spectrum of $(\mathbf{2})_{18}$ (t_R =13.61 min) from the LC-MS analysis of a DCL made from **2**. $(\mathbf{2})_{18}$: m/z calculated: 1711.30 $[M+3H]^{3+}$; m/z observed: 1711.25 $[M+3H]^{3+}$.

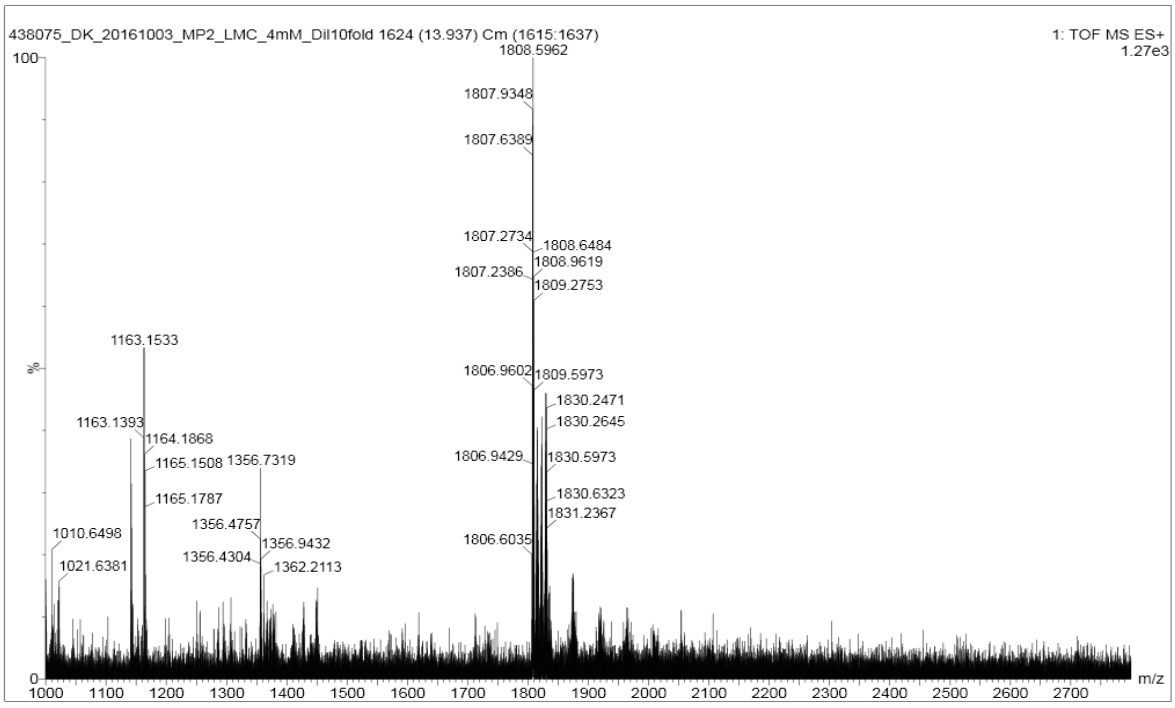

Figure S 52. Mass spectrum of $(\mathbf{2})_{19}$ (t_R =13.94 min) from the LC-MS analysis of a DCL made from **2**.
$(\mathbf{2})_{19}$: m/z calculated: 1806.32 $[M+3H]^{3+}$; m/z observed: 1806.30 $[M+3H]^{3+}$.

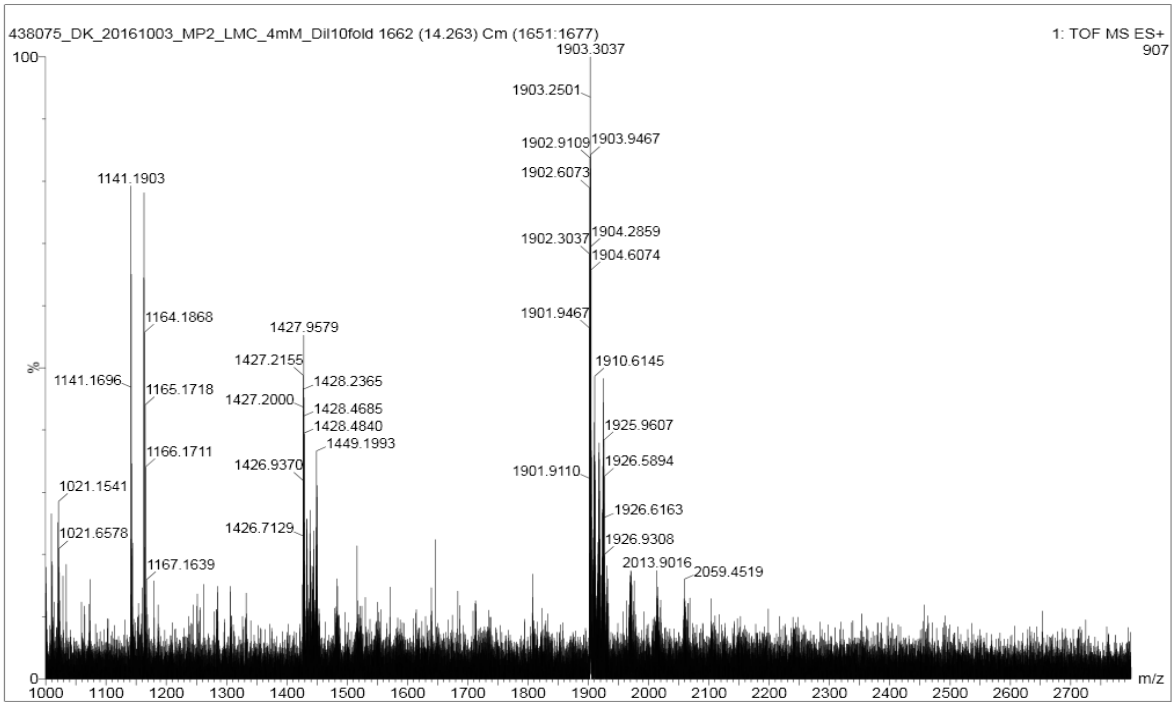

Figure S 53. Mass spectrum of $(\mathbf{2})_{20}$ (t_R =14.26 min) from the LC-MS analysis of a DCL made from **2**.
$(\mathbf{2})_{20}$:m/z calculated: 1901.34 $[M+3H]^{3+}$, 1426.25 $[M+4H]^{4+}$; m/z observed: 1901.27 $[M+3H]^{3+}$, 1426.23 $[M+4H]^{3+}$.

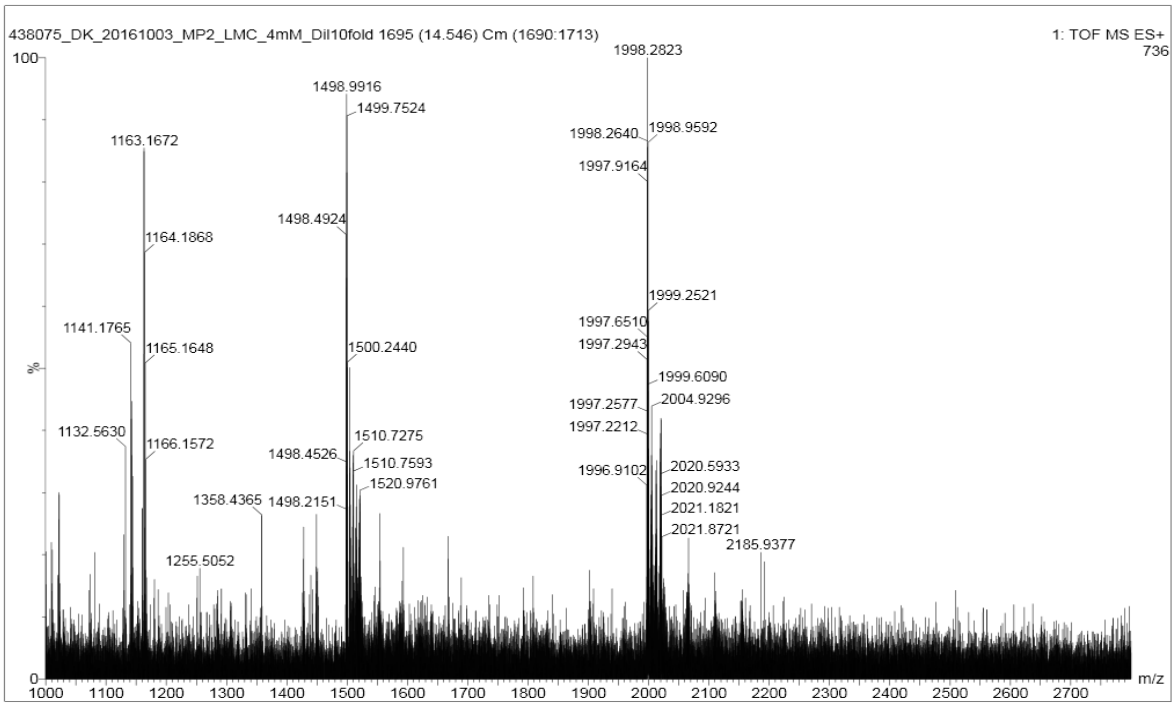

Figure S 54. Mass spectrum of $(\mathbf{2})_{21}$ (t_R =14.55 min) from the LC-MS analysis of a DCL made from **2**.
$(\mathbf{2})_{21}$:m/z calculated: 1996.35 $[M+3H]^{3+}$, 1497.52 $[M+4H]^{4+}$; m/z observed: 1996.31 $[M+3H]^{3+}$, 1497.53 $[M+4H]^{4+}$.

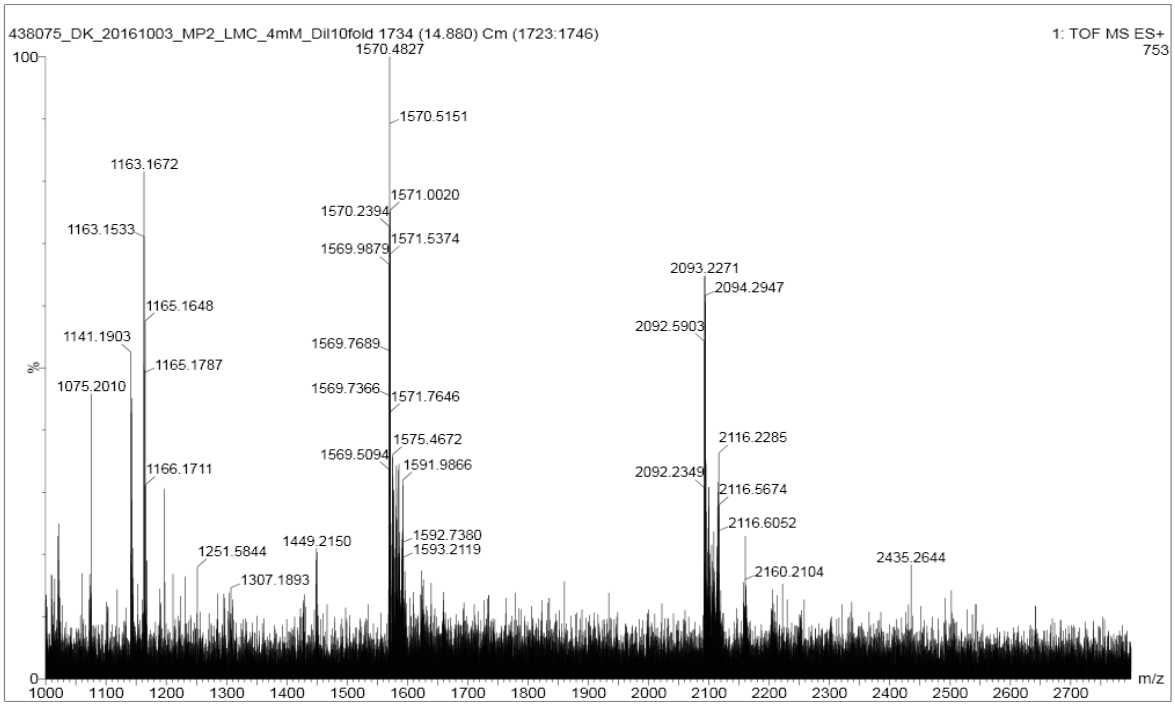

Figure S 55. Mass spectrum of $(\mathbf{2})_{22}$ (t_R =14.86 min) from the LC-MS analysis of a DCL made from **2**.
$(\mathbf{2})_{\mathbf{22}}$:m/z calculated: 2091.37 $[M+3H]^{3+}$, 1568.78 $[M+4H]^{4+}$; m/z observed: 2091.33 $[M+3H]^{3+}$, 1568.73 $[M+4H]^{4+}$.

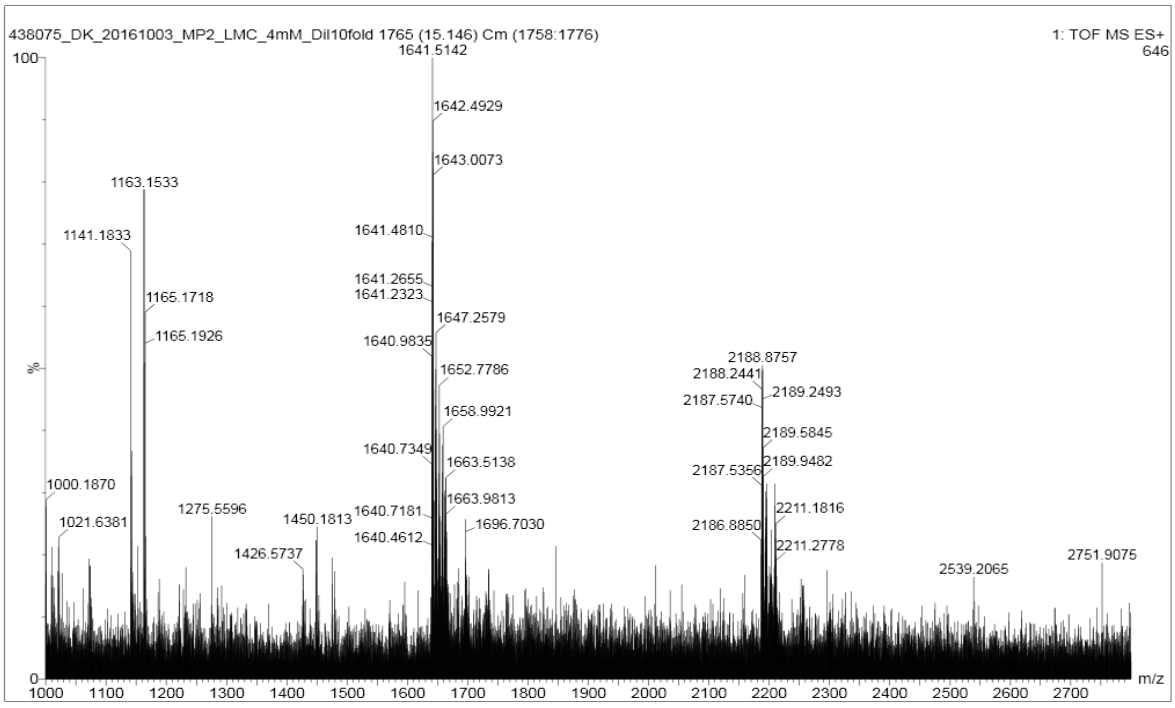

Figure S 56. Mass spectrum of $(\mathbf{2})_{23}$ (t_R =15.15 min) from the LC-MS analysis of a DCL made from **2**. $(\mathbf{2})_{23}$:m/z calculated: 2186.39 $[M+3H]^{3+}$, 1640.04 $[M+4H]^{4+}$; m/z observed: 2186.25 $[M+3H]^{3+}$, 1639.96 $[M+4H]^{4+}$.

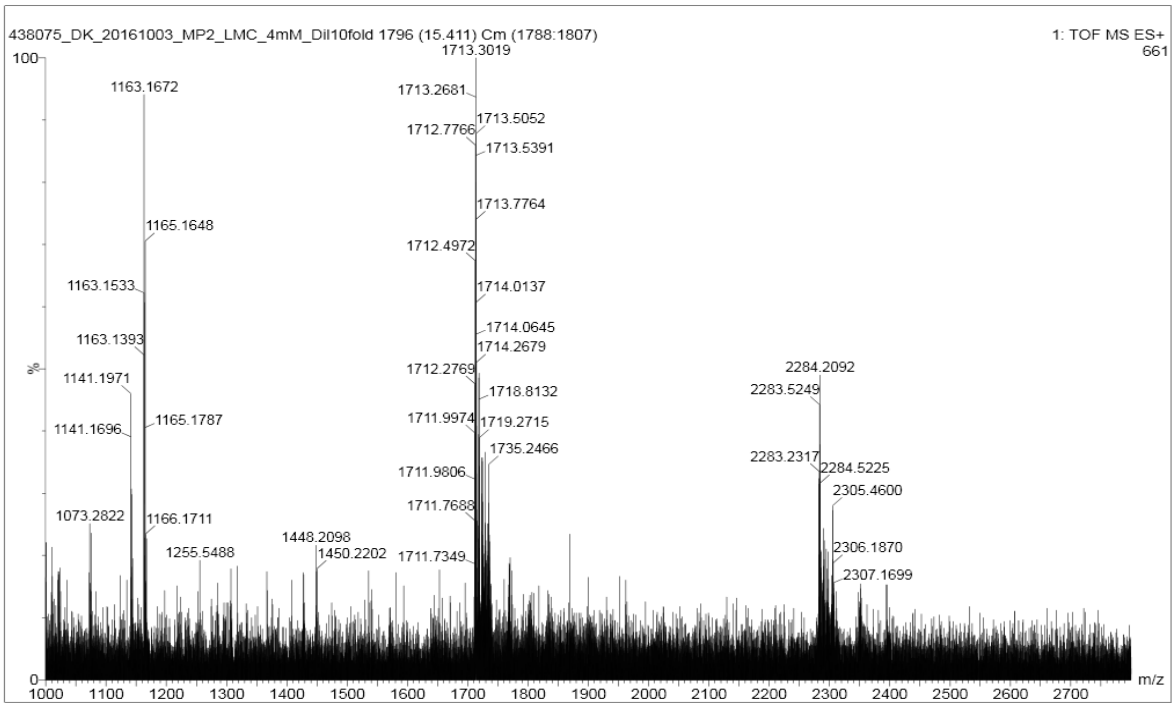

Figure S 57. Mass spectrum of $(\mathbf{2})_{24}$ (t_R =15.41 min) from the LC-MS analysis of a DCL made from **2**. $(\mathbf{2})_{24}$:m/z calculated: 2281.40 $[M+3H]^{3+}$, 1711.30 $[M+4H]^{4+}$; m/z observed: 2281.47 $[M+3H]^{3+}$, 1711.25 $[M+4H]^{4+}$.

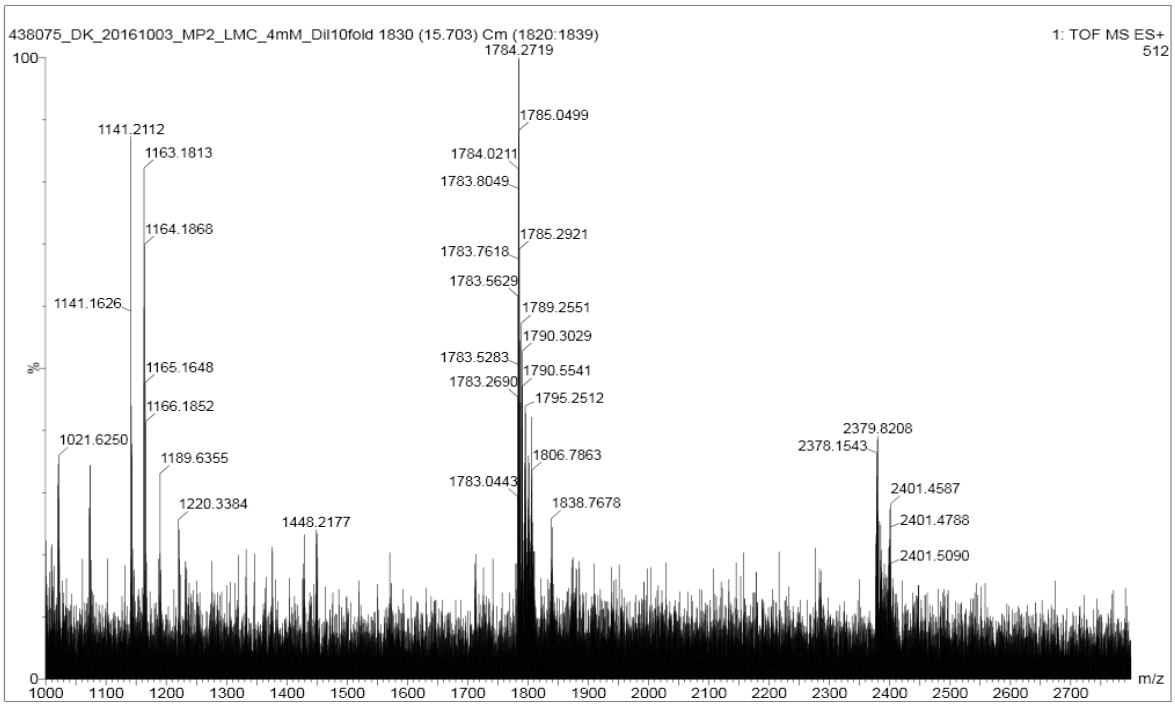

Figure S 58. Mass spectrum of $(\mathbf{2})_{25}$ (t_R =15.70 min) from the LC-MS analysis of a DCL made from **2**. $(\mathbf{2})_{25}$:m/z calculated: 2376.42 $[M+3H]^{3+}$, 1782.57 $[M+4H]^{4+}$; m/z observed: 2376.56 $[M+3H]^{3+}$, 1782.49 $[M+4H]^{4+}$.

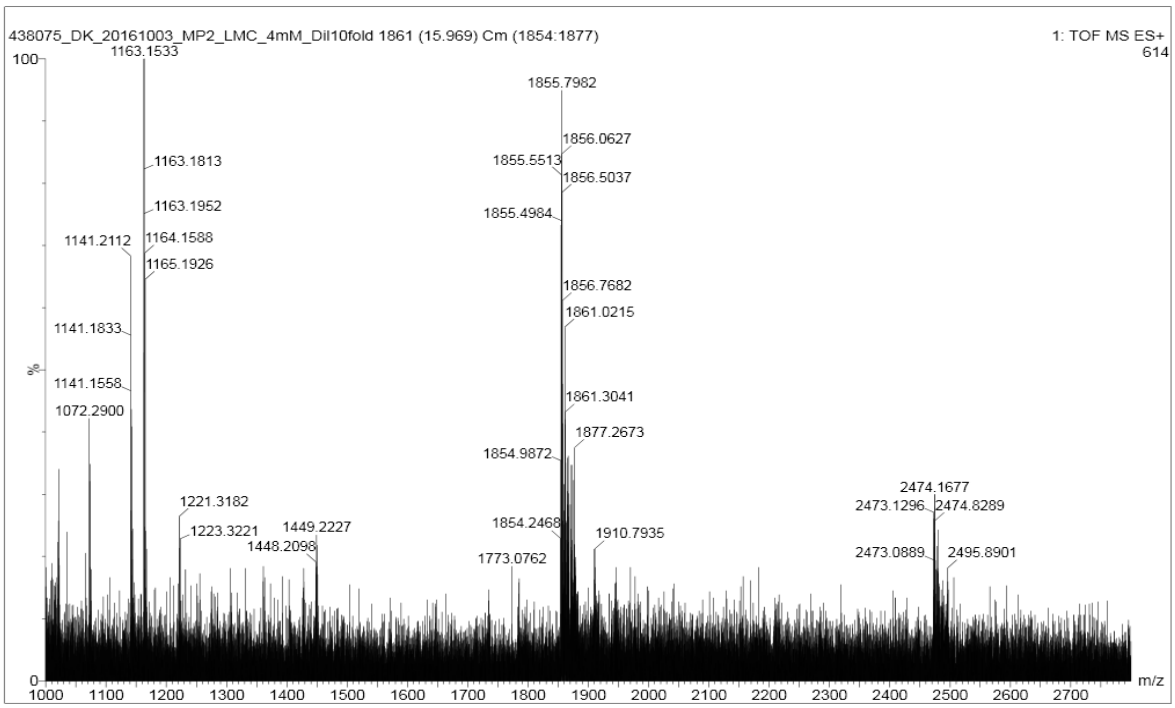

Figure S 59. Mass spectrum of $(\mathbf{2})_{26}$ (t_R =15.97 min) from the LC-MS analysis of a DCL made from **2**. $(\mathbf{2})_{26}$:m/z calculated: 2471.44 $[M+3H]^{3+}$, 1853.83 $[M+4H]^{4+}$; m/z observed: 2471.45 $[M+3H]^{3+}$, 1853.75 $[M+4H]^{4+}$.

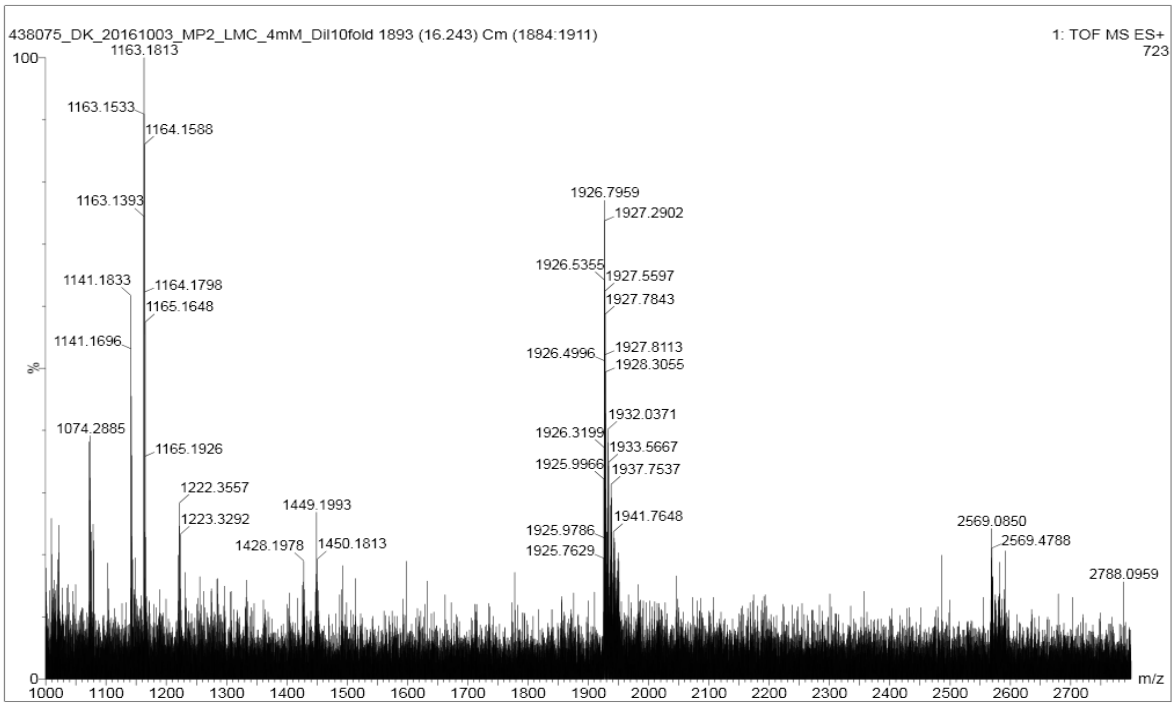

Figure S 60. Mass spectrum of $(\mathbf{2})_{27}$ (t_R =16.24 min) from the LC-MS analysis of a DCL made from **2**. $(\mathbf{2})_{27}$:m/z calculated: 2566.45 $[M+3H]^{3+}$, 1925.09 $[M+4H]^{4+}$; m/z observed: 2566.50$[M+3H]^{3+}$, 1925.30 $[M+4H]^{4+}$.

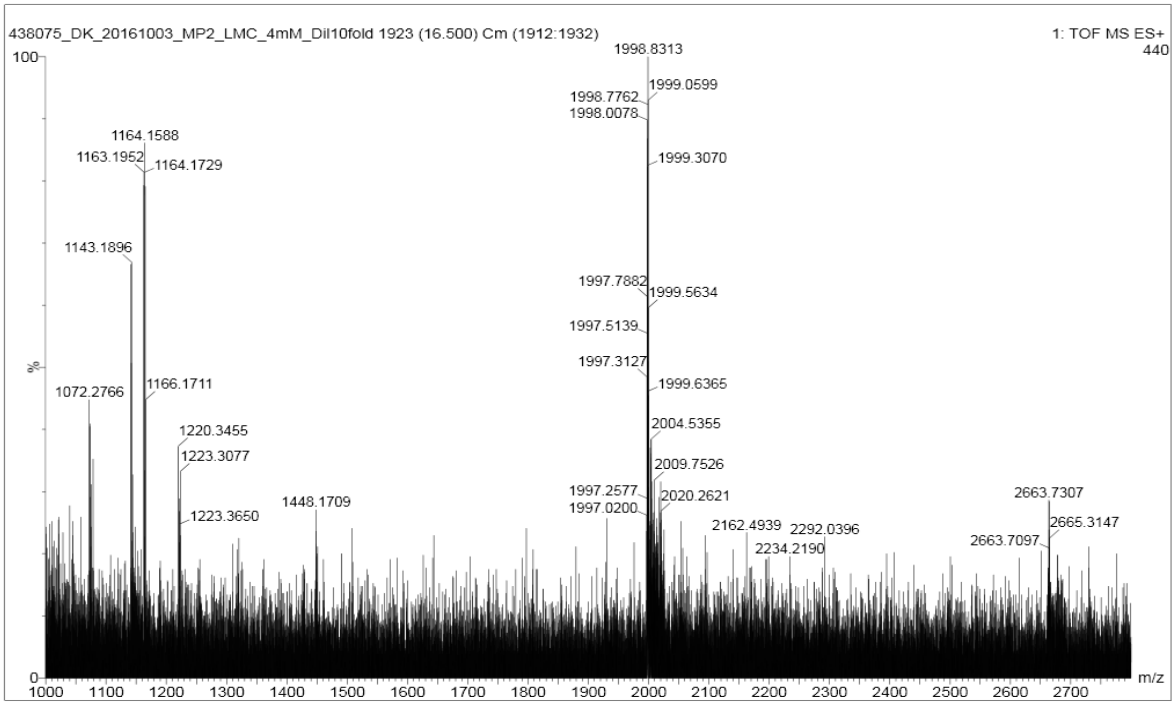

Figure S 61. Mass spectrum of $(\mathbf{2})_{28}$ (t_R =16.50 min) from the LC-MS analysis of a DCL made from **2**. $(\mathbf{2})_{28}$:m/z calculated:, 1996.35 $[M+4H]^{4+}$; m/z observed: 1996.51 $[M+4H]^{4+}$.

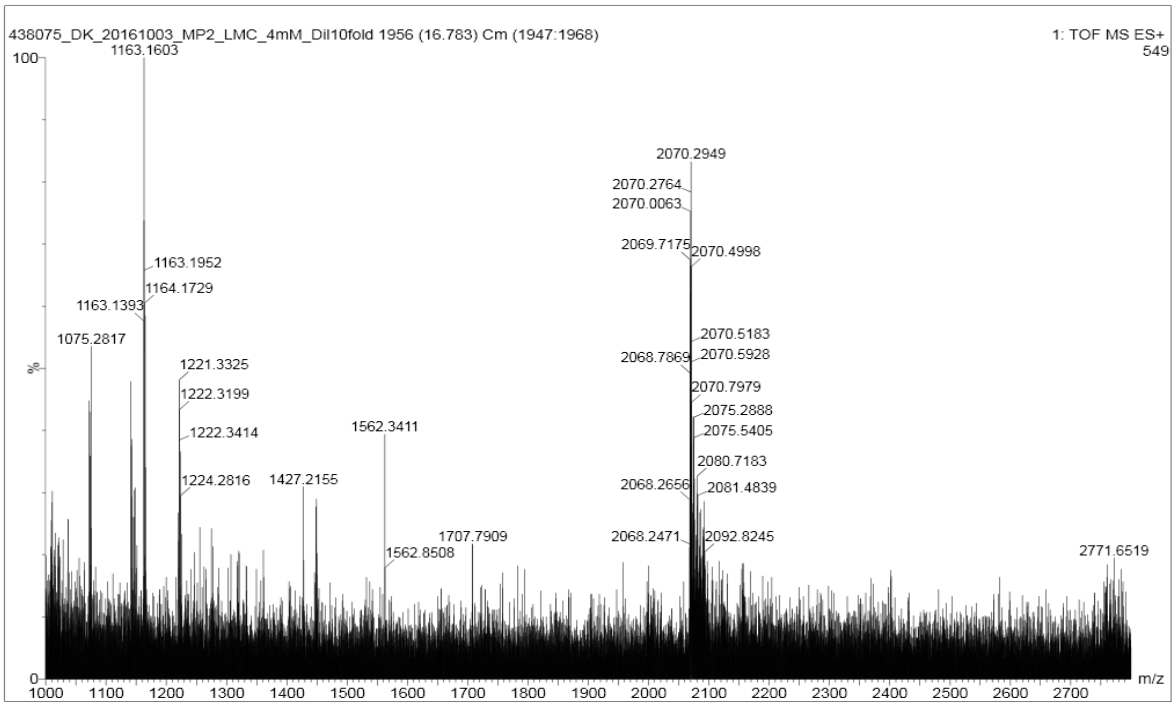

Figure S 62. Mass spectrum of $(\mathbf{2})_{29}$ (t_R =16.78 min) from the LC-MS analysis of a DCL made from **2**. $(\mathbf{2})_{29}$:m/z calculated:, 2067.62 $[M+4H]^{4+}$; m/z observed: 2067.82 $[M+4H]^{4+}$.

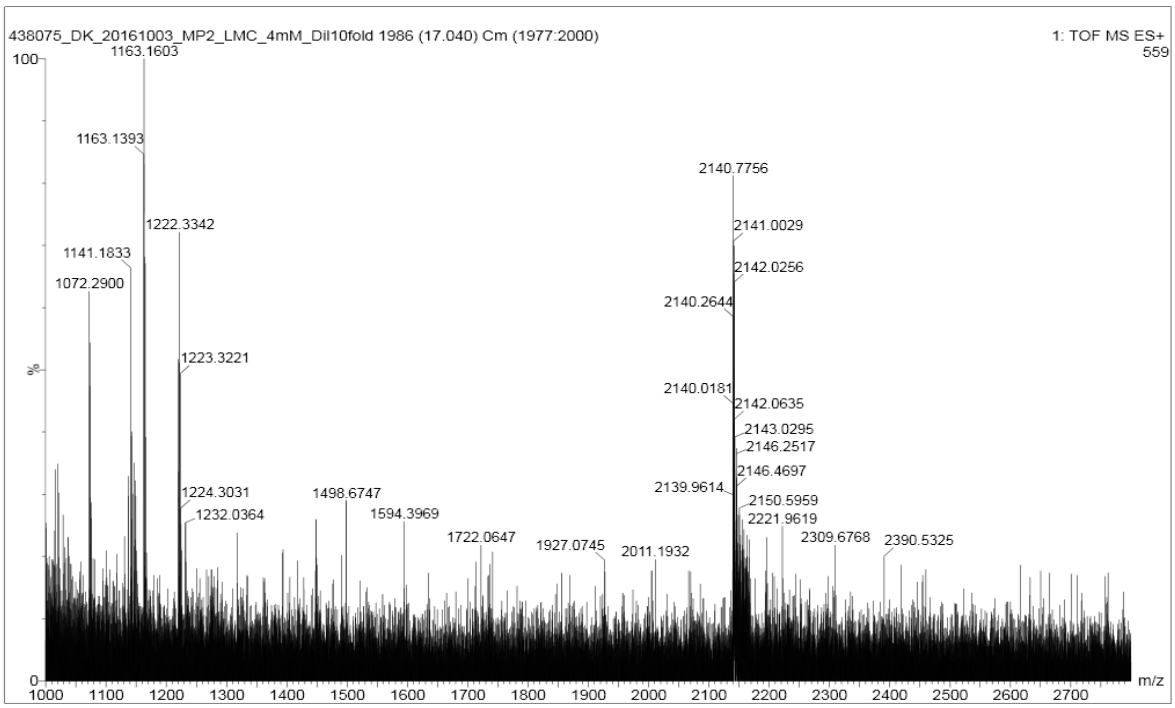

Figure S 63. Mass spectrum of $(\mathbf{2})_{30}$ (t_R =17.04 min) from the LC-MS analysis of a DCL made from **2**. $(\mathbf{2})_{30}$:m/z calculated:, 2138.88 $[M+4H]^{4+}$; m/z observed: 2139.01 $[M+4H]^{4+}$.

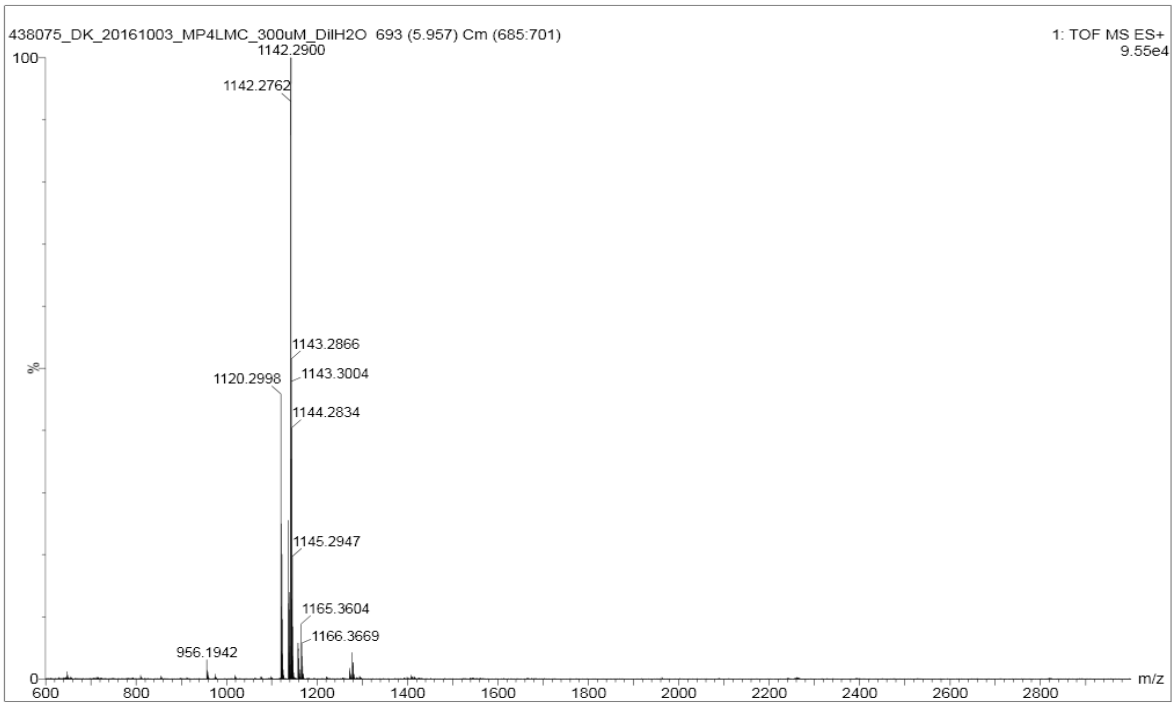

Figure S 64. Mass spectrum of $(\mathbf{3})_3$ (t_R =5.96 min) from the LC-MS analysis of a DCL made from **3**. $(\mathbf{3})_3$:m/z calculated: 1120.31 $[M+H]^+$, 1142.30 $[M+Na]^+$; m/z observed: 1120.30 $[M+H]^+$, 1142.29 $[M+Na]^+$.

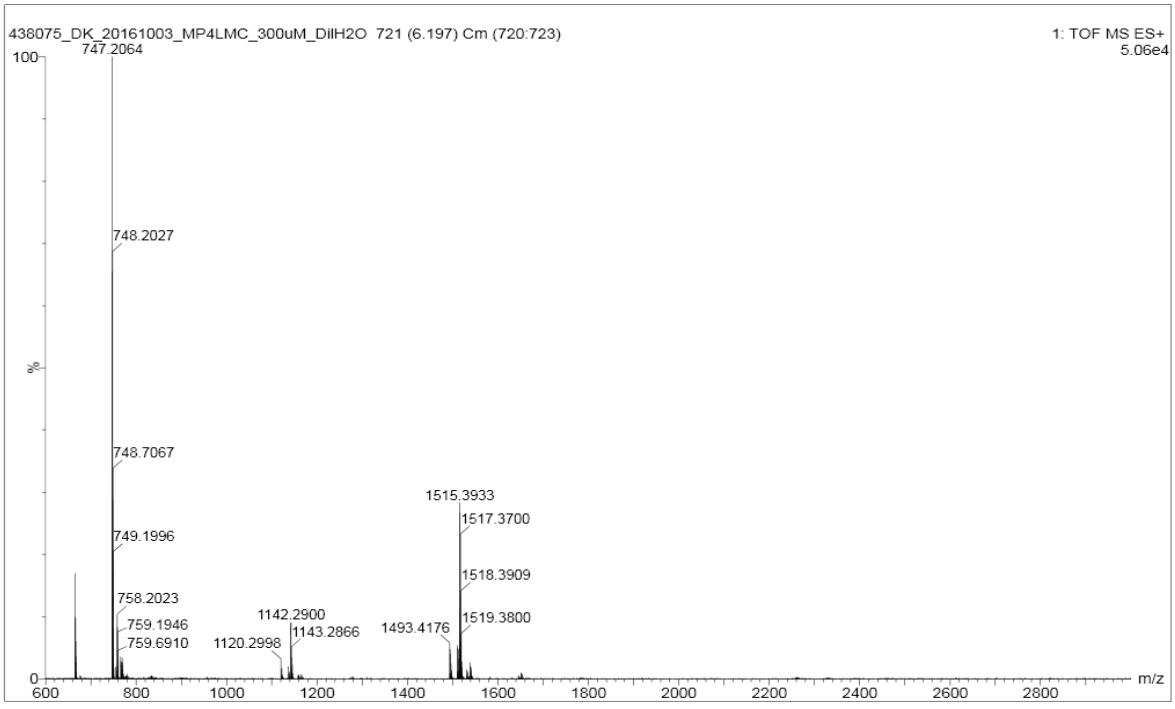

Figure S 65. Mass spectrum of $(\mathbf{3})_4$ (t_R =6.20 min) from the LC-MS analysis of a DCL made from **3**. $(\mathbf{3})_4$:m/z calculated: 1515.40 $[M+Na]^+$, 747.21 $[M+2H]^{2+}$; m/z observed: 1515.39 $[M+Na]^+$, 747.21 $[M+2H]^{2+}$.

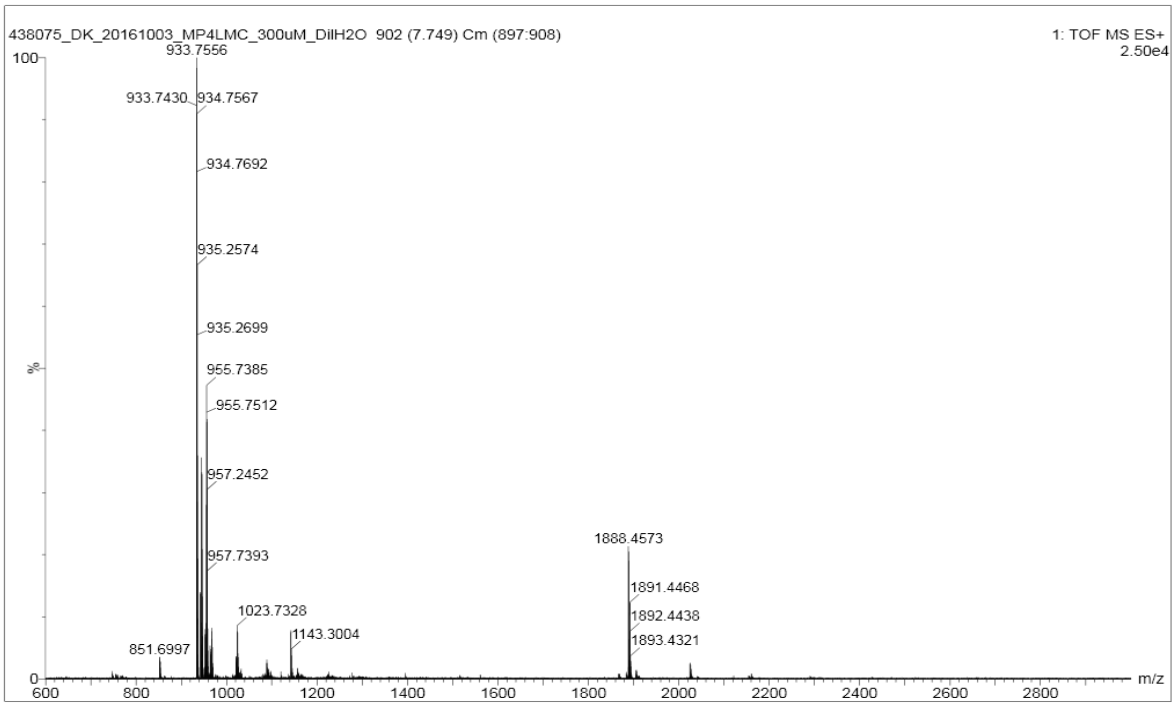

Figure S 66. Mass spectrum of $(\mathbf{3})_5$ (t_R =7.75 min) from the LC-MS analysis of a DCL made from **3**.
$(\mathbf{3})_5$:m/z calculated: 1888.50 $[M+Na]^+$, 933.76 $[M+2H]^{2+}$; m/z observed: 1888.46 $[M+Na]^+$, 933.75 $[M+2H]^{2+}$.

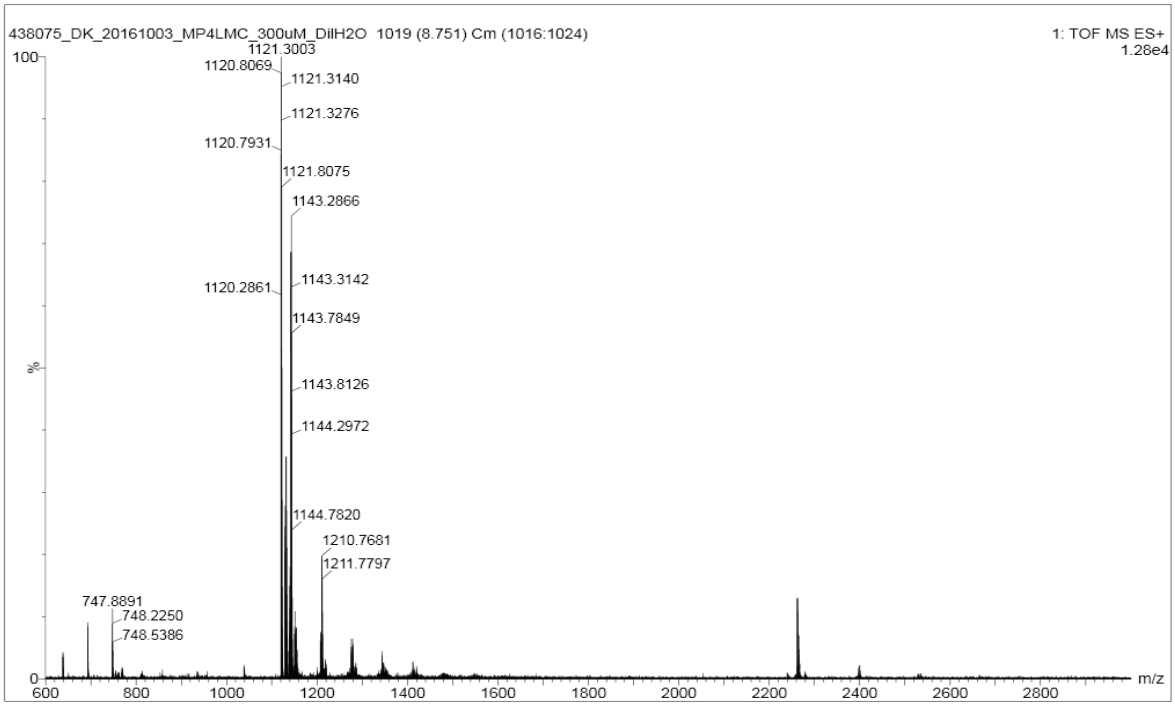

Figure S 67. Mass spectrum of $(\mathbf{3})_6$ (t_R =8.75 min) from the LC-MS analysis of a DCL made from **3**.
$(\mathbf{3})_6$:m/z calculated: 1142.30 $[M+2Na]^{2+}$, 1120.31 $[M+2H]^{2+}$; m/z observed: 1142.29 $[M+2Na]^{2+}$, 1120.29 $[M+2H]^{2+}$.

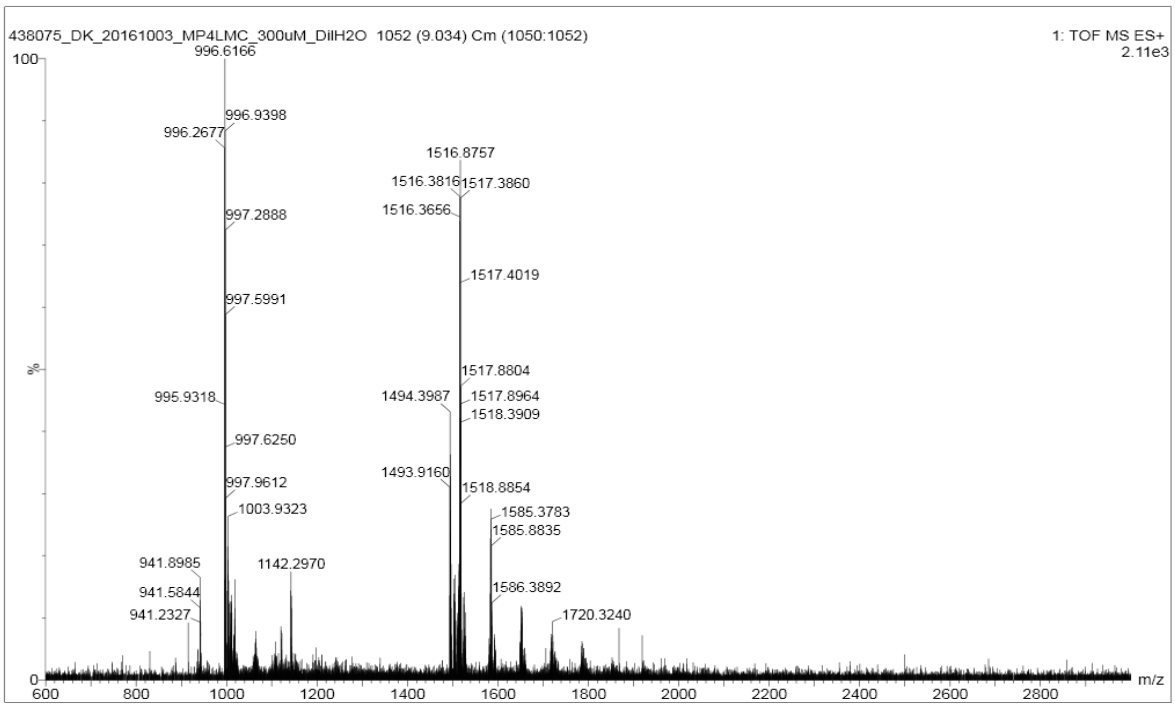

Figure S 68. Mass spectrum of $(\mathbf{3})_8$ (t_R =9.03 min) from the LC-MS analysis of a DCL made from **3**.
$(\mathbf{3})_8$**:** m/z calculated: 1515.40 $[M+2Na]^{2+}$, 995.95 $[M+3H]^{3+}$; m/z observed: 1515.36 $[M+2Na]^{2+}$, 995.93 $[M+3H]^{3+}$.

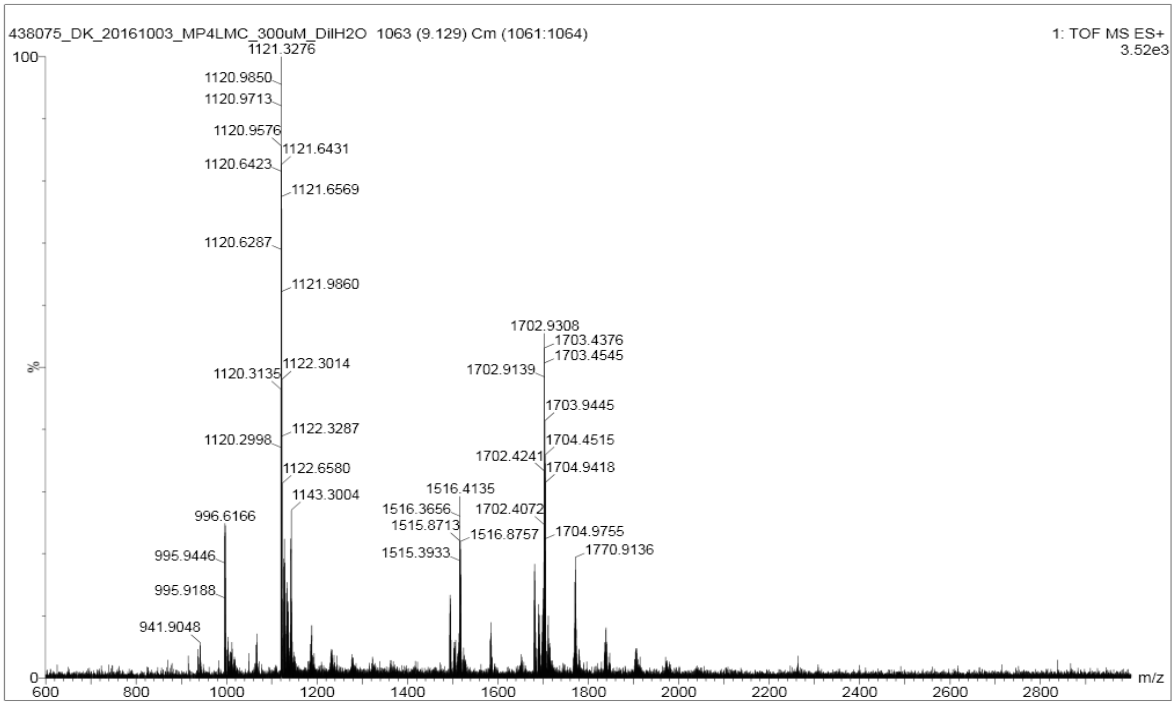

Figure S 69. Mass spectrum of $(\mathbf{3})_9$ (t_R =9.13 min) from the LC-MS analysis of a DCL made from **3**.
$(\mathbf{3})_9$**:** m/z calculated: 1701.95 $[M+2Na]^{2+}$, 1120.31 $[M+3H]^{3+}$;m/z observed: 1701.94 $[M+2Na]^{2+}$, 1120.31 $[M+3H]^{3+}$.

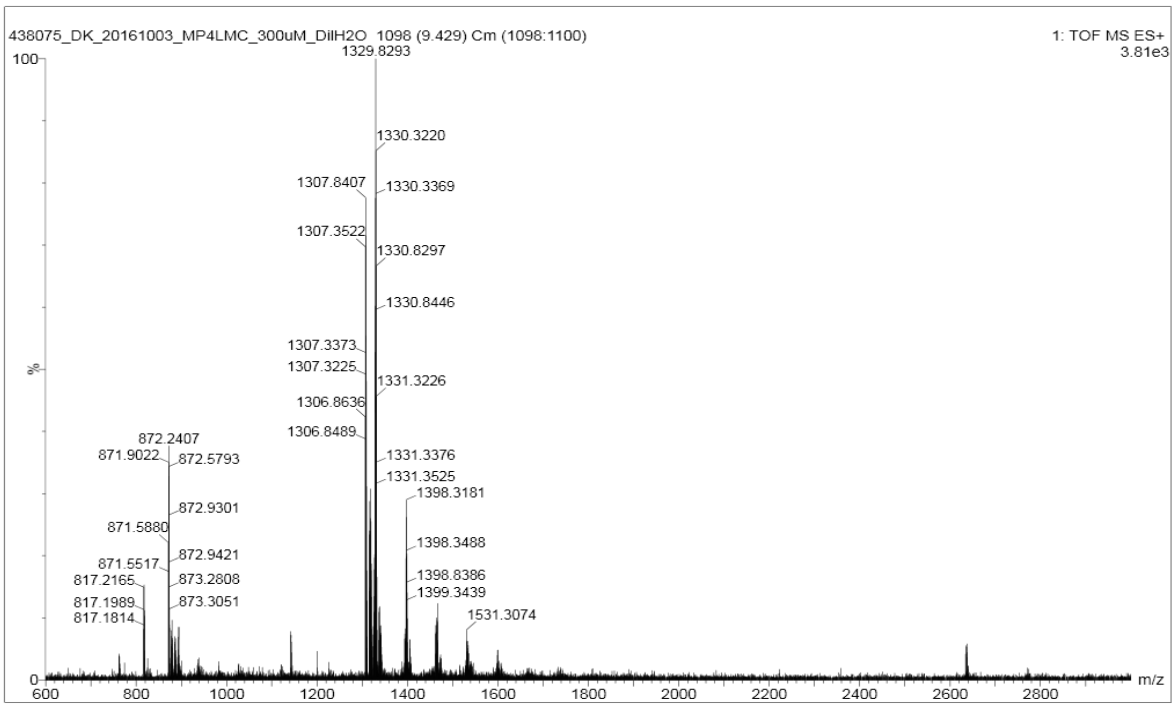

Figure S 70. Mass spectrum of $(\mathbf{3})_7$ (t_R =9.43 min) from the LC-MS analysis of a DCL made from **3**.
$(\mathbf{3})_7$ **:** m/z calculated: 1306.86 $[M+2H]^{2+}$, 871.58 $[M+3H]^{3+}$;m/z observed: 1306.85 $[M+2H]^{2+}$, 871.59 $[M+3H]^{3+}$.

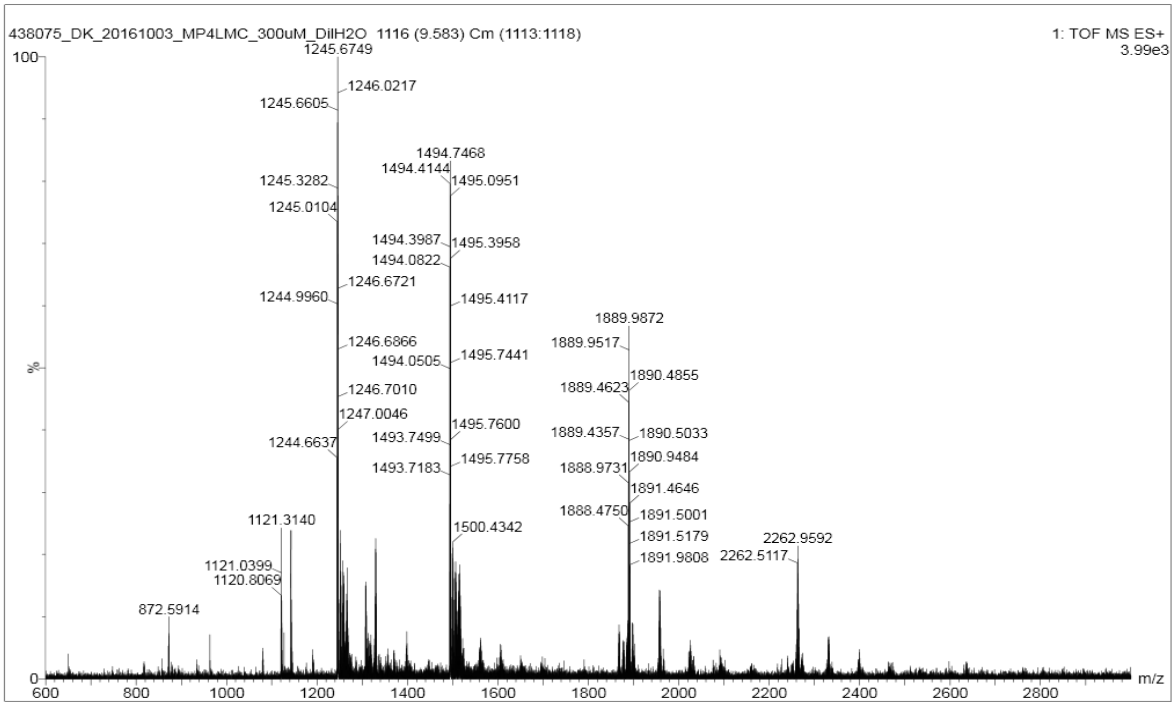

Figure S 71. Mass spectrum of $(\mathbf{3})_{10}$ and $(\mathbf{3})_{12}$ (t_R =9.58 min) from the LC-MS analysis of a DCL made from **3**.
$(\mathbf{3})_{10}$ **:** m/z calculated: 1888.50 $[M+2Na]^{2+}$, 1244.68 $[M+3H]^{3+}$;m/z observed: 1888.48 $[M+2Na]^{2+}$, 1244.66 $[M+3H]^{3}$.
$(\mathbf{3})_{12}$ **:** m/z calculated: 2261.61 $[M+2Na]^{2+}$, 1493.42 $[M+3H]^{3+}$;m/z observed: 2261.42 $[M+2Na]^{2+}$, 1493.42 $[M+3H]^{3}$.

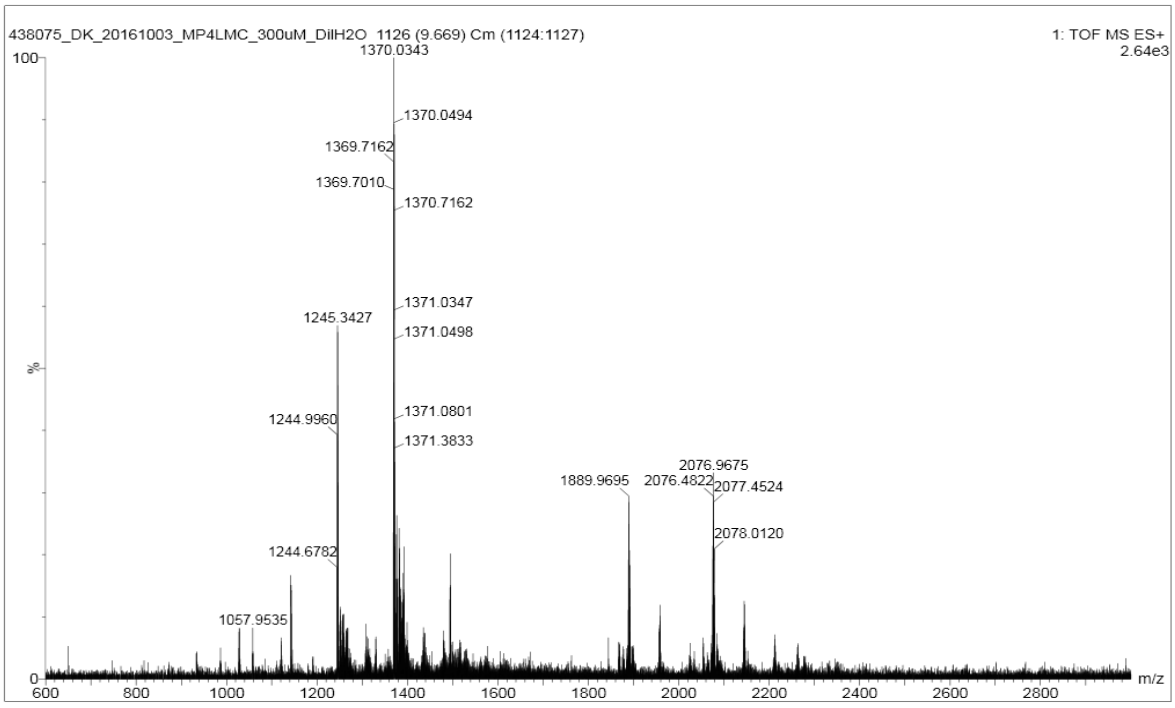

Figure S 72. Mass spectrum of $(\mathbf{3})_{11}$ (t_R =9.67 min) from the LC-MS analysis of a DCL made from **3**. $(\mathbf{3})_{11}$**:**m/z calculated: 2075.05 $[M+2Na]^{2+}$, 1369.05 $[M+3H]^{3+}$; m/z observed: 2075.05 $[M+2Na]^{2+}$, 1369.03 $[M+3H]^{3+}$.

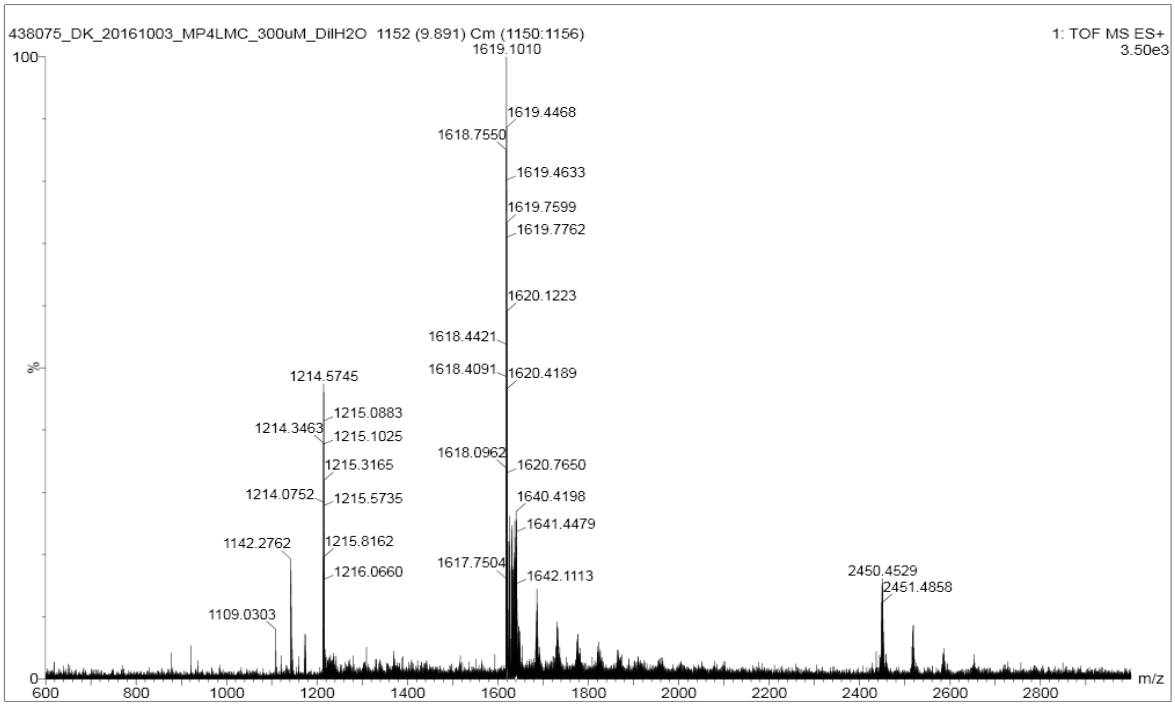

Figure S 73. Mass spectrum of $(\mathbf{3})_{13}$ (t_R =9.89 min) from the LC-MS analysis of a DCL made from **3**. $(\mathbf{3})_{13}$: m/z calculated: 1617.78 $[M+3H]^{3+}$, 1213.59 $[M+4H]^{4+}$; m/z observed: 1617.75 $[M+3H]^{3+}$, 1213.55 $[M+4H]^{4+}$.

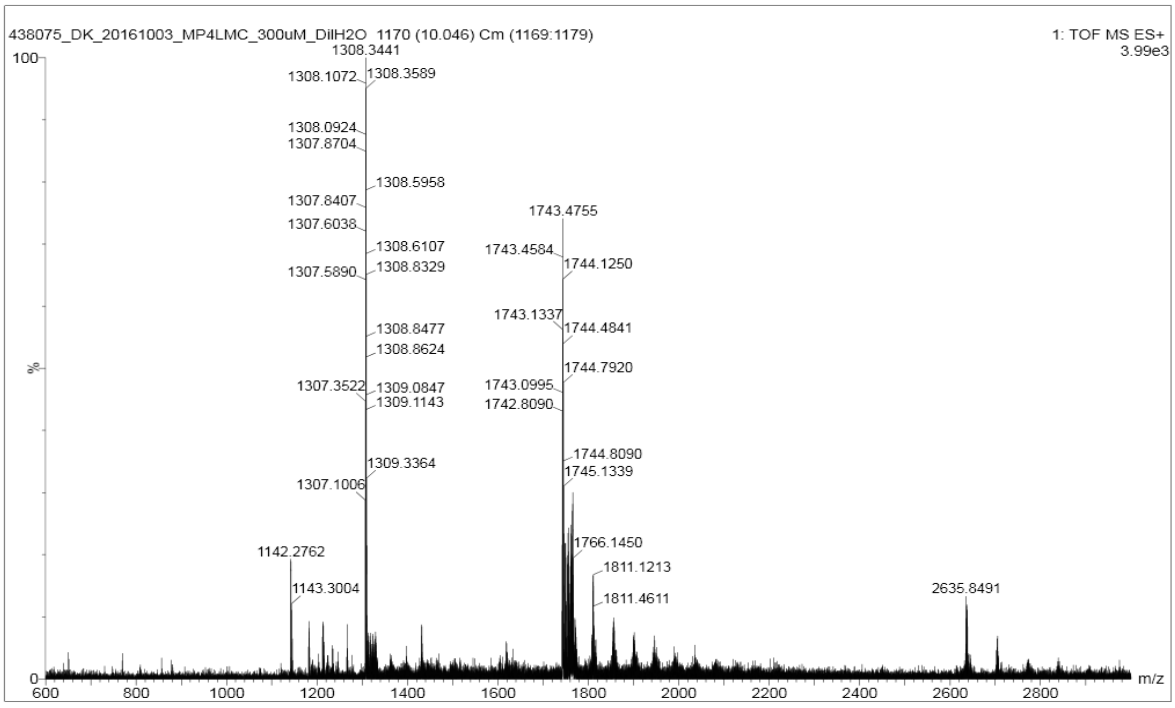

Figure S 74. Mass spectrum of $(\mathbf{3})_{14}$ (t_R =10.05 min) from the LC-MS analysis of a DCL made from **3**.
$(\mathbf{3})_{14}$: m/z calculated: 1742.15 $[M+3H]^{3+}$, 1306.86 $[M+4H]^{4+}$; m/z observed: 1742.13 $[M+3H]^{3+}$, 1306.86 $[M+4H]^{4+}$.

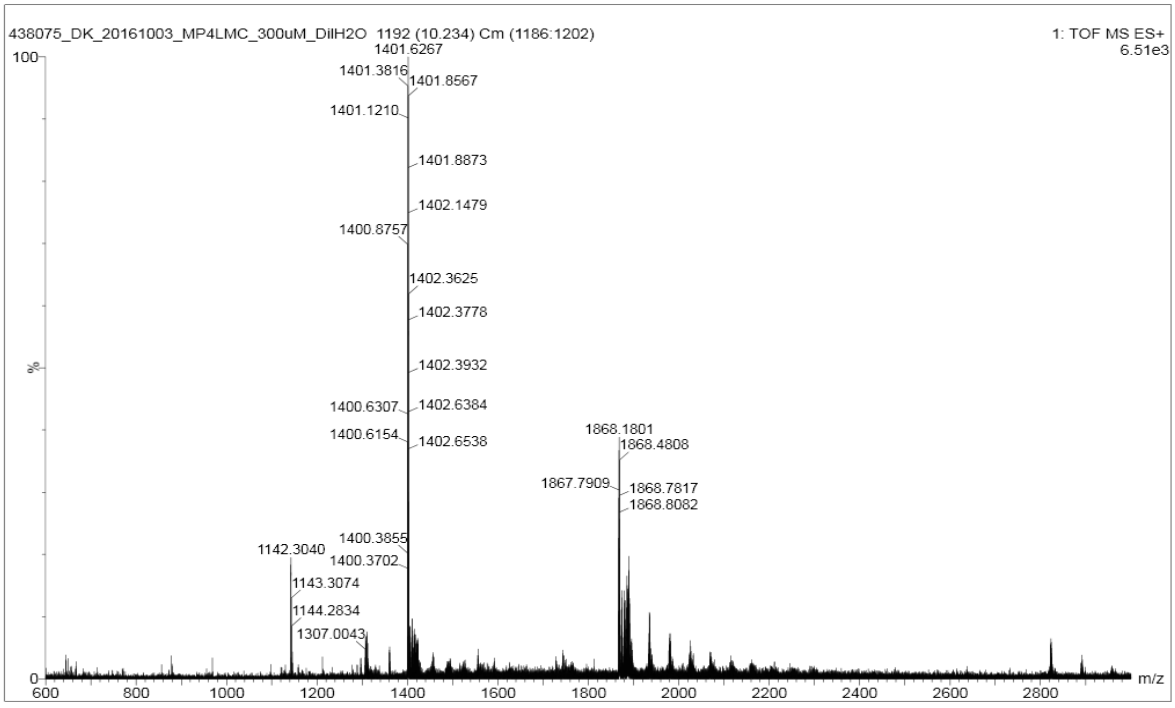

Figure S 75. Mass spectrum of $(\mathbf{3})_{15}$ (t_R =10.23 min) from the LC-MS analysis of a DCL made from **3**.
$(\mathbf{3})_{15}$: m/z calculated: 1866.52 $[M+3H]^{3+}$, 1400.14 $[M+4H]^{4+}$; m/z observed: 1866.50 $[M+3H]^{3+}$, 1400.11 $[M+4H]^{4+}$.

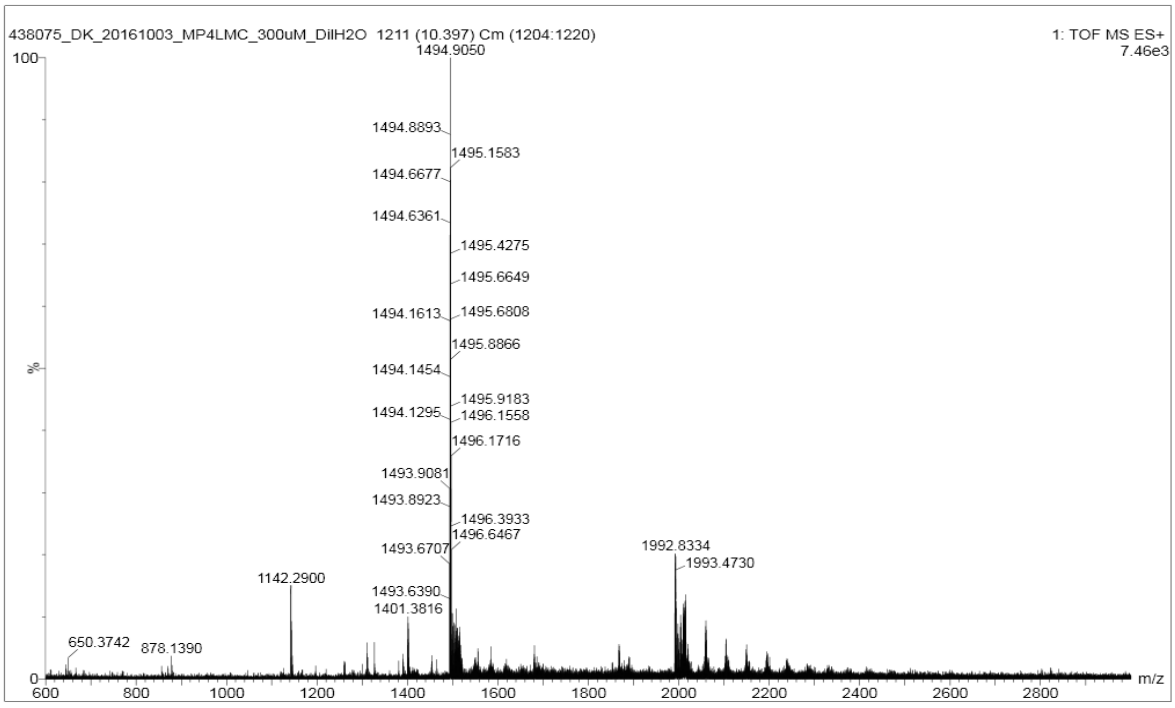

Figure S 76. Mass spectrum of $(\mathbf{3})_{16}$ (t_R =10.40 min) from the LC-MS analysis of a DCL made from **3**.
$(\mathbf{3})_{16}$: m/z calculated: 1990.88 $[M+3H]^{3+}$, 1493.42 $[M+4H]^{4+}$; m/z observed: 1990.81 $[M+3H]^{3+}$, 1493.42 $[M+4H]^{4+}$.

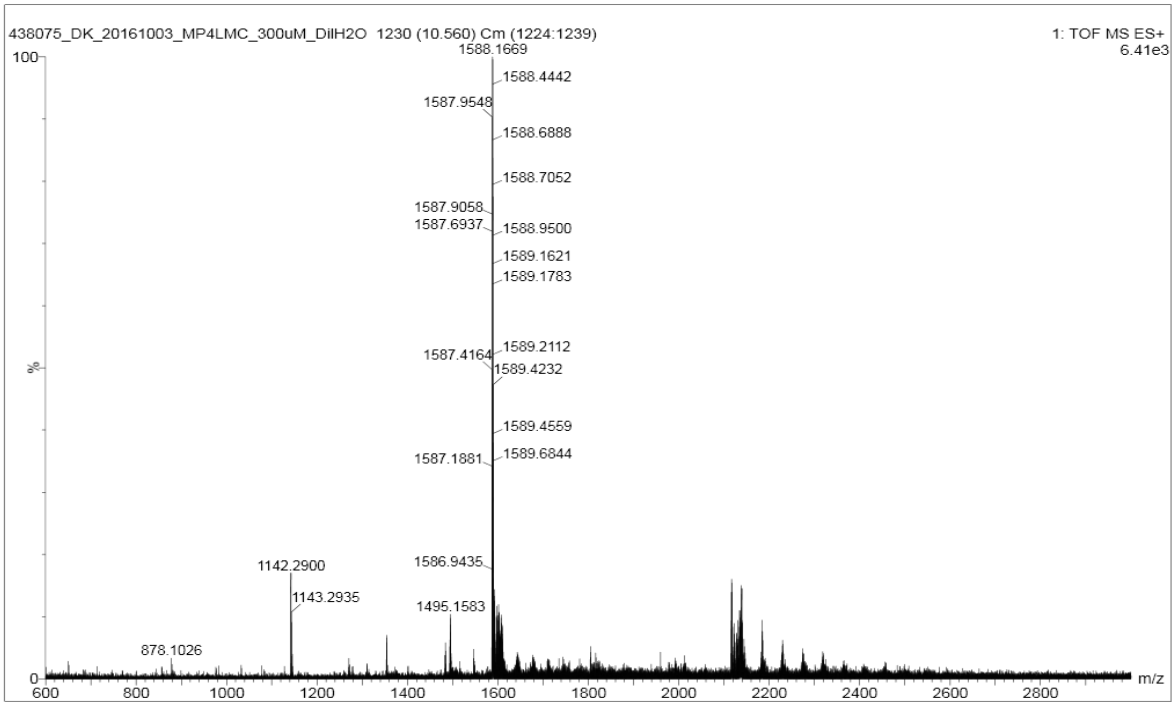

Figure S 77. Mass spectrum of $(\mathbf{3})_{17}$ (t_R =10.56 min) from the LC-MS analysis of a DCL made from **3**.
$(\mathbf{3})_{17}$: m/z calculated: 2115.25 $[M+3H]^{3+}$, 1586.69 $[M+4H]^{4+}$; m/z observed: 2115.17 $[M+3H]^{3+}$, 1586.70 $[M+4H]^{4+}$.

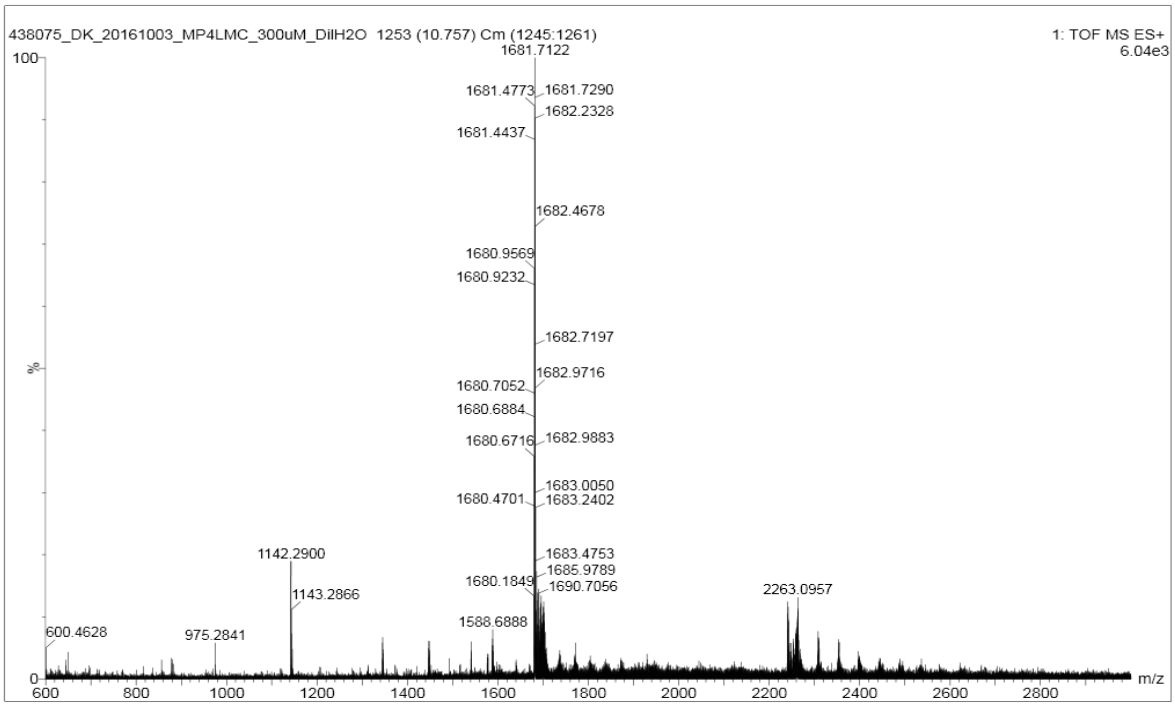

Figure S 78. Mass spectrum of $(\mathbf{3})_{18}$ (t_R =10.76 min) from the LC-MS analysis of a DCL made from **3**.
$(\mathbf{3})_{18}$: m/z calculated: 2239.62 $[M+3H]^{3+}$, 1679.97 $[M+4H]^{4+}$; m/z observed: 2239.77 $[M+3H]^{3+}$, 1679.95 $[M+4H]^{4+}$.

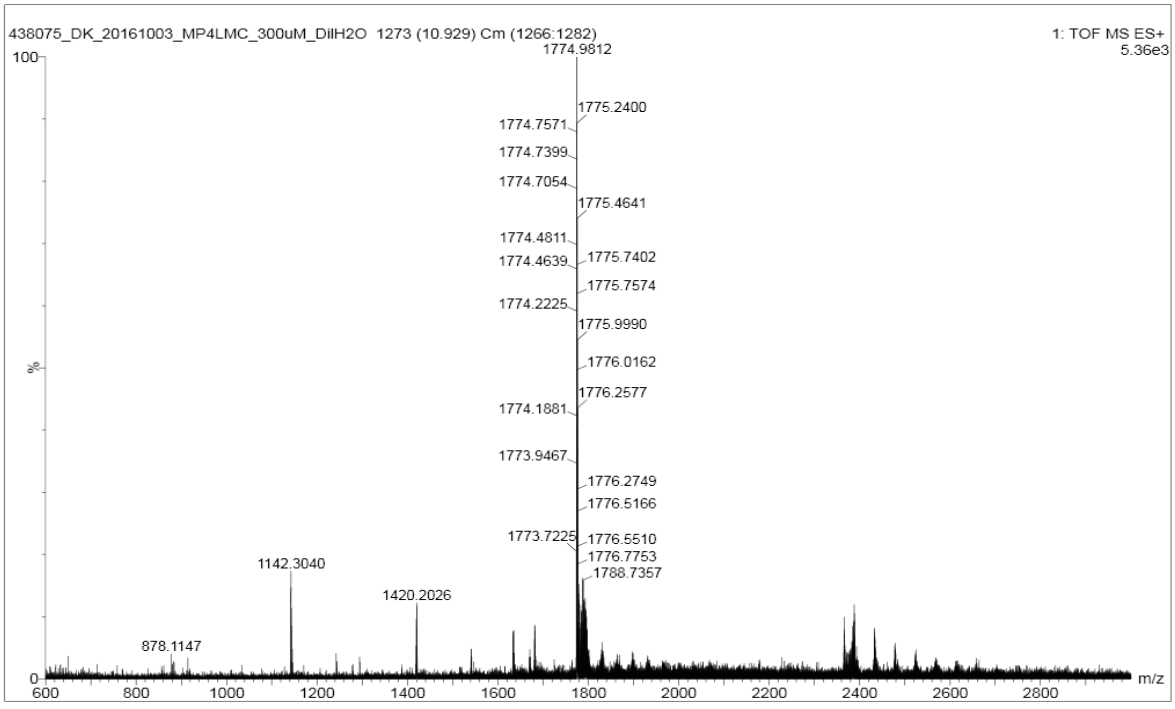

Figure S 79. Mass spectrum of $(\mathbf{3})_{19}$ (t_R =10.93 min) from the LC-MS analysis of a DCL made from **3**.
$(\mathbf{3})_{19}$: m/z calculated: 1773.24 $[M+4H]^{4+}$; m/z observed: 1773.22 $[M+4H]^{4+}$.

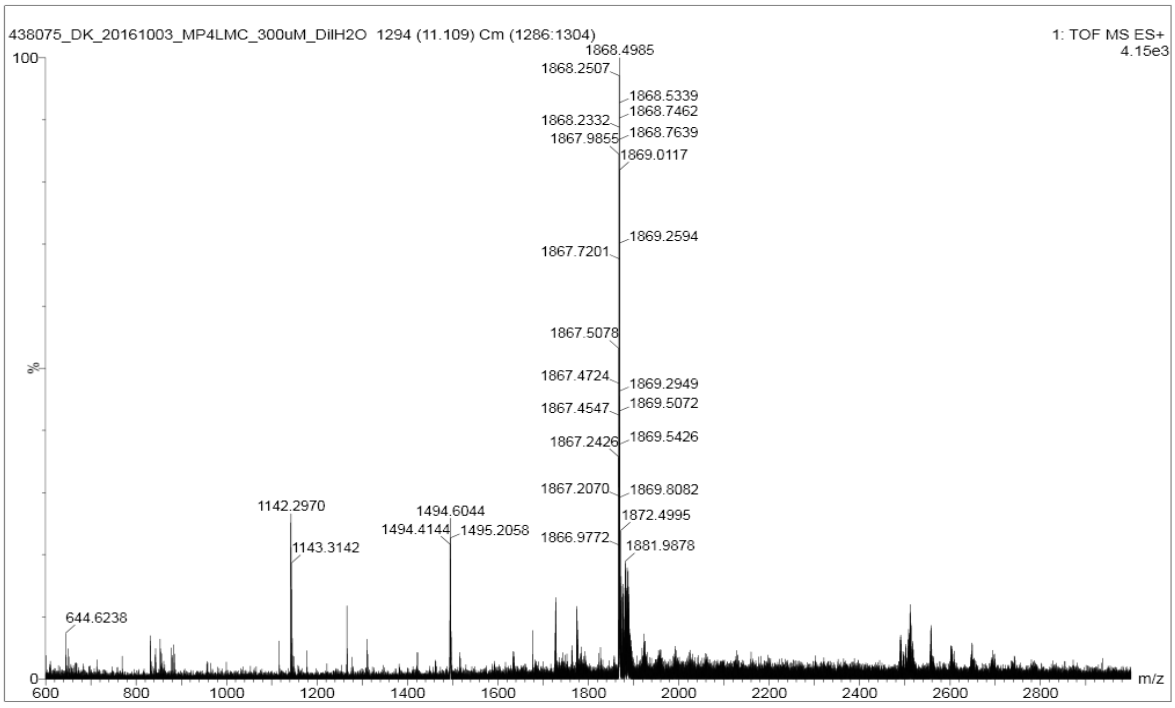

Figure S 80. Mass spectrum of $(\mathbf{3})_{20}$ (t_R =11.11 min) from the LC-MS analysis of a DCL made from **3**.
$(\mathbf{3})_{20}$: m/z calculated: 1866.52 $[M+4H]^{4+}$; m/z observed: 1866.52 $[M+4H]^{4+}$.

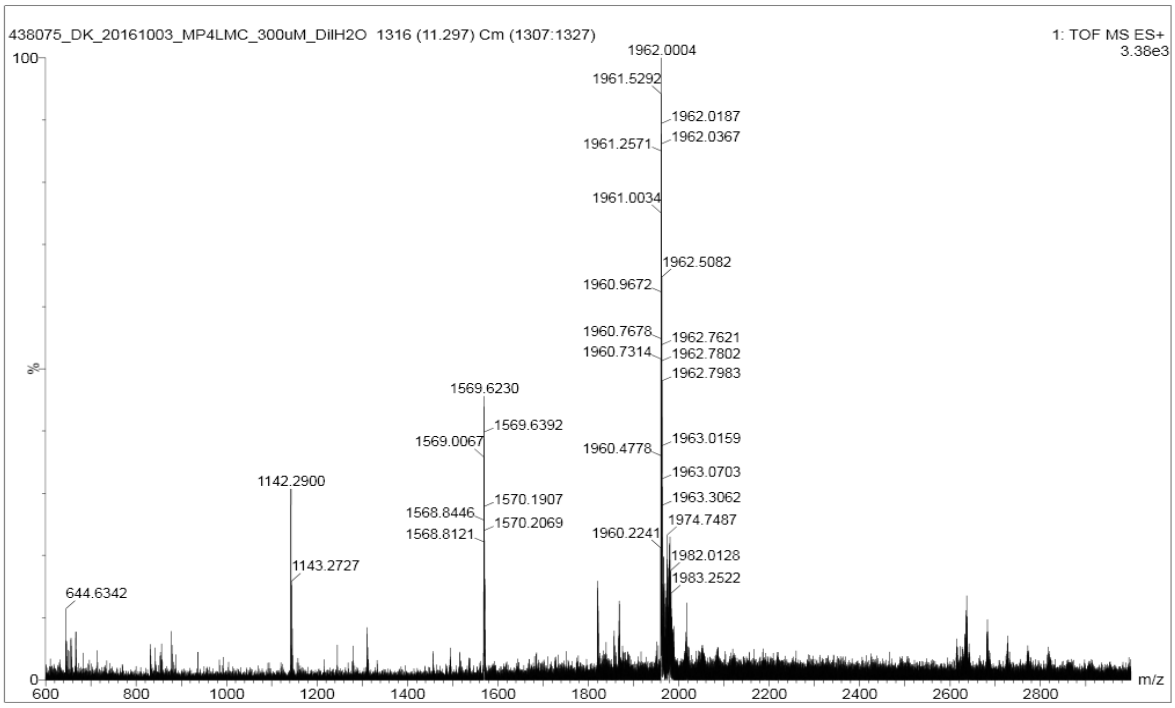

Figure S 81**.** Mass spectrum of $(\mathbf{3})_{21}$ (t_R =11.23 min) from the LC-MS analysis of a DCL made from **3**.
$(\mathbf{3})_{21}$: m/z calculated: 1959.79 $[M+4H]^{4+}$, 1568.03 $[M+5H]^{5+}$; m/z observed: 1959.73 $[M+4H]^{4+}$, 1568.07 $[M+5H]^{5+}$.

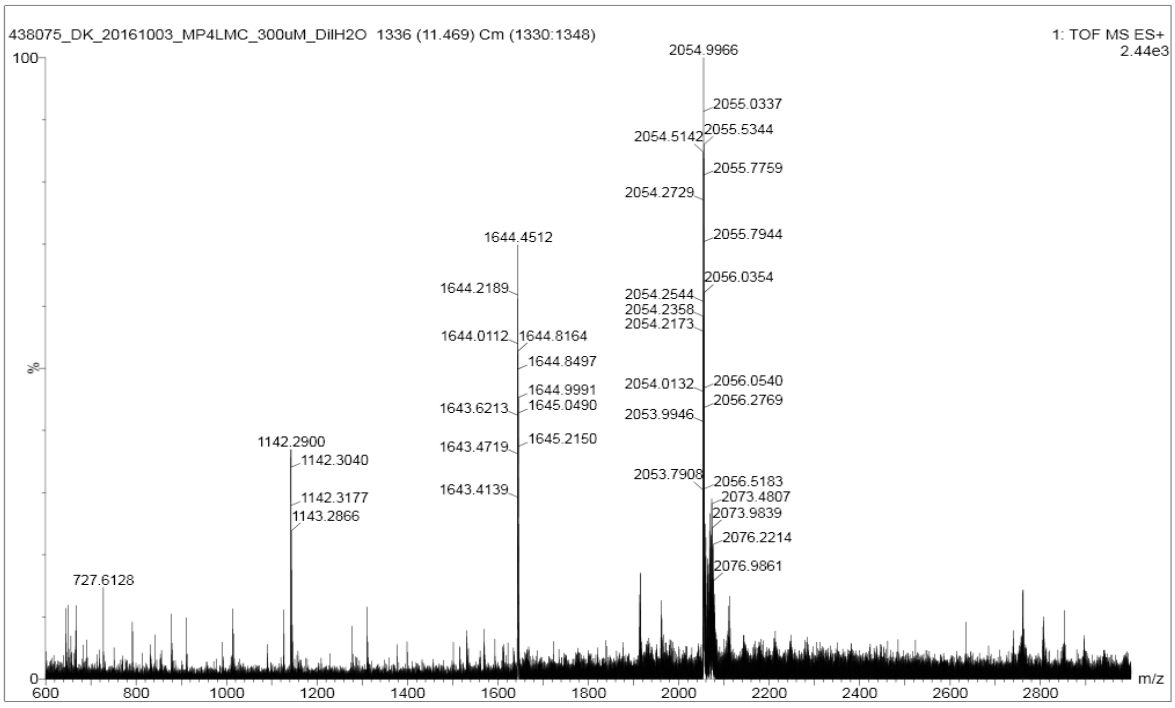

Figure S 82. Mass spectrum of $(\mathbf{3})_{22}$ (t_R =11.47 min) from the LC-MS analysis of a DCL made from **3**.
$(\mathbf{3})_{22}$: m/z calculated: 2053.07 $[M+4H]^{4+}$, 1642.66 $[M+5H]^{5+}$; m/z observed: 2052.98 $[M+4H]^{4+}$, 1642.63 $[M+5H]^{5+}$.

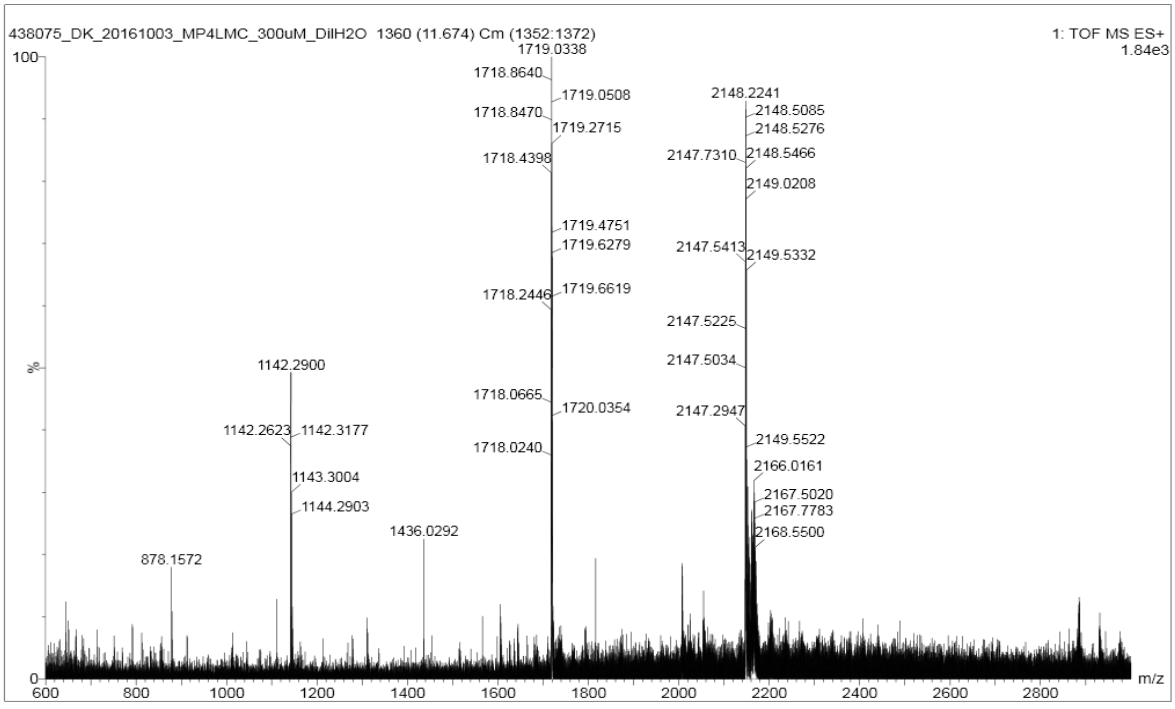

Figure S 83. Mass spectrum of $(\mathbf{3})_{23}$ (t_R =11.67 min) from the LC-MS analysis of a DCL made from **3**.
$(\mathbf{3})_{23}$: m/z calculated: 2146.34 $[M+4H]^{4+}$, 1717.28 $[M+5H]^{5+}$; m/z observed: 2146.26 $[M+4H]^{4+}$, 1717.24 $[M+5H]^{5+}$.

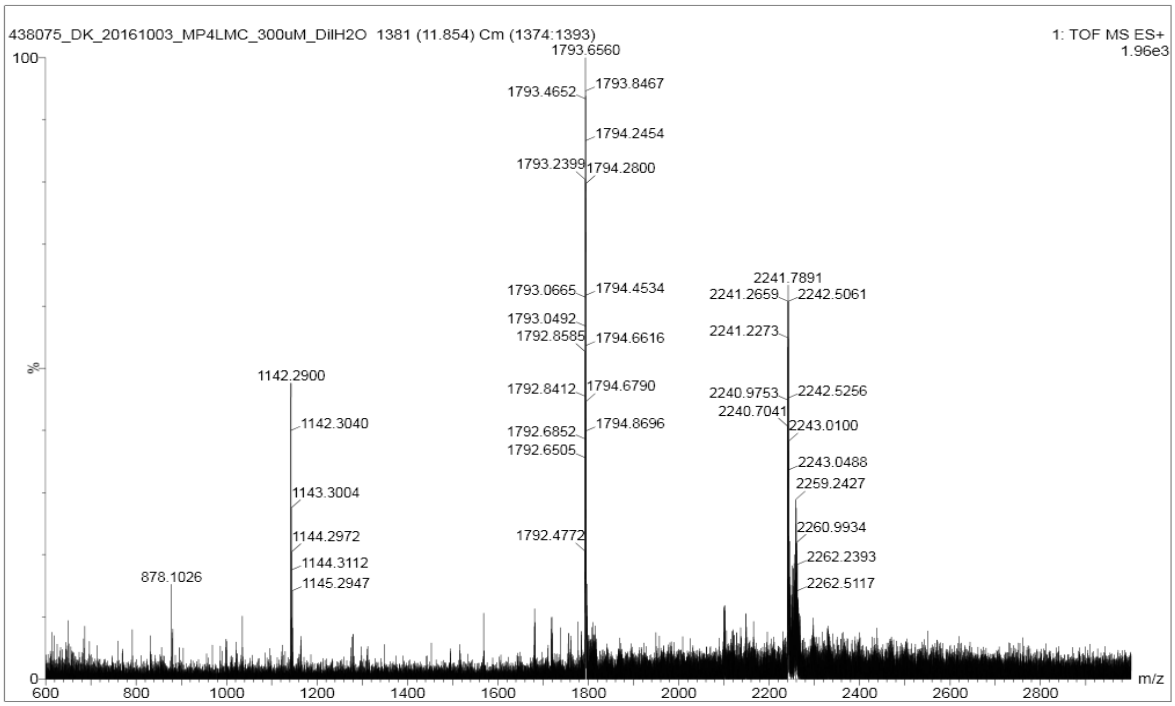

Figure S 84. Mass spectrum of $(\mathbf{3})_{24}$ (t_R =11.85 min) from the LC-MS analysis of a DCL made from **3**.
$(\mathbf{3})_{24}$: m/z calculated: 2239.62 $[M+4H]^{4+}$, 1791.90 $[M+5H]^{5+}$; m/z observed: 2239.76 $[M+4H]^{4+}$, 1791.88 $[M+5H]^{5+}$.

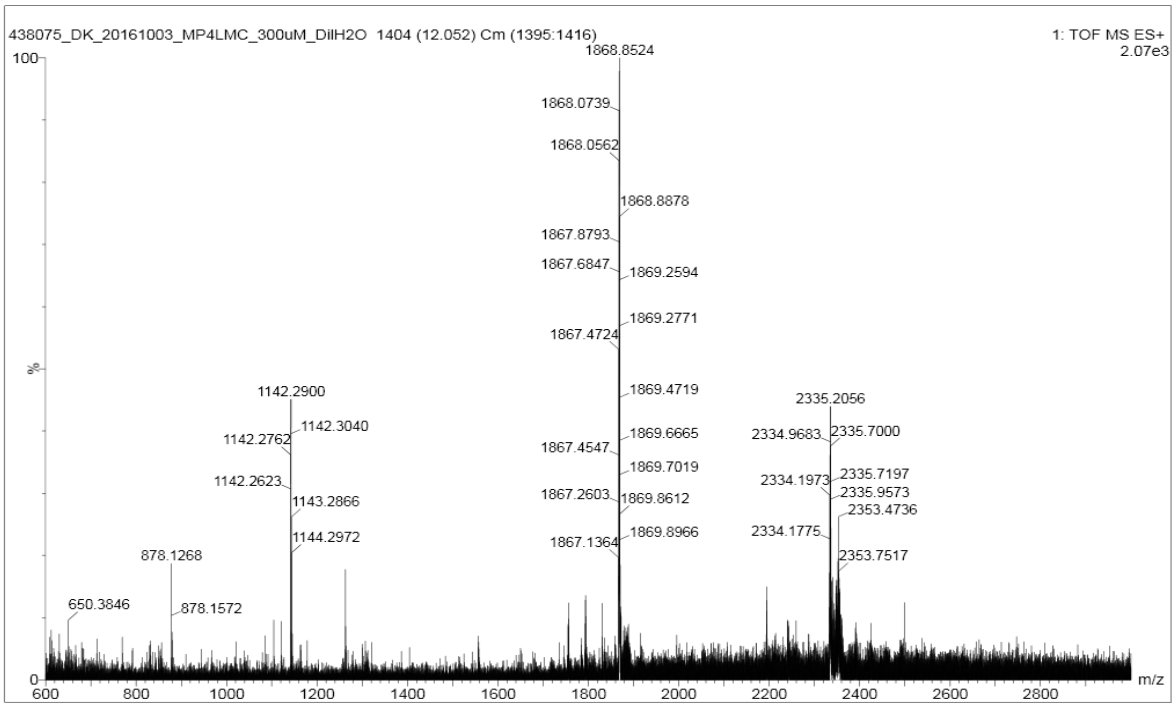

Figure S 85. Mass spectrum of $(\mathbf{3})_{25}$ (t_R =12.05 min) from the LC-MS analysis of a DCL made from **3**.
$(\mathbf{3})_{25}$: m/z calculated: 2332.89 $[M+4H]^{4+}$, 1866.52 $[M+5H]^{5+}$; m/z observed: 2332.85 $[M+4H]^{4+}$, 1866.52 $[M+5H]^{5+}$.

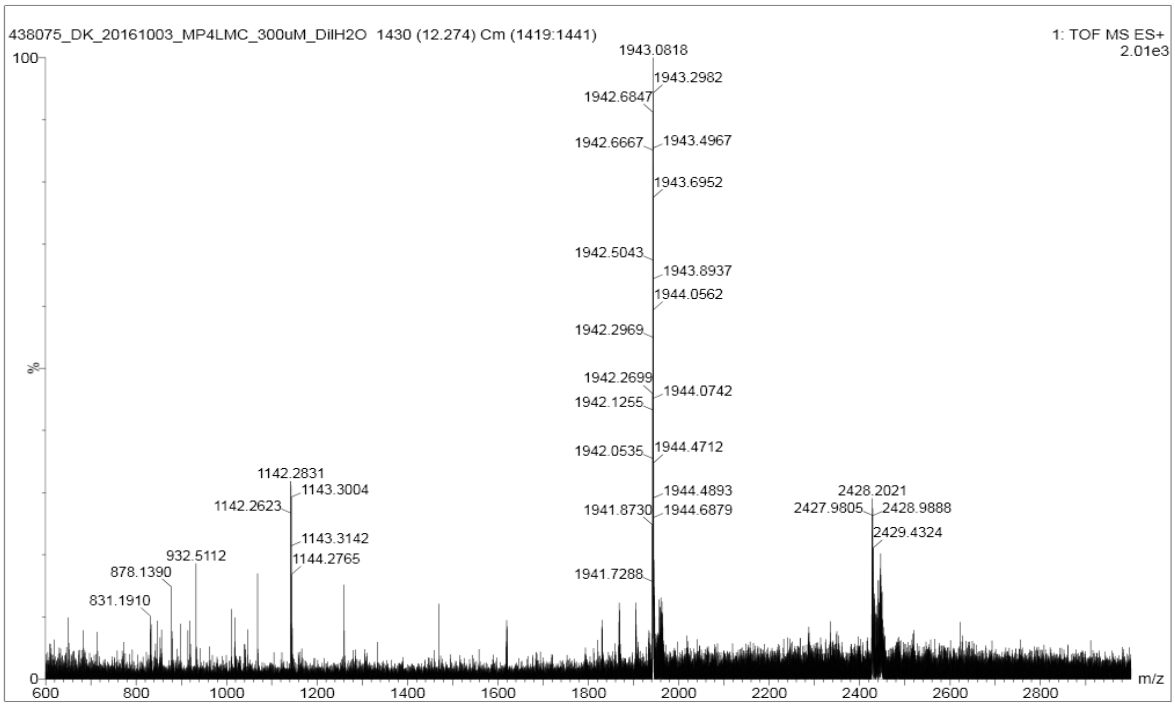

Figure S 86. Mass spectrum of $(\mathbf{3})_{26}$ (t_R =12.27 min) from the LC-MS analysis of a DCL made from **3**. $(\mathbf{3})_{26}$: m/z calculated: 2426.17 $[M+4H]^{4+}$, 1941.37 $[M+5H]^{5+}$; m/z observed: 2426.15 $[M+4H]^{4+}$, 1941.33 $[M+5H]^{5+}$.

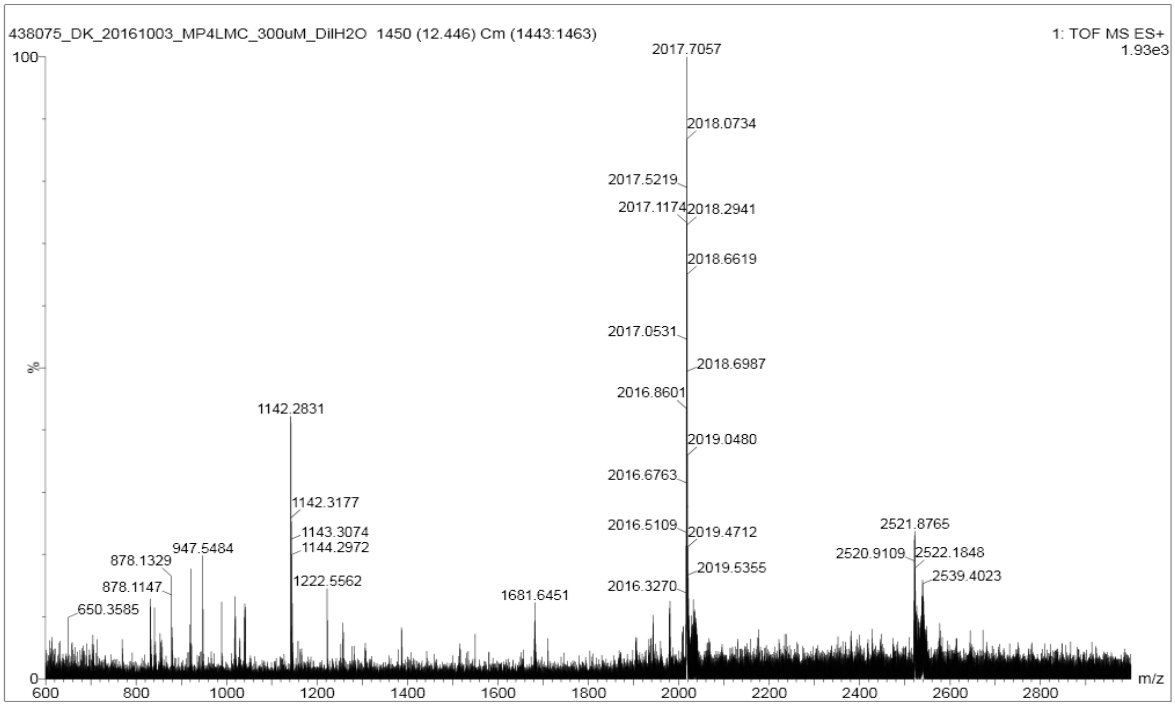

Figure S 87. Mass spectrum of $(\mathbf{3})_{27}$ (t_R =12.45 min) from the LC-MS analysis of a DCL made from **3**. $(\mathbf{3})_{27}$: m/z calculated: 2519.45 $[M+4H]^{4+}$, 2015.76 $[M+5H]^{5+}$; m/z observed: 2519.46 $[M+4H]^{4+}$, 2016.07 $[M+5H]^{5+}$.

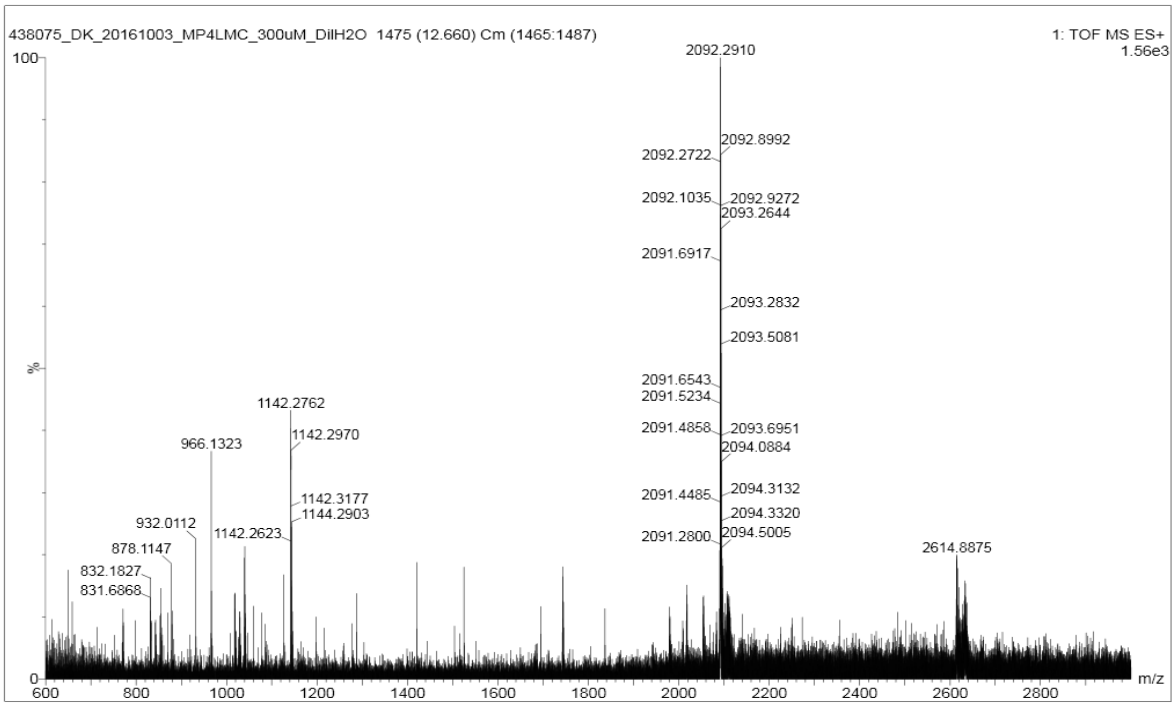

Figure S 88. Mass spectrum of $(\mathbf{3})_{28}$ (t_R =12.67 min) from the LC-MS analysis of a DCL made from **3**. $(\mathbf{3})_{28}$: m/z calculated: 2090.38 $[M+5H]^{5+}$; m/z observed: 2090.55$[M+5H]^{5+}$.

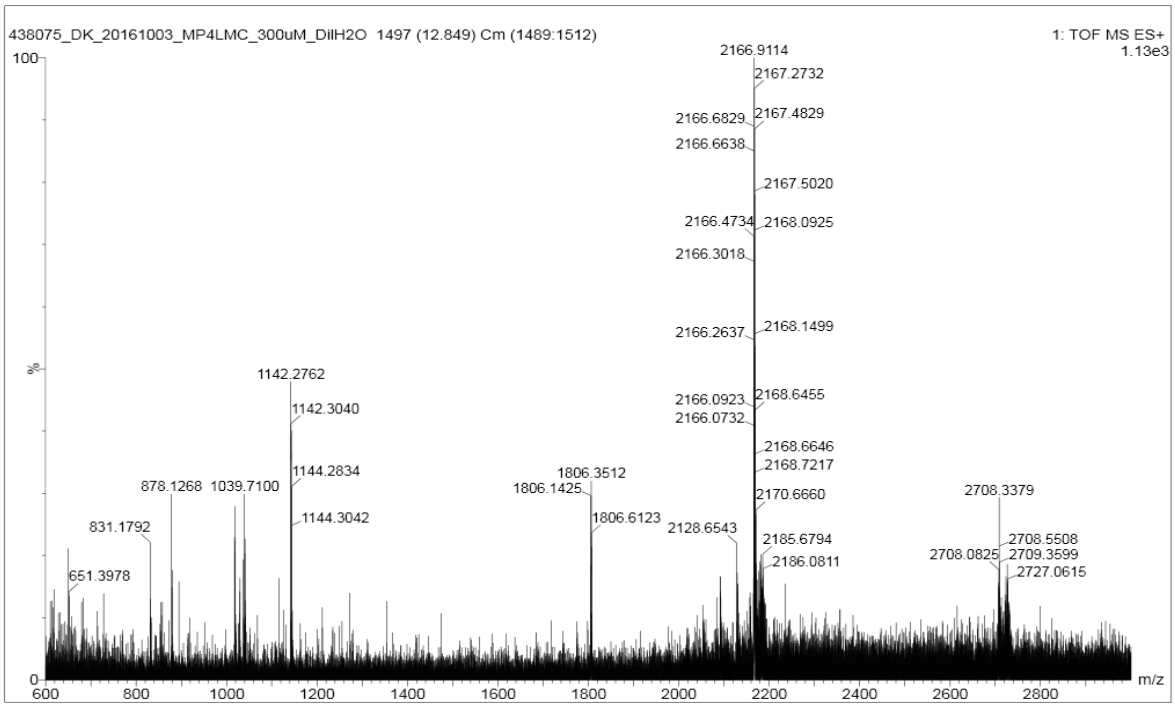

Figure S 89. Mass spectrum of $(\mathbf{3})_{29}$ (t_R =12.85 min) from the LC-MS analysis of a DCL made from **3**. $(\mathbf{3})_{29}$: m/z calculated: 2165.00 $[M+5H]^{5+}$; m/z observed: 2165.31 $[M+5H]^{5+}$.

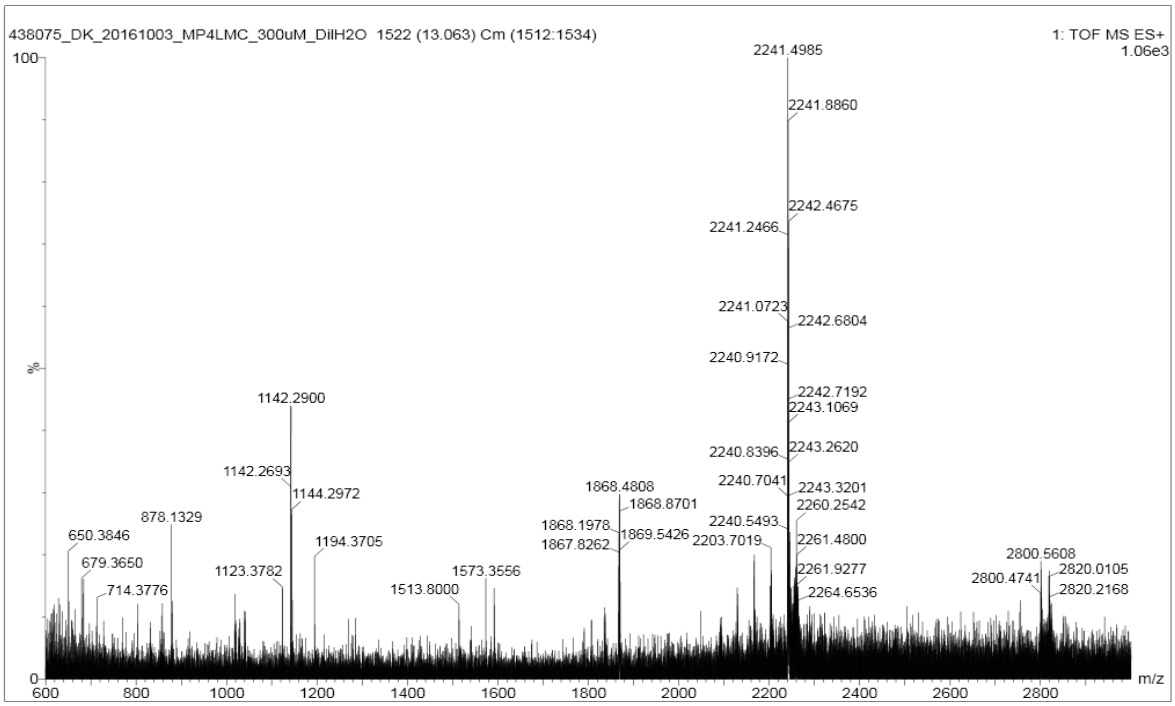

Figure S 90. Mass spectrum of $(\mathbf{3})_{30}$ (t_R =13.06 min) from the LC-MS analysis of a DCL made from **3**. $(\mathbf{3})_{30}$: m/z calculated: 2239.62 $[M+5H]^{5+}$; m/z observed: 2239.92 $[M+5H]^{5+}$.

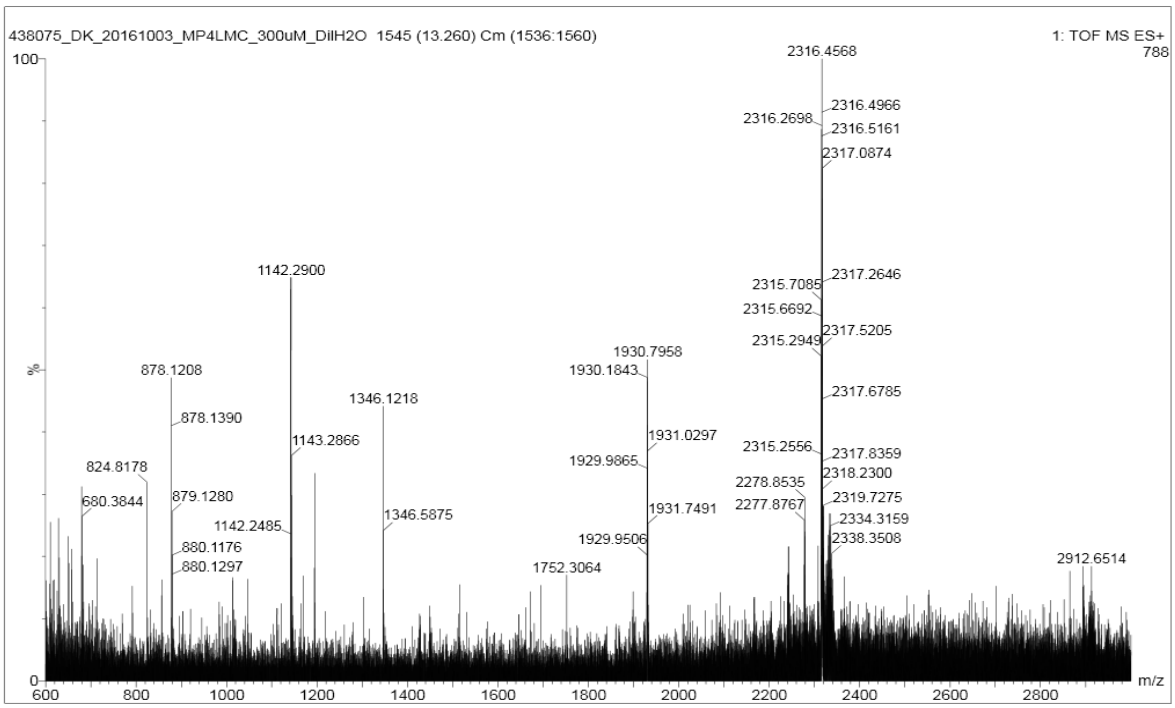

Figure S 91. Mass spectrum of $(\mathbf{3})_{31}$ (t_R =13.26 min) from the LC-MS analysis of a DCL made from **3**. $(\mathbf{3})_{31}$: m/z calculated: 2314.24 $[M+5H]^{5+}$; m/z observed: 2314.74 $[M+5H]^{5+}$.

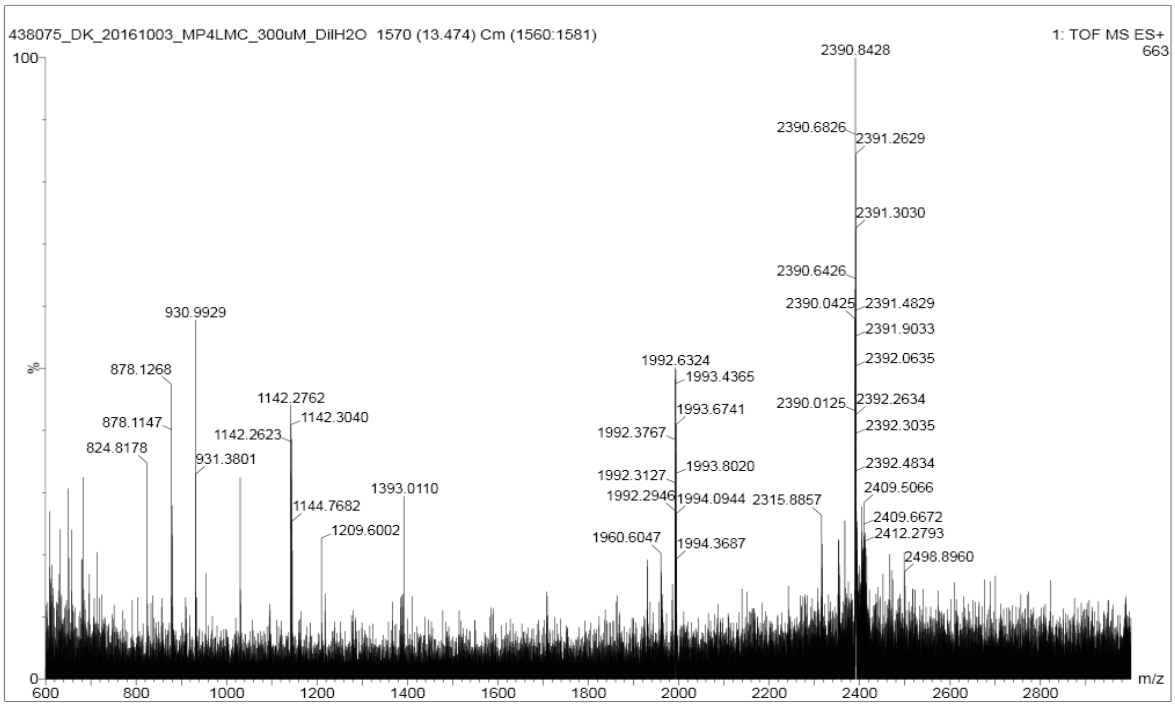

Figure S 92. Mass spectrum of $(\mathbf{3})_{32}$ (t_R =13.47 min) from the LC-MS analysis of a DCL made from **3**. $(\mathbf{3})_{32}$: m/z calculated: 2388.86 $[M+5H]^{5+}$; m/z observed: 2389.24 $[M+5H]^{5+}$.

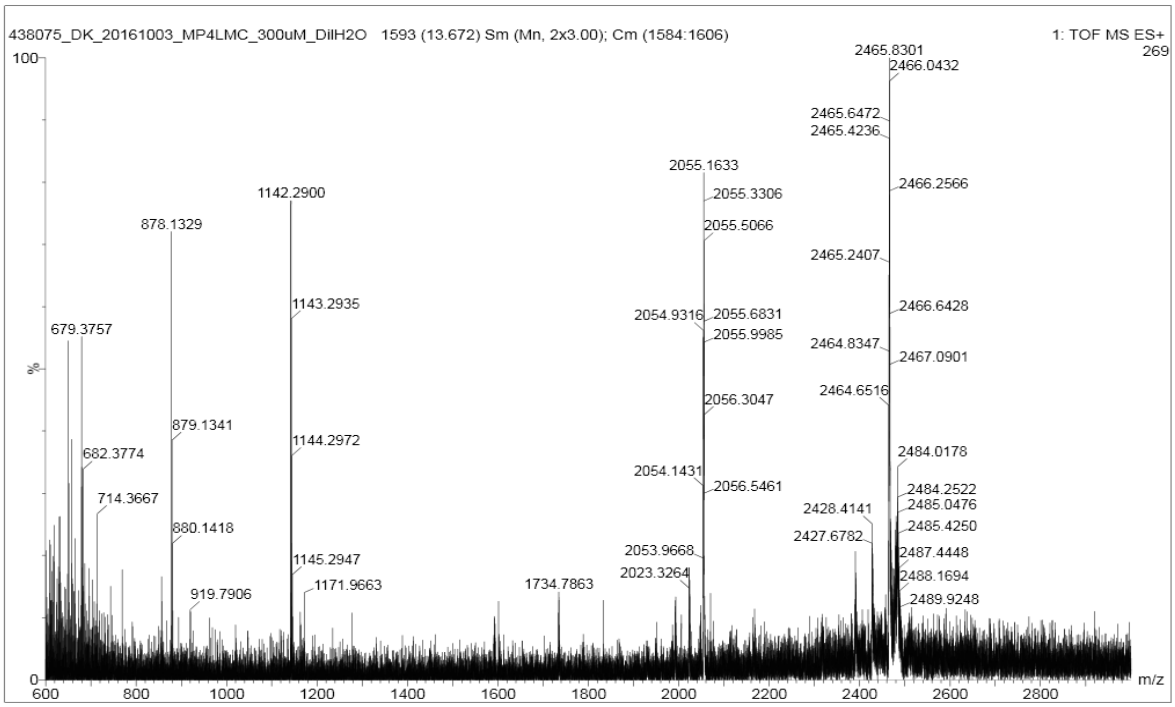

Figure S 93. Mass spectrum of $(\mathbf{3})_{33}$ (t_R =13.67 min) from the LC-MS analysis of a DCL made from **3**. $(\mathbf{3})_{33}$: m/z calculated: 2463.48 $[M+5H]^{5+}$; m/z observed: 2464.03 $[M+5H]^{5+}$.

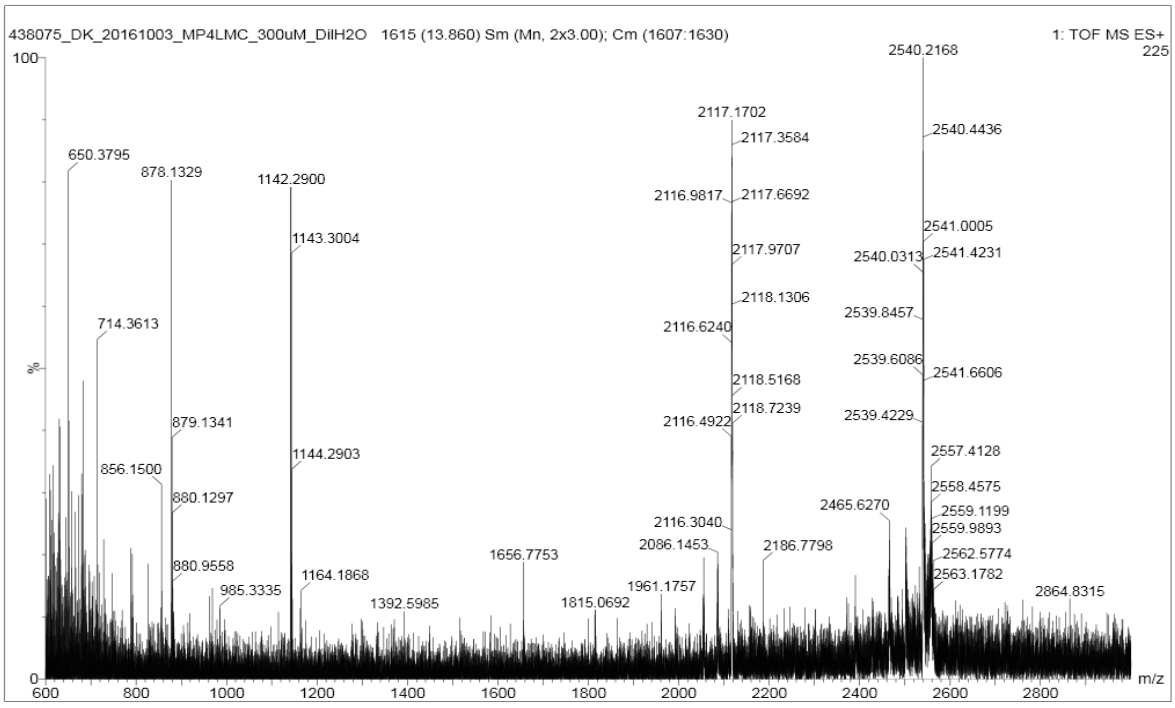

Figure S 94. Mass spectrum of $(\mathbf{3})_{34}$ (t_R =13.86 min) from the LC-MS analysis of a DCL made from **3**.
$(\mathbf{3})_{34}$: m/z calculated: 2115.25 $[M+6H]^{6+}$, 2538.10 $[M+5H]^{5+}$; m/z observed: 2115.80 $[M+6H]^{6+}$, 2538.36 $[M+5H]^{5+}$.

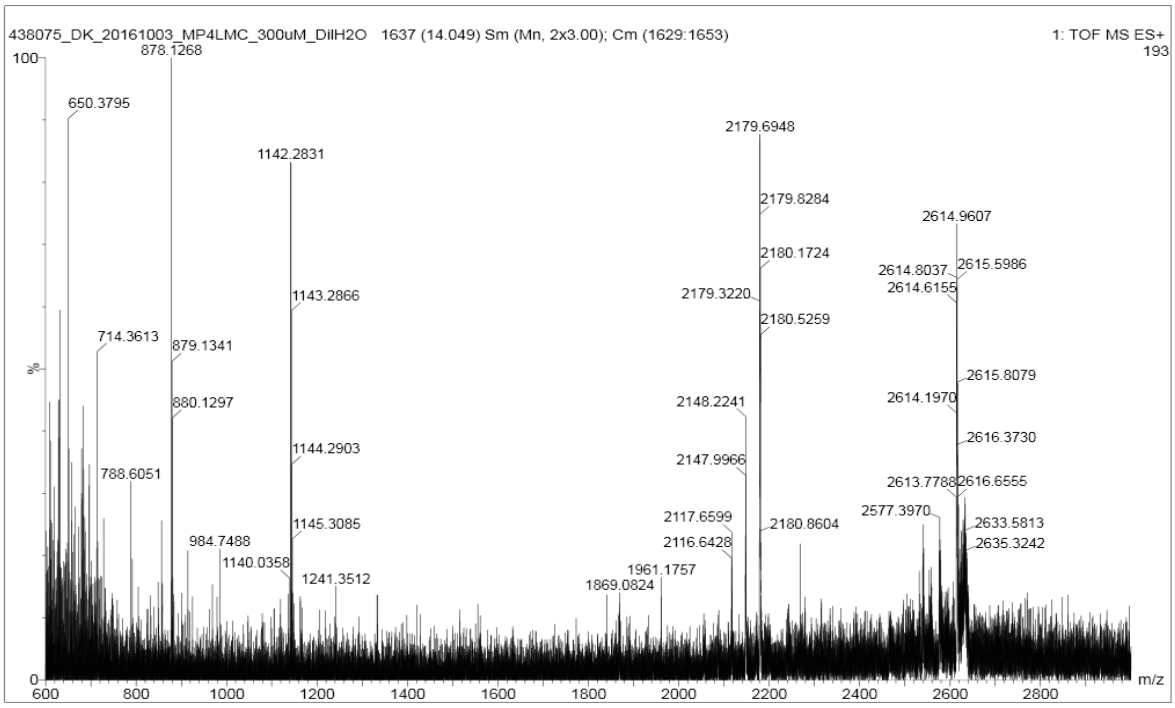

Figure S 95. Mass spectrum of $(\mathbf{3})_{35}$ (t_R =14.05 min) from the LC-MS analysis of a DCL made from **3**.
$(\mathbf{3})_{35}$: m/z calculated: 2177.44 $[M+6H]^{6+}$, 2612.72 $[M+5H]^{5+}$; m/z observed: 2177.87 $[M+6H]^{6+}$, 2613.21 $[M+5H]^{5+}$.

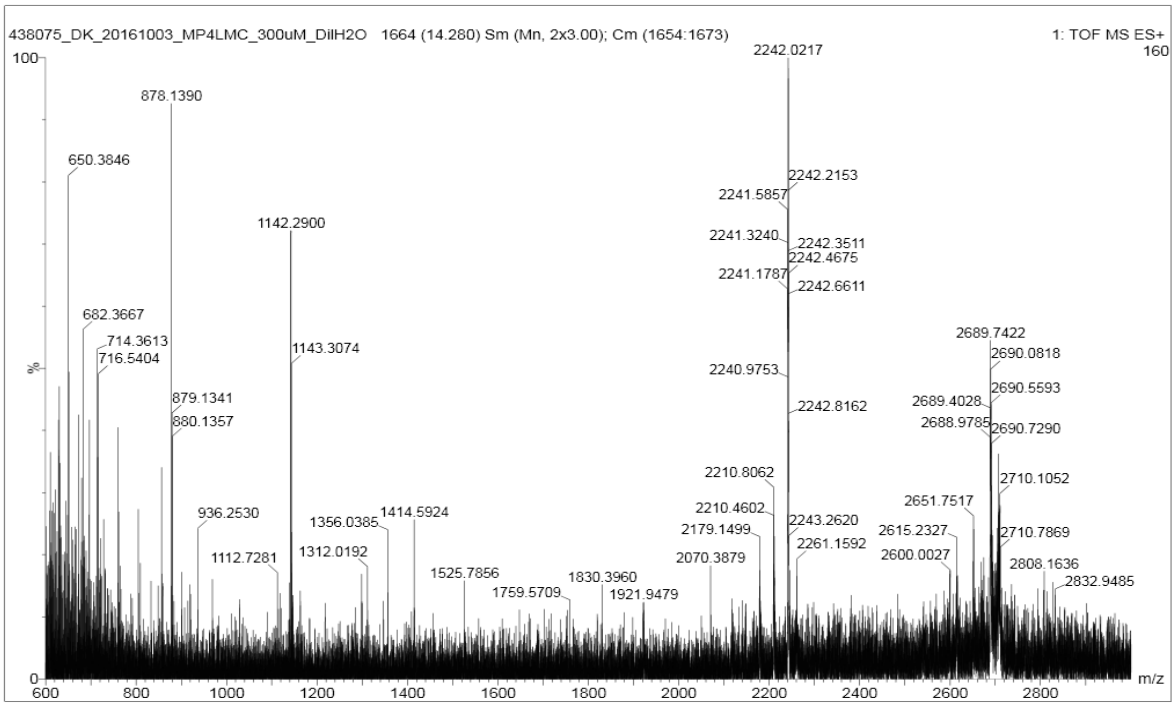

Figure S 96. Mass spectrum of $(\mathbf{3})_{36}$ (t_R =14.28 min) from the LC-MS analysis of a DCL made from **3**.
$(\mathbf{3})_{36}$: m/z calculated: 2239.62 $[M+6H]^{6+}$, 2687.34 $[M+5H]^{5+}$; m/z observed: 2239.90 $[M+6H]^{6+}$, 2687.396$[M+5H]^{5+}$.

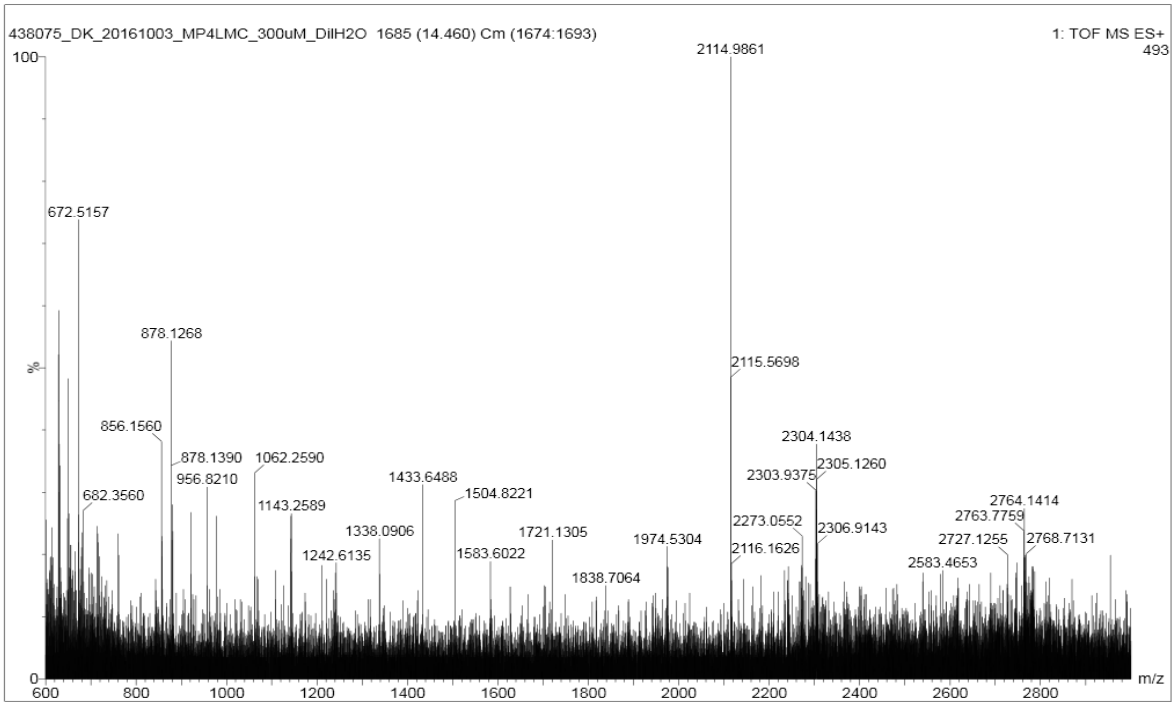

Figure S 97. Mass spectrum of $(\mathbf{3})_{37}$ (t_R =14.46 min) from the LC-MS analysis of a DCL made from **3**.
$(\mathbf{3})_{37}$: m/z calculated: 2301.80 $[M+6H]^{6+}$, 2761.96 $[M+5H]^{5+}$; m/z observed: 2302.30 $[M+6H]^{6+}$, 2762.32 $[M+5H]^{5+}$.

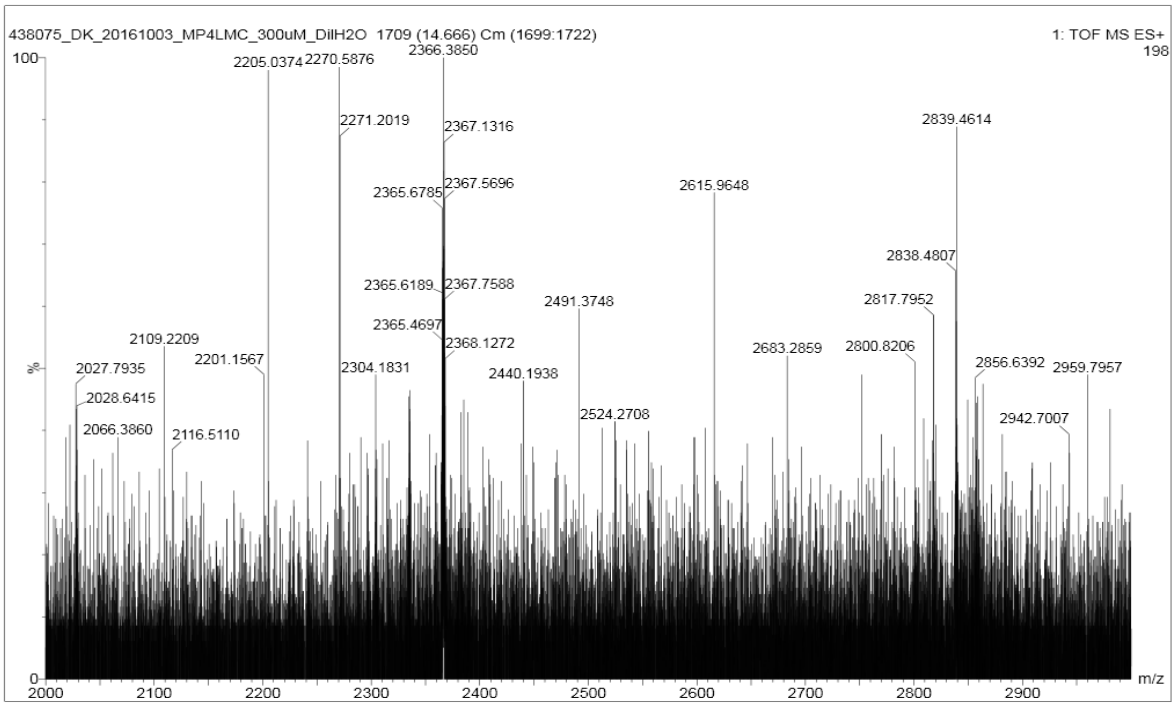

Figure S 98. Mass spectrum of $(\mathbf{3})_{38}$ (t_R =14.67 min) from the LC-MS analysis of a DCL made from **3**.
$(\mathbf{3})_{38}$: m/z calculated: 2363.99 $[M+6H]^{6+}$, 2836.58 $[M+5H]^{5+}$; m/z observed: 2364.64 $[M+6H]^{6+}$, 2837.11 $[M+5H]^{5+}$.

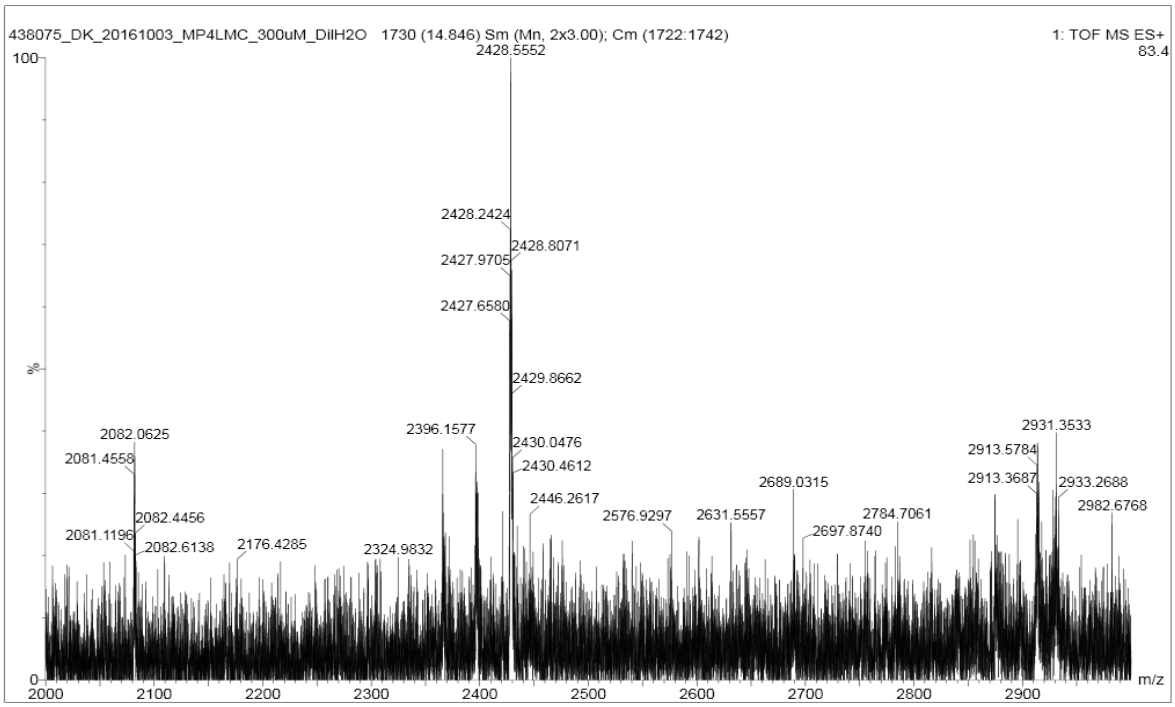

Figure S 99. Mass spectrum of $(\mathbf{3})_{39}$ (t_R =14.85 min) from the LC-MS analysis of a DCL made from **3**.
$(\mathbf{3})_{39}$: m/z calculated: 2426.17 $[M+6H]^{6+}$; m/z observed: 2426.68 $[M+6H]^{6+}$.

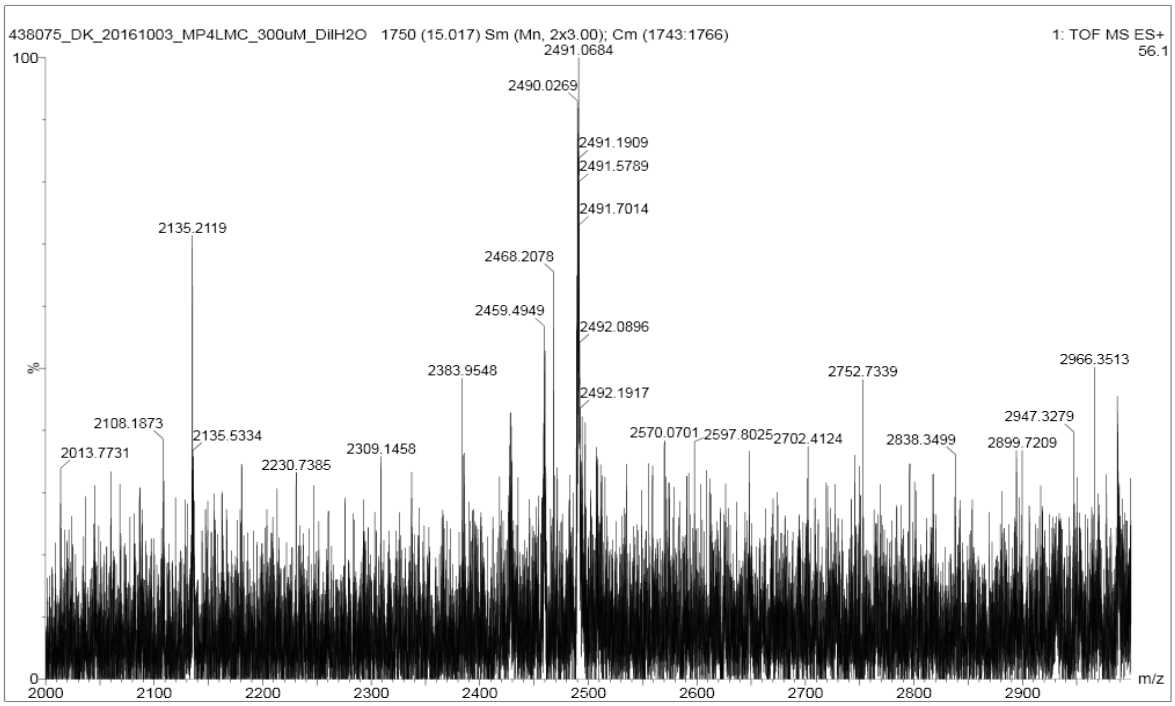

Figure S 100. Mass spectrum of $(\mathbf{3})_{40}$ (t_R =15.02 min) from the LC-MS analysis of a DCL made from **3**. $(\mathbf{3})_{40}$: m/z calculated: 2488.35 $[M+6H]^{6+}$; m/z observed: 2488.61 $[M+6H]^{6+}$.

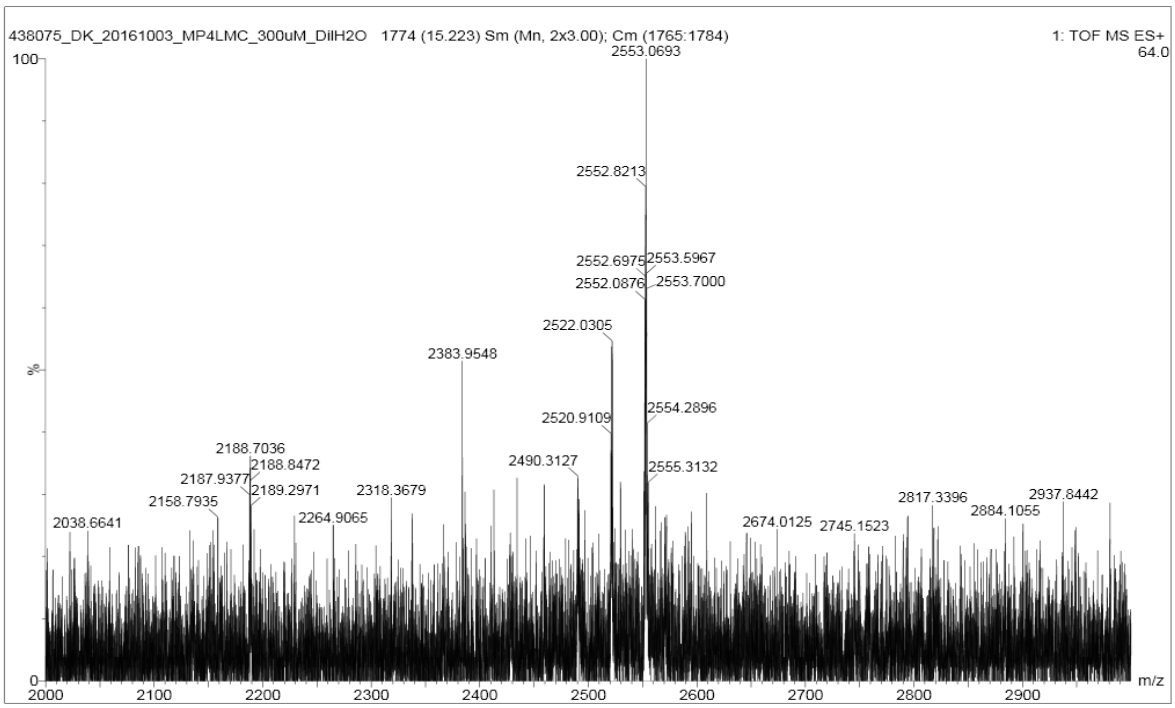

Figure S 101. Mass spectrum of $(\mathbf{3})_{41}$ (t_R =15.22 min) from the LC-MS analysis of a DCL made from **3**. $(\mathbf{3})_{41}$: m/z calculated: 2550.54 $[M+6H]^{6+}$; m/z observed: 2550.97 $[M+6H]^{6+}$.

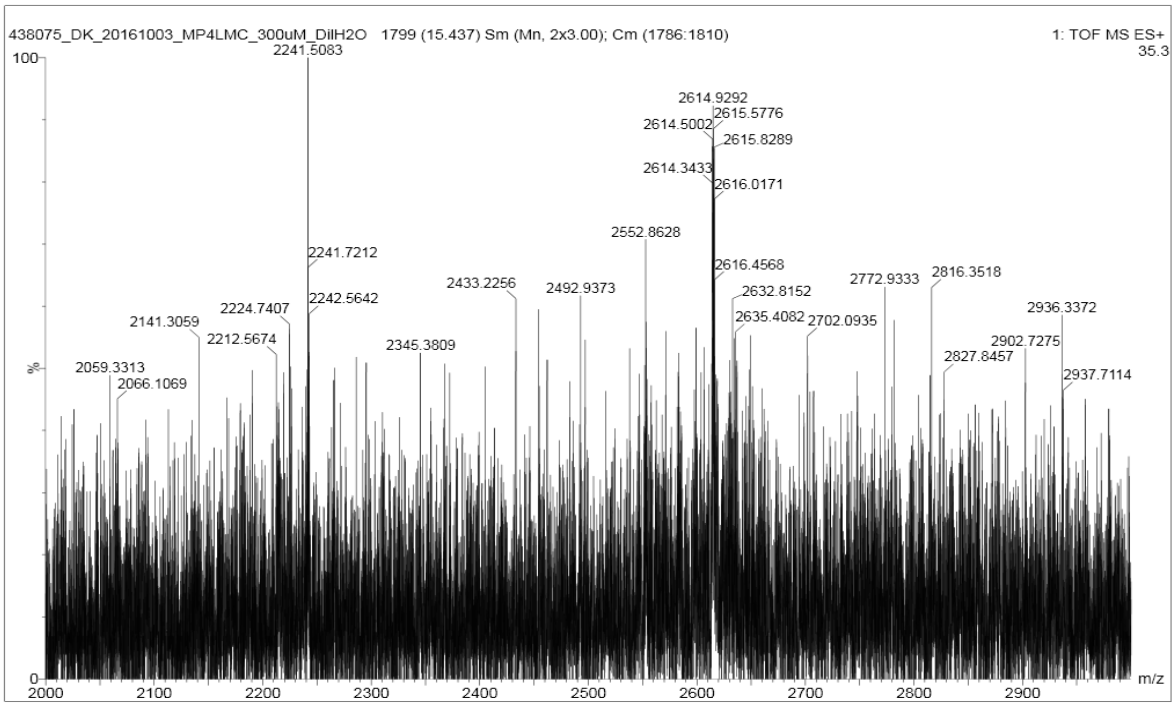

Figure S 102. Mass spectrum of $(\mathbf{3})_{42}$ (t_R =15.44 min) from the LC-MS analysis of a DCL made from **3**. $(\mathbf{3})_{42}$: m/z calculated: 2612.72 $[M+6H]^{6+}$; m/z observed: 2613.52 $[M+6H]^{6+}$.

Remark: For the large oligomers, UPLC-TOF-MS can in principle distinguish between cyclic and linear species as the latter ones would contain two extra hydrogen atoms at the chain ends. In practice, as the amount of the corresponding oligomers (and thus the corresponding signal intensities and signal-to-noise ratios) decrease with increasing oligomer length, we could only confirm the presence of cyclic oligomers up to 35^{mer}s, based only on the MS analysis. Furthermore, the low abundance hampered the MS detection of oligomers above 38-mer (building block **1**) and 42-mer (building block **3**), respectively. Additional peaks most likely corresponding to even larger oligomers were clearly observed in the UPLC chromatograms (see Figure S 107 and Figure S 114).

If linear oligomers were present in considerable amount, thiols and linear dimers would also be detectable in similar concentrations, due to thiol-disulfide exchange. UPLC analysis of fully oxidized samples show that the amount of these free thiol-containing species are below the detection limit. One can argue that for larger oligomers, the linear and cyclic species composed of the same number of monomer units cannot be separated by UPLC because the difference in polarity conferred by the presence of two thiol groups is relatively small due to the large size of both species. Thus, we performed the following experiment: For each building block **1**-**3**, a UPLC spectrum of a fully oxidized library (6 mM), containing considerable amounts of LMCs, alongside with a low amount of organic co-solvent, was recorded. Subsequently, a 100 µL portion of each sample was diluted with 900 µL isopropanol, resulting in DCLs (1.2 mM) containing 90 V/V % organic co-solvent. As discussed in detail in the main text, these libraries contained only neglectable amounts of LMCs as the hydrophobicity-driven aggregation of trimers and tetramers, which is necessary

for the formation of large oligomers, is far less pronounced in mainly organic media (see Figure 2 in the Main Text).

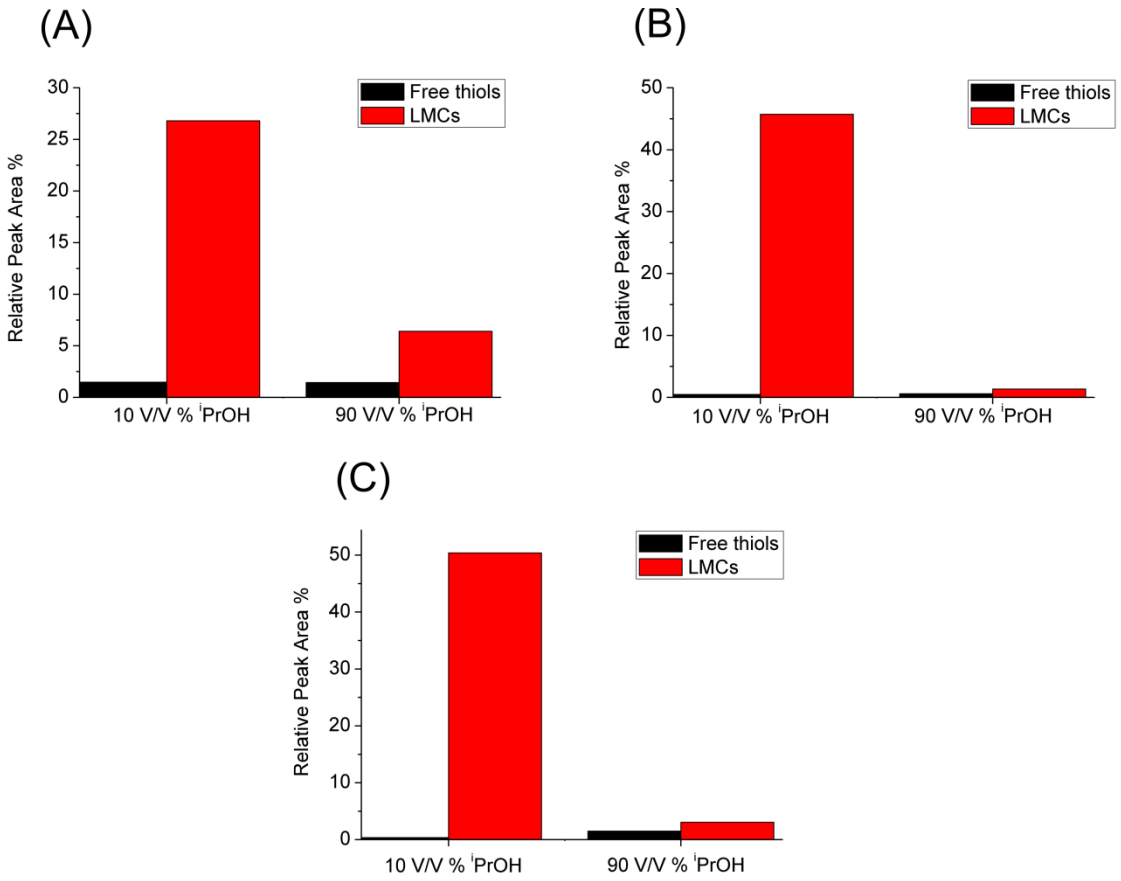

Figure S 103. Free thiol (calculated as c(SH) = c(monomer)+0.5×c(dimer); black bars) and LMC (red bars) content of fully-oxidized, non-stirred DCLs (6 mM) prepared from building block (A) **2**, (B) **1**, (C) **3** before (left-side bars) and after (right-side bars) diluting into 90 V/V% isopropanol.

If there were a considerable amount of linear large oligomers containing free thiol groups, these would cause a considerable increase in the amount of free thiols (monomer and linear dimer). However, the linear thiol concentration increased only by a negligible amount (0.1 % and 1.1 % for building block **1** and **3**, respectively, whereas in the case of building block **2**, no change was detectable), as shown in Figure S 103. Thus, based on our analytical data, the detected large oligomers are most probably macrocyclic species, with at most a few percent of linear species present.

7. *Additional characterization of the LMCs formed from building block 1.*

Remark: In oxidized, non-stirred DCLs prepared from **1,** stable colloids are formed at concentrations below 1 mM. In contrast, in libraries with a DMF content less than 10 V/V % and building block concentration higher than 1 mM, phase separation occurred (Figures S104-106). This process was also evident from UPLC analysis of the samples, showing extensive peak area loss for samples that exhibited phase separation (Figure S104). After re-dissolving phase-separated material in MeCN, UPLC analysis revealed that it had a composition similar to that of the solution phase, consisting mainly of trimers and tetramers (Figure S 106). Consistently, upon the addition of increasing amounts of co-solvent, the phase-separated material could be re-dissolved as evidenced by the increase in the overall UPLC peak area.

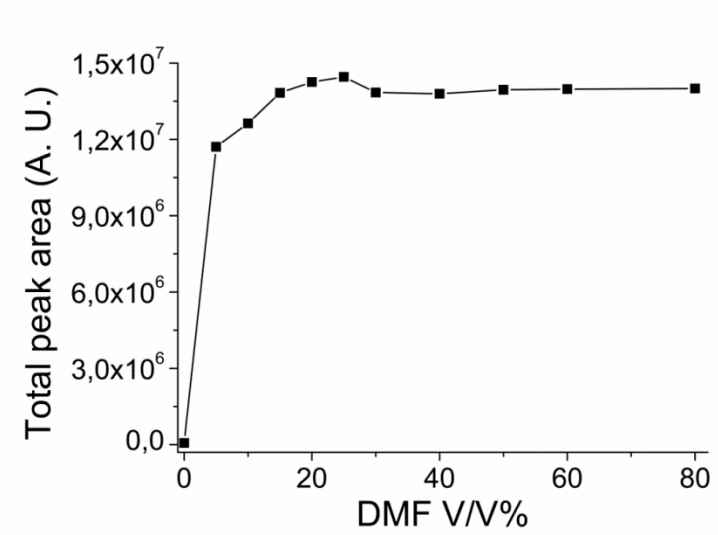

Figure S104. Total UPLC peak area of a DCL prepared from **1** (6.0 mM) with different amounts of DMF as a co-solvent.

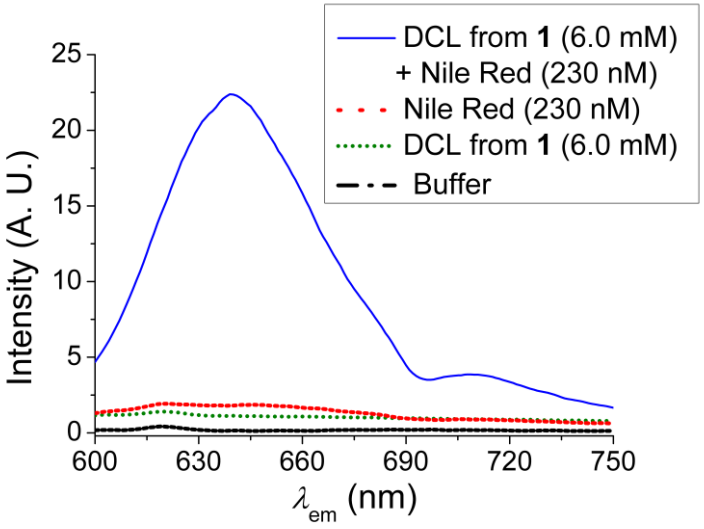

Figure S 105. Fluorescent emission spectrum of a solution containing a DCL prepared from **1** (6.0 mM) in the absence of agitation and 230 nM Nile Red in 50 mM borate buffer (pH = 8.2, without co-solvent) at λ_{exc} = 553 nm (blue line) and the fluorescent emission spectra of Nile Red (red dots), a DCL prepared from **1** at a total concentration of 6.0 mM (green dots) and buffer (black line) recorded under the same conditions.

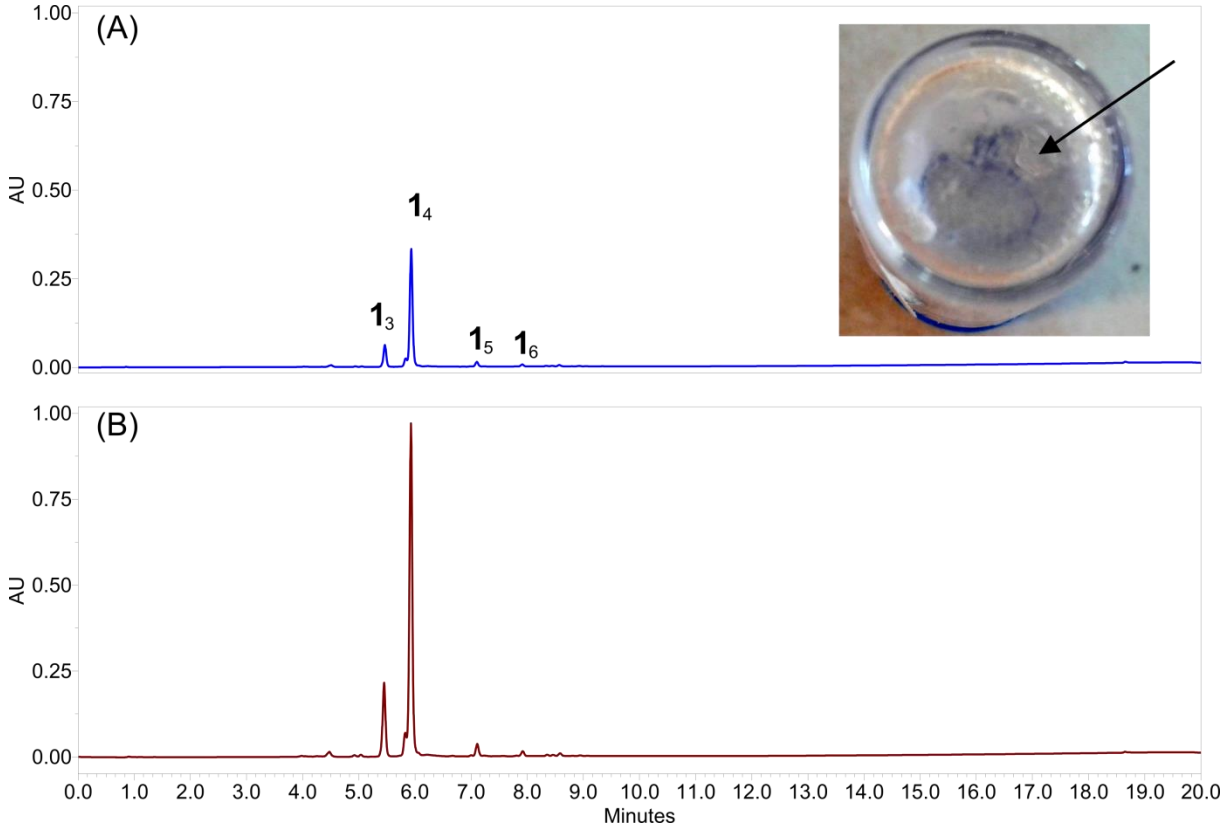

Figure S 106. A sample prepared by isolating the oily substrate (see inset, arrow pointing towards an oil droplet), formed in a vial containing a 2 months old non-agitated DCL prepared from **1**. The oil was dissolved in MeCN and UPLC chromatograms were recorded by adding (A) 0% (B) 10 % DMSO to the sample. Note that the intensity scales of the two chromatograms are the same.

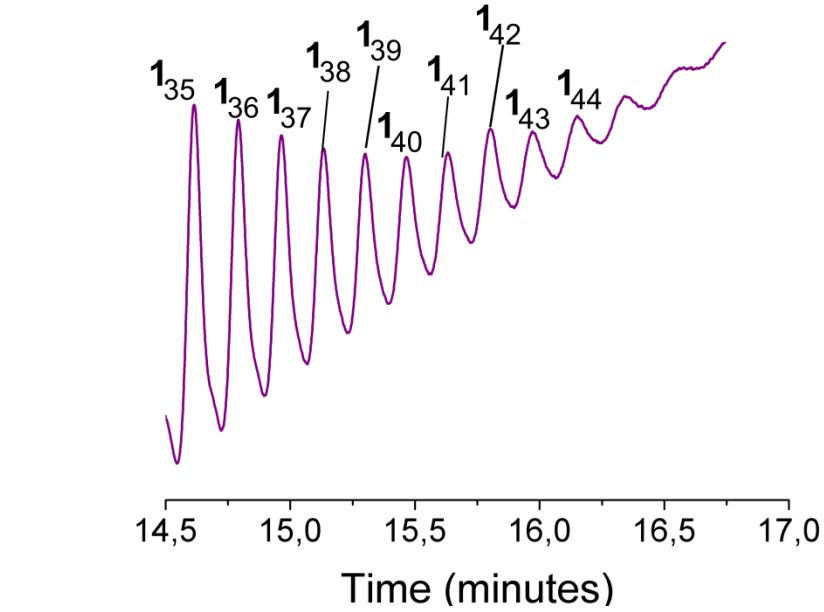

Figure S 107. Partial UPLC chromatogram of a DCL prepared from **1**, showing peaks most likely corresponding to oligomers $\mathbf{1}_{39}$-$\mathbf{1}_{44}$ (not detected in LC-MS due to low signal intensity).

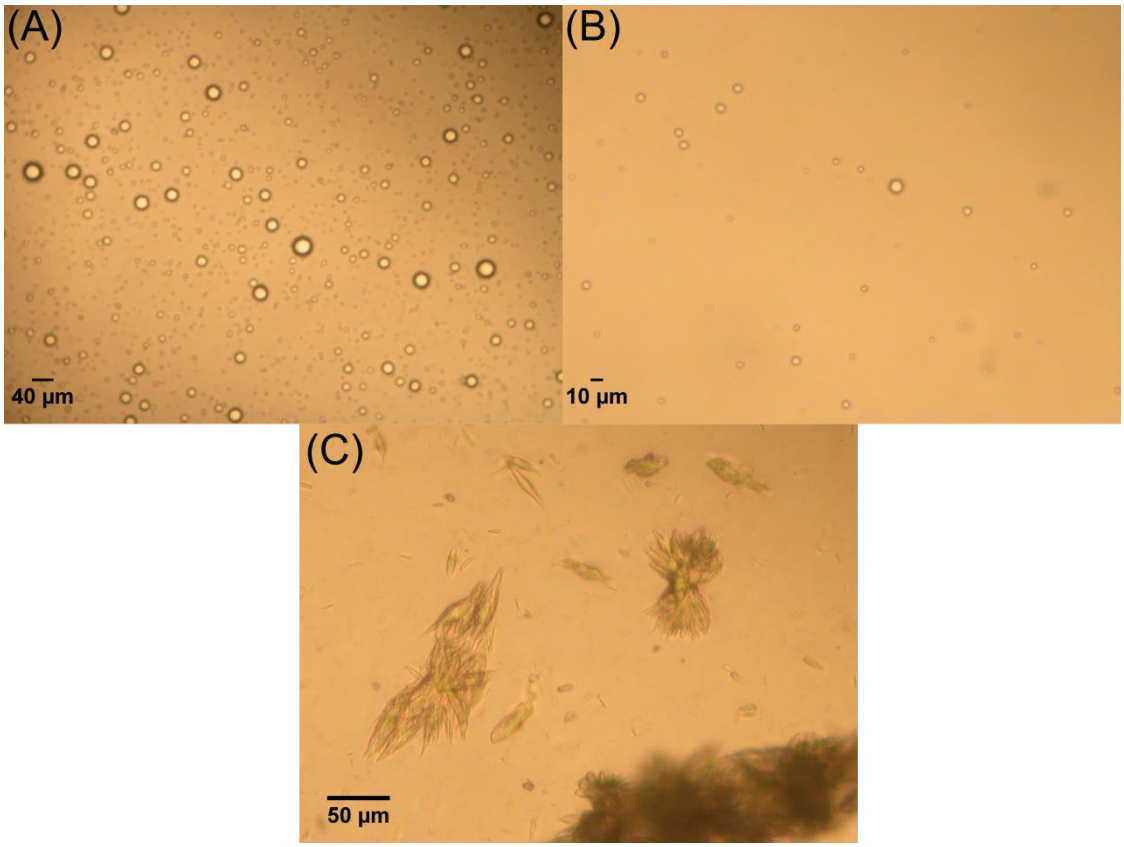

Figure S 108. Optical microscopy images taken of a non-agitated DCL prepared of **1** (6.0 mM) in borate buffer (50 mM, pH = 8.2), pre-oxidized 80 % with sodium perborate (A) 1 hour (B) 1 day (C) 4 months after preparation. Note the presence of spherical aggregates in the fresh samples.

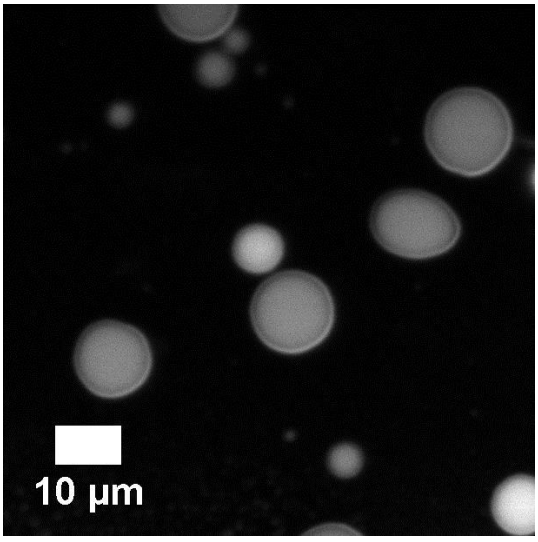

Figure S 109. Fluorescence micrscopy image of an oxidized sample of building block **1** (6.0 mM in 50 mM borate buffer, pH = 8.2) containing trimers, tetramers and LMCs, stained with Nile Red (100 nM).

8. Additional characterization of the LMCs formed from building block 2.

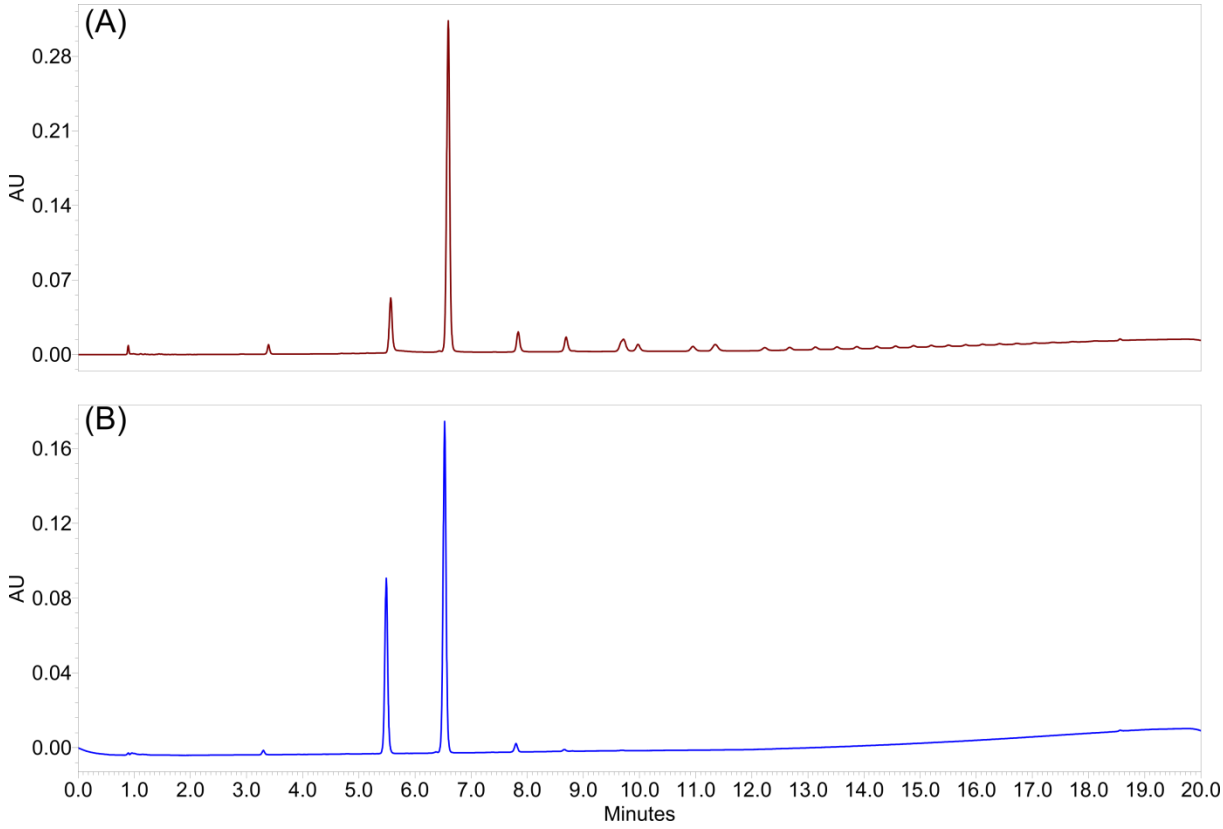

Figure S 110. UPLC chromatograms of a DCL prepared from building block **2** (4 mM), oxidized to 95% with sodium perborate in aqueous borate buffer (50 mM, pH = 8.2) containing (A) 5 V/V % DMSO (B) 75 V/V % MeCN.

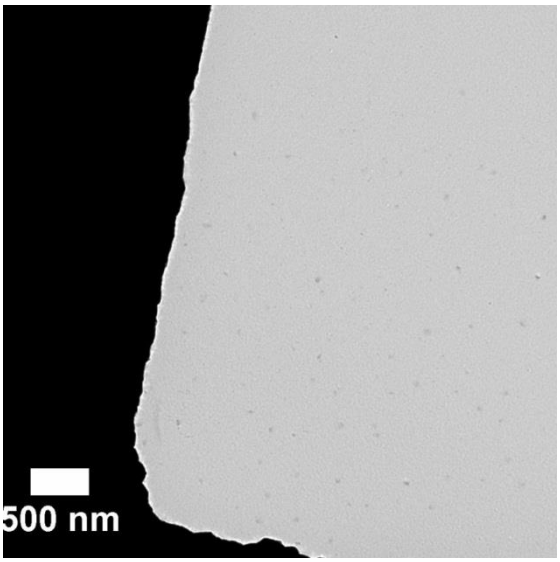

Figure S 111. Negative staining TEM image of a DCL prepared from building block **2** (4 mM) in borate buffer (50 mM, pH = 8.2), oxidized to 90% with sodium perborate. According to the UPLC analysis, the sample contained trimers, tetramers and large macrocycles, whereas TEM shows no indication for the presence of nanoscale objects.

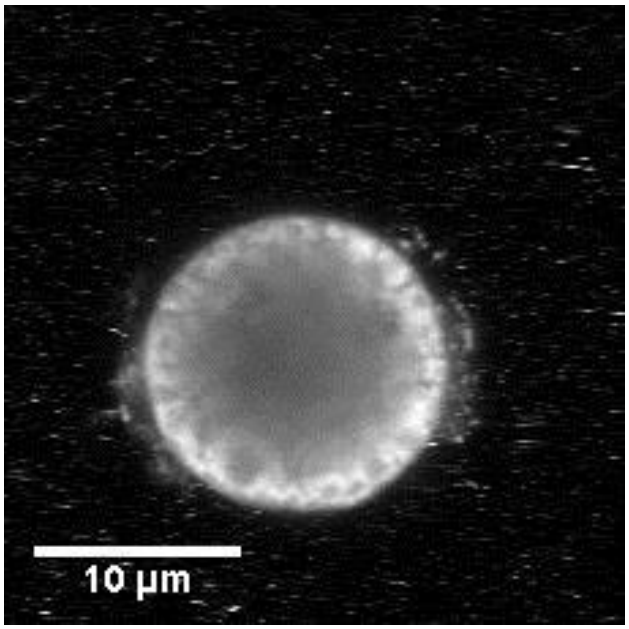

Figure S 112. Confocal fluorescence microscopy image of a freshly oxidized sample of building block **2** (4.0 mM in 50 mM borate buffer, pH = 8.2) containing trimers, tetramers and LMCs, stained with Nile Red (100 nM).

9. Additional characterization of the LMCs formed from building block 3.

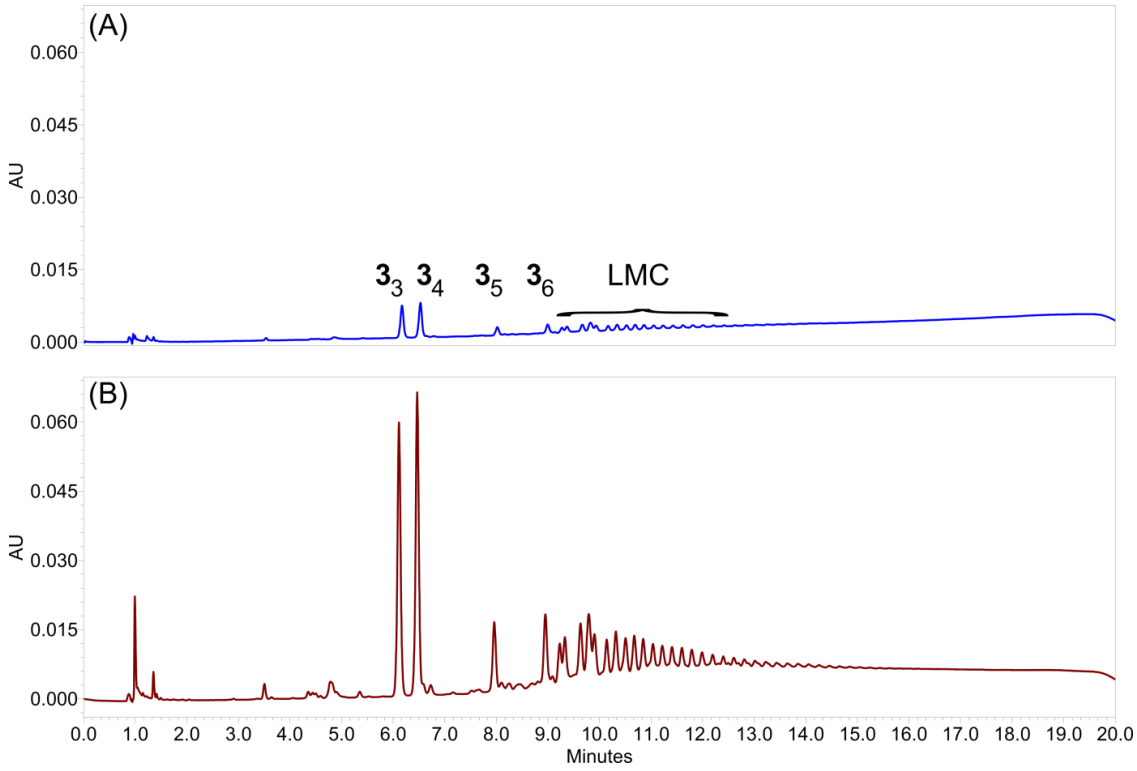

Figure S 113. A sample prepared by injecting a 2 months old, non-agitated DCL prepared from **3** after adding (A) 0% (B) 10 % DMSO to the sample. Note that the intensity scales of the two chromatograms are the same.

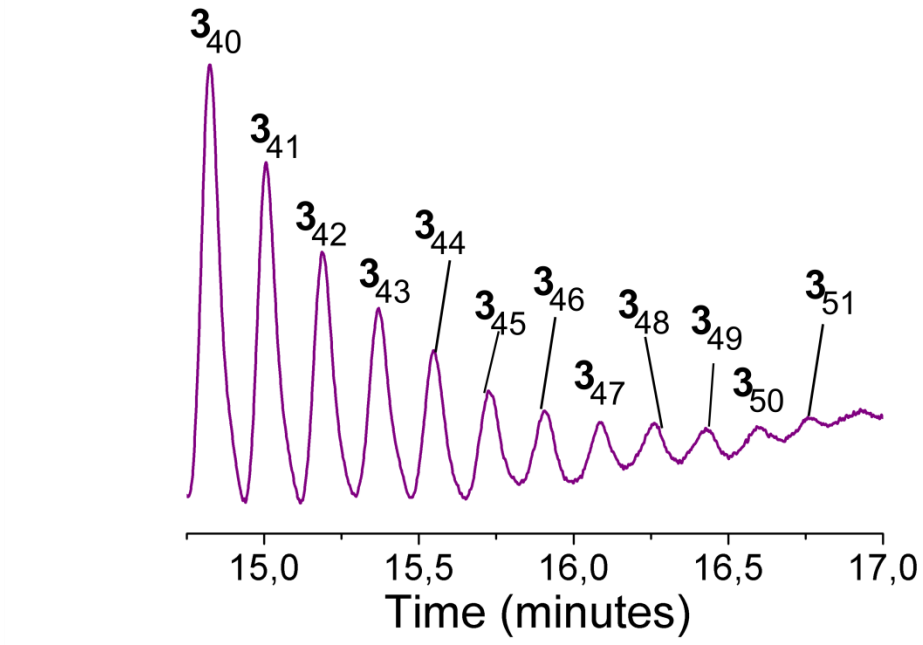

Figure S 114. Partial UPLC chromatogram of a DCL prepared from **3**, showing peaks most likely corresponding to oligomers $\mathbf{3}_{40}$-$\mathbf{3}_{51}$ (not detected in LC-MS due to low signal intensity).

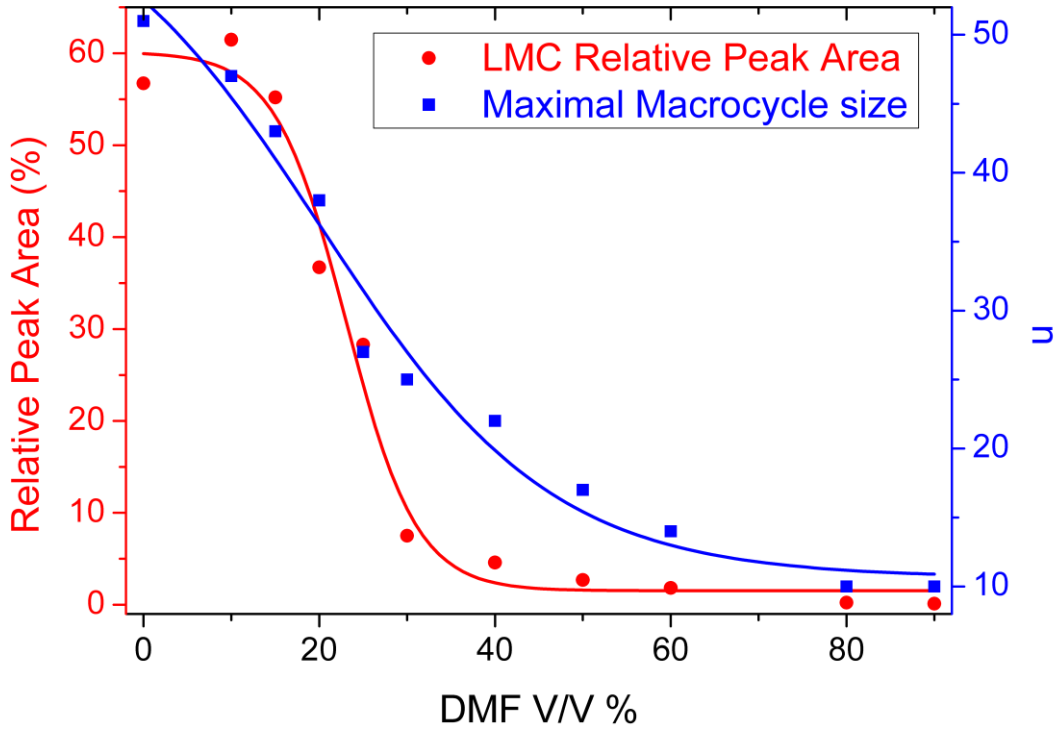

Figure S115. LMC percentage (left axis) and maximal detected LMC size *n* (right axis) of DCLs prepared from **3** (6.0 mM) with different amounts of DMF as a co-solvent. Lines are drawn to guide the eye.

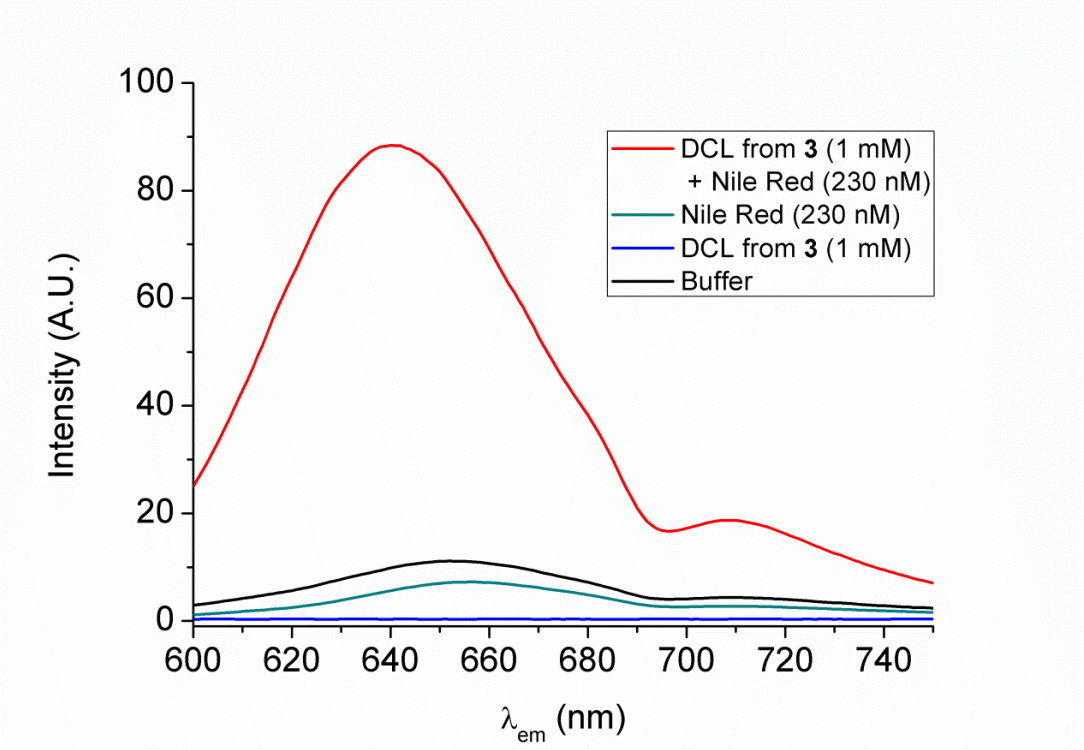

Figure S116. Fluorescent emission spectrum of a solution containing a DCL (total concentration 1.0 mM) prepared from **3** (in the absence of agitation) and 240 nM Nile Red in 50 mM borate buffer (pH = 8.2) at λ_{exc} = 553 nm (blue line). The fluorescent emission spectrum of Nile Red (green), a DCL prepared from **3** at a total concentration of 1.0 mM (blue) and buffer (black) recorded under the same conditions is also indicated.

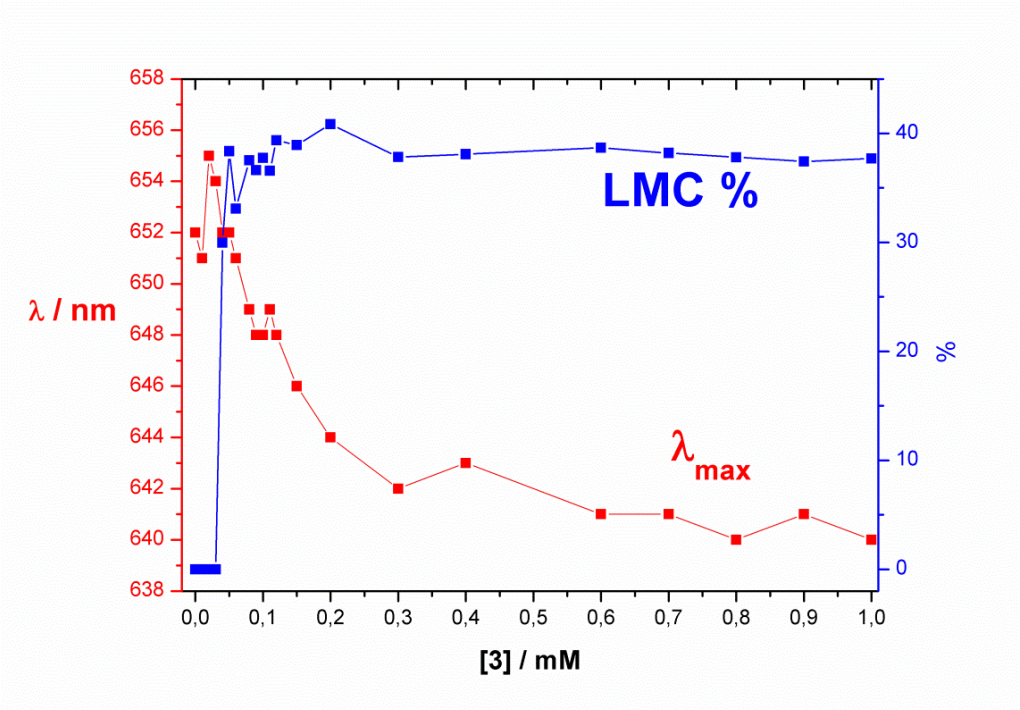

Figure S117. Fluorescent emission maximum (left axis, λ_{exc} = 553 nm) and LMC content (right axis) of solutions containing 240 nM Nile Red and a pre-oxidized DCL prepared from **3** (50 mM borate buffer, pH = 8.2), at different building block concentrations.

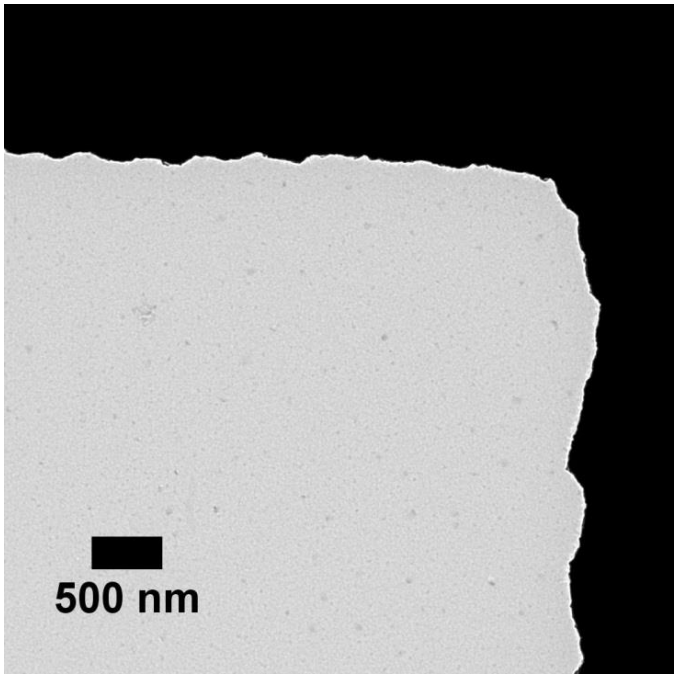

Figure S 118. Negative staining TEM image of a DCL prepared from building block **3** (6 mM) in borate buffer (50 mM, pH = 8.2), fully oxidized by air. According to the UPLC analysis, the sample contained trimers, tetramers and large macrocycles, whereas TEM shows no evidence for the presence of any nanoscale objects.

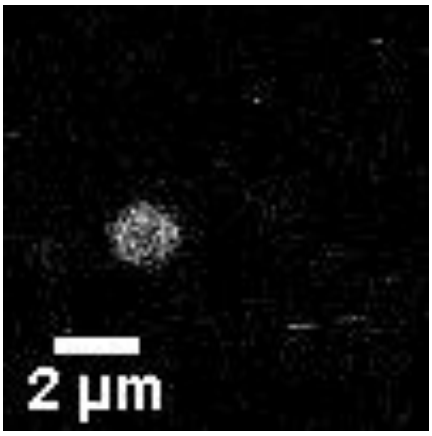

Figure S 119. Confocal fluorescence microscopy image of a freshly oxidized sample of building block **3** (6.0 mM in 50 mM borate buffer, pH = 8.2) containing trimers, tetramers and LMCs, stained with Nile Red (100 nM).

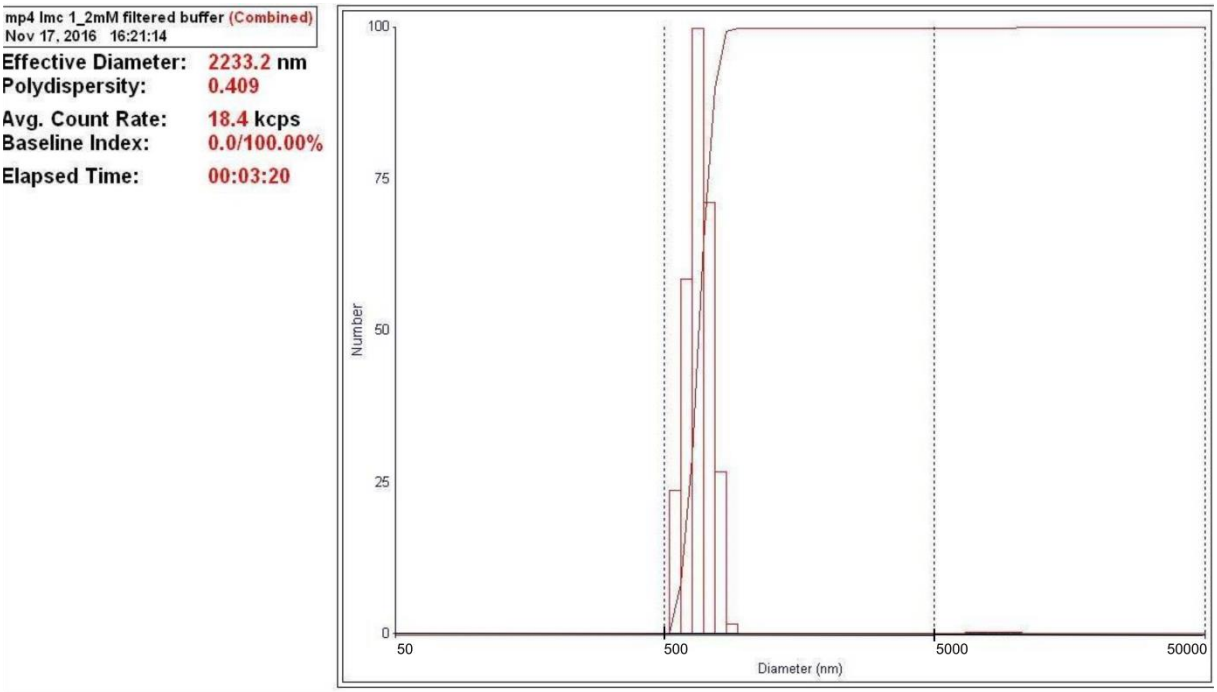

Figure S 120. Particle size distribution in a non-agitated DCL prepared from building block **3** (6.0 mM) in aqueous borate buffer (50 mM, pH = 8.2), measured with dynamic light scattering.

10. Additional characterization of the formation and structure of hexamer 1_6

Synthesis of **1_6** from **1**:

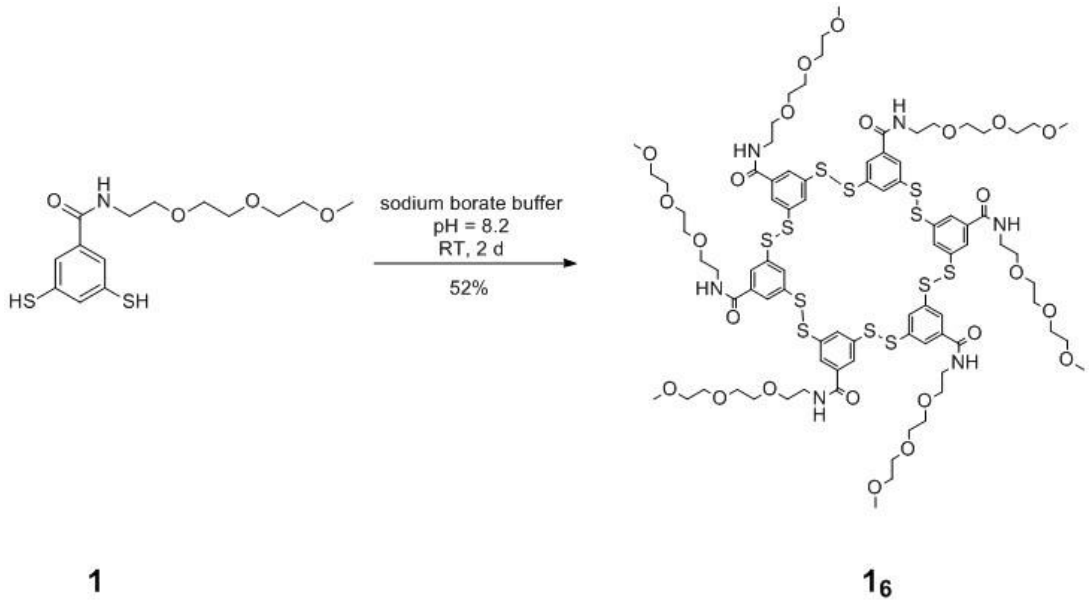

1 **1_6**

1 (7.7 mg, 23 µmol) was suspended in aqueous sodium borate buffer (1.2 mL, 50 mM, pH = 8.2) and was left standing for 1 day. Subsequently, it was stirred for one day. At this time, UPLC analysis showed complete conversion of the monomer to hexamer. The resulting suspension was centrifuged (17 min, 3900 rpm). The pellet was washed with doubly distilled water (2×1200 µL) to remove excess sodium borate and centrifuged. The residue was freeze-dried overnight to yield **1_6** (4.0 mg, 2.0 µmol) as a white solid in 52 % yield. The purity of the product was confirmed by UPLC.

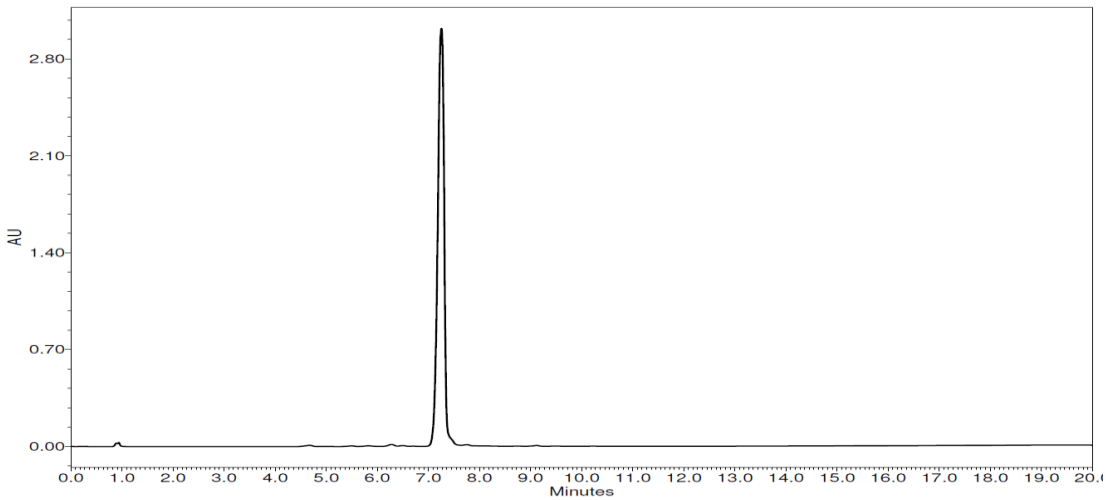

Figure S 121. UPLC chromatogram of isolated **1_6**, freshly dissolved in MeCN.

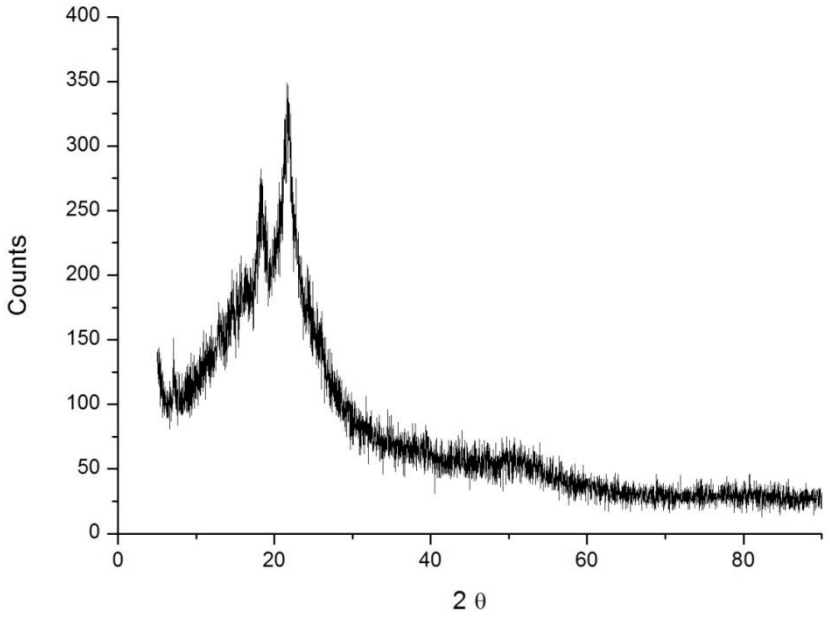

Figure S122. Powder X-ray diffractogram of isolated $\mathbf{1}_6$.

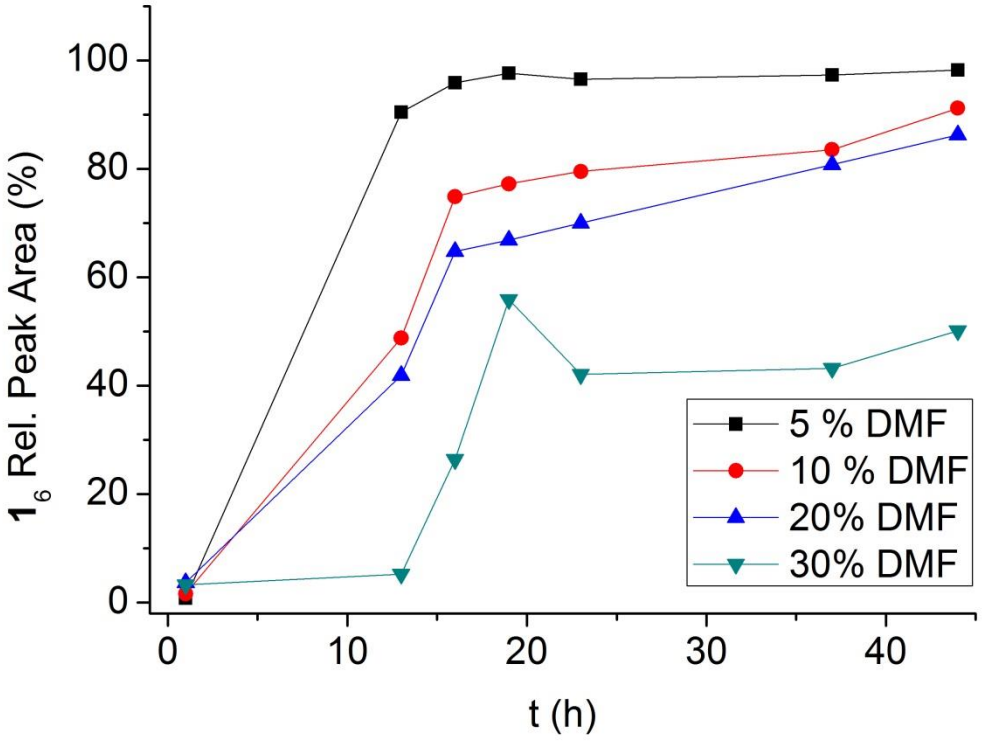

Figure S123. Time evolution of stirred DCLs prepared from **1** (6.0 mM) with different amounts of co-solvent (DMF), pre-oxidized with $NaBO_3$.

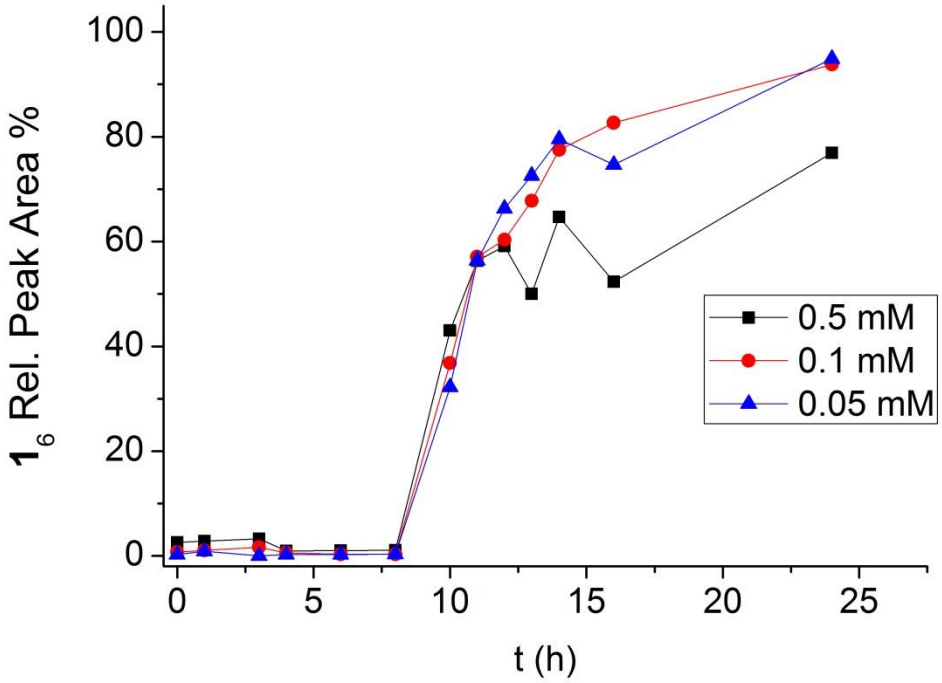

Figure S 124. Change of the relative concentration of **1$_6$** in agitated libraries prepared from **1** at 0.05, 0.1 and 0.5 mM concentrations, in aqueous sodium borate buffer (50 mM, pH = 8.2).

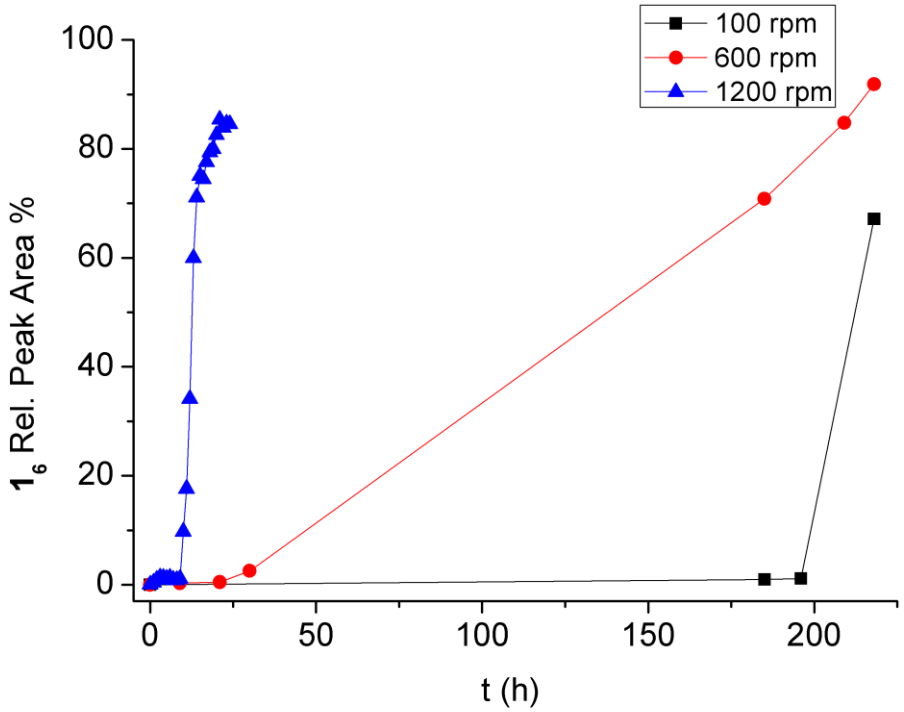

Figure S 125. Change of the relative concentration of **1$_6$** in libraries agitated at different stirring rates (100, 600 and 1200 rpm) prepared from **1** at 2 mM concentrations, in aqueous sodium borate buffer (50 mM, pH = 8.2). The data points corresponding to 1200 rpm stirring rate were taken from **Figure 4**A of the main text.

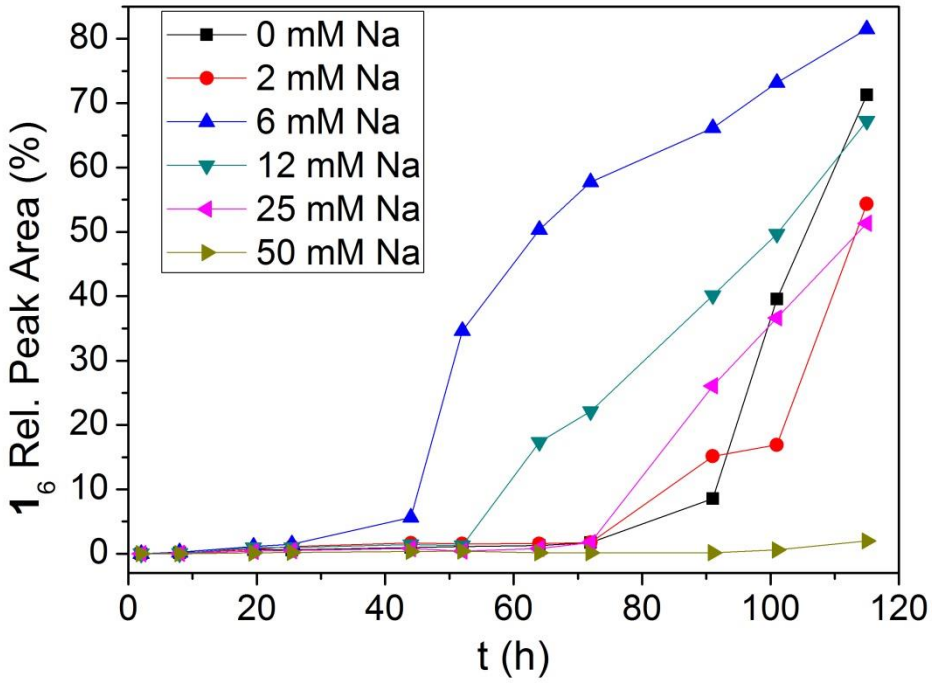

Figure S126. Change of the relative concentration of the hexamer of **1** in a DCL prepared from **1** (6.0 mM) in UPLC grade water with different concentrations of NaCl. The time evolution of the hexamer shows no readily interpretable correlation between the replication rate and the concentration of Na^+ ions, thus ruling out that Na^+ ions promote the association of hexamers by inserting between the oligo(ethylene oxide) chains, forming a crown ether-type chelate. Note that replication is also relatively fast in the absence of Na^+ ions.

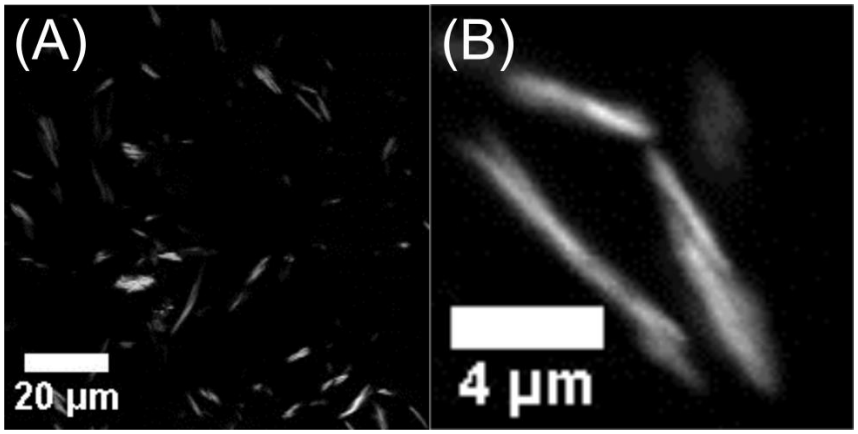

Figure S 127. Confocal fluorescence microscopy image of a sample containing exclusively $\mathbf{1_6}$ (6.0 mM) in borate buffer (50 mM, pH = 8.2) stained with Nile Red (100 nM).

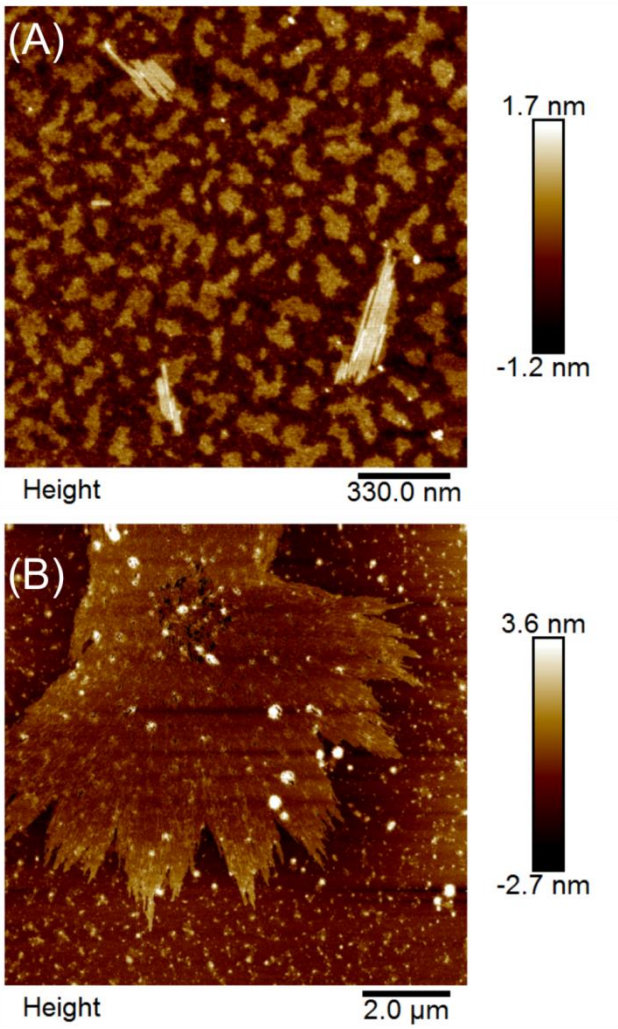

Figure S 128. AFM images of a library prepared from **1** (6.0 mM) by oxidizing it to 80 % with $NaBO_3$ in aqueous borate buffer and subsequently stirred for (A) 8.5 hours (early stage of self-assembly) and (B) 12 hours (late stage of self-assembly). Note that at the early stage of self-assembly aggregates of 4-5 nanoribbons (150 – 300 nm long) are observed, whereas at the late stage of self-assembly several tens of nanoribbons self-assemble to give large aggregates (more than 6 µm long).

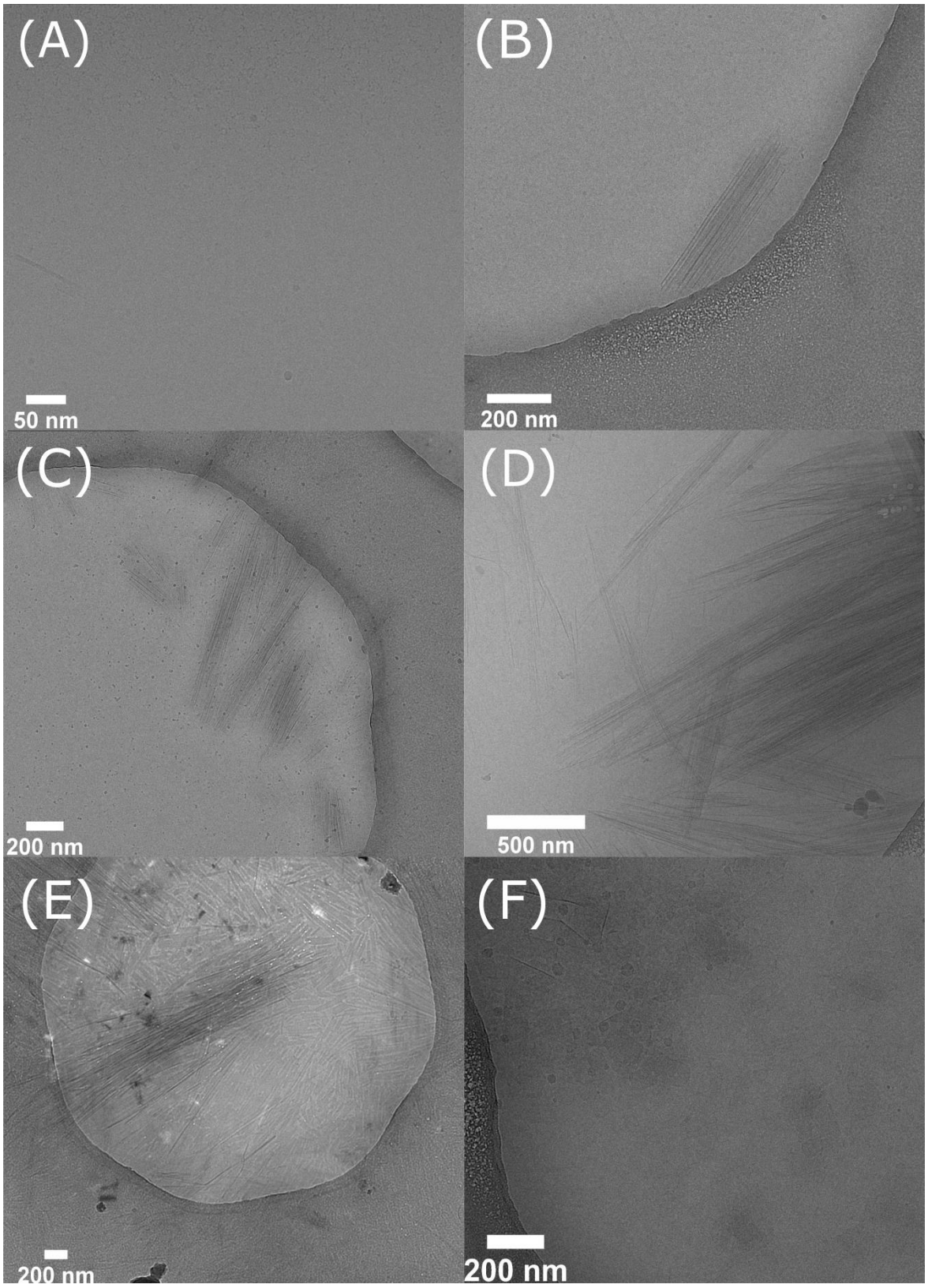

Figure S 129. TEM images taken of samples from of a DCL prepared from **1** (6.0 mM) in borate buffer (50 mM, pH = 8.2), pre-oxidized 80 % with sodium perborate, after stirring for (A) 0 hours , (B) 2 hours, (C) 3.5 hours, (D) 17 hours, (E) 20 hours, (F) 72 hours. All images were recorded with cryo-TEM, except for the image shown in (G), which was recorded with negative staining. Note the absence of nanoribbons at 0-1 hour, the presence of increasingly elongated and laterally associated nanoribbons (associated with the self-replication and self-assembly of $\mathbf{1}_6$) from 2-43 hours, as well as the presence of nanoplatelets at 72 hours.

11. Additional characterization of the formation and structure of tetramer 2_4

Synthesis of $\mathbf{2_4}$ from **2**:

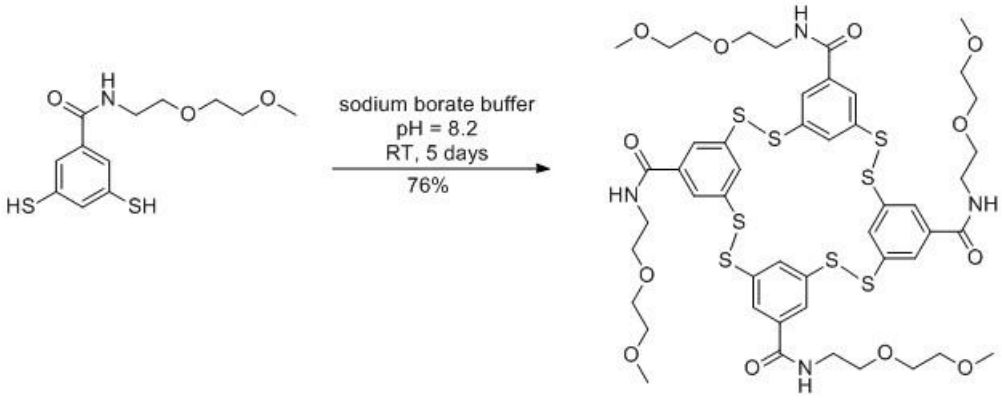

2 $\qquad\qquad$ $\mathbf{2_4}$

2 (5.2 mg, 15 µmol) was suspended in aqueous sodium borate buffer (2.74 mL, 50 mM, pH = 8.2). Sodium borate (60mM, 304 µL in sodium borate buffer) was added in portions of 12.2 µL over the course of 25 minutes. Subsequently, the reaction mixture was stired for 5 days until UPLC analysis showed complete conversion of the monomer to the tetramer. The resulting suspension was centrifuged (5 min, 5000 rpm). The pellet was washed with doubly distilled water (1 mL) to remove excess sodium borate and centrifuged. The residue was freeze-dried overnight to yield $\mathbf{2_4}$ (4.0 mg, 3.5 µmol) as a white solid in 76 % yield. The purity of the product was confirmed by UPLC.

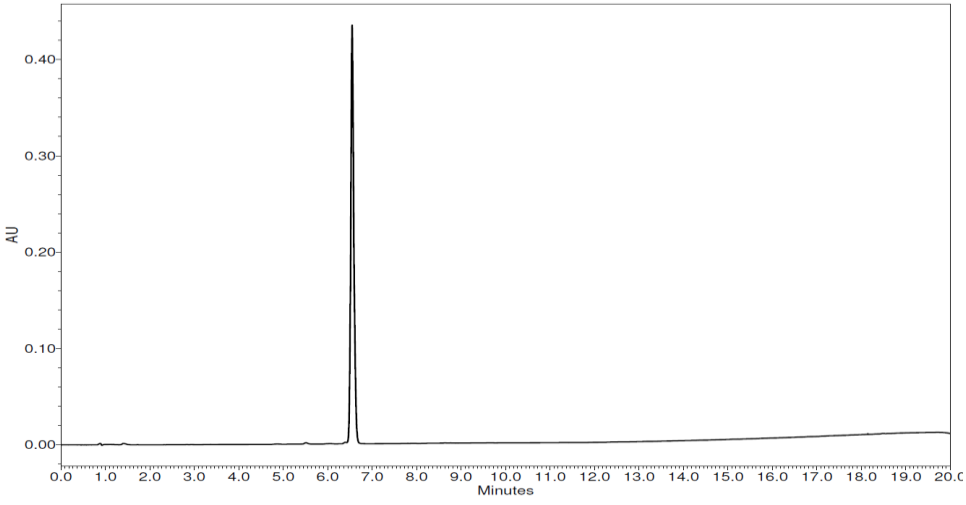

Figure S 130. UPLC chromatogram of isolated $\mathbf{2_4}$, freshly dissolved in 2-propanol.

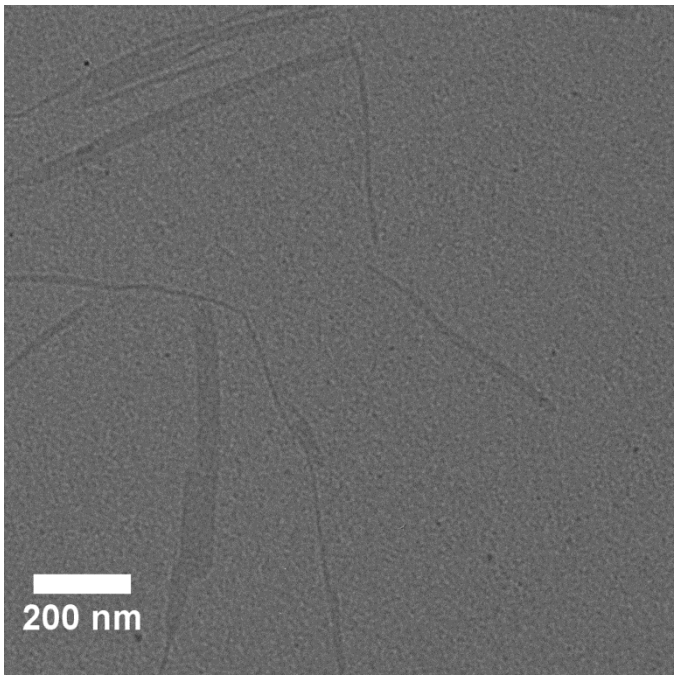

Figure S131. Negative stain TEM image of a stirred DCL prepared from building block **2** (3.84 mM), containing exclusively the cyclic tetramer $\mathbf{2_4}$. Note the presence of nanoribbons similar to those observed in the case of $\mathbf{1_6}$, which suggests a similar mode of self-assembly of the two species.

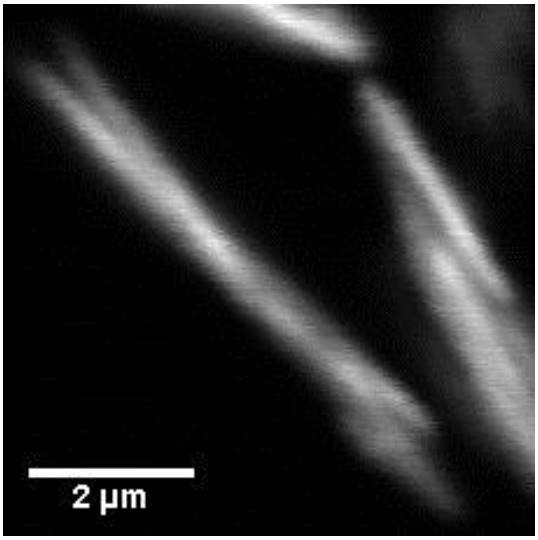

Figure S 132. Confocal fluorescence microscopy image of a sample containing exclusively $\mathbf{2_4}$ (3.84 mM) in borate buffer (50 mM, pH = 8.2) stained with Nile Red (100 nM).

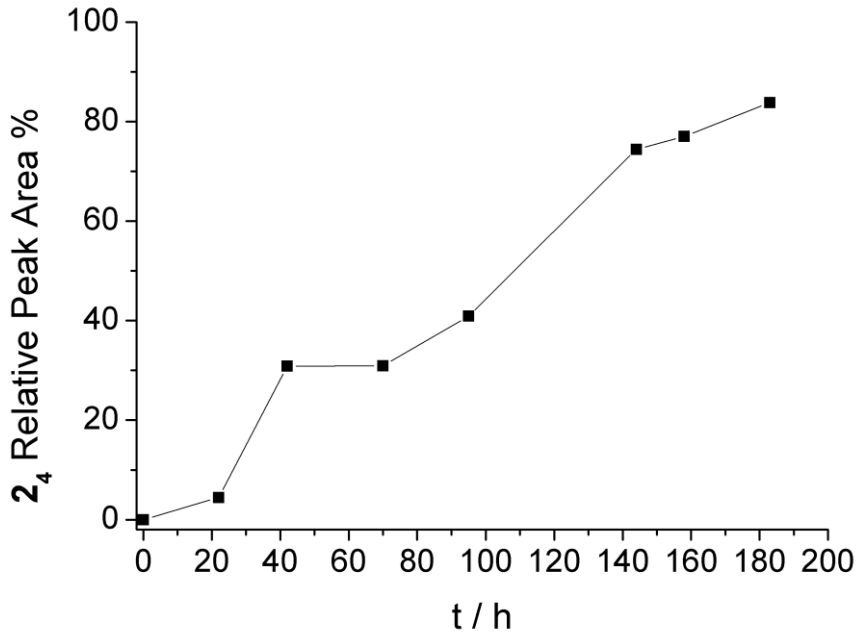

Figure S 133. Change of the relative concentration of $\mathbf{2}_4$ in an agitated (880 rpm) library prepared from **2** (4 mM) in aqueous sodium borate buffer (50 mM, pH = 8.2).

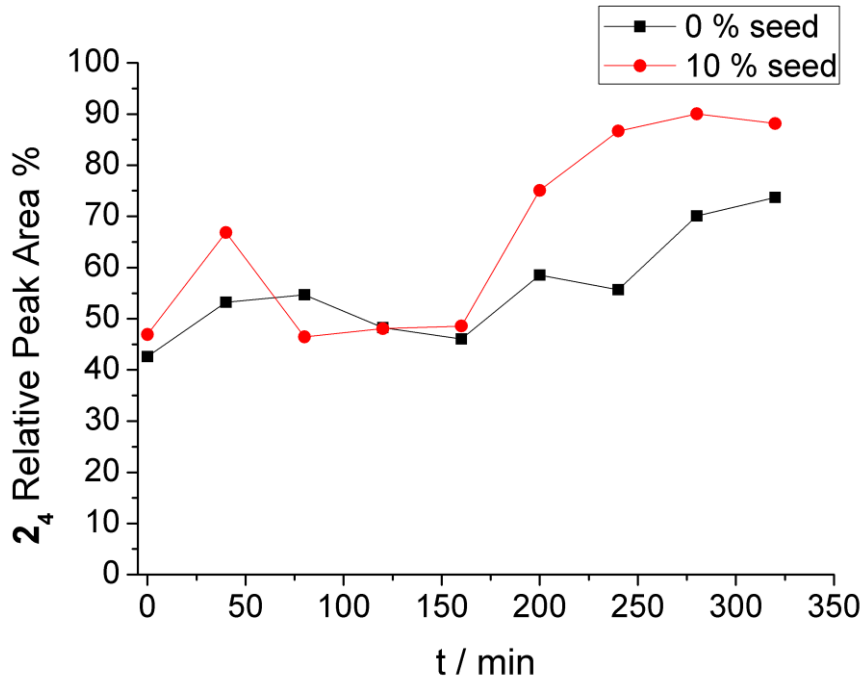

Figure S 134. Change of the relative concentration of $\mathbf{2}_4$ in a non-agitated DCL prepared from **2** (4.0 mM in 50 mM borate buffer, containing 10 V/V % DMF) by fast oxidation with sodium borate (90% oxidation level) without seeding (squares) and upon seeding with 10 % (circles) preformed tetramer seed at t = 0 min.

12. References

1. Carnall, J. M. A.; Waudby, C. A.; Belenguer, A. M.; Stuart, M. C. A.; Peyralans, J. J.-P.; Otto, S. *Science* **2010**, *327* (5972), 1502–1506.
2. Wei, T.; Jung, J. H.; Scott, T. F. *J. Am. Chem. Soc.*, **2015**, *137*, 16196–16202.
3. Wendeln, C.; Rinnen, S.; Schulz, C.; Kaufmann, T.; Arlinghaus, H. F.; Ravoo, B. J. *Chem. Eur. J.* **2012**, *18*, 5880-5888.